UCL SCHOOL OF PHARMACY
BRUNSWICK SQUARE

Formulation strategies for dermal delivery of angiotensin converting enzyme inhibitors

Fouad Helal

This thesis submitted in fulfilment of the requirements for the degree of Doctor of Philosophy

UCL School of Pharmacy
29-39 Brunswick Square
London, WC1N 1AX

2020

Thesis declaration

I, Fouad Helal, confirm that the work presented in this thesis is my own. Where information has been derived from other sources, I confirm that this has been indicated in the thesis.

Fouad Helal

Abstract

Each year, a large number of people develop scars all over the world as a result of abnormal wound healing. However, the current treatment strategies available have demonstrated insufficient outcomes and limitations. Even though studies have shown that angiotensin converting enzyme inhibitors (ACEIs) can be a cutting edge scar treatment, licensed topical formulations of ACEIs have not been yet available for use. Therefore, an attempt has been made in the present work to design stable topical formulations of ACEIs and evaluate the percutaneous absorption of the drugs across porcine ear skin as a surrogate model of human skin. Since the quality of any formulation relies on its stability and efficacy, three different ACEIs, moexipril (MOX), ramipril (RAM), and cilazapril (CILA), were underwent stability studies at 32 ˚C in a wide range of dermal vehicles. Among these three compounds, CILA exhibited good stability while the others were degraded under the experimental conditions resulting in diketopiperazine formation. Based on the findings of the stability studies, simple and complex topical formulations of CILA were developed. The permeation data demonstrated the feasibility of dermal delivery of CILA across porcine skin. Furthermore, the results indicated that the complexity of the topical formulation had a pronounced effect on the permeation rate. The hydrolysed form of CILA, cilazaprilat, was also found in the receptor phase, indicating that CILA may undergo metabolism during the permeation. This was confirmed by evaluating the susceptibility of CILA to metabolism by porcine skin homogenate. Overall, the findings indicated that CILA was extensively metabolized by skin esterases leading to metabolite formation, specifically, cilazaprilat. We reported for the first time the possibility of the topical delivery of cilazapril. Ultimately, the work described here will lead to the design and development of new and better topical formulations for the management of wounds.

Acknowledgments

It is my pleasure to show my gratitude to many people who made this thesis possible.

I would like to thank my supervisors, Dr. Majella E. Lane and Prof. Jonathan Hadgraft, for their guidance throughout my PhD.

I would also like to thank my colleagues for sharing their enthusiasm for and comments on my work.

The assistance received from the technical staff at UCL School of Pharmacy during the lab work is greatly appreciated.

I am also indebted to my sponsor, Damascus University, for providing the financial support and giving me the opportunity to pursue my postgraduate studies in UK. I would also like to extend my appreciation to the academic staff at the department of Pharmaceutics and Pharmaceutical Technology for constant encouragement, invaluable guidance and suggestions.

Heartfelt thanks to my sister, Rana and my brother in law, Hanna for keeping me motivated. Their words of encouragement will never be forgotten.

And most importantly, I wish to thank my parents (Mufid and Amira). They bore me, raised me, supported me, taught me, and loved me. To them I dedicate this thesis.

Last but not least, thanks to God for every success I achieved in my life. You have made my life more bountiful. May your name be exalted, honored, and glorified.

Fouad Helal

Table of Contents

List of Figures

List of Tables

List of Abbreviations

ACE	Angiotensin converting enzyme
ACEIs	Angiotensin converting enzyme inhibitors
Ang II	Angiotensin II
API	Active pharmaceutical ingredient
AT1-R	Angiotensin type 1 receptors
AT2-R	Angiotensin type 2 receptors
BP	British Pharmacopoeia
b-FGF	Basic fibroblast growth factor
CAP	Capryol®
CILA	Cilazapril
cm	centimeter
CPEs	Chemical permeation enhancers
C_v	Concentration of drug in a vehicle
D	Diffusion coefficient
DMI	Dimethyl isosorbide
DPG	Dipropylene glycol
DSC	Differential scanning calorimetry
ECM	Extracellular matrix
EPA	The Environmental Protection Agency
EtOH	Ethanol
GC	Gas chromatography
h	Diffusion pathlength
Homo	Homogenate
HPLC	High performance liquid chromatography
ICH	The International Conference on Harmonisation

IL-1	Interleukin 1
IPM	Isopropyl myristate
J	Flux
J_{ss}	Steady state flux
K	Partition coefficient
k_p	Permeability coefficient
LA	Lactic acid
LAB	Labrafac®
LOD	Limit of detection
LOQ	Limit of quantification
min	minute
MOX	Moexipril
MOX-DKP	Moexipril diketopiperazine
MS	Mass spectrometry
MW	Molecular weight
OECD	The Organisation for Economic Co-operation and Development
P/S	Penicillin and streptomycin
PBS	Phosphate buffer saline
PDGF	Platelet derived growth factor
PEG	Polyethylene glycol
PG	Propylene glycol
PGL	Propylene glycol laurate
PGML	Propylene glycol monolaurate
PMSF	Phenylmethanesulfonyl fluoride
Q	The cumulative amount of a drug permeated
RAM	Ramipril
RAM-DKP	Ramipril diketopiperazine

RAS	Renin angiotensin system
RSD	Relative standard deviation
SB	Stratum basale
SC	Stratum corneum
SD	Standard deviation
SG	Stratum granulosum
SGS	Silicone gel sheet
SL	Stratum lucidum
SS	Stratum spinosum
TCL	Transcutol®
TGF-β	Transforming growth factor
t_{lag}	Lag time
TNF-α	Tumor necrosis factor alpha
δ	Solubility parameter
δ_D	Solubility parameter of a drug
δ_{mix}	Solubility parameter of a mixture of solvents
δ_V	Solubility parameter of a solvent
a	Thermodynamic activity
µg	microgram

Chapter 1

Introduction

1 Introduction

1.1 Skin structure and function

The skin forms the largest and heaviest body organ with a surface area of ~2 m^2 and a weight of ~5 kg (Wolff, 2009; Tobin, 2011). It can be regarded as a physical barrier, regulating water loss from the body and preventing the permeation of foreign substances and microorganisms from the skin surface. While the function of the gastrointestinal tract is to render the ingested materials suitable for absorption, the skin's function is to maintain homeostasis and keep compounds out of the body. Skin is also considered a metabolizing organ. It possesses many enzymes responsible for metabolizing topically applied compounds (Wilkinson and Williams, 2007). An understanding of the skin structure and function is vital to the design of optimal dermal formulations. Anatomically, human skin is made up of three distinct layers: the epidermis, the dermis, and the subcutaneous fat layer (Figure 1-1). In these layers are found the epidermal appendages: nails, hair follicles, and glands.

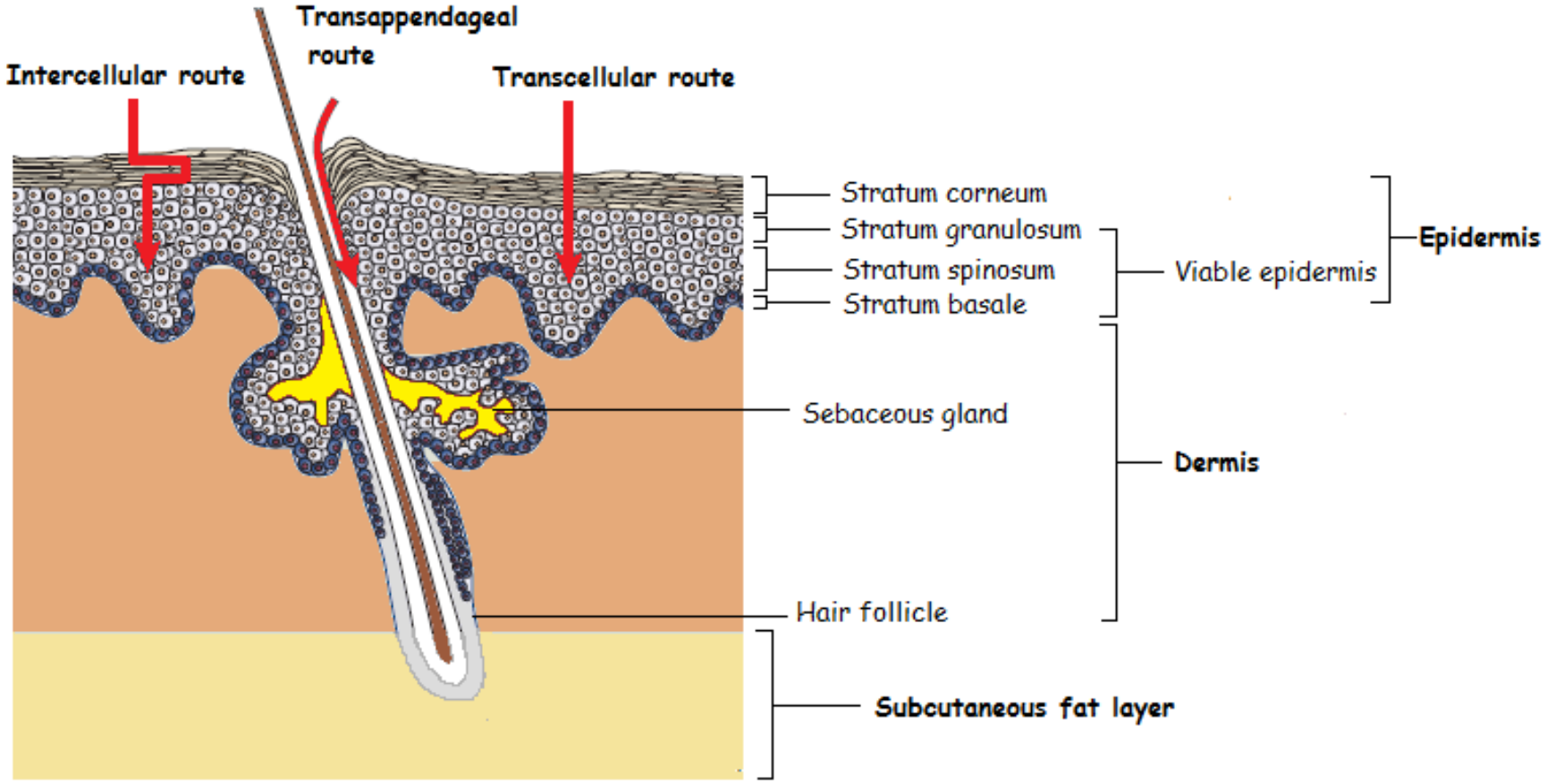

Figure 1-1 A cross-section through human skin. Adapted from Prausnitz et al. (2004)

1.1.1 The epidermis

The epidermis is the upper layer of skin with a thickness varies between 0.05 and 1 mm, depending upon the anatomical site (Chilcott, 2008; Kusuma et al., 2010; McGrath and Uitto, 2010). It is a non-vascular layer. Therefore, it has access to nutrients and removes waste by diffusion across the dermal-epidermal basement membrane to the vascular dermis (Kusuma et al., 2010). The main cell within the epidermis is called the keratinocyte. The epidermis is differentiated into four main layers (Gawkrodger, 2003), namely, from deep to superficial: stratum basale (SB), stratum spinosum (SS), stratum granulosum (SG), and stratum corneum (SC) (Figure 1-2). The cells of these layers start to loose viability while migrating from the basal layer toward the skin surface. The cycle of the migration and differentiation of keratinocytes is known as epidermal turnover (Houben et al., 2007) and takes about 5-30 days in normal skin, depending on the anatomical site (Chilcott, 2008).

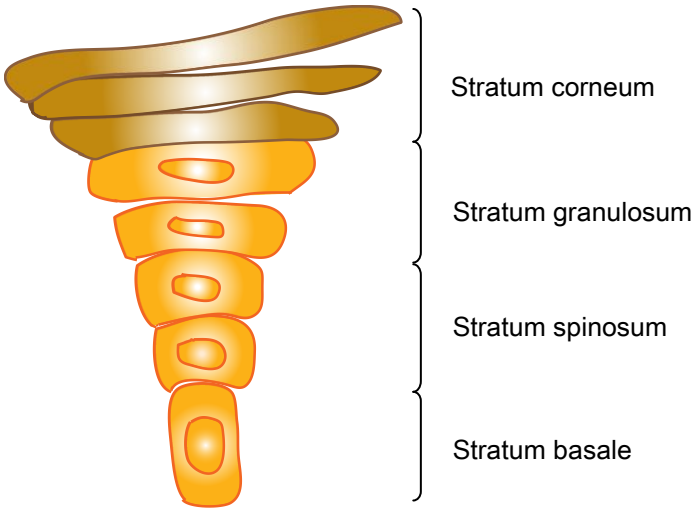

Figure 1-2 The process of epidermal differentiation

1.1.1.1 Viable epidermis

The term “viable epidermis” is used for the epidermal layers located underneath the SC. The SB is the deepest layer of the viable epidermis. It is a single layer of columnar cells and the only cells within the epidermis that divide giving new cells that migrate toward the skin surface (Kusuma et al., 2010; McGrath and Uitto, 2010). The keratinocytes of the SB are connected to the dermal-epidermal membrane by hemi-desmosomes. In addition to the keratinocytes, the SB contains other non-keratinized cell types: melanocytes which synthesise the pigment melanin, the Langerhans cells which are involved in the body immune system, and the Merkel cells which have a role in cutaneous sensation (McGrath and Uitto, 2010; Tobin, 2011). The SS is located on top of the SB. The keratinocytes of this layer change from a columnar to polygonal shape. They are connected to each other and to SB cells with fine bridges known as desmosomes. These have the appearance of spines, giving the name SS and maintaining the integrity of the epidermis (Graham-Brown and Burns, 2007). Desmosomes can break and reform thus allowing the migration of cells (Walters and Roberts, 2002; Thappa, 2009). The third layer is the SG. In this layer, the keratinocytes start to flatten and compact to form the stratum lucidum (SL) or SC. The nuclei and other cytoplasmic organelles of the cells start to be degraded by enzymes. The cytoplasm of the granular cells contains keratohyalin granules and lipid-rich lamellar granules. The former play a role in keratinization and the latter release their lipid content into the intercellular space between the SG and the SC (Graham-Brown and Burns, 2007). The uppermost layer of the viable epidermis is the SL. This layer is only found on the palms of the hands and the soles of the feet (Kusuma et al., 2010). The cells of this layer are flattened and compacted.

1.1.1.2 The stratum corneum

The SC, the 11-20 μm top layer of the epidermis (Sandby-Moller et al., 2003), has a unique morphology which has been extensively studied using conventional and advanced visualization techniques reviewed by Menon et al (2012). This layer varies in thickness across all body regions and between species (Monteiro-Riviere et al., 1990; Graham-Brown and Burns, 2007). It consists of 15-25 layers of hexagonal, flattened, and fully keratinized dead cells (corneocytes) embedded in an intercellular multiple bilayered lipid (Walters and Roberts, 2002; Wilkinson, 2008). Each corneocyte is approximately 40 μm in diameter and 0.5 μm thick. The SC has been described as the "brick and mortar" model (Figure 1-3) in which the corneocytes form the hydrophilic bricks and the intercellular lipid is the mortar (Michaels et al., 1975).

The corneocytes are composed of ~70 % protein predominantly alpha-keratin and ~20 % lipid, and are joined together with corneodesmosomes (Walters and Roberts, 2002; Wilkinson, 2008). Each corneocyte is surrounded by several cross linked proteins known as the corneocyte envelope. Filaggrin is the main protein of the SC and is stored as profilaggrin in the keratohyalin granules. During differentiation, the profilaggrin undergoes an enzymatic cleavage to form filaggrin. The latter binds to the keratin cytoskeleton, resulting in compaction of the keratinocytes into corneocytes. The lipid components of the SC are synthesized in the lamellar granules of the SG prior to be released into the space surrounding the corneocytes and form the intercellular lipid content of the SC barrier (Wilkinson, 2008; Irion, 2010a). This lipid is arranged in a multi-bilayered structure in which water molecules are trapped (Figure 1-3). Its composition is unique compared with any other biological membranes, phospholipids are absent but a large amount of ceramides (~50 %), cholesterol (~25 %), fatty acids

(~15 %) and other lipids (~10 %) such as cholesterol sulfate, cholesterol esters, and glucosylceramides are present (Wertz et al., 1987; Weerheim and Ponec, 2001; Johnson, 2009).

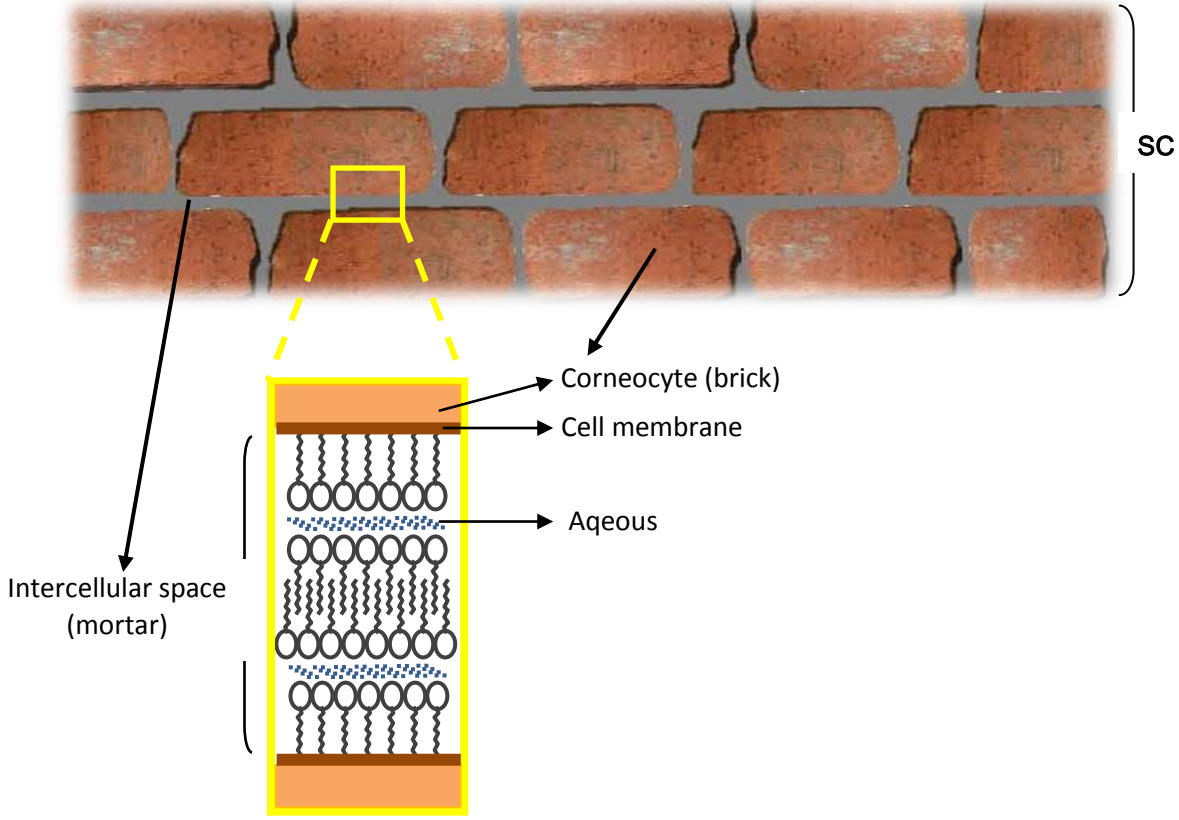

Figure 1-3 Schematic representation of the SC. The "brick and mortar" model

The lipid content varies between individuals and with the anatomical site (Lampe et al., 1983; Norlen et al., 1999). The ceramides consist of a sphingosine base to which a fatty acid is chemically linked. They have been classified into 12 subclasses (Janssens et al., 2012). The free fatty acids of the SC mainly consist of saturated acids with chain lengths of C22 and C24 (Bouwstra and Ponec, 2006). The SC is the main barrier within the skin especially for hydrophilic compounds because of its hydrophobic nature and tortuous path available for permeation. However, substances having both

lipophilic and hydrophilic properties will have a better chance of penetrating the SC because of the hydrophilic regions in the SC lipid.

1.1.2 The dermis

This layer lies immediately underneath the epidermis and is about 0.5 -3 mm thick (McGrath and Uitto, 2010). It is subdivided into the upper papillary dermis and the lower reticular dermis. Unlike the epidermis, the dermis contains a network of capillaries that transport absorbed compounds into the systemic circulation. This network is located in the papillary layer whereas the deeper layer is avascular (Irion, 2010a; Kusuma et al., 2010). The dermis is composed of connective tissue embedded in a network of mucopolysaccharide and proteins (McGrath and Uitto, 2010). The fibroblasts are the main cells in the dermis. They produce collagen and elastin which are the constituent of the extracellular matrix (ECM) (Graham-Brown and Burns, 2007; Kusuma et al., 2010). Lymphocytes, macrophage and mastocytes are other cell types also found in the dermis. Hair follicles, sweat and sebaceous glands, blood supply, and nerves are also present in this layer. The dermis structure does not challenge drug permeation but may act as a barrier for delivering highly lipophilic compounds (Chilcott, 2008). It is also a site of both inflammation triggered by skin injury and metabolic activity (Wilkinson and Williams, 2007).

1.1.3 The subcutaneous fat layer

The subcutaneous fat layer is the thickest layer in human skin and is of the order of several millimetres. It lies below the dermis and acts as an insulator and a physical shock absorber (Walters and Roberts, 2002). This layer is not important in terms of

drug absorption as drugs enter the microcirculation in the dermis before reaching this layer.

1.2 Permeation pathways through the stratum corneum.

There are three pathways (Figure 1-1) by which a molecule can traverse the SC: (I) the transcellular route through the hydrophilic keratinised cells by partitioning into and out of the cell membrane, (II) the intercellular route through the lipid channels between the cells, and (III) the transappendageal route via the hair follicles, sweat and sebaceous glands. Among the three permeation routes, the intercellular SC lipid was suggested to be the main route for the transport of water and other molecules across the skin (Albery and Hadgraft, 1979; Nemanic and Elias, 1980; Bodde et al., 1991). Since the appendages cover a very small portion of the skin surface area (~0.1 % of the total skin surface area), the transappendageal route is considered not very significant compared to the other routes (Hadgraft, 2001). In order for a molecule to traverse the skin by one of the routes mentioned above, they should possess favourable physicochemical characteristics. These will be discussed in the following sections.

1.3 The physicochemical properties of a permeant:

Some substances can penetrate and reach the underlying tissues and blood vessels. These substances are characterized by having a low molecular weight (MW ≤ 500 Da), a degree of lipophilicity and if required to have a therapeutic action then effectiveness at low dosage (Prausnitz et al., 2004). Therefore, the fundamental

physicochemical properties of a permeant that affect the percutaneous absorption are illustrated in Figure 1-4 and will be discussed in the following sections.

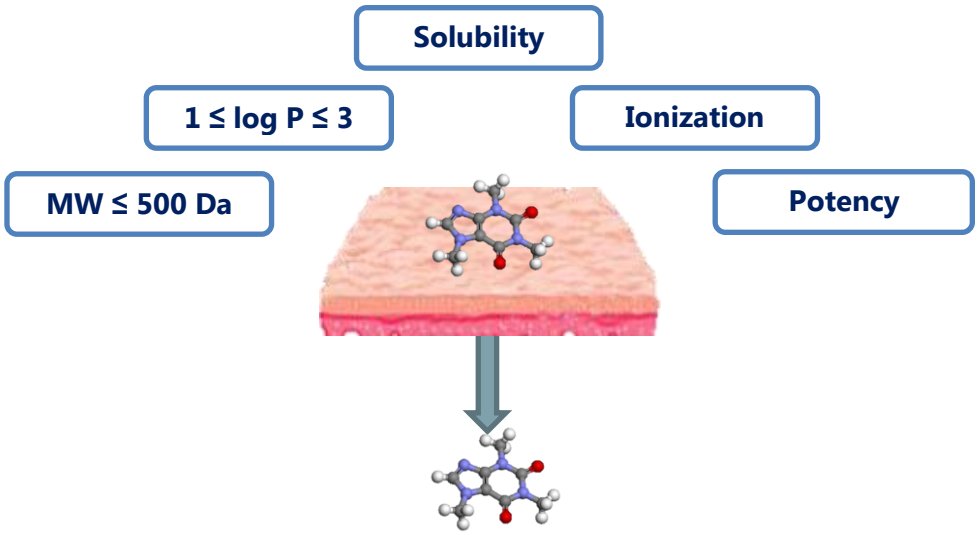

Figure 1-4 The physicochemical properties of a candidate for transdermal drug delivery

1.3.1 Partition coefficient

When a molecule is applied to the skin surface, it has first to partition into the outermost layer of the SC, then to diffuse through the SC and finally to partition into the viable epidermis and dermis (Lane et al., 2012). The SC to vehicle partition coefficient is then very important to achieve a high initial concentration of the permeant in the outer layer of skin. The partition of the molecule into the SC of skin is related to its solubility in both the formulation and the SC (Lane et al., 2012). Molecules with a log P value of 1 to 3 will be good candidates for topical delivery (Hadgraft, 2001). Therefore, drugs should have affinity for both lipid vehicles and water in order to partition into the skin and reach the hydrophilic site of absorption, the dermis.

1.3.2 Molecular weight

Since drug permeation across the skin is governed by passive diffusion, small molecules traverse human skin faster than larger molecules. The drug flux (J) is inversely proportional to the molecular weight of the permeant. A relationship between the permeability coefficient (k_p) of a molecule, the partition coefficient (K_{oct}), and its molecular weight (MW) was defined by Potts and Guy (1992) according to Equation 1-1

$$\log k_p = 0.71 \log K_{oct} - 0.0061\ MW - 2.7 \qquad n = 93 \qquad r^2 = 0.67 \quad \ldots\ldots (1\text{-}1)$$

As the molecule becomes larger its diffusion in the skin is reduced. Bos and Meinardi (2000) proposed the "500 Dalton" rule for skin permeation of compounds, where a remarkable decrease in human skin absorption was recorded with molecules over 500 Dalton. A correlation between MW and J_{max} was also observed, where MW was found to be the main predictor of J_{max} for 87 compounds (Magnusson et al., 2004) as shown in Equation 1-2.

$$\log J_{max} = -3.90 - 0.0190\ MW \qquad n = 87, \qquad r^2 = 0.85 \quad \ldots\ldots (1\text{-}2)$$

1.3.3 Solubility in the SC lipid and vehicles

The solubility of a drug in the intercellular SC lipid influences its permeation across the skin. Moreover, drug concentration in the applied vehicle is also an important factor. According to Fick's first law, J is linearly related to the concentration of solute in the vehicle C_v, up to the saturated solubility of the solute in the vehicle, i.e., increasing the concentration of the solute in the formulation resulted in enhanced flux (Lippold and Schneemann, 1984).

1.3.4 pH variation and ionization

Because of the lipophilic nature of the SC, most compounds are better absorbed in the non-ionized form. Therefore, the ionisation state of the permeant plays a role in skin permeability. Ionisation influences both the solubility of the permeant in the applied vehicle and its partition into the skin (Hadgraft, 2004). Since the majority of drugs are weak acids or weak bases, their degree of ionization depends on the pH of the applied vehicle and the pK_a of the molecule. Thus, the pH of the topically applied formulation is important in the penetration of an ionized molecule through the skin (Wester and Maibach, 1985). Henderson–Hasselbalch equation (Equation 1-3) allows calculation of the extent of ionisation of an acidic or basic drug as a function of pH if the pK_a is known. When the pH is 2 units below the pK_a, a weakly acidic drug will be completely un-ionised and when the pH is 2 units above the pK_a, it will be fully ionised. However, in case of a weakly basic drug, when the pH is 2 units below the pK_a, the drug will be completely ionised.

$$\mathrm{pH} = \mathrm{p}K_\mathrm{a} + \log \frac{[\text{conjugate base}]}{[\text{conjugate acid}]} \quad \ldots\ldots \text{(1-3)}$$

Besides the physicochemical properties of the permeant described above, the rate and extent of skin absorption of the permeant depend on other factors, which are illustrated in Figure 1-5

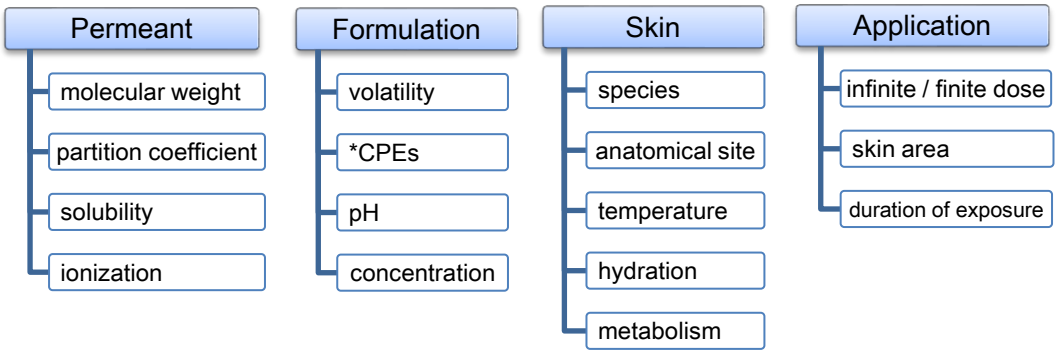

Figure 1-5 Factors affecting drug permeation through porcine or human skin (Howes et al., 1996). *Chemical penetration enhancers

1.4 Passive diffusion and Fick's first law of diffusion

In general, permeation of a molecule across the SC is basically a passive diffusion process which is described by Fick's first law (Equation1-4)

$$J_{ss} = \frac{DK(C_v - C_r)}{h} = k_p(C_v - C_r) \qquad (1-4)$$

Where J_{ss} (μg/cm²/h) is the steady-state flux of the permeant through a membrane, D (cm²/h) is the diffusion coefficient, K is the vehicle-membrane partition coefficient, C_v -C_r (μg/cm³) is the concentration gradient of the permeant between the vehicle and the receptor phase, h (cm) is the length of the diffusion path within the membrane, and k_p (cm/h) is the permeability coefficient of the permeant in the SC. As in most cases C_v >> C_r, Equation 1-4 can be rewritten in the following form.

$$J_{ss} = \frac{DKC_v}{h} = k_p C_v \qquad (1-5)$$

As shown from Equation 1-5, J_{ss} is directly proportional to D, K and C_v, and inversely proportional to h. Typically, J_{ss} can be obtained from *in vitro* experiments

under infinite dose conditions where the slope of the linear portion of the permeation curve represents Jss (Figure 1-6). This curve is the plot of the cumulative amount (Q) penetrated as a function of time. The lag time (t_{lag}) is the intercept of the straight line of the curve with the time axis as shown in Figure 1-6.

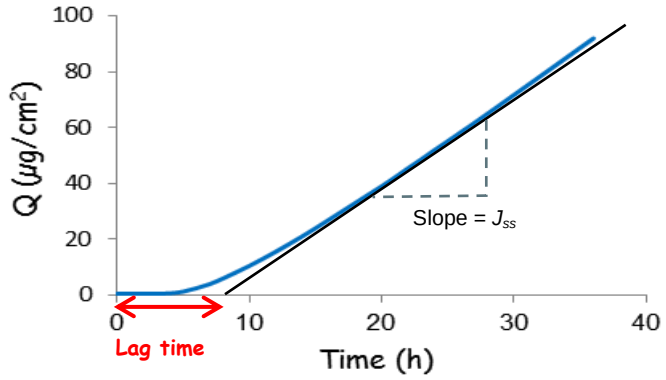

Figure 1-6 Typical permeation profile for an infinite dose. Q is the cumulative amount of the drug permeated per unit area.

From Equation 1-5, D, K and C_v are the main determinants that govern the drug permeation through the skin. Therefore, the flux across the skin may be enhanced by increasing D, K and/or C_v. These parameters can be affected by interactions between the vehicle and skin and between the vehicle and drug (Figure 1-7).

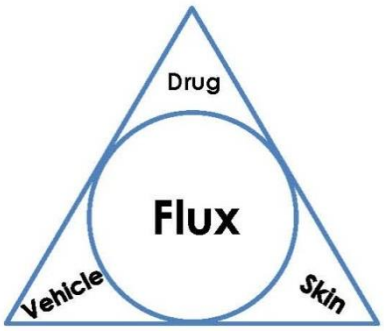

Figure 1-7 Interactions between a drug, vehicle, and skin. Adapted from Lippold (1992)

Increasing D or K can be achieved by incorporating chemical penetration enhancers (CPEs) which can either interact with the SC lipid or increase the solubility of the permeant in the skin. Sometimes, CPEs can act on both the solubility and diffusion coefficient of drugs (Hadgraft and Lane, 2011). However, increasing C_v leads to an enhanced thermodynamic activity of the permeant in the vehicle which, in turn, increases the drug permeation. An alternative form of Equation 1-5 uses thermodynamic activities (Higuchi, 1960) as shown in Equation 1-6

$$J_{ss} = \frac{\partial D}{\gamma h} \qquad (1-6)$$

Where ∂ is the thermodynamic activity (unitless) of the permeant in its vehicle and γ is the activity coefficient of the permeant in the skin barrier. The thermodynamic activity describes the tendency of the permeant to leave the vehicle and go into the skin and is the actual driving force for diffusion (Otto et al., 2009). For maximum flux, the drug should be in saturated solutions. Generally, saturated solutions of a given drug are at equal thermodynamic activities and hence should give the same flux (despite differences in the solubility of the drug in different vehicles) as long as the vehicle does not affect the barrier properties (Higuchi, 1960; Twist and Zatz, 1986). Ideally, it is difficult to maintain this as most topical vehicles interact with the SC.

1.5 Chemical penetration enhancers (CPEs)

In the previous sections it was outlined that the structural arrangement of the SC, with packed layers of protein-rich corneocytes embedded in a multi-bilayered lipid, has implications for the drug permeation. Therefore, one of the strategies developed to overcome this obstruction and facilitate drug permeation is chemical penetration

enhancers (CPEs). CPEs are substances that can reduce the resistance of the skin barrier by interacting with skin constituents to accelerate skin permeability. Figure 1-8 illustrates the chemical structures of some frequently used CPEs.

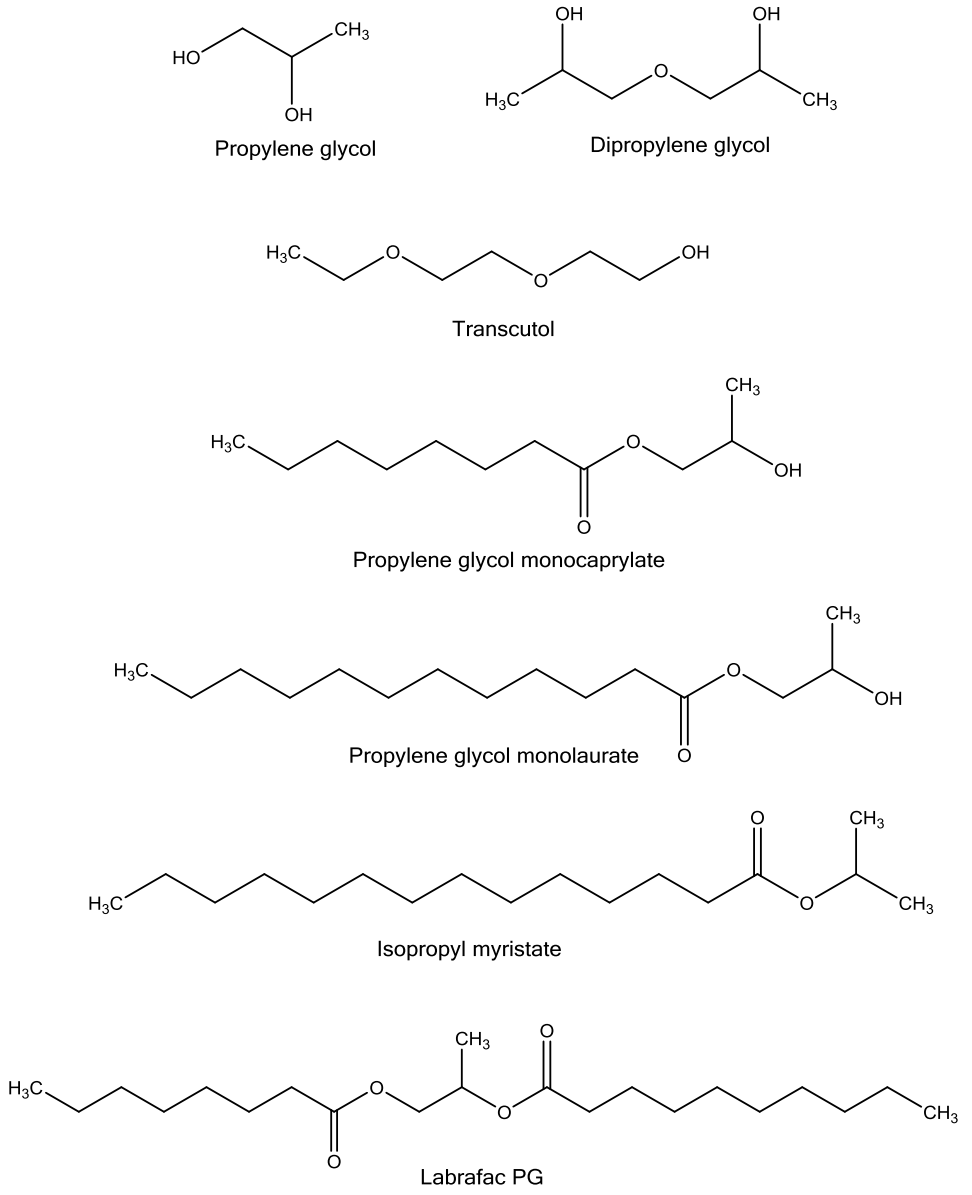

Figure 1-8 Chemical penetration enhancers.

They should be nontoxic, nonirritant, nonallergenic, pharmacologically inert, reversible in action, compatible with the drug and other excipients in the formulation,

and cosmetically acceptable (Hadgraft and Lane, 2011). However, it is unlikely that one compound will possess all these properties. The mechanisms by which CPEs overcome the impermeability of the SC should be understood. CPEs are believed to affect permeation by interacting with the intercellular domain at three main sites, A, B and C (Barry, 1988) as shown in Figure 1-9

1. Interaction with the aqueous region of the lipid bilayers (**Site A**)
2. Interaction with the lipid hydrophobic chain (**Site B**)
3. Interaction with the polar head groups of the lipids (**Site C**)

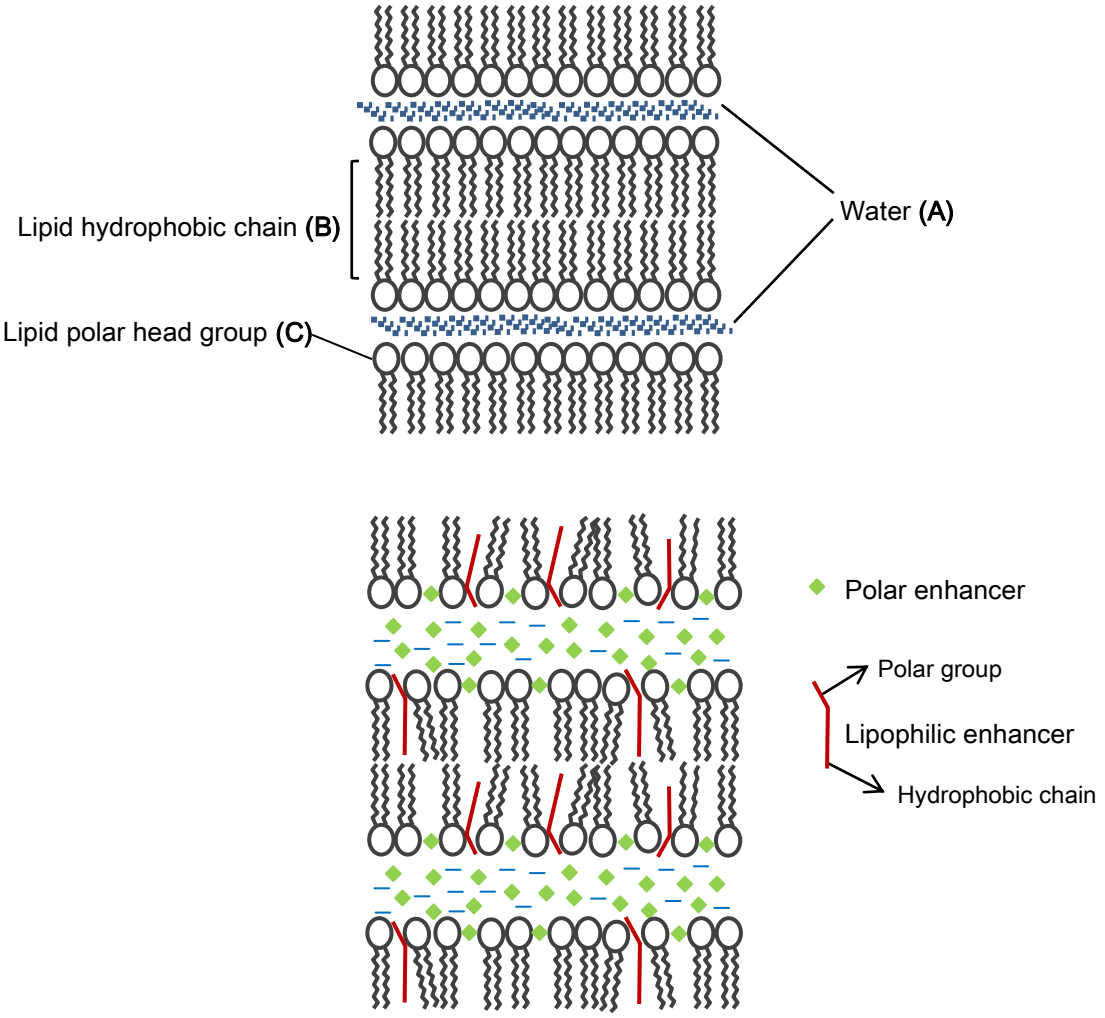

Figure 1-9 Mechanisms of action of CPEs. Adapted from Barry (1988)

Isopropyl myristate (IPM) is an aliphatic fatty acid ester which has been widely studied for its chemical enhancement properties. IPM has been demonstrated to enhance drug permeation through both porcine and human skin. The penetration of melatonin in IPM through porcine skin increased in a study which investigated the effect of a number of vehicles on melatonin permeation (Kikwai et al., 2002). IPM also exhibited an enhancing effect with 5-fluorouracil through excised human SC (Singh et al., 2005). Leopold and Lippold (1995) used differential scanning calorimetry (DSC) in an attempt to clarify the mechanism of enhancing effects of IPM. The authors correlated the reduction of the enthalpy and phase transition temperatures of the SC lipid with the SC lipid fluidisation. This led to disorder in the organized structure of the SC lipid. The effect of IPM on human SC was also studied using DSC and X-ray diffraction. It was concluded that IPM integrated into the lipophilic areas of the SC lipid matrix with lateral insertion of IPM between lipid molecules of the SC bilayers and with anchoring of the isopropyl group in the polar region of the layer (Brinkmann and Muller-Goymann, 2005). In a very recent study, the impact of IPM on the structure of a SC lipid model membrane was also investigated (Engelbrecht et al., 2012). The results not only supported those obtained by Brinkmann and Muller-Goymann (2005) but also suggested the possibility of a complete immersion of IPM into the SC lipid, leading to a phase separation in the lipid bilayer.

Propylene glycol (PG) is widely used as a solvent or co-solvent in variety of pharmaceutical formulations. PG enhanced the skin permeability of metronidazole by altering the solubility parameter of the SC and shifting it towards that of the drug (Wotton et al., 1985). This increases the drug solubility in the SC, thus enhancing the

flux. Increased concentration of PG was also noted to enhance the permeation of ibuprofen from formulations of PG:water saturated binary mixtures (Watkinson et al., 2009). In order to elucidate the mode of action of PG on the human SC, several techniques such as X-ray scattering and diffraction, DSC, and differential thermal analysis were used. The findings of one study indicated that PG did not interfere with the SC lipids (Bouwstra et al., 1991). However, it is likely that PG incorporated laterally with the head group region of the lipid bilayers. The data from another study indicated the lateral and perpendicular integration of PG molecules between the polar head groups of the lipid bilayers (Brinkmann and Muller-Goymann, 2005).

Transcutol® (TCL), monoethyl ether of diethylene glycol, is a water miscible solvent which is also used in topical formulations as a penetration enhancer. Its mechanism of action was reported by increasing the solubility of drugs in the skin (Harrison et al., 1996). Studies showed the use of TCL alone or in combination with other CPEs increased the percutaneous penetration of various drugs (Puglia and Bonina, 2008; Hirata et al., 2013). Hirata and colleagues (2013) reported that incorporation of TCL in carbenoxolone binary and ternary formulations of CPEs resulted in higher fluxes compared with the other formulations in the absence of TCL.

Propylene glycol monolaurate (PGML), propylene glycol laurate (PGL), and propylene glycol monocaprylate (CAP) are lipophilic penetration enhancers that have been used in topical formulations. PGML and PGL are composed of varying amounts of mono- and di-esters of lauric acid and propylene glycol. PGML contains approximately not less than 90 % of the monoester (Gattefosse, 2010a) whereas PGL contains 45–70 % of the monoester (Gattefosse, 2010b). PGL, PGML and CAP

significantly decreased the lag time when they were used for delivery of melatonin across excised hairless mouse skin (Gwak et al., 2002). The permeation rate of ketorolac from 15 pure hydrophilic and lipophilic vehicles was reported to be the highest with PGML (Cho and Gwak, 2004). Based on the recent investigation about the feasibility of delivery of levodopa transdermally, CAP and PGML showed the highest permeation enhancing effects across hairless mouse skin (Lee et al., 2013). Takahashi et al. (2001) and Moghimipour et al. (2013) attempted to clarify the mechanism of CAP enhancement effect by Fourier transform infrared spectroscopy and DSC. They suggested that CAP interacts with the hydrophobic chain of the SC lipid resulting in a lipid fluidization. CAP significantly enhanced skin permeation of 5-fluorouracil in all tested formulations compared with those which lacked CAP (Takahashi et al., 2011).

1.6 Experimental design

When designing permeation experiments, the experimental conditions should be as close as possible to the *in vivo* situation in order to provide useful data. Therefore, several factors should be taken into account (Figure 1-10):

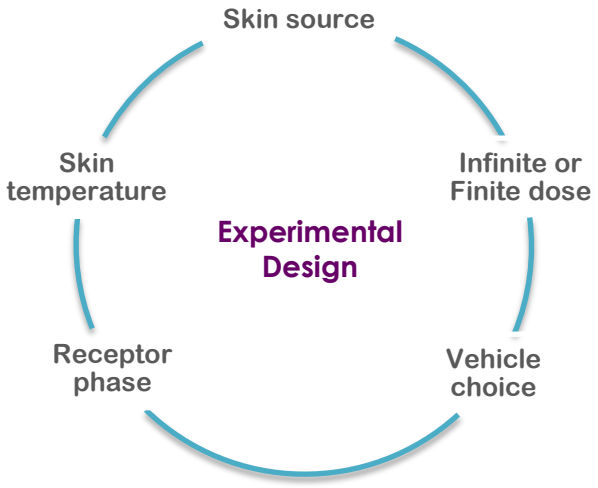

Figure 1-10 The factors to be considered when designing permeation studies.

1.6.1 The choice of skin source

The choice of membrane is of vital importance *in vitro* skin penetration and depends on several factors such as use of a relevant model, price, and availability. The most appropriate membrane for dermal drug delivery studies is human skin. It is preferred over animal skin because of large differences in barrier properties between species in terms of structure, lipid composition and thickness (Sato et al., 1991). Therefore, they vary in their permeability characteristics (Bartek et al., 1972; Sato et al., 1991). Animal skin generally is more permeable than human skin. The most relevant animal model for human skin in assessing percutaneous absorption is porcine skin due to its similarity to human skin in terms of the SC thickness and lipid composition (Sato et al., 1991). Porcine skin also gives comparable results to human skin in terms of the permeability (Bartek et al., 1972). The histological and biochemical properties of porcine skin were shown to be similar to human skin (Kong and Bhargava, 2011). However, it is slightly more permeable than human skin (Sato et al., 1991; Singh et al., 2002). Porcine ear skin, in particular, gave comparable results to human skin and thus has been used as a surrogate for human skin (Dick and Scott, 1992; Bhatia and Singh, 1996; Herkenne et al., 2006). The outer side of porcine ear skin represents the area of porcine tissue with the highest similarity to human skin, with regards to the thickness and structure of both the SC and viable epidermis (Jacobi et al., 2007). At the formulation development stage, alternative membranes such as animal skin and artificial membranes may be used because of the ethical constraints and high cost on obtaining and using human tissues. Full thickness skin (OECD, 2004b) and epidermal membranes (Kligman and Christophers, 1963) are mainly used. Furthermore, the

integrity of human and porcine skin is maintained under storage at -20˚C for up to one year (Harrison et al., 1984; Steiling et al., 2001).

1.6.2 Finite or infinite dose application

There are two dosing applications: finite and infinite dose. Formulations are usually applied to the skin surface as a finite dose where a small amount of formulation (≤10 µl or mg/cm^2) is applied to the skin surface (Finnin et al., 2012). This dose depletes on the skin surface leading to a reduction in the permeation rate and an eventual plateau in the cumulative permeation profile (Figure 1-11-B). However, for permeants with low permeability, the depletion of the applied dose is negligible and therefore the shape of the permeation profile obtained is characteristic for infinite dose conditions (Figure 1-11-A). On the other hand, application of an infinite dose to the skin is usually used to obtain steady state flux data and therefore evaluate the permeation profiles of a compound. This can be achieved by preparing a suspension of drug where an excess amount of drug is added to the donor phase.

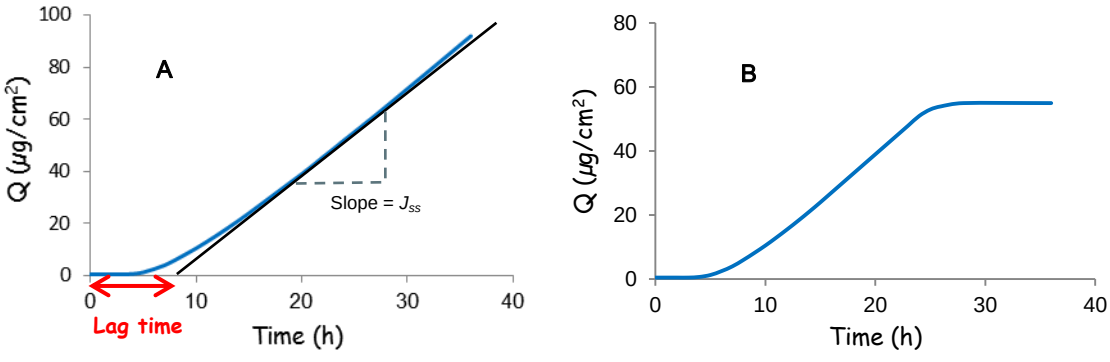

Figure 1-11 Typical permeation profiles for an infinite (A) and finite (B) dose

1.6.3 The choice of vehicle

Vehicles in which the drug is incorporated can have a significant effect on the drug flux through the membrane by modifying the nature of the membrane barrier either by disrupting the lipid domains or by altering partitioning of the permeant into the membrane (Watkinson et al., 1995; Otto et al., 2008; Lane, 2013). These vehicles should be inert, inexpensive, nontoxic, and well tolerated. Furthermore, the stability and compatibility of the vehicles with the active pharmaceutical ingredient are of the greatest importance in the development of topical products (Sinha and Kaur, 2000; Allen et al., 2011b).

1.6.4 Static diffusion cells

Most measurements of *in vitro* absorption through excised skin have been performed using static diffusional cells (Franz, 1975). As shown in Figure 1-12, the cell consists of a donor compartment and a receptor compartment between which the skin is mounted. Both the volume of the receptor compartment and diffusion area are measured for each cell individually. The receptor compartment is filled with phosphate buffer saline (PBS) solution pH 7.4. At predetermined time intervals, samples are collected from the receptor medium via the sampling port of the cell and then analysed using high performance liquid chromatography (HPLC). This analytical technique was used in order to separate and quantify low concentrations of organic compounds in a solution.

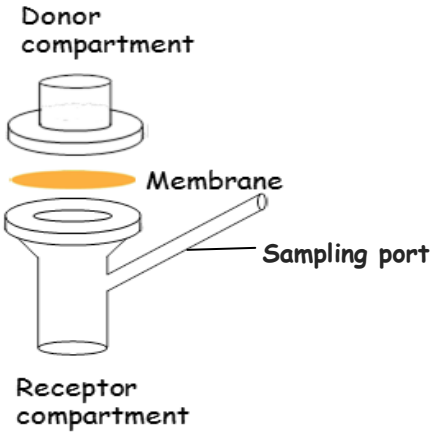

Figure 1-12 Static diffusion cell

Depending on the aim of the experiment, donor compartments may or may not be occluded (OECD, 2004b). During the diffusion experiment, the receptor phase needs to be stirred and replaced with fresh receptor fluid to ensure the existence of the sink conditions.

1.6.5 Temperature and humidity

When performing topical or transdermal drug delivery experiments, the temperature of the skin surface should be 32 ºC in order to mimic the *in vivo* conditions (OECD, 2004b). Humidity should preferably be between 30 and 70 % (OECD, 2004b).

1.6.6 Receptor phase for *in vitro* studies

The selected receptor fluid should simulate the *in vivo* scenario, not affect the integrity of skin, and maintain sink conditions throughout the experiment (OECD, 2004b). Phosphate Buffer Saline (PBS), pH 7.4, is most commonly used for hydrophilic and moderately lipophilic compounds. Preservatives are added into the receptor phase to prevent the microbial growth, particularly for long term experiments. The highest

concentration of the permeant in the receptor phase should not exceed 10 % of its solubility to maintain sink conditions.

1.6.7 Duration of experiment and sampling times

Permeation experiments are usually run between 24 and 48 h (Howes et al., 1996; OECD, 2004b). However, under infinite dose conditions, this duration may be extended further if the steady state flux is not obtained at 48 h, taking into account the skin integrity. Samples from the receptor fluid are required to be collected at regular time intervals (at least ten time points) in order to allow determining lag time and steady state flux (Howes et al., 1996; OECD, 2004a).

1.7 The role of renin angiotensin system (RAS) in wound healing and scar tissue formation

The anatomy of normal human skin was discussed in the first section of this chapter. However, following skin injury, this normal architecture of the skin is disrupted and a sequence of biochemical events is triggered in order to repair the damage. Failure of a wound to progress the normal stages of healing results in abnormal healing and scar formation. Steckelings et al. (2004) demonstrated the existence of a local RAS in human skin. Further studies have showed that the components of RAS are an integral part of the wound healing process. To aid understanding of the role of RAS in cutaneous wound repair and formation of scar tissue, it is essential to have background knowledge of wound classifications and the different phases of wound repair process which are outlined in the following sections.

1.7.1 Wound classification

Wounds are classified based on the depth of the injury (Irion, 2010b) as being:

- *Superficial* if the damage limited to the epithelial tissue alone (epidermis).
- *Partial thickness* if the damage involved the dermis including blood vessels.
- *Full thickness* if the damage involved the dermis, subcutaneous fat layer, and sometimes bone.

The wound healing process can be divided into four main stages: coagulation, inflammation, proliferation (granulation), and remodelling (Figure 1-13)

Figure 1-13 Phases of the wound repair process.

1.7.2 Phases of wound healing

1.7.2.1 Coagulation

Following initial wounding, the permeability of blood vessels is increased to allow neutrophils, lymphocytes, platelets and plasma proteins to enter the wound site (Clark, 1996). The two main components of coagulation are platelets and fibrin (Figure 1-14). Coagulation occurs when platelets aggregate with fibrin. The platelets are activated by exposure to collagen and to the platelet-derived growth factor (PDGF) produced by erythrocytes damaged during injury (Irion, 2010b). Platelets release several growth factors, including PDGF, epidermal growth factor (EGF), transforming growth factor beta (TGF-β) and platelet factor IV (Enoch and Leaper, 2008). These proteins initiate the wound healing process by attracting polymorphonuclear neutrophils (PMNs),

macrophages, and fibroblasts into the injured site. Platelets increase the vascular permeability by secreting serotonin and histamine. This allows more inflammatory cells to enter the wound (Clark, 1996).

1.7.2.2 Inflammation

The inflammatory phase can be divided into the early and late inflammatory response (Beanes et al., 2003). In the early response (days 1-2) the predominant PMNs attracted by TGF-β and peptide products enter the wound. PMNs do not affect the wound healing process. Their main function is to clear out debris and bacteria of the wound, thus preventing infection (Irion, 2010b). After 48 h, in the late inflammatory response (days 2-3), the macrophages replace PMNs as principal inflammatory cells and are drawn to the wound by TGF-β, PDGF and other components (Figure 1-14). One of the more important roles of the macrophage in wound healing is the secretion of growth factors such as TGF-β, PDGF, basic fibroblast growth factor (b-FGF), TGF-α and insulin-like growth factor 1 (IGF-1) (Irion, 2010b). These growth factors are essential to wound healing by regulating the production and organization of the extracellular matrix (ECM) by fibroblasts, and the proliferation of smooth muscle cells and endothelial cells necessary for angiogenesis (Clark, 1996).

1.7.2.3 Proliferation

The proliferative phase starts at about the third day after injury and lasts for 2-4 weeks. It is characterized by angiogenesis, collagen deposition, granulation tissue formation, and re-epithelialization. In angiogenesis, new blood vessels are formed from pre-existing vessels. This phase is marked by the appearance and dominance of

dermal fibroblasts (Figure 1-14). On the third or fourth day after injury, fibroblasts attracted to the wound by TGF-β and PDGF begin to proliferate and produce fibronectin, hyaluronan, proteoglycans, elastin and collagen in the wound. These components comprise the ECM in which collagen constitutes the major component. PDGF, TGF-β, b-FGF, tumor necrosis factor alpha (TNF-α) and interleukin 1 (IL-1) induce collagen synthesis during the proliferative and remodelling phases. Collagen imparts strength to wounds and plays a crucial role in wound closure. Furthermore, its metabolism is a key factor in scar formation (Clark, 1996).

1.7.2.4 Remodelling

The remodelling phase of wound healing begins when collagen synthesis and breakdown equilibrate to a steady state approximately three weeks after injury, and can last for two years after wounding (Figure 1-14) (Clark, 1996). Serious injuries may disrupt this balance and lead to abnormalities in collagen metabolism. Collagen degradation is achieved by matrix metalloproteinases (MMPs) including collagenases that are produced by fibroblasts, neutrophils and macrophages at the wound site (Enoch and Leaper, 2008). Wound contraction occurs through the interactions between fibroblasts and the surrounding ECM and is regulated by PDGF and TGF-β. Imbalance in this stage of the healing process may result in overproduction of collagen and therefore an increased risk of scar formation.

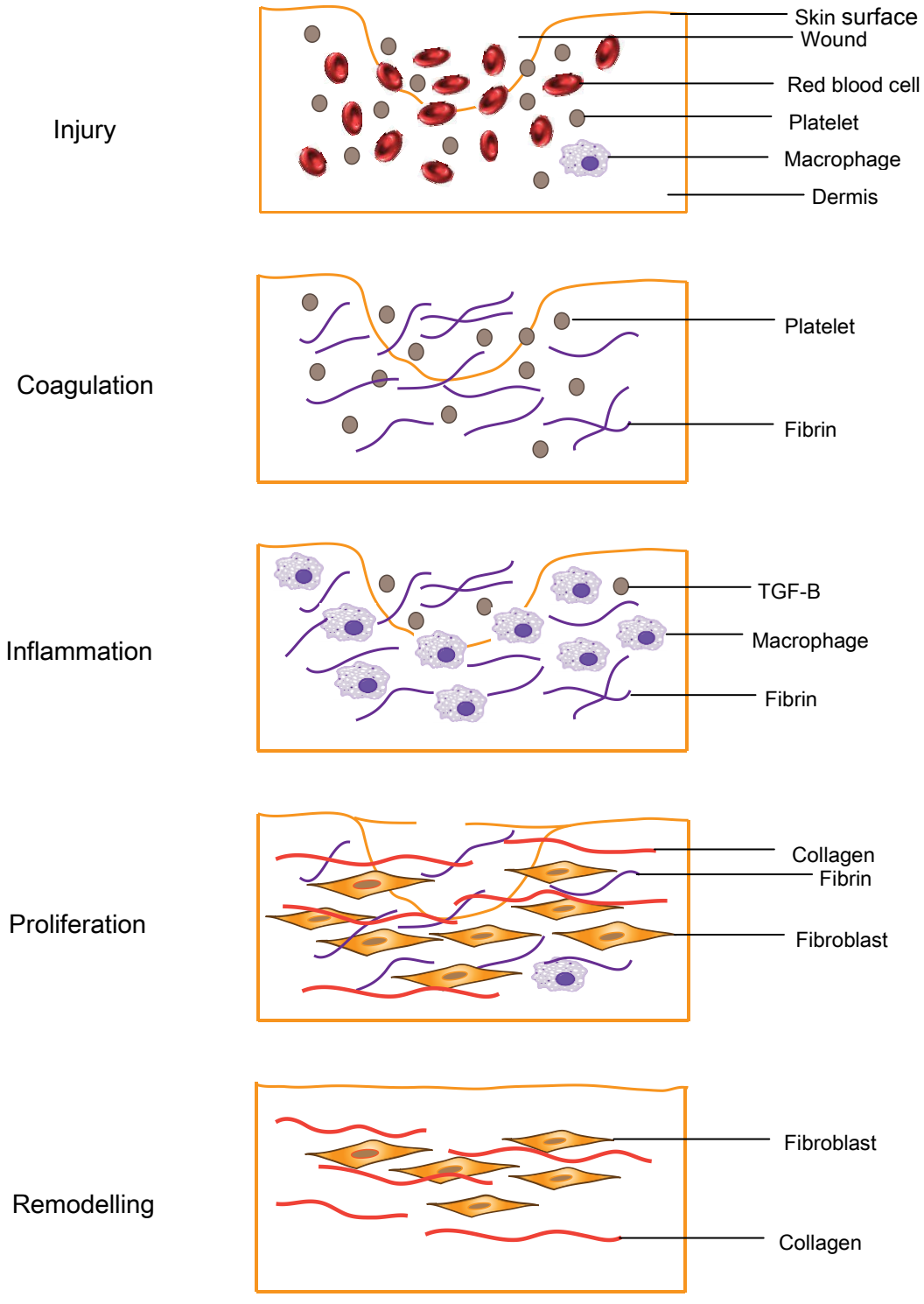

Figure 1-14 The main stages of the wound healing process. Adapted from Beanes et al. (2003).

The wound healing process varies from one individual to another and is usually associated with a risk of scar formation if the blood vessels are damaged. Dunkin et al. (2007) quantified the critical depth of dermal injury (0.56 ± 0.03 mm) at which a wound heals with a scar, where digital image analysis software and high frequency ultrasound scanner were used to assess the appearance and depth of wound as well as scar development. It was reported that dermal fibroblasts, the key cells involved in scarring, from different layers of normal skin have different characteristics (Wang et al., 2008). Fibroblasts from the deep layers resembled those from hypertrophic scars and thus they contributed to scar formation (Wang et al., 2008)

1.7.3 The existence of a local RAS in human skin

An increasing number of studies have demonstrated the existence of a local (tissue) RAS in a number of organs including the heart (Lindpaintner et al., 1988), adipose tissue (Karlsson et al., 1998), liver (Bataller et al., 2003), brain (Paul et al., 1993), and eye (Wagner et al., 1996). Recently, a RAS has also been detected in human skin (Steckelings et al., 2004). The local RAS works, in whole or in part, independently of the circulating RAS. The production of angiotensin within a tissue may be either intracellular or extracellular where angiotensinogen and renin enzyme may be either locally synthesized or taken up by the cell (Campbell, 1987) as shown in Figure 1-15

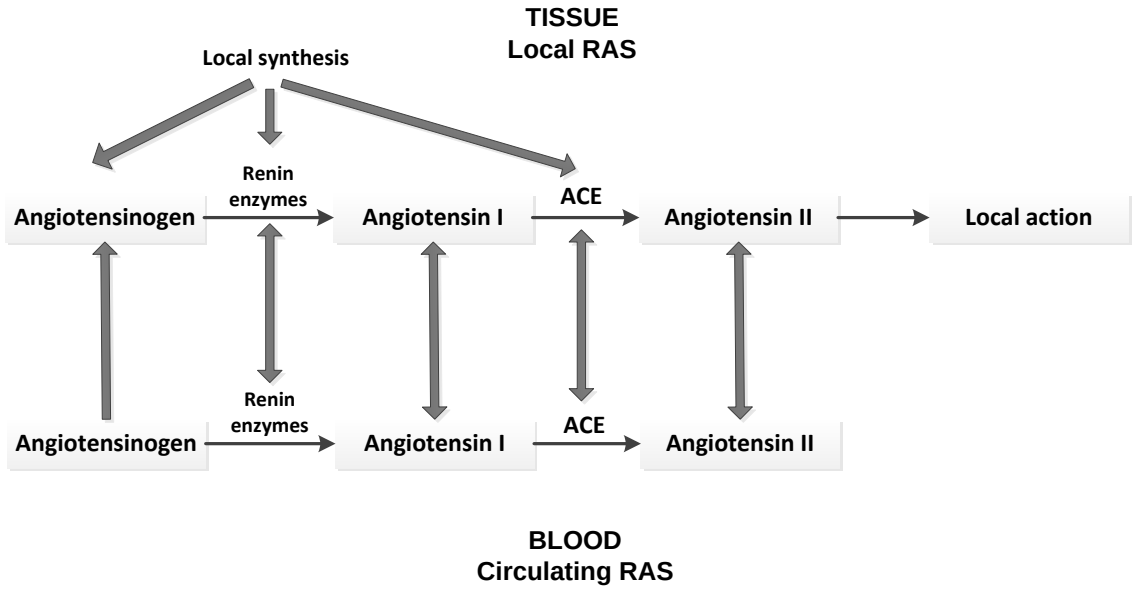

Figure 1-15 The relationship between the circulating and local renin angiotensin system. Adapted from Campbell (1987).

The expression of all components of the local RAS in human cutaneous cells was investigated by Steckelings and colleagues (2004). The data showed that human skin expresses a complete RAS including precursor (angiotensinogen) and enzymes (renin and ACE) essential to synthesize Ang II as well as angiotensin type 1 (AT1-R) and angiotensin type 2 (AT2-R) receptors within the epidermis and dermis. All the components were detected immunohistochemically in the cutaneous cells. These findings confirmed that human skin is not just a source of, but also a target organ for, Ang II (Steckelings et al., 2004).

1.7.4 The role of various components in wound healing.

With evidence for the existence of a local RAS in human skin (Steckelings et al., 2004), understanding the mechanism by which Ang II takes part in wound healing is a vital importance in wound healing and scar management.

1.7.4.1 Angiotensin II and skin wound repair

The association between Ang II receptor levels and the wound repair process was evident from a number of studies. Abiko et al. (1996) noticed a significant increase in the number of Ang II receptors on the fifth day after a full thickness excisional injury in adult rats, where AT1-R were predominant. In contrast, Viswanathan and Saavedra (1992) who used young, two week-old rats found that the major proportion of the Ang II receptors expression was due to AT2-R. The reason for the potential differences between these results was due to the age of rats used. Takeda et al. (2004) proposed that wound healing was governed by a balance between AT1-R and AT2-R signaling with the prominence of AT1-R signal, where AT1-R activation enhanced fibroblast proliferation and re-epithelisation and AT2-R activation suppressed these effects. The involvement of Ang II in cutaneous wound healing was also examined using AT1-R deficient mice (Yahata et al., 2006). A marked delay in wound healing was observed in these mice compared with normal mice. Moreover, Ang II induced keratinocyte and fibroblast migration which was mediated via AT1-R and inhibited by AT1-R blockers (Yahata et al., 2006).

Studies have also demonstrated that the exogenous administration of Ang II accelerated cutaneous wound healing (Rodgers et al., 1997). The authors found that wounds treated with Ang II closed more rapidly than wounds which received a vehicle alone. Based on the significance of fibroblasts in collagen synthesis and skin wound healing, Tang and his colleagues (2009) investigated the effect of Ang II on collagen gene expression in human dermal fibroblasts. Ang II induced the expression of collagen and this effect was completely blocked by AT1-R antagonist but not by the

AT2-R antagonist. Furthermore, the synthesis of collagen was increased by Ang II in a dose dependent manner (Tang et al., 2009).

Since angiogenesis plays a key role in granulation formation and re-epithelisation, Kurosaka et al. (2009) attempted to determine whether there is a relationship between Ang II and wound-induced angiogenesis. The data showed significantly reduced vascular endothelial growth factor (VEGF) levels and microvessel density as well as a marked delay in wound closure in mice treated with an AT1-R blocker or lacking AT1-R. These findings indicated that AT1-R signaling induces angiogenesis in wound granulation tissue during the wound healing process (Kurosaka et al., 2009).

In a recent study, alterations in Ang II levels and the expression of its receptors, AT1-R and AT2-R, were observed during cutaneous wound healing (Wu et al., 2011). The expression of Ang II and its receptors increased in wounded skin to reach a maximum at the end of the first week after injury.

1.7.4.2 Angiotensin II and scar tissue formation

In order to evaluate the role of Ang II in collagen synthesis and tissue fibrosis, Kawaguchi et al. (2004) conducted a study on patients with systemic sclerosis. Their findings showed that (i) Ang II levels were significantly higher in the patients than in healthy volunteers, (ii) the abnormal production of Ang II contributed to skin fibrosis via the excessive production of ECM, and (iii) the administration of Ang II increased the production of procollagen and TGF-β which was inhibited by an AT1-R antagonist. Another investigation was carried out to determine the relationship between the ACE

and cutaneous scar formation during wound healing (Morihara et al., 2006). The authors compared the activity of ACE in normal human skin, wounded skin, and scars. The ACE activity in the scar tissue was the highest followed by the wounded skin and then normal skin. Furthermore, the up-regulated ACE contributed to the development of cutaneous scar formation (Morihara et al., 2006). The findings suggested that Ang II levels increased under these abnormal conditions because of the existence of the local RAS in human skin which was confirmed by Steckelings et al (2004). Detection of changes in the expression of Ang II receptors in human skin during cutaneous wound healing was reported by Steckelings (Steckelings et al., 2005). The data indicated a marked increase in the expression of Ang II receptors within the epidermis and dermis of cutaneous scar tissue. This supports what it was previously reported regarding the elevated expression of AT1-R in diverse organs undergoing wound repair (Steckelings et al., 2005). It was also found that in the dermis of scar tissue, there were more AT1-R and AT2-R than in normal and wounded skin (Morihara et al., 2006). As a result, ACE inhibitors as well as AT1-R antagonists were suggested to be innovative strategies for the treatment of scars.

1.7.4.3 Transforming growth factor beta (TGF-β) and collagen expression

Among several molecules known to mediate cutaneous wound healing TGF-β plays a vital role in stimulating dermal fibroblasts to proliferate. It was reported that the administration of growth factors accelerates the wound healing process (Lynch et al., 1989). TGF-β encouraged fibroblasts to contract collagen-matrix in order to accelerate wound healing (Montesano and Orci, 1988) and stimulated the synthesis of collagen by keloid fibroblasts (Bettinger et al., 1996). Humans with a delay in wound healing

exhibited reduced TGF-β expression (Schmid et al., 1993). In contrast, the overexpression of TGF-β was often associated with the development of keloids and hypertrophic scars (Lee et al., 1999; Abdou et al., 2011). Tang et al. (2009) investigated the role of TGF-β in the Ang II induced fibrosis using human dermal fibroblasts. Ang II, via AT1-R, enhanced the expression and release of TGF-β that in turn was responsible for the increase in collagen expression. In addition, this expression was markedly inhibited by blockade of TGF-β, establishing that endogenous TGF-β was a major pathway for collagen synthesis (Tang et al., 2009).

A very recent study showed that during the wound healing process the expression of TGF-β started to increase after injury, reaching a peak level on day 4-7 and then dropped to a minimal value on day 35 (Abramov et al., 2013). Furthermore, a good relationship was observed between TGF-β expression and the wound closure rate, suggesting the involvement of this factor in the process of wound repair.

1.7.4.4 Angiotensin converting enzyme inhibitors (ACEIs) and collagen synthesis

The overproduction of Ang II during the wound healing process participated in the formation of scars (Kawaguchi et al., 2004; Morihara et al., 2006). Based on the significance of Ang II in wound healing and fibrosis, a number of studies have been performed to evaluate the effect of ACEIs on the prevention of fibrosis in different organs including skin.

In a clinical study conducted with patients who developed a postsurgical keloid scar, a marked improvement in the scar was observed after 4-6 months treatment with a low dose (10 mg/day) of enalapril (Iannello et al., 2006). The authors concluded that

early treatment with ACEIs after injury or surgical operations would be useful to achieve the best possible outcomes. Another study was carried out to determine the ability of the topical application of the ACEI, captopril, to prevent scar formation in rabbit skin (Ardekani et al., 2008). The formulation demonstrated its efficacy in the reduction of collagen synthesis and scar formation. After the promising results obtained from this study, Ardekani and colleagues tested the same formulation on humans (Ardekani et al., 2009), where keloid scars were topically treated with 5 % captopril cream, twice daily for 6 weeks. A marked improvement was achieved in terms of the height, redness and pruritus of the lesion. Interestingly, no local or systemic adverse effects were associated with the treatment. Captopril inhibited the conversion of Ang I to Ang II which in turn suppressed the expression of TGF-β, the potent enhancer of collagen synthesis in dermal fibroblasts.

In a very recent study, Kim and colleagues (2012) evaluated the efficacy of topical formulations containing captopril 5 % or celecoxib 0.5 % alone, and a combination of these drugs to reduce scarring. The data demonstrated that wounded skin treated with the formulations containing captopril had a significantly lower scar elevation index compared with the control (Kim et al., 2012). These preliminary observations will need to be validated by large scale clinical studies in order to verify the potential use of ACEIs as novel therapeutic agents for the treatment of scars.

To date, there are no topical products containing ACEIs on the market and the currently available products for scar treatment will be discussed in section 1.8.

1.8 Topical treatments for scars

Abnormal wound healing results in hypertrophic scar and keloid formation, causing cosmetic defects and patient dissatisfaction. A wide range of nonsurgical treatment strategies are currently available for the management of scars. However, these treatments have not proved to be completely effective and satisfactory. Furthermore, the treatment usually continues over several weeks to months.

1.8.1 Corticosteroids

Steroid injections have been widely used for minimizing scar appearance. They act by suppressing inflammation, reducing fibroblast proliferation and collagen synthesis (Cruz and Korchin, 1994; Wu et al., 2006) as well as suppressing the expression of TGF-β (Stojadinovic et al., 2007). In the 1960s, the intralesional injection of triamcinolone acetonide (TA) (Figure 1-16) was first reported by Ketchum et al. (1966). Several researchers have reported the effectiveness of TA in scar improvement. A three to five year study of injection of TA into 109 keloid scars on 94 Asian patients was conducted by Muneuchi et al (2006). One third of the patients discontinued the treatment because of the pain accompanied by injection and slow improvement. The assessment of objective and subjective symptoms was not satisfactory. Ma et al. (2012) assessed the effect of TA on hypertrophic scars using skin roller needles as a delivery device. The colour, thickness, and texture of scars were significantly different in the treated area compared with the control. In comparison with TA alone, a treatment with a combination of TA and 5-Fluorouracil (5-FU) resulted in more effective and rapid response with fewer adverse effects (Darougheh et al., 2009). The results were in line with the previous ones of Apikian and Goodman (2004).

Hypopigmentation, atrophy and telangiectasia were recorded from intralesional corticosteroid injections as adverse effects (Fitzpatrick, 1999). Other undesirable effects were pain on injection and the risk of skin atrophy if the drug was injected superficially.

1.8.2 Fluorouracil

5-fluorouracil (5-FU) (Figure 1-16), a pyrimidine analog, has been used extensively in the treatment of cancer. It targets rapidly proliferating fibroblasts in dermal wounds, thus inhibiting excessive collagen production (Bulstrode et al., 2005). 5-FU was intralesionally injected as monotherapy (Nanda and Reddy, 2004; Kontochristopoulos et al., 2005) or in combination with low dose corticosteroids (Fitzpatrick, 1999; Apikian and Goodman, 2004). The data showed a regression in the objective symptoms of scars, i.e. size, redness, and prominence. This combination was more effective and less painful and had fewer complications than the intralesional corticosteroid injection. In addition, the degree and rapidity of response depended on the early stages of treatment, dose, and frequency of injections (Fitzpatrick, 1999). 5-FU was found to interfere with TGF-β and thus inhibits TGF-β induced collagen production in human fibroblasts (Wendling et al., 2003). Hatamipour et al (2011) evaluated the efficacy of a formulation containing both 5-FU and topical silicone in the prevention of keloids. The findings demonstrated that this formulation was more effective than the control (silicone alone). Like corticosteroid treatment, pain was recorded during the injection. Moreover, ulceration and hyperpigmentation were the undesirable effects recorded with 5-FU (Apikian and Goodman, 2004; Kontochristopoulos et al., 2005).

1.8.3 Onion extract

Mederma®, a topical product containing an onion extract, has been formulated by Merz Pharmaceuticals, Germany in order to improve the appearance of scars. It also has anti-inflammatory, antibacterial, and fibrinolytic properties (Augusti, 1996). The onion extract contains quercetin (Figure 1-16) which plays a role in supressing fibroblast proliferation and collagen synthesis (Phan et al., 2003). Studies on its effect on scars showed inconsistent results. The effect of Mederma® on hypertrophic scars was investigated by Saulis et al. (2002). The data demonstrated the inability of the product to reduce both scar hypertrophy and erythema, yet it improved collagen organization. Another clinical study conducted with 60 patients by Hosnuter et al (2007) showed the ineffectiveness of onion extract in treating hypertrophic scars in terms of scar elevation and itching. However, it was more effective in reducing scar redness. Further studies using Mederma® gels have also shown treatment with this extract did not result in any improvement in scar appearance, erythema, and elevation when compared with a petroleum based ointment as a control (Jackson and Shelton, 1999; Chung et al., 2006). While former clinical studies showed disappointing results in terms of improving scar height, a very recent study demonstrated the opposite (Chanprapaph et al., 2012). This study was carried out on Asian women who underwent caesarean section and confirmed the benefit of onion extract in reducing scar height and symptoms. However, the differences between these results and those from previous studies were attributed to the variability in the study design (Chanprapaph et al., 2012). Interestingly, no side effects were recorded in all cases.

1.8.4 Imiquimod

Imiquimod cream 5 % (Aldara®), a topical immune response modifier, is an effective treatment for warts (Berman, 2002). Imiquimod (Figure 1-16) stimulates the synthesis and release of interferon alpha (IFN-α), a cytokine that increases collagen breakdown. Topical application of imiquimod cream 5 % following surgical removal of keloids reduced the recurrence rates of keloids (Berman and Kaufman, 2002). However, discouraging results were obtained from recent clinical studies (Malhotra et al., 2007; Cacao et al., 2009), where the daily application of imiquimod cream 5 % for 8 weeks after surgical excision resulted in recurrence of keloids in the majority of patients. Thus further investigations may be necessary to determine the ultimate success rates. Mild and local site reactions including erythema and hyperpigmentation were recorded.

1.8.5 Silicone based products

Silicone based products have been widely used for over 20 years to prevent and treat scars. They were first introduced in the early 1980s for the treatment of burn scars (Perkins et al., 1983). Silicone (Figure 1-16) is a polymer of dimethylsiloxane used as a topical silicone gel sheet (SGS) or gel with the advantages of being inexpensive, non-invasive, and easy to apply.

The precise mechanism by which silicone exerts its effect is not yet clear. It was suggested that SGS increases skin temperature which in turn increases collagenase activity (Krieger et al., 1993). It was also shown that SGS reduced collagen synthesis by downregulating TGF-β (Kuhn et al., 2001). Further experiments, however, suggested that the mode of action of SGS may be attributed to its occlusive and

hydration effects, and not to the chemistry of the compound. Sawada and Sone (1992) and de Oliveira et al. (2001) demonstrated that occlusion was the primary basis for improving hypertrophic scars and keloids regardless of the presence of silicone, but the magnitude of occlusion was critical for effective treatment (Saulis et al., 2002). SGS induced a mild hydration of the SC compared to a plastic film (Suetake et al., 2000). This hydration is likely the underlying mechanism of silicone by preventing the development of hydration dermatitis which was observed with the plastic film.

It was found that transepidermal water loss (TEWL) was higher with hypertrophic scars and keloids than normal skin (Suetake et al., 1996). In a study where cultured human keratinocytes and fibroblasts were treated with high osmotic NaCl in order to simulate *in vivo* dehydration when the skin barrier is disrupted, levels of proinflammatory cytokines were increased (Terunuma et al., 2001). Therefore, it seems likely that occlusive silicone based products could decrease TEWL and return the hydration of keratinocytes to normal conditions. This resulted in suppression of production of cytokines that activate fibroblasts to produce ECM. Recent studies confirmed that the occlusion induced by SGS led to modification in the cytokine levels, decreasing the profibrotic cytokine (IL-1) and increasing the antifibrotic cytokine (TNF-α). This in turn altered the activity of dermal fibroblasts, resulting in a decrease in both ECM synthesis and scar development (Tandara et al., 2007; Gallant-Behm and Mustoe, 2010).

Results of comparative clinical studies indicated that silicone gel (Dermatix®) was an effective treatment for the management of abnormal scarring (Chan et al., 2005; Chernoff et al., 2007; Signorini and Clementoni, 2007). The scars showed significant

improvements in redness, elevation, hardness, itching and pain compared with those untreated or received placebo treatment. However, 5-FU was more effective than silicone in the prevention of keloids (Hatamipour et al., 2011). The findings indicated that the recurrence of keloids was five times higher in patients treated with silicone alone.

1.8.6 Bleomycin

Bleomycin (Figure 1-16), a cytotoxic antibiotic, has been widely used in the treatment of warts (Shumer and O'Keefe, 1983). Its exact mode of action by which it reduces hypertrophic scars and keloids remains unclear. A study showed that incubation of human fibroblasts with bleomycin resulted in inhibition of DNA synthesis in the fibroblasts (Hendriks et al., 1993). The findings of clinical studies demonstrated the effectiveness of bleomycin to treat both hydrotropic scars and keloid (Espana et al., 2001; Saray and Gulec, 2005; Naeini et al., 2006). The main adverse effect of bleomycin administered intralesionally is hyperpigmentation and dermal atrophy (Saray and Gulec, 2005).

1.8.7 Tamoxifen

Tamoxifen (Figure 1-16) is used in the treatment of breast cancer. It was reported to decrease the production of TGF-β in a dose dependent manner (Chau et al., 1998). Mousavi et al (2010) assessed the efficacy of tamoxifen administered orally in the prevention of postsurgical scars. 52 % of patients developed scars compared with 92 % of the control group. In addition, topical application of 0.1 % tamoxifen resulted in

scar improvement after treatment (Gragnani et al., 2010). Flushing and nausea were reported as adverse effects.

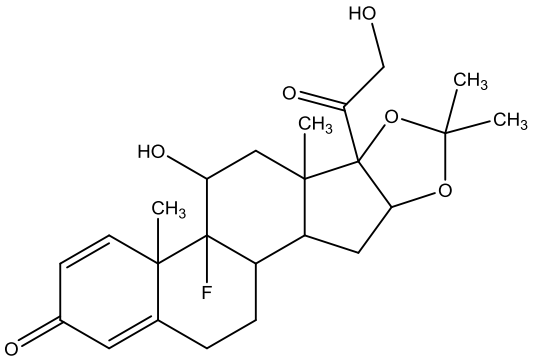

Triamcinolone acetonide

MW: 434.5 Da
Log P: 0.59
pK_a: 12.8, 13.4

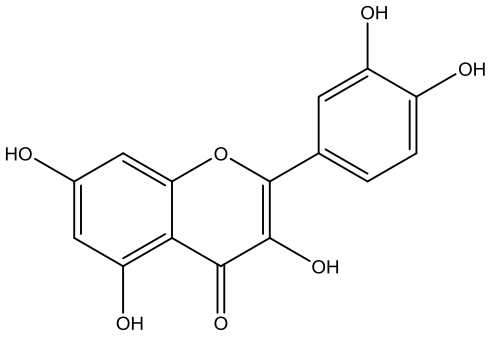

Quercetin

MW: 302.2 Da
Log P: 0.35
pK_a: 6.9, 7.8, 10.9, 12.5, 16.7

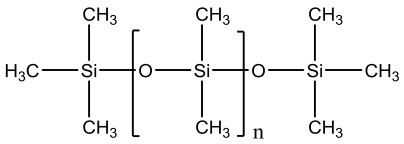

Silicone

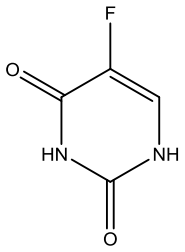

Fluorouracil

MW: 130.1 Da
Log P: -1.31
pK_a: not available

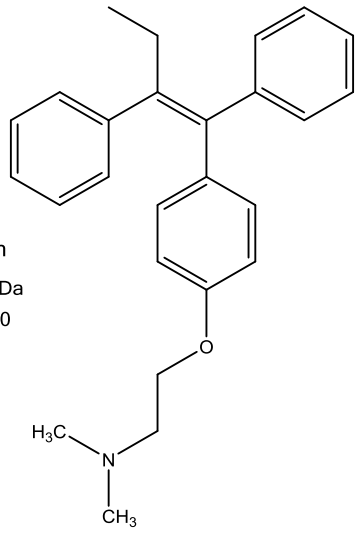

Tamoxifen

MW: 371.5 Da
Log P: 6.10
pK_a: 9.2

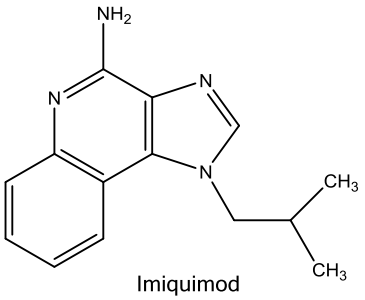

Imiquimod

MW: 240.3 Da
Log P: 2.27
pK_a: not available

Figure 1-16 Chemical structures of different drugs used for scar treatment. MW, Log P and pK_a were calculated using ChemDraw® software.

1.9 Drugs under investigation

Moexipril, ramipril, and cilazapril are among the ACEIs which are generally well tolerated and have been widely used in oral solid dosage forms for the treatment of hypertension and congestive heart failure (Jackson, 2006; BNF, 2012). They are prodrugs which are hydrolyzed in the liver to the active forms, moexiprilat, ramiprilat, and cilazaprilat, respectively (Figure 1-17).

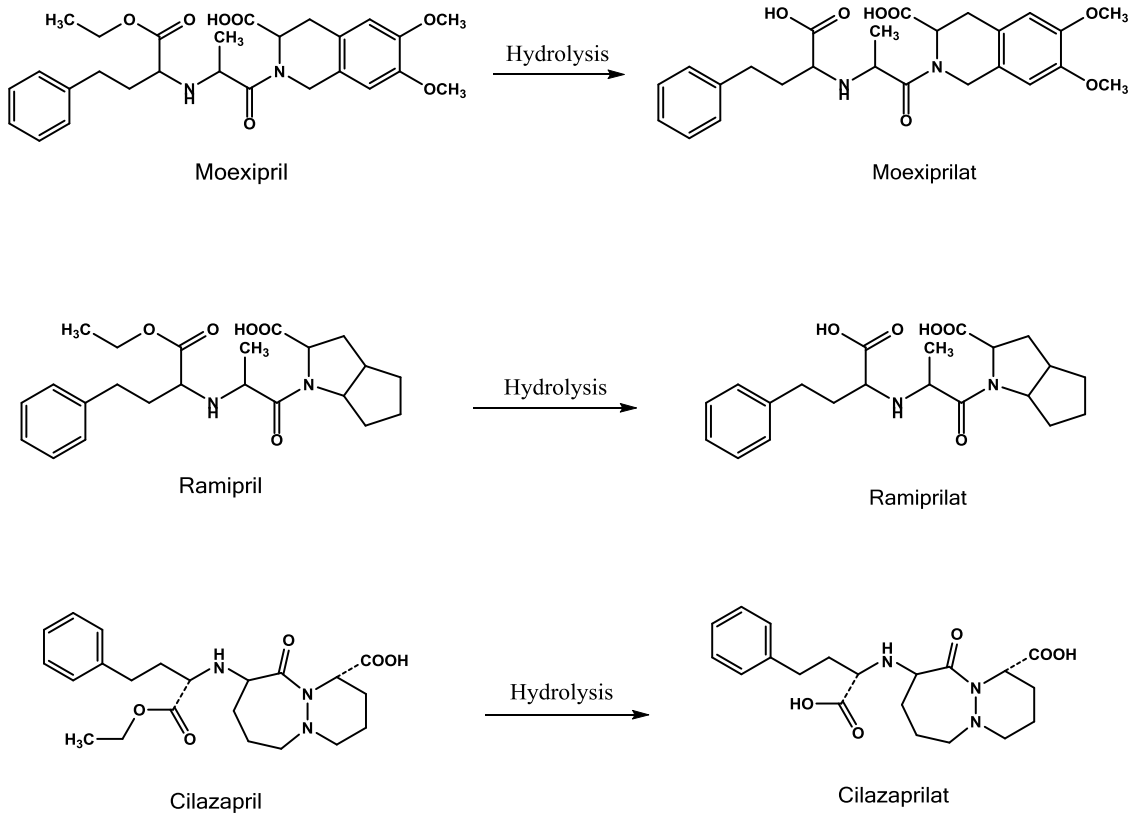

Figure 1-17 Chemical structures of moexipril, ramipril, and cilazapril and their metabolites

Based on their potency and physicochemical properties (Table 1-1), these drugs are suitable candidates for transdermal and topical drug delivery.

Table 1-1 Physicochemical properties of moexipril, ramipril, and cilazapril

Physicochemical properties	Moexipril	Ramipril	Cilazapril
Daily dose [a] (mg)	7.5 - 15	1.25 - 10	1 - 5
MW [a] (g/mole)	498.6	416.5	435.5
Log P [b]	3.4	3.3	0.7
pK_a [c]	2.7, 4.4	3.0, 4.6	2.9, 4.6
MP [a] (°C)	141 - 161	109	95 - 97

[a] Clarke's Analysis of Drugs and Poisons.

[b] ChemSpider (http://www.chemspider.com)

[c] Calculated using ChemDraw® software

Interestingly, the existence of a local RAS in human skin (Steckelings et al., 2004) and its role via Ang II in skin wound healing and scar formation has been demonstrated as outlined in section 1.7.4. Therefore, these candidates might be innovative strategies for wound management.

1.10 Aims of the thesis

This thesis focuses on the design of stable topical formulations for delivery of ACEIs as a novel treatment strategy for the management of hypotrophic scars and keloid. Therefore, the following points are addressed:

1. The stability of moexipril (MOX), ramipril (RAM), and cilazapril (CILA) in a range of hydrophilic and lipophilic vehicles at 32 ˚C over a period of five days.
2. Development of topical formulations of RAM and CILA and assessment of percutaneous absorption of the drugs across human and porcine skin.
3. Evaluation of the fate of CILA in porcine skin homogenate.

Chapter 2

Stability of angiotensin converting enzyme inhibitors (ACEIs) in a range of vehicles

2 Stability of angiotensin converting enzyme inhibitors (ACEIs) in a range of vehicles

2.1 Introduction

The selection of active pharmaceutical ingredients (API) for the manufacture of a successful formulation should be based not only on their physicochemical properties but also on their chemical and physical stability when combined with excipients (Allen et al., 2011b). It is estimated that the majority of pharmaceutical dosage forms are manufactured as tablets and capsules because of stability issues which arise from the liquid formulations (Allen et al., 2011a).

In general, pharmaceutical dosage forms contain both API and excipients which make up more than 90 % of the final product in order to aid the manufacturing process (Rowe et al., 2009). Although excipients are usually biologically inactive, they can stabilise (Ren et al., 2008; Jain et al., 2012) or destabilise (Gu et al., 1990; Stanisz et al., 2013) drug products. Therefore, the assessment of API stability in the presence of commonly selected excipients is of vital importance in outlining possible interactions between formulation components. This eliminates any risks of incompatibility at an early stage of the formulation development.

Incompatibility between the drug and excipients can alter drug stability and bioavailability and thereby affect its safety and efficacy (Bharate et al., 2010). Unfortunately, drugs are more vulnerable to chemical degradation when they are in solution compared with the solid state (Parmar et al., 2012). Therefore, when a drug is formulated into a liquid dosage form, a stability study is necessary to ensure that the drug will not degrade under the manufacturing and storage conditions. Drug

degradation can lead not only to a loss in effectiveness, but sometimes to formation of toxic products. Therefore, the degradation products and their levels must be monitored during the preformulation stage (FDA, 2006).

One of the approaches to investigate excipient-drug compatibility is based on conducting a stability study under normal and stressed conditions (ICH, 2003). The latter are useful to identify the potential degradation products, which can in turn help to identify the degradation pathways (Reynolds et al., 2002; ICH, 2003). The stability study can be divided into three steps. Firstly, solutions of a given drug in a pure solvent or mixture of solvents are prepared. Secondly, the samples are kept under specific storage conditions in terms of temperature and humidity over a convenient time period. Finally, a validated stability-indicating analytical method is applied in order to determine the concentration of the intact drug. Whenever feasible, the degradation products are identified by mass spectrometry (MS) (Ren et al., 2008; Modhave et al., 2011; Pan et al., 2012) and/or nuclear magnetic resonance (NMR) (Shetgiri et al., 2008).

The influence of several formulation factors on the chemical stability of MOX and RAM along with other ACEIs in both solid state (Al-Omari et al., 2001; Stanisz, 2004; Amaral et al., 2011; Stanisz et al., 2013) as well as aqueous solutions (Gu and Strickley, 1987; Boulton et al., 1994; Allen et al., 1995; Schlatter and Saulnier, 1997; Hanysova et al., 2005; Roskar et al., 2009) was previously evaluated. The findings of these studies revealed that these ACEIs were sensitive to the type of excipients, temperature, moisture, and pH. The degradation occurred mainly via two pathways: the hydrolysis and/or the intramolecular cyclization. Furthermore, the formation of the two degradation products was pH dependent. The diketopiperazine form (DKP) is not the

active metabolite of the parent drug whereas the hydrolysed form is the active diacid form. The effect of organic solvents on MOX and RAM stability has not been extensively examined. Gu and Strickley (1990) reported the stability of MOX in water-ethanol mixtures. Interestingly, the stability of CILA which has a different chemical structure has not been reported to date.

2.2 Aims

The goals of this study were (i) to evaluate the stability of MOX, RAM, and CILA in a range of hydrophilic and lipophilic vehicles at 32 ˚C and (ii) to identify the main degradation products, whenever feasible, during the stability studies by MS.

2.3 Materials

MOX, RAM and CILA (purity: unknown) were a donation from Ranbaxy Laboratories Ltd (Punjab, India). Ramipril diketopiperazine (RAM-DKP) was purchased from LGC Standards (Middlesex, UK). Dimethyl isosorbide (DMI) of different grades (Arlasolve® DMI-PC) and (Super refined Arlasolve® DMI-LQ) were a gift from Croda, UK. Pentanediol (PENTA), propylene glycol (PG), isopropyl myristate (IPM), and sodium perchlorate monohydrate ($NaClO_4.H_2O$, ≥99 % HPLC grade) were purchased from Sigma-Aldrich, UK. Absolute ethanol (EtOH) was from Hayman Ltd (Essex, UK). Lactic acid (LA), and polyethylene glycol (PEG) 200 and 400 were from Fluka, UK. Propylene glycol monocaprylate or Capryol® 90 (CAP), propylene glycol monolaurate (PGML), propylene glycol laurate (PGL), dipropylene glycol (DPG), diethyleneglycol monoethyl ether or Transcutol® (TCL), and propylene glycol dicaprylate/dicaprate or Labrafac PG® (LAB) were a gift from Gattefosse (Cedex, France). Acetonitrile (ACN),

methanol (MeOH), water, potassium dihydrogen phosphate (KH_2PO_4), orthophosphoric acid (H_3PO_4), and formic acid (all HPLC grade) were purchased from Fisher Scientific Ltd (Leicestershire, UK). Deionized water was prepared using a USF ELGA Option 3 water purifier system.

2.4 Methods

2.4.1 Development of HPLC methods used for analysis of MOX, RAM, and CILA.

HPLC separation for MOX, RAM and CILA was performed with an Agilent 1200 series HPLC System (Agilent Ltd, UK) which consisted of a G1311A quaternary pump, G1316A UV detector, G1329A auto-sampler, G1322A vacuum degasser, and a solvent module. The data were acquired and processed using HP Chemstation software and Computer control. Since MOX, RAM and CILA were insoluble in the non polar solvents used in a normal phase HPLC mode but soluble in water and metanol, a reversed phase (RP) HPLC mode was selected. The wavelength for the analysis was determined from the UV spectrum of MOX, RAM and CILA by scanning in the range of 200 - 400 nm. From this, the wavelength of 210 nm was selected for the final method as these drugs have shown good absorbances at 210 nm. For HPLC analysis, initially various mobile phases and stationary phases were tried in attempts to obtain the best peak parameters in terms of the retention time, peak width, and asymmetry. Two RP-HPLC columns (250 x 4.6 mm) were selected, Capcell® packed with octadecylsilyl silica gel (Shiseido, Japan) and Synergi Polar-RP, an ether-linked phenyl phase (Phenomenex, UK). In order to determine the best compostion of the mobile phase, gradient conditions were initially tried using a binary solvent system (acetonitrile/buffer or methanol/buffer). Two different buffers were used: potassium dihydrogen phosphate

(0.01 M) and sodium perchlorate (0.7 % w/v). After the compostion of the mobile phase was determined, the HPLC run under an isocratic mode. A flow rate of 1 ml/min was used initially. Temperature was set at 25 or 40 ˚C. Temperature was used for good resolution and faster elution of compounds. The chromatographic conditions for MOX, RAM and CILA were adjusted in order to obtain the desired separation and peak parameters and are listed in Table 2-1.

Table 2-1 HPLC chromatographic conditions for the analysis of MOX, RAM, and CILA

Conditions	Drug		
	MOX	RAM	CILA
HPLC column (250 x 4.6 mm)	Synergi Polar-RP (Phenomenex, UK)	Capcell® packed with octadecylsilyl silica gel (Shiseido, Japan)	
Mobile phase (45:55 v/v)	ACN: KH_2PO_4 (0.01 M, pH 2.5)	ACN: $NaClO_4$ (0.7 % w/v, pH 2.5)	MeOH: KH_2PO_4 (0.02 M, pH 2.5)
Injection volume (µl)	15	20	25
Flow rate (ml/min)	1	1.5	1
Column temperature (˚C)	40	25	40
UV detection (nm)	210	210	210
Assay range (µg/ml)	5 - 70	5 - 100	0.5 - 70

2.4.2 HPLC method validation

All the HPLC methods have been validated prior to use for parameters such as linearity, specificity, limits of detection and quantification, system suitability, accuracy, and precision according to the British Pharmacopeia (BP, 2013b) and the International Conference on Harmonization (ICH) guidelines Q2 (R1) for validation of analytical procedures (ICH, 2005).

2.4.2.1 Linearity

The linearity is the capability of an analytical method to achieve results that are directly proportional to the concentration of drug (ICH, 2005). Linearity was evaluated for a minimum of five concentrations as recommended by ICH guidelines Q2 (R1). It was performed by analysis of working standard solutions of MOX, RAM, and CILA at different concentrations 5, 10, 20, 50, 70 μg/ml; 5, 15, 45, 70, 100 μg/ml and 0.5,1, 2, 5, 10, 20, 40, 70 μg/ml, respectively. Each concentration was prepared in triplicate.

2.4.2.2 Specificity

Specificity is the ability of the method to assure that a drug can be assessed specifically in the presence of other substances, which may be present in the product (ICH, 2005). These substances might be impurities, degradation products, or matrix. The specificity of the method was evaluated by injecting the blank and the drug standard solution separately into the HPLC and then comparing the chromatograms obtained. The concentrations were 15, 40 and 50 μg/ml for RAM, CILA, and MOX, respectively. The peak of MOX, RAM, and CILA in the tested formulations was compared with both the blank peaks resulting from the mobile phase and vehicles used, and the peaks of known and unknown degradation products.

2.4.2.3 Limits of detection (LOD) and quantitation (LOQ)

LOD is the lowest amount of drug which can be detected but not necessarily quantified. However, LOQ is the minimum concentration at which the drug can be quantified (ICH, 2005). LOD and LOQ were determined by calculating the signal-to-

noise (S/N) ratio of a diluted standard solution which were 3:1 for LOD and 10:1 for LOQ.

2.4.2.4 System suitability

The system suitability is to verify that the chromatographic system is suitable for the intended analysis. It was performed by analyzing the standard solution (10 μg/ml) six times (n=6) and evaluating the following parameters: peak area, retention time, and asymmetry. A RSD value equal or less than 2 % was an indication of the suitability of the HPLC system. The value of each parameter was obtained from by HP Chemstation software.

2.4.2.5 Accuracy

The accuracy of the analytical method expresses the closeness between the obtained (experimental) value and the theoretical value (ICH, 2005). It was evaluated by the analysis of mobile phase spiked with known amounts of the analyte and expressed as the % accuracy. Spiked samples were prepared in triplicate at three concentration levels within the specified experimental range (lower, medium and upper concentration) and then analyzed by the HPLC. The concentration levels were 1, 20, 70 μg/ml; 5, 45, 100 μg/ml; and 0.5, 20, 70 μg/ml for MOX, RAM, and CILA, respectively.

2.4.2.6 Precision

Precision expresses that all measurements of a drug at the same concentration should be very close to each other (ICH, 2005). Precision was assessed at two levels,

repeatability (intra-day) and intermediate (inter-day) precision. It was determined from three concentration levels, three repetitions each. The concentration levels were 1, 20, 70 µg/ml; 5, 45, 100 µg/ml; and 0.5, 20, 40 µg/ml for MOX, RAM, and CILA, respectively. The intermediate precision was conducted to study the variations at different days which might affect chromatographic performance. The relative standard deviation (% RSD) of the measured concentrations was calculated and used as an indicator of the precision of the system. A RSD value equal or less than 2 % was an indication of the precision of the HPLC method.

2.4.3 Stability studies of ACEIs in a range of vehicles

2.4.3.1 Moexipril

The stability of MOX in different vehicles EtOH, CAP, DMI, PGML, PGL, PG, PEG 200, TCL, and water was investigated for up to five days with 24 h intervals at 32 ˚C. The rationale for this temperature was that the topical formulations of the present study were prepared and assessed in terms of their percutaneous absorption at skin temperature (32 ˚C). To start the stability study, known concentrations of the drug solutions in the selected vehicles were prepared as follows: known amounts of the drug substance were individually transferred to capped soda glass specimen tubes (50 x 25 mm) containing 5 ml of each vehicle, stirred with the aid of magnetic followers for 15 min. Since the concentration of the drug was high, the sorption to vessel walls was considered minimal. Triplicate test solutions of MOX in each vehicle were prepared. Physical stability was assessed by visual examination of the test solutions in natural light. At the end of the experiment, if these solutions did not exhibit any colour changes or precipitation, they were considered physically stable. Figure 2-1 illustrates

the stages of conducting the stability study. After the initial sampling (t_0), the tubes containing the test solutions were placed in a water bath (Grant SUB Aqua 26, UK) held at 32 °C throughout the investigation in order to examine the effect of vehicles and temperature on drug stability. The chemical stability was assessed using the HPLC analytical technique based on the determination of drug concentrations initially and at predetermined time intervals over the study period in order to make valid conclusions about the stability of the drug. Fresh standard solutions of MOX were prepared at each time interval and then injected before running the samples in order to make sure that the decrease in the peak area was related to the drug degradation. Stability of the drug was defined as not less than 90 % of the initial drug concentration remaining in the solutions in accordance with FDA drug stability guidelines (FDA, 2008).

Figure 2-1 The stability study diagram.

2.4.3.2 Ramipril

The stability of RAM in different solvents CAP, LA, PG, PGML, PGL, DMI, TCL, PEG 200, PENTA, IPM, EtOH, and water was investigated for up to five days with 24 h intervals at 32 °C. Samples preparation, sampling, and analysis procedures were the same as described in section 2.4.3.1

2.4.3.3 Cilazapril

The stability of CILA in different solvents PEG 200, EtOH, water, IPM, PG, DPG, PGL, PGML, TCL, LAB and CAP was evaluated at 32 °C for up to five days at 24 h intervals. Triplicate test solutions of CILA in each vehicle were prepared. Sample preparation, sampling, and analysis procedures were the same as described in section 2.4.3.1

2.4.4 Identification of the degradation products

2.4.4.1 Forced degradation studies

Forced degradation studies were conducted for determining the main degradation products and therefore the degradation pathways of the drug (ICH, 2003; De Diego et al., 2010). The experiments were performed by preparing solutions of the model drugs in PG and EtOH. These solutions were exposed to a high temperature condition at 60 °C. Separations were performed using the HPLC with the same chromatographic conditions described in section 2.4.1. The degradant was collected from the HPLC eluate. The fraction collections were combined and re-injected to ensure that they contained a single product. The molecular mass of the degradation compound was then determined by MS (Ren et al., 2008; Rao et al., 2011).

2.4.4.2 Identification of degradation products of MOX and RAM using MS

MOX and RAM and their degradation products in the stress testing samples were detected by MS as follows: the effluent from the liquid chromatography was introduced into an ion trap mass spectrometer (Finnigan LCQDuo, Thermo Scientific,

UK) equipped with electrospray ionization (ESI) probe operated in positive-ion mode. The data was acquired in the m/z range 50–1900. The temperature of the ESI ion source was kept at 180°C. The capillary voltage was set at 45 V for positive-ion ESI. The ion spray voltage was 1-1.5 kV with a spray current of 0.34 µA.

2.4.4.3 Confirmation of the degradation product of RAM by HPLC using RAM-DKP standard.

A standard stock solution of RAM-DKP was prepared by dissolving 10 mg of this material in 1 ml of a mixture of acetonitrile and water (50:50). The resultant solution was diluted and then separately injected into the HPLC with the degradation product collected from the stress degradation study. The two resultant HPLC chromatograms were compared according to the retention times.

2.5 Results and discussion

2.5.1 HPLC method validation

2.5.1.1 Linearity

A linear calibration curve was obtained from plotting mean peak areas (y) as a function of the concentration (x) of each working standard solution (Figure 2-2). The linearity was expressed as a correlation coefficient by linear regression analysis. The regression equation for MOX, RAM and CILA was y = 67.68 x + 0.81, y = 26.44 x + 4.64, and y = 37.39 x - 1.29, respectively; where x is the drug concentration (µg/ml) and y is the peak area. The corresponding correlation coefficient (r^2) was 0.99 in all cases. The results showed that within this concentration range there was an excellent correlation between the peak area and concentration of drug.

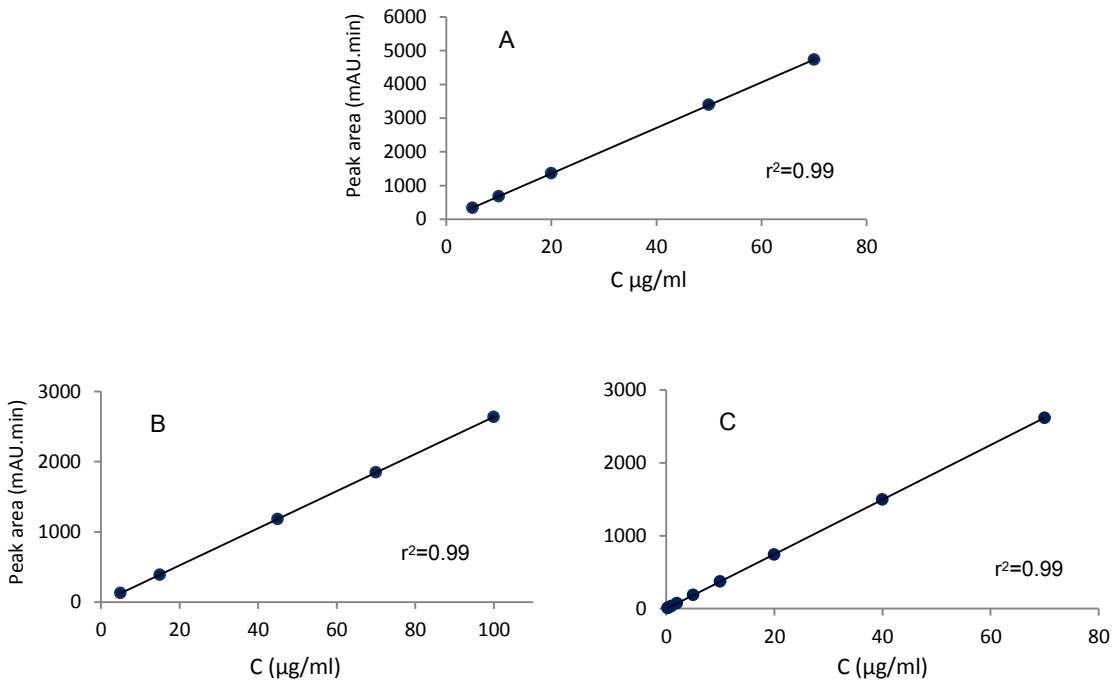

Figure 2-2 Graphical presentation of linearity plots of MOX (A), RAM (B), and CILA (C) (Mean ± SD, n=3); the SD error bars are too small to be visible.

2.5.1.2 Specificity

From the concentration HPLC chromatogram overlays of both MOX, RAM and CILA and their mobile phases (Figure 2-3), it was observed that these drugs eluted at 5.0, 6.2, and 8.5 min, respectively. No interfering substances were found at the retention times corresponding to the analyte peaks, indicating the specificity of the methods for the analysis of MOX, RAM, and CILA.

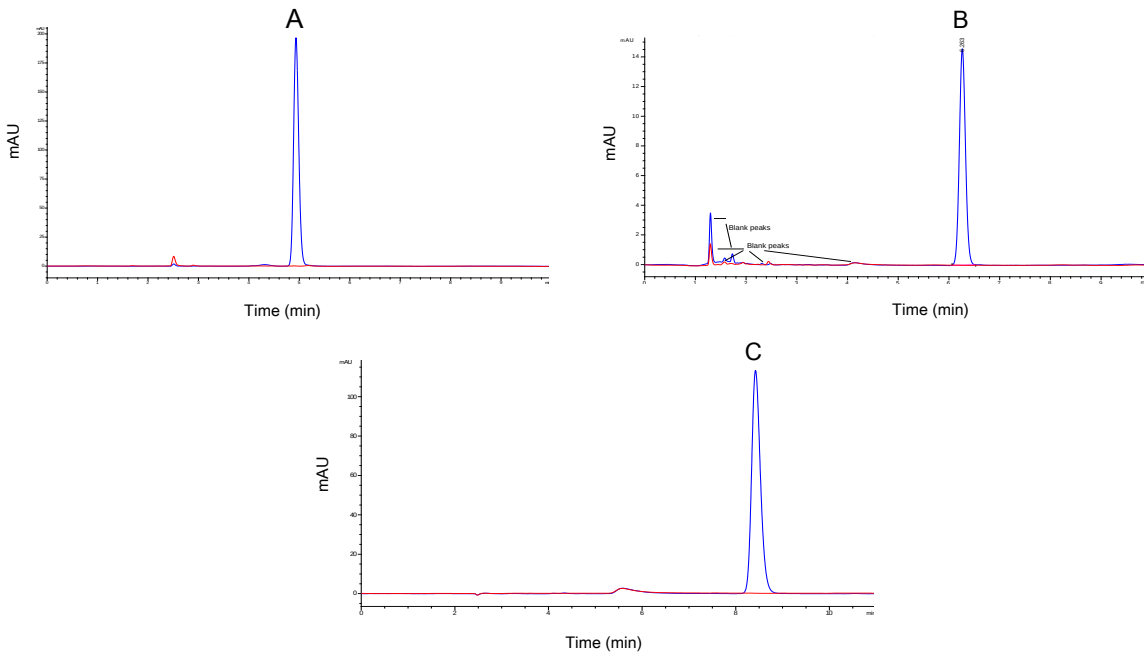

Figure 2-3 Overlaid HPLC chromatograms of MOX (A), RAM (B), and CILA (C) along with the mobile phase. The red line represents the chromatogram of the mobile phase.

2.5.1.3 Limits of detection (LOD) and quantification (LOQ)

The LOD and LOQ for MOX, RAM and CILA were 0.2 and 0.5 µg/ml, respectively. These low values were an indication of the sensitivity of the method.

2.5.1.4 System suitability

The results obtained from the system suitability test are shown in Table 2-2. In all cases, % RSD values were less than 2 %, which confirmed the reliability of the methods.

Table 2-2 Results obtained from the system suitability test. Each value represents the mean ± SD (RSD); n=6

Parameter	MOX (20 µg/ml)	RAM (15 µg/ml)	CILA (10 µg/ml)
Retention time (min)	4.93 ± 0.01 (0.13)	6.29 ± 0.02 (0.08)	8.60 ± 0.01 (0.08)
Peak area (mAU.min)	1411.10 ± 1.84 (0.13)	390.09 ± 0.10 (0.18)	291.43 ± 4.27 (1.46)
Asymmetry	0.83 ± 0.01 (1.04)	0.89 ± 0.01 (0.00)	0.82 ± 0.01 (0.91)

2.5.1.5 Accuracy

Data listed in Table 2-3 show that the percent accuracy values were within the range from 98 to 103 %. These results were an indication of good accuracy for the methods being validated.

Table 2-3 Results obtained from the accuracy test. Each value represents the mean ± SD; n=3

Drug	C (µg/ml)		Accuracy (%)
	Spiked	Measured	
MOX	1	0.98 ± 0.02	98.10
	20	20.06 ± 0.27	100.28
	70	69.90 ± 1.24	99.86
RAM	5	4.91 ± 0.05	98.21
	45	44.50 ± 0.19	98.88
	100	99.84 ± 1.32	99.84
CILA	0.5	0.52 ± 0.01	103.16
	20	19.70 ± 0.25	98.48
	70	69.67 ± 0.37	99.53

2.5.1.6 Precision

The resulting data for intra- and inter-day precision are provided in Table 2-4. In all cases, the % RSD values of the measured concentrations were all found to be equal or less than 2 %. The low RSD values demonstrated the repeatability and intermediate precision of the proposed methods.

Table 2-4 Results of the precision test. Each value represents the mean ± SD (RSD); n=3

Drug	C	*Intra-day*			*Inter-day*	
	(µg/ml)	Day 1	Day 2	Day 3		
MOX	1	0.95 ± 0.02	0.93 ± 0.06	0.91 ± 0.02	0.93 ± 0.02	(1.83)
	20	20.05 ± 0.27	20.16 ± 0.51	19.50 ± 0.04	19.91 ± 0.36	(1.80)
	70	69.90 ± 1.24	70.14 ± 1.75	68.89 ± 1.25	69.64 ± 0.67	(0.96)
RAM	5	4.91 ± 0.05	5.07 ± 0.06	5.10 ± 0.07	5.0 ± 0.08	(1.66)
	45	44.50 ± 0.19	44.71 ± 0.19	44.56 ± 1.00	44.6 ± 0.09	(0.20)
	100	99.84 ± 1.32	99.50 ± 0.25	101.05 ± 1.41	100.0 ± 0.67	(0.66)
CILA	0.5	0.51 ± 0.01	0.52 ± 0.01	0.53 ± 0.01	0.52 ± 0.01	(1.14)
	10	9.98 ± 0.21	10.07 ± 0.12	10.00 ± 0.14	10.02 ± 0.04	(0.43)
	40	40.08 ± 0.19	39.74 ± 0.53	39.32 ± 0.27	39.71 ± 0.18	(0.44)

2.5.2 Stability studies

2.5.2.1 Moexipril stability

All the test solutions were initially clear and colourless under natural light. Some solutions exhibited colour change or precipitation during the study. The colour of DMI solution has changed from colourless, to light yellow and then to dark yellow at 48, 72, and 96 h, respectively whereas no change in the colour of MOX solutions in water, CAP, PGML, and PEG 200 throughout the study. MOX solutions in PG exhibited a slight colour change at 120 h from colourless to clear light pink (Figure 2-4). However, at 72 h, visible particulate matter was observed in the water samples. A sample of this matter was collected, dissolved, and then analysed using the HPLC and MS in order to identify the content.

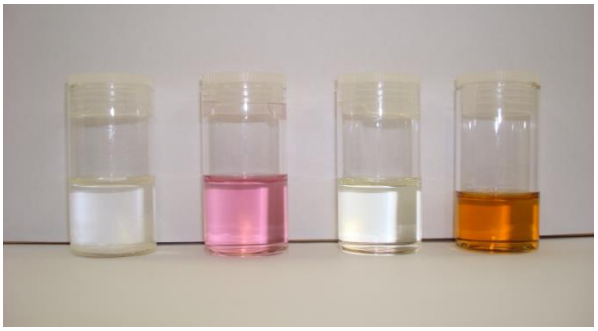

Figure 2-4 MOX in various vehicles from left to right water, PG, PEG 200, DMI at 120 h.

The HPLC chromatograms obtained from the drug assay at t_0 and t_{120} in the different vehicles are shown in Figure 2-5. These chromatograms revealed the main peak of MOX along with other related substances. The pure vehicles were firstly injected into the HPLC after dilution at the same dilution factor as the samples in order to see if there was any interference between the solvent peak and drug peak. As shown in Figure 2-5 (the red line), all the peaks of solvents appeared early around 3 min whereas the drug and its degradant eluted at 5 and 15 min, respectively. However, when CAP was analysed, two peaks appeared. The first one was at the beginning and the other was around 12 min. No interfering substances were found at the retention time corresponding to MOX peak, indicating the specificity of the method for the analysis of MOX.

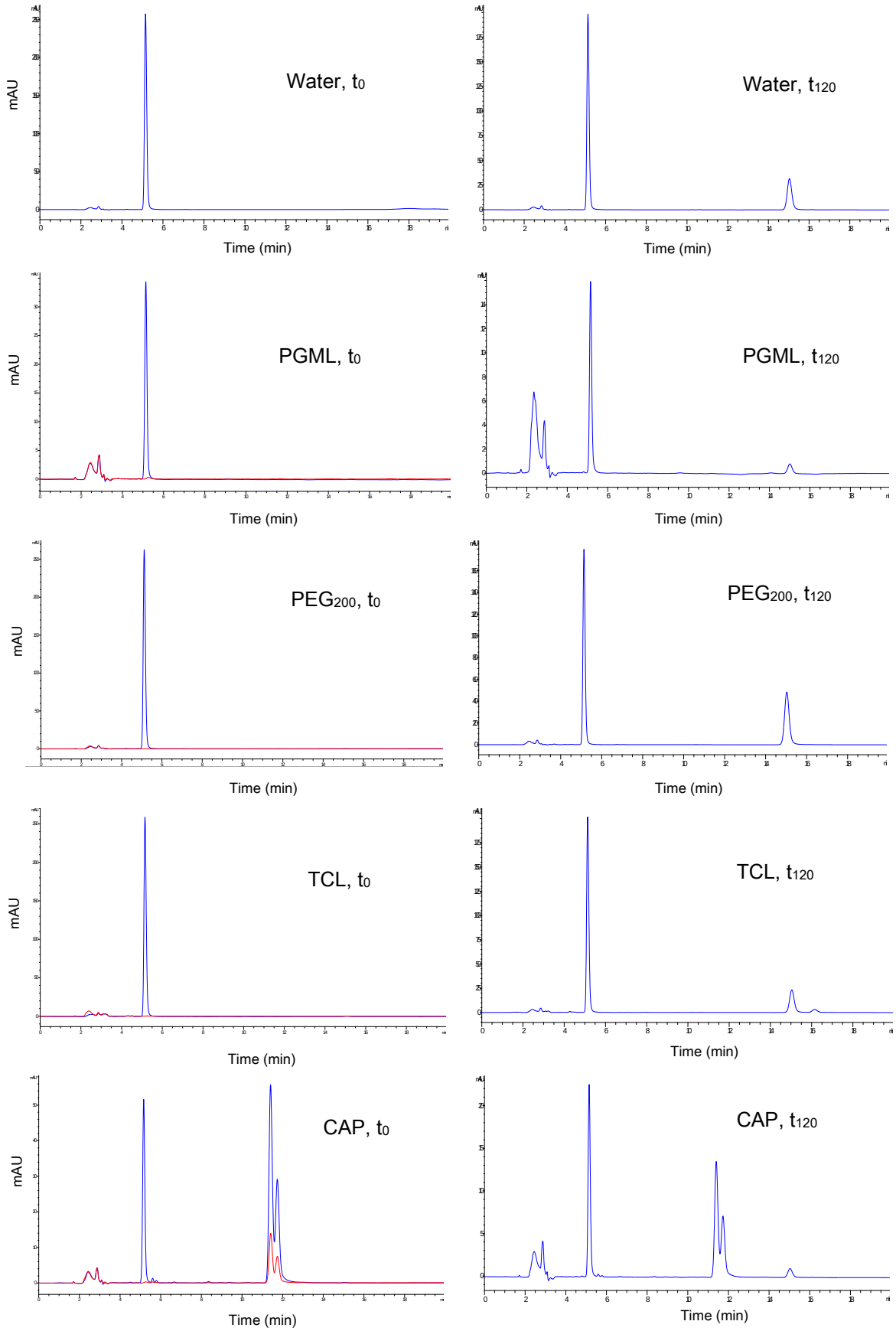

Figure 2-5 HPLC chromatograms of MOX in different vehicles at the initial time (t_0) and after 120 h (t_{120}). The red line represents HPLC chromatograms of the pure vehicles.

MOX was degraded under the stability conditions. However, the drug degradation rate depended on the vehicle in which it was dissolved. The quantity of MOX and the other compound changed over the testing period. However, the identification of the degradation products was confirmed by the MS technique as described in section 2.5.4. The initial concentrations of MOX in each vehicle were defined as 100 %, and subsequent sample concentrations were expressed as percentages of the initial concentrations as listed in Table 2-5. The drug was considered stable if not less than 90 % of the initial drug concentration remaining in the solutions at the end of study (FDA, 2008).

Rapid degradation was observed in PEG 200 and DMI at 24 h where 88.91 ± 1.61 and 82.26 ± 1.94 % of the initial concentrations remained in the solutions, respectively. However, a slower degradation rate of the drug occurred in water, PG, TCL, EtOH, PGL, PGML, and CAP solutions. Except for CAP, these solutions lost more than 10 % of their original potency for up to 120 h. At this time point, 82.39 ± 0.65, 78.33 ± 0.70, 89.96 ± 0.28, 88.76 ± 0.62, 85.51 ± 2.15, and 88.33 ± 4.04 % of MOX remained in these vehicles, respectively.

Table 2-5 The percentage of initial concentrations remaining of MOX in various vehicles at 32 °C during the stability study. Each value represents the mean ± SD; n=3.

Time (h)	Water	PG	TCL	PEG 200	DMI
0	100	100	100	100	100
24	96.17 ± 2.76	94.74 ± 2.36	94.11 ± 0.36	88.91 ± 1.61	82.26 ± 1.94
48	94.77 ± 1.18	92.56 ± 0.25	92.98 ± 1.21	83.62 ± 0.81	68.68 ± 1.72
72	88.86 ± 1.16	88.20 ± 1.54	88.68 ± 0.42	75.96 ± 1.99	52.44 ± 1.52
96	86.55 ± 1.15	83.09 ± 0.33	87.90 ± 0.41	71.79 ± 0.53	38.23 ± 0.96
120	82.39 ± 0.65	78.33 ± 0.70	89.96 ± 0.28	65.63 ± 2.15	25.61 ± 2.07

Time (h)	EtOH	PGL	PGML	CAP
0	100	100	100	100
24	94.08 ± 0.85	93.82 ± 1.75	95.79 ± 4.14	96.05 ± 0.72
48	91.35 ± 0.88	93.22 ± 2.32	91.12 ± 3.22	92.93 ± 1.38
72	88.46 ± 1.86	90.65 ± 1.72	89.95 ± 3.14	90.45 ± 1.11
96	88.99 ± 0.24	87.15 ± 0.44	89.50 ± 3.56	89.78 ± 1.39
120	88.76 ± 0.62	85.51 ± 2.15	88.33 ± 4.04	90.33 ± 2.16

In an earlier study conducted by Streinberg and Bada (1983), the thermal decomposition of peptides at neutral pH via diketopiperazine formation was demonstrated. The effect of temperature and pH on the stability of MOX in aqueous solution was previously reported (Gu and Strickley, 1987). It was found that the degradation pathway of this drug depended on the pH. At pH ≤ 4, moexipril diketopiperazine (MOX-DKP) was subject to intermolecular cyclization. In addition a small amount of moexiprilat (MOX-LAT) was formed. At pH > 5, the hydrolysis of the ester bond was responsible for giving the active diacid form. However, the effect of temperature on the distribution of degradation products was quite similar. The researchers concluded that the findings might be applied to other ACEIs which have a similar chemical structure.

The addition of organic solvent had also a profound effect on the degradation rate of MOX (Gu and Strickley, 1990). The authors investigated the stability of MOX in mixed aqueous-organic solutions at different percentages. The hydrolysis was inhibited with added organic solvent due to the decrease in water content. However, the formation of diketopiperazine increased with additional organic solvent. The effect of relative humidity and temperature on MOX stability during storage in the solid state was also evaluated (Stanisz, 2004). In the humidity and temperature ranged from 50 to 75 % and 60 to 90 °C, respectively, MOX degraded to form MOX-LAT and MOX-DKP.

2.5.2.2 Ramipril stability

All of the RAM mixtures were initially clear and colourless under natural light. The appearance of these solutions did not change throughout the study except for DMI where its colour turned yellow. Figure 2-6 shows HPLC chromatograms of RAM in different solvents at t_0 and t_{72}. These chromatograms revealed the main peak of analyte along with other related substances. The peak of a degradation product was detected in all the HPLC chromatograms, and at the same time it was clearly separated from the main peak. The unknown degradant was eluted [~13.5 min] after the elution of the main compound [~6.4 min]. Under reversed phase liquid chromatographic conditions, the more hydrophobic a compound is, the more it will be retained (Watson, 2012). A comparison of the retention time of RAM with that of its degradation product indicated that the latter was more hydrophobic than the former. Ren et al. (2008) and Pan et al. (2012) demonstrated that the elution of the degradation product depended on its polarity compared with the parent compound.

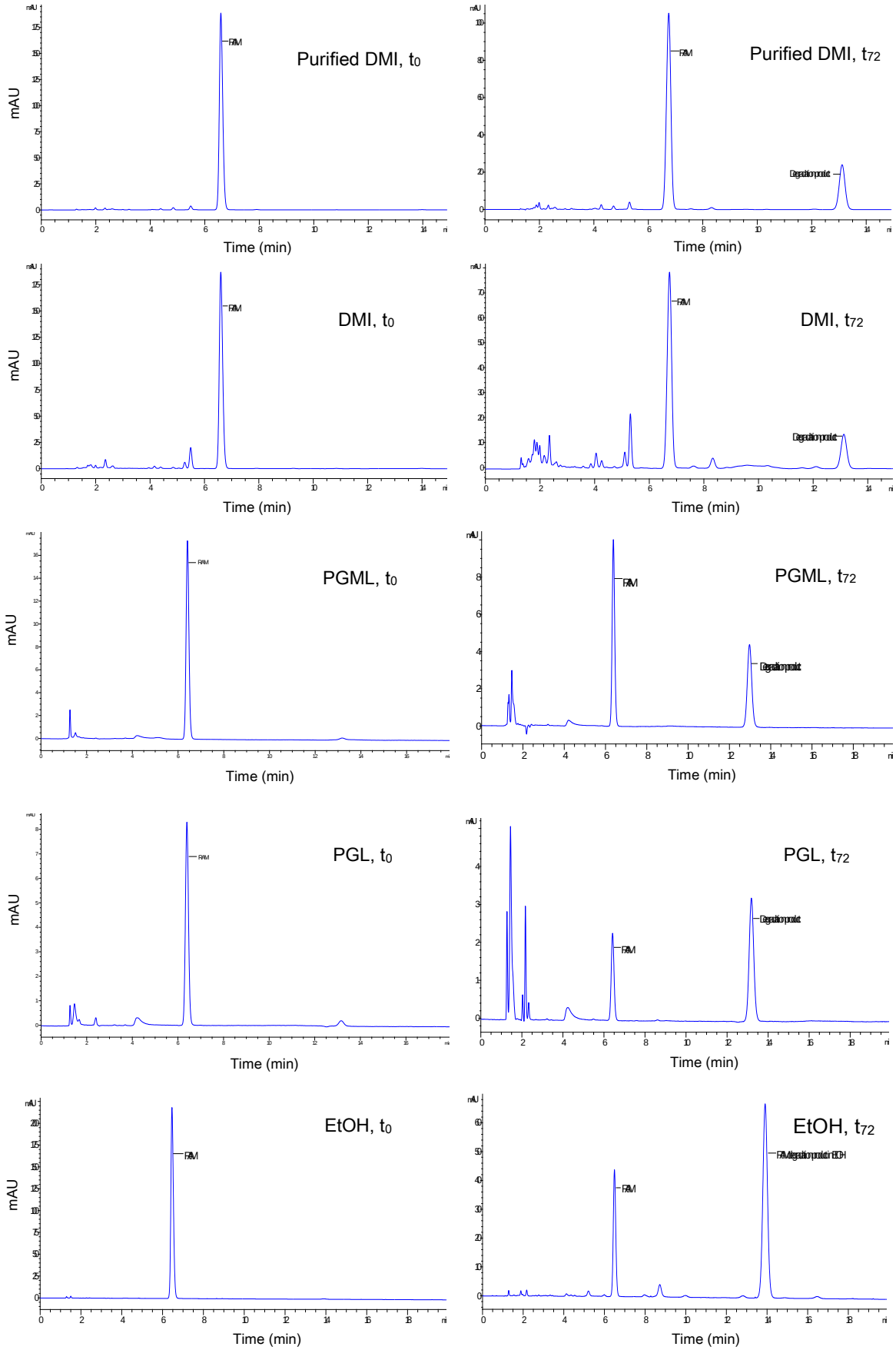

Figure 2-6 HPLC chromatograms of RAM in different vehicles at the initial time (t_0) and after 72 h (t_{72}).

As seen in Figure 2-6, the height of the RAM peak and the other compound changed over the testing period. HPLC analysis indicated that RAM underwent degradation in all the samples. Results of the percentage of unaltered concentration of drug in the different types of vehicles as a function of sampling times are listed in Table 2-6. RAM was most stable in LA, PG, PEG 200 and water. Less than 10 % loss occurred after five days at 32 ˚C.

It was also observed that RAM levels dropped below 90 % of the initial concentration at 24 h in both super refined DMI-LQ and DMI-PC where 89.66 ± 0.45 and 86.00 ± 0.28 % remained in these solutions, respectively (Table 2-6). However, after 96 h the degradation of RAM in DMI-PC was much more rapid than that in the purified DMI and therefore RAM showed higher stability in the latter vehicle. This might be attributed to the solvent purity. In the samples prepared in PGML, IPM, and PGL, RAM loss was more than 19 % at 24 h. The percentage of intact drug in these vehicles was 80.98 ± 0.33, 75.03 ± 1.76, and 62.67 ± 1.26 %, respectively, but after five days the loss had increased to about 60-75 %. Therefore, RAM underwent rapid degradation in these vehicles. These findings illustrated that the type of vehicle in which the drug was dissolved played an important role in the degradation process.

Table 2-6 The percentage of initial concentrations remaining of RAM in various vehicles at 32 °C during the stability study. Each value represents the mean ± SD; n=3.

Time (h)	LA	PGML	PGL	IPM	CAP	DMI	DMI (Purified)
0	100	100	100	100	100	100	100
24	98.35 ± 0.72	80.98 ± 0.33	62.67 ± 1.26	75.03 ± 1.76	90.50 ± 1.52	86.00 ± 0.28	89.66 ± 0.45
48	97.46 ± 0.11	69.03 ± 1.61	49.50 ± 2.50	57.58 ± 1.22	83.61 ± 2.18	70.48 ± 0.45	80.63 ± 0.63
72	97.19 ± 0.43	57.38 ± 1.46	36.69 ± 0.37	45.34 ± 0.28	77.34 ± 1.93	54.27 ± 0.27	72.42 ± 0.40
96	95.92 ± 0.32	49.79 ± 1.19	30.73 ± 0.66	36.76 ± 0.43	71.20 ± 0.97	40.76 ± 0.46	65.57 ± 0.61
120	94.74 ± 1.19	42.29 ± 1.03	25.67 ± 1.72	33.02 ± 1.08	65.88 ± 1.47		

Time (h)	TCL	PG	PENTA	PEG 200	PEG 400	EtOH	Water
0	100	100	100	100	100	100	100
24	97.83 ± 0.79	98.27 ± 0.48	96.64 ± 1.49	98.49 ± 0.66	94.56 ± 0.91	86.16 ± 1.70	100.01 ± 1.53
48	95.25 ± 0.15	98.31 ± 0.42	95.55 ± 1.85	98.24 ± 0.32	89.06 ± 0.33	77.47 ± 0.82	96.78 ± 1.87
72	92.15 ± 0.26	95.95 ± 0.54	92.50 ± 0.79	96.20 ± 0.06	85.79 ± 0.53	71.29 ± 1.07	99.21 ± 1.84
96	89.55 ± 0.69	95.43 ± 0.37	88.90 ± 1.10	95.64 ± 0.46	82.97 ± 0.52	64.32 ± 1.25	100.97 ± 2.29
120	87.89 ± 0.36	92.06 ± 0.76	84.63 ± 1.19	93.46 ± 0.48	77.72 ± 0.66	58.18 ± 1.96	98.69 ± 1.71

RAM stability in aqueous media has been previously reported (Allen et al., 1995; Hanysova et al., 2005). In the former study the drug mixed with water, apple juice, and apple sauce remained stable for 24 h at 23°C and for 48 h at 3°C (Allen et al., 1995). In the latter the effect of pH on RAM stability was examined (Hanysova et al., 2005). RAM was unstable in both alkaline and acidic media and the percentages of its related substances were pH-dependent. A recent study showed that aqueous solutions of enalapril and perindopril which have similar structure to RAM were prone to degradation (Roskar et al., 2009). Temperature and pH were the most important factors that affected the degradation rate. Furthermore, it was also shown that the structural element had a significant impact on the stability properties of ACEIs. Therefore, a further molecule, CILA, was selected to determine whether its chemical structure could be linked to the stability properties of the molecule.

2.5.2.3 Cilazapril stability

Like RAM, all CILA solutions were initially clear and colourless and remained colourless under normal light throughout the study. No precipitation was also observed with all tested solutions. The concentration of CILA at the initial time was used as a reference to determine the relative stability. The percentage of unaltered concentration of drug in each vehicle as a function of sampling times was calculated and tabulated in Table 2-7. Interestingly, CILA exhibited a very good stability in all the vehicles. Less than 6 % loss occurred after 5 days in the samples prepared in IPM, PGL, EtOH, water, PEG 200, LAB, PGML, CAP, and TCL. The percentage of intact drug in these vehicles ranged from 98.30 to 100.49 %.

Table 2-7 The percentage of initial concentrations remaining of CILA in various vehicles at 32 °C during the stability study. Each value represents the mean ± SD; n=3.

Time (h)	IPM	PGL	EtOH	Water	PEG 200
0	100	100	100	100	100
24	102.14 ± 3.52	100.63 ± 1.68	102.37 ± 0.77	99.26 ± 0.56	98.56 ± 0.39
48	100.76 ± 1.41	102.17 ± 1.56	103.17 ± 0.66	99.33 ± 1.41	97.59 ± 0.43
72	100.91 ± 1.56	99.62 ± 2.75	100.92 ± 0.32	98.77 ± 0.98	97.54 ± 0.36
96	101.77 ± 2.19	99.64 ± 3.88	100.06 ± 1.03	98.94 ± 0.87	98.13 ± 0.21
120	100.10 ± 1.66	99.79 ± 1.97	100.49 ± 0.53	99.69 ± 1.06	98.38 ± 0.22

Time (h)	PG	LAB	PGML	CAP	TCL	DPG
0	100	100	100	100	100	100
24	99.46 ± 0.57	101.58 ± 6.15	101.17 ± 1.51	101.01 ± 0.58	100.32 ± 0.48	99.23 ± 0.76
48	100.10 ± 0.74	96.30 ± 5.27	102.84 ± 2.12	103.97 ± 2.43	100.62 ± 0.71	98.51 ± 1.24
72	97.50 ± 0.53	101.31 ± 9.02	102.21 ± 2.30	101.86 ± 1.39	100.59 ± 0.22	98.01 ± 0.48
96	96.29 ± 0.84	102.92 ± 3.26	101.67 ± 1.57	102.46 ± 1.43	100.91 ± 0.37	96.64 ± 1.16
120	96.24 ± 0.77	98.59 ± 5.87	100.01 ± 1.57	100.21 ± 1.24	100.33 ± 0.65	93.88 ± 1.22

2.5.3 Comparison of the stability profiles of MOX, RAM, and CILA

As illustrated in Figure 2-7, CILA exhibited good stability compared with MOX and RAM. Examination of the chemical structure of a compound may provide some indication of chemical reactivity.

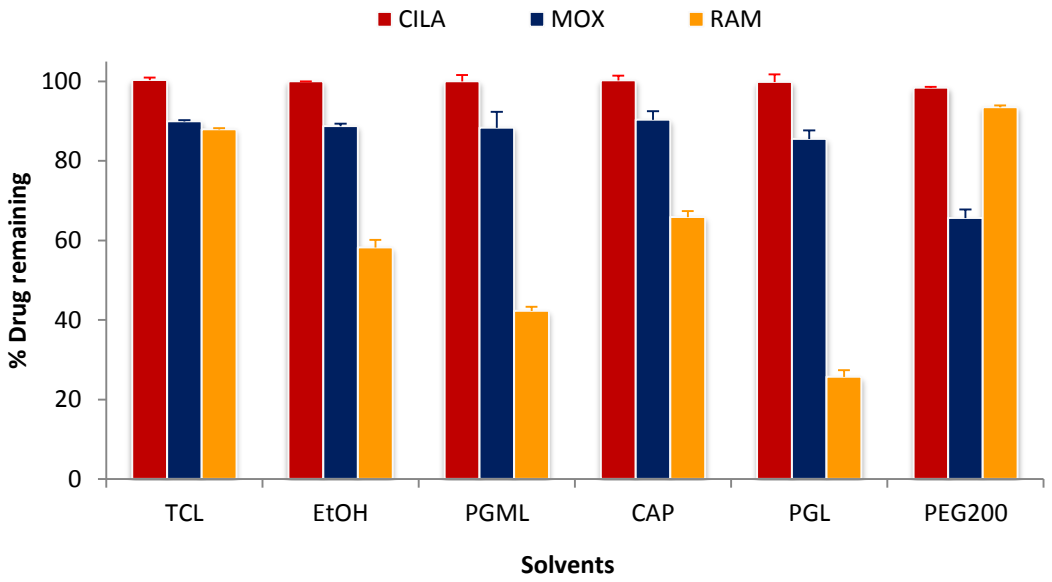

Figure 2-7 The percentage of each drug remaining after five days of the stability studies at 32 °C (mean ± SD; n=3)

As Figure 2-8 shows, MOX and RAM have a similar chemical structure and were prone to degradation as displayed in the present results. Their structure included an ester group and a similar structure, which suggested that the hydrolysis and cyclization processes were the most likely pathways of degradation (Roskar et al., 2009; Stanisz et al., 2013). The diketopiperazine form (DKP) is not active at all. However, CILA which had a different structure displayed good stability in all the selected vehicles. Based on the obtained stability results of MOX, RAM, and CILA and the comparison of the chemical structure of CILA with MOX and RAM it was concluded that the structural element had a marked influence on the stability properties of ACEIs.

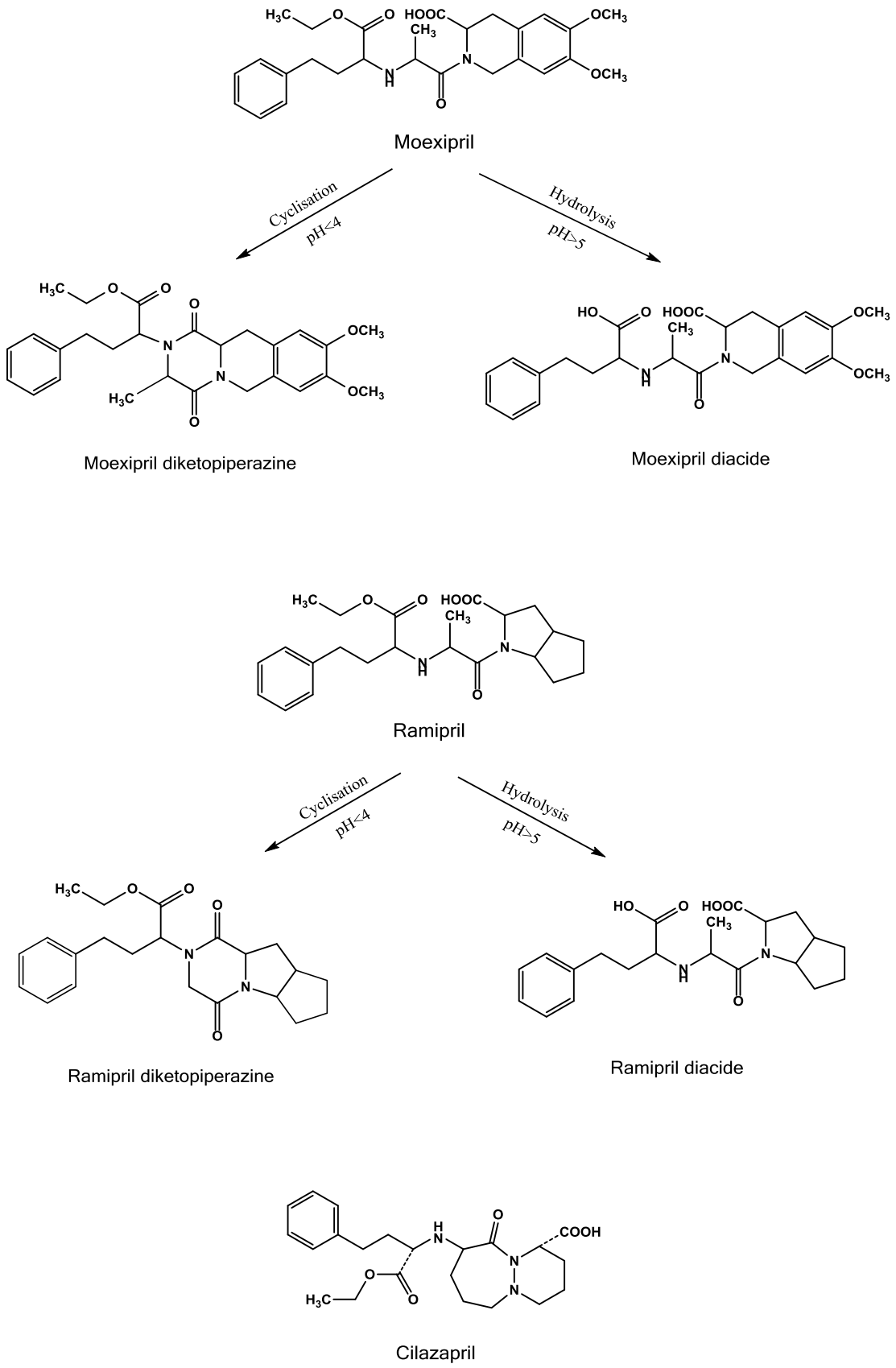

Figure 2-8 The relationship between the chemical structure of ACEIs and the degradation process.

2.5.4 Identification of the degradation products

2.5.4.1 Stress degradation studies

The separation and identification of all significant degradation products is required by the U.S. Food and Drug Administration (FDA, 2006). RAM in propylene glycol and ethanol underwent degradation under the thermal conditions (60 °C). These forced degradation studies showed the potential degradation product (Fauzee and Walker, 2013). The HPLC chromatograms obtained from samples prepared in PG and EtOH (Figure 2-9) treated with heat showed a well separated peak of RAM from an additional peak at different retention times (6.4 and 13.9 min for RAM and its main degradant, respectively).

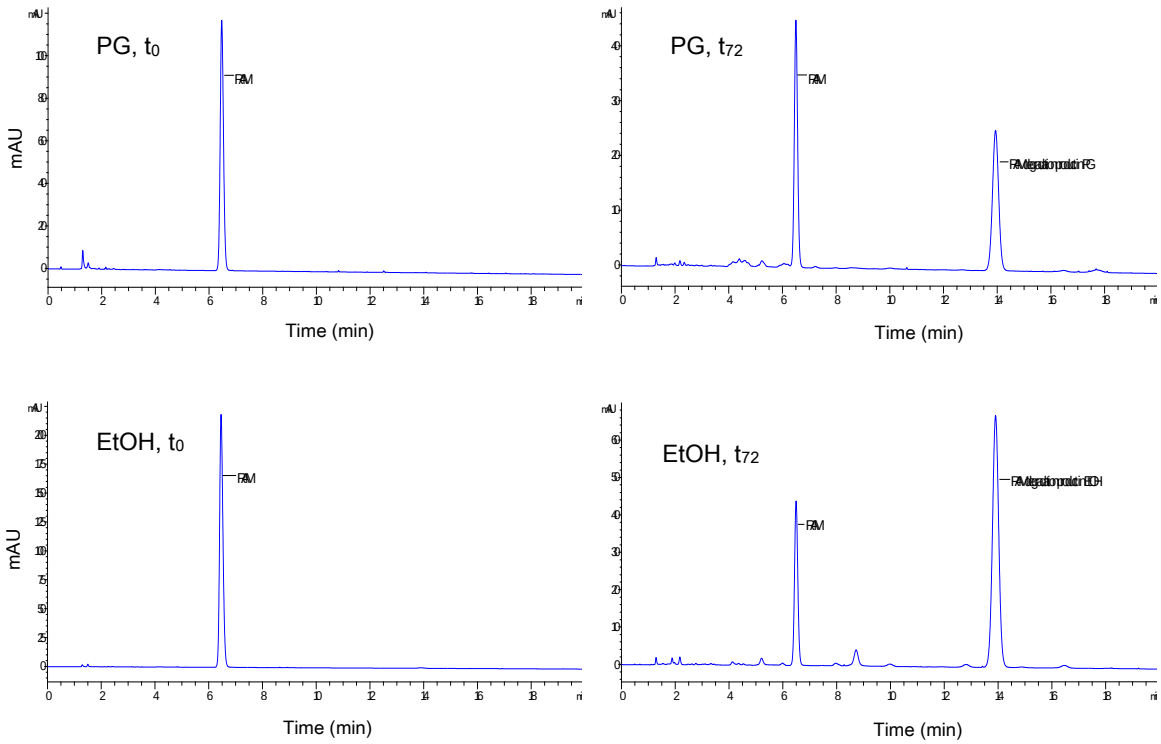

Figure 2-9 HPLC chromatograms of RAM in PG and EtOH at t_0 and at t_{72}

Figure 2-10 illustrates the peak of degradant collected from the HPLC effluent and then re-injected into the HPLC. The degradation compound was then analyzed by MS (section 2.5.4.2).

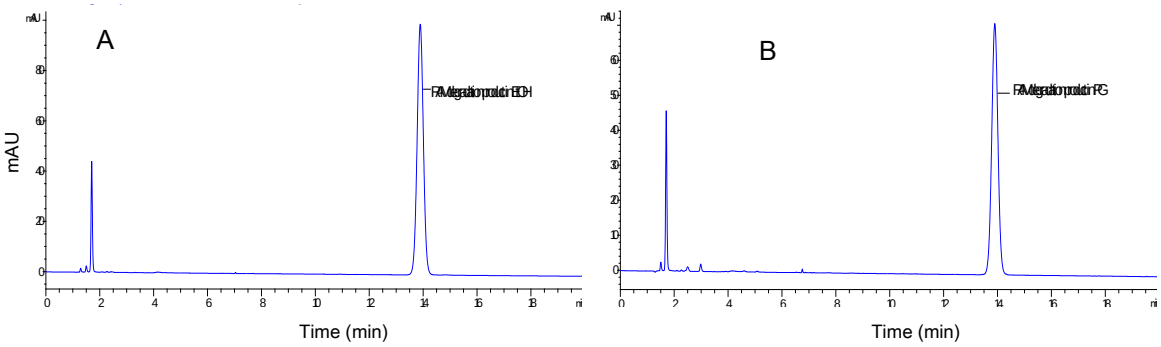

Figure 2-10 HPLC chromatograms of the main degradation product of RAM in EtOH (A) and PG (B).

Several impurities related to the degradation of RAM have been reported in literature (Shetgiri et al., 2008; De Diego et al., 2010) and British Pharmacopoeia (BP, 2013a). Shetgiri et al. (2008) and De Diego et al. (2010) reported RAM-DKP as the main degradant of RAM. The identity of the resultant degradation product was discovered by MS (section 2.5.4.2)

2.5.4.2 Mass Spectra interpretation

RAM in a water-methanol mixture was introduced into MS. Figure 2-11 shows the mass spectrum of the main compound, RAM. The mass spectrum was a plot of relative ion abundance versus m/z ratio. The peak produced at m/z=417 was called the base peak. This represented the commonest fragment ion formed and was assigned a height of 100, and the height of everything else was measured relative to this. From the positive-ion ESI mass spectrum of RAM, a molecular weight of 416 Da could be easily

determined as only the following ion was found in the mass spectrum: $[M+H]^+$ (m/z 417, relative abundance 100 %) with no sign of degradation.

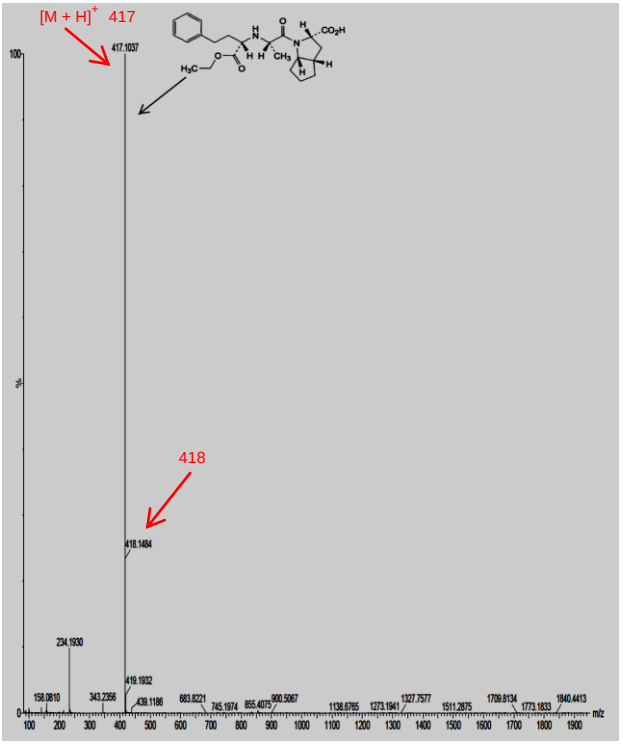

Figure 2-11 The mass spectrum of RAM obtained by ESI in the positive detection mode.

The positive-ion ESI mass spectra of the degradation product in EtOH and PG (Figure 2-12) show that intense peaks appeared at m/z 399 and 399, respectively with a relative abundance of 100 %. The mass of each peak corresponds to the mass of RAM-DKP, one of the specific impurities of RAM listed in the British Pharmacopeia (2013a). These results were in agreement with those of Shetgiri et al. (2008). The mass spectra also contained peaks at m/z 421 which were 23 mass units higher than the expected molecular mass. This was due to the addition of the sodium cation $[Na^+]$ instead of a proton $[H^+]$ during the ionization stage.

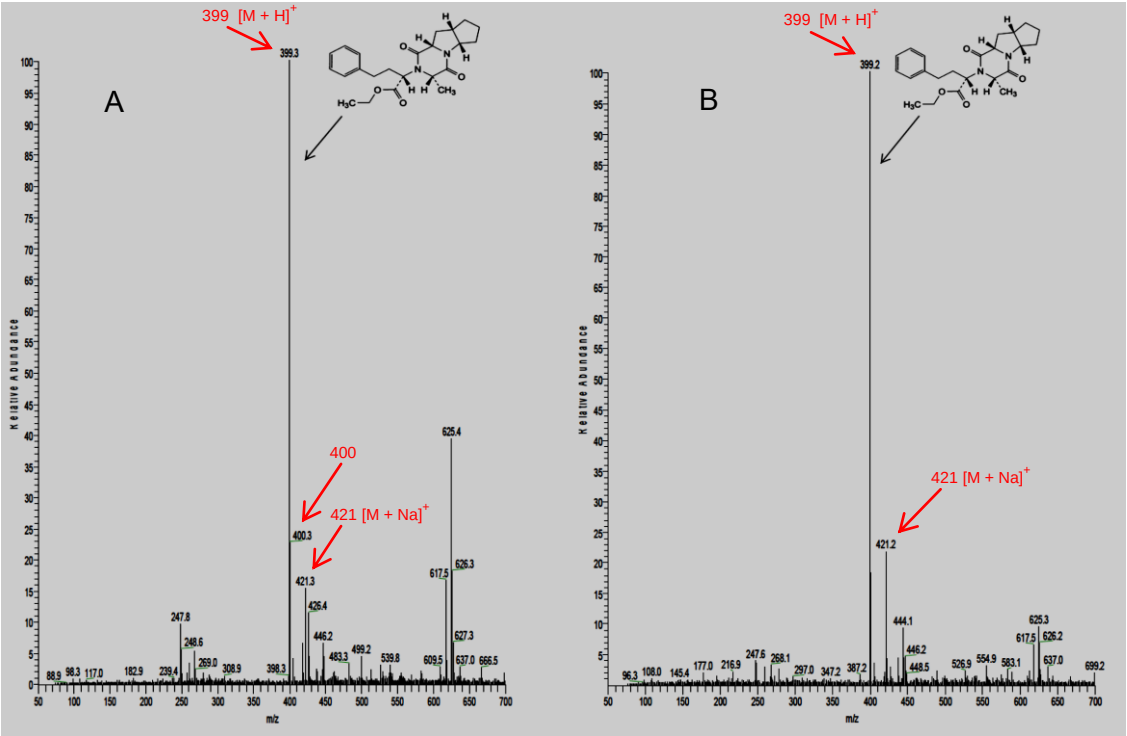

Figure 2-12 The mass spectrum of the RAM degradation product in EtOH (A) and PG (B) obtained by ESI in the positive detection mode.

Molecules in nature do not occur as isotopically pure species. Therefore, in Figure 2-11 the small peak (m/z = 418) located at one mass unit higher than the pseudo-molecular ion peak (m/z = 417) was due to the natural abundance of ^{13}C isotope. The same case was observed in the mass spectra of the degradant (Figure 2-12) where a small peak was found at m/z = 400. This peak was an isotope peak and had a much lower intensity than the pseudo-molecular ion peak as ^{13}C makes up about 1.1 % of the ^{12}C containing peak.

The MS spectra of RAM and its degradation product have shown that the difference in mass of the degradant pseudo-molecular ion and the RAM pseudo-molecular ion was 18. This was associated with the loss of the H_2O group. Therefore, the main compound underwent a cyclization process leading to RAM-DKP formation.

In comparison, the ESI mass spectrum of the degradation product of MOX (Figure 2-13) illustrates a protonated pseudo-molecular ion $[M+H]^+$ at m/z 481 in the positive ion mode, which was 18 units less than that of the MOX protonated pseudo-molecular ion (m/z=499). The MS spectrum also shows ions peak at m/z 503 $[M+Na]^+$ and 518 $[M+K]^+$ as sodium and potassium adducts, respectively. MOX, the main compound, was also detected as $[M+H]^+$ of m/z 499. These data confirmed that the major degradation product observed in Figure 2-5 was MOX-DKP with the molecular formula of $C_{27}H_{32}N_2O_6$.

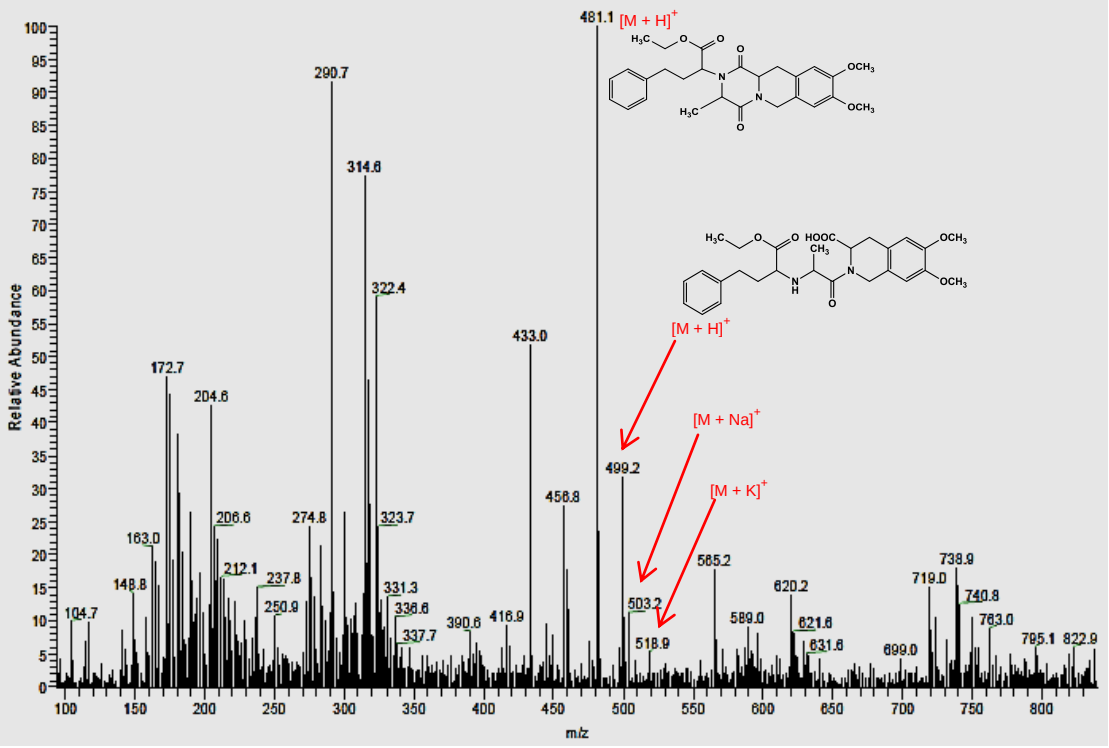

Figure 2-13 The mass spectrum of the MOX degradation product in water residue obtained by ESI in the positive detection mode

As seen in Figure 2-14, the MS spectrum of MOX shows the presence of a protonated pseudo-molecular ion $[M+H]^+$ that was identified at m/z 499 with a sign of degradation at m/z 481 which represented the chemical formula of MOX-DKP.

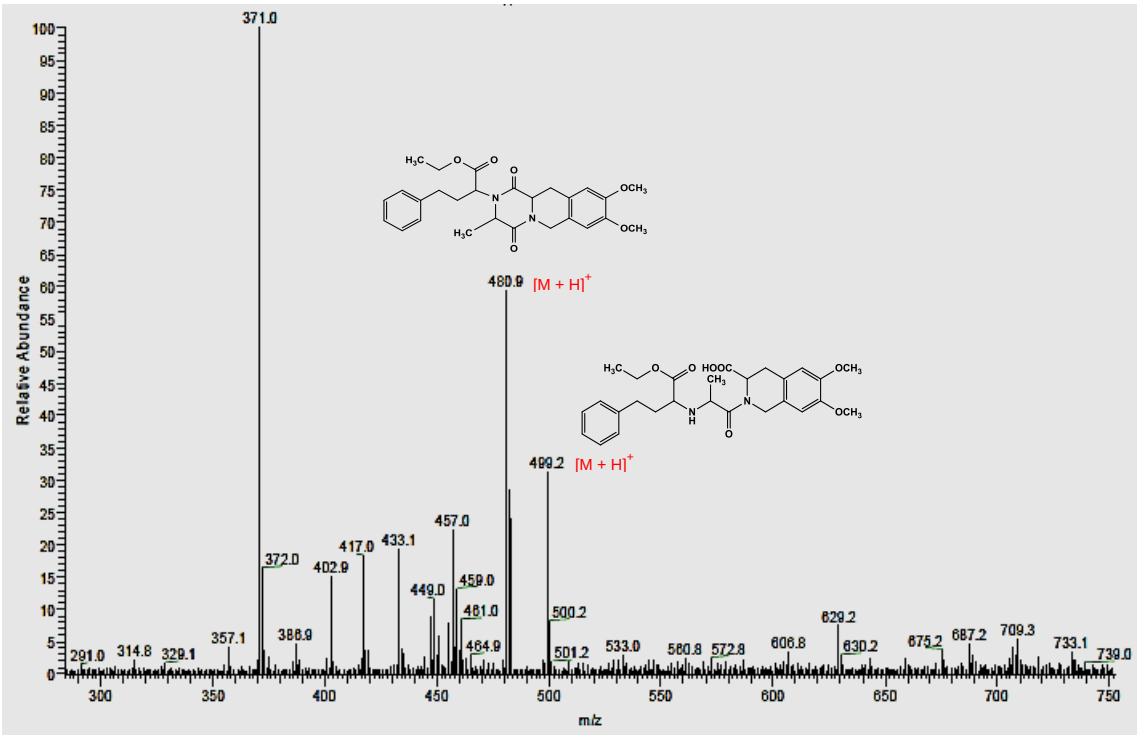

Figure 2-14 The mass spectrum of the MOX degradation product in DMI obtained by ESI in the positive detection mode.

2.5.4.3 Confirmation of RAM degradation product by HPLC using RAM-DKP standard.

As shown in Figure 2-15 the retention time of RAM-DKP standard was 13 min. This retention time matched that of the degradation product observed in the HPLC chromatograms (Figure 2-6) in different types of vehicles. As a result, the main degradation compound of RAM in the selected vehicles at 32 °C was RAM-DKP.

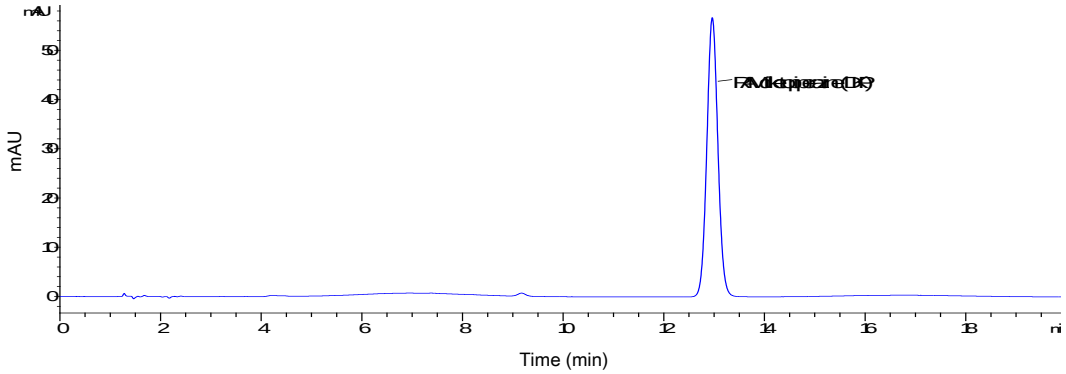

Figure 2-15 HPLC chromatograms of RAM-DKP standard

2.6 Conclusions

Designing and conducting a proper stability study that would generate appropriate stability data are essential for the safety, efficacy, and quality of pharmaceutical products. In the present study, HPLC methods for the determination of MOX, RAM and CILA were developed and validated. These validated HPLC methods were demonstrated to be linear, specific, accurate, precise, and robust within the specified range. They allowed quantification of the selected ACEIs in the presence of their degradation products. Stability data of MOX and RAM in different solvents showed that these drugs were prone to degradation, irrespective of the vehicle used. However, the type of vehicle in which the drug was dissolved played an important role in the degradation process. In contrast, CILA exhibited very good stability in all the selected vehicles. Roskar et al. (2009) concluded that the chemical structure of ACEIs might have an impact on their stability properties. Based on the findings of Roskar et al. (2009) and the present results, it was confirmed that the stability of CILA in a wide range of vehicles was attributed to its chemical structure which was different from that of MOX and RAM. As recommended by the US FDA, the isolation and identification of MOX-DKP and RAM-DKP as the main degradation products of MOX and RAM, respectively were achieved using MS. The findings demonstrated that the formation of DKP occurred from the intramolecular cyclization process. We report for the first time that CILA was stable in a range of hydrophilic and lipophilic vehicles. Therefore, it appears to be a promising candidate in terms of its stability and physicochemical properties for design stable formulations. These formulations will be tested on porcine skin in order to investigate of the possibility of delivering this compound across the skin.

Chapter 3

Development of topical formulations containing ACEIs

3 Development of topical formulations containing ACEIs

3.1 Introduction

A successful formulation must (i) be physically and chemically stable (Allen et al., 2011b), (ii) release the active pharmaceutical ingredient (API) from the formulation and deliver it into the skin (Lane et al., 2012), and (iii) be easy to apply to patients. Therefore, preformulation studies are conducted at an early stage. The stability and solubility of the API in a range of vehicles are assessed, and compatibility studies with solvent combinations and excipients are performed. In the previous chapter, the stability of ACEIs in a range of hydrophilic and lipophilic vehicles was evaluated. In this chapter, the solubility of RAM and CILA in various solvent systems will be initially determined followed by the design of topical formulations of ACEIs. Furthermore, the amount of the drug permeated through porcine and human skin will be measured by conducting *in vitro* permeation studies in order (i) to ensure that drug is released from the formulation and (ii) to measure the rate and extent of the drug permeation across the skin. This will allow us to identify the most promising formulations. Figure 3-1 illustrates the stages of developing topical products.

Skin absorption of compounds is a passive diffusion process that can be described by Fick's first law of diffusion $J=DKC/h$, where J is the steady-state flux of the permeant through a membrane, D is the diffusion coefficient, K is the vehicle-membrane partition coefficient, C is the concentration of the permeant, h is the length of the diffusion path. As described in chapter one, the primary factors affecting percutaneous absorption of a compound are its physicochemical properties, in particular, molecular weight, solubility, lipophilicity, ionization, and melting point (Lane

et al., 2012). These factors can enable formulators to make a reasonable judgment about the possibility of a given compound to cross the SC.

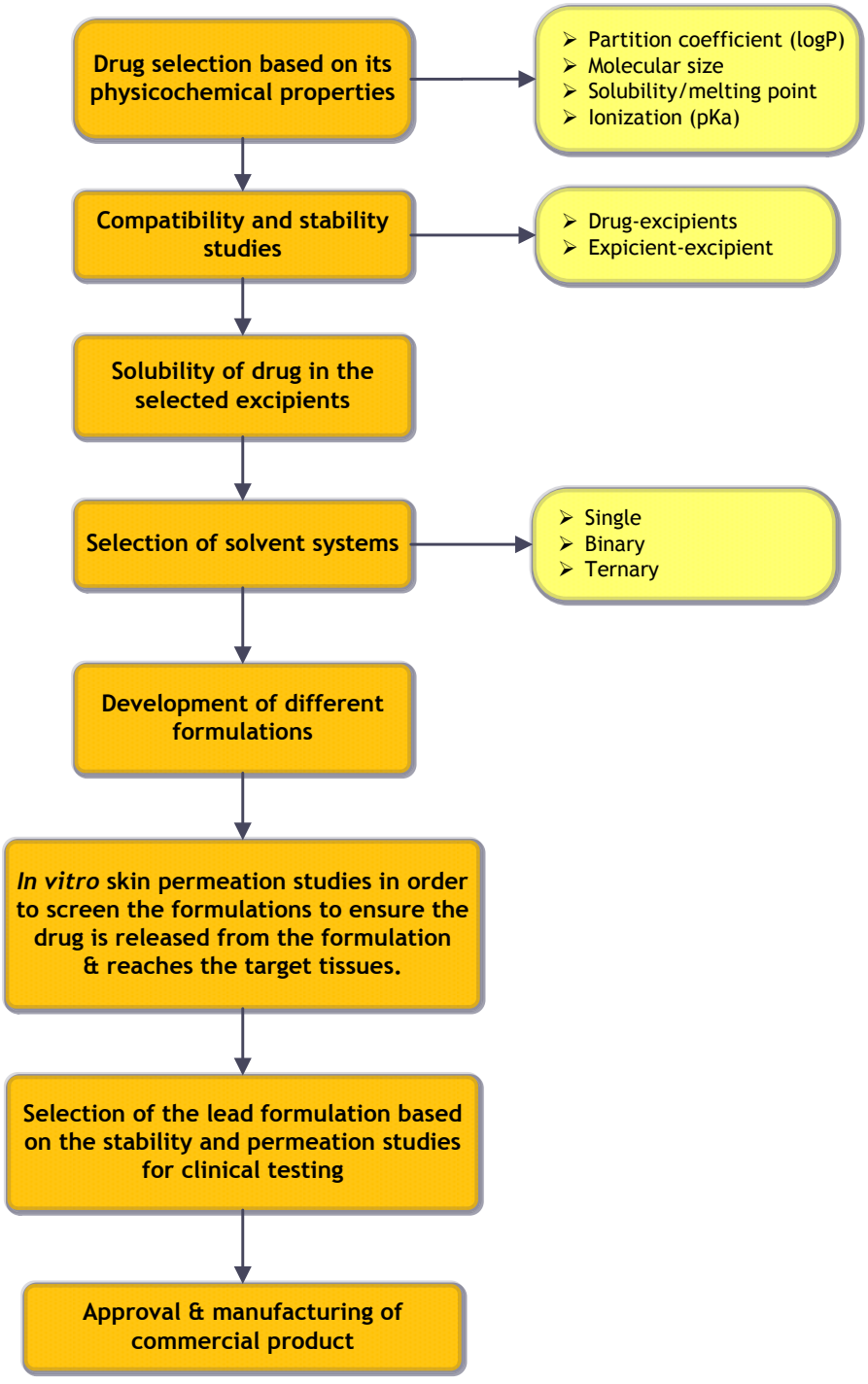

Figure 3-1 Topical formulation development flowchart

Drug candidates for transdermal delivery should possess a suitable molecular weight ≤ 500 Da, appropriate lipophilicity (log P = 1-3), and high potency ≤ 20 mg/day. Although the lipophilicity of the permeant is very important because of the lipophilic nature of the SC, its aqueous solubility is equally important because of the water content of the SC. RAM and CILA are good candidates to be formulated in topical formulations because of their physicochemical characteristics as shown in Table 1-1.

Besides the physicochemical properties of the compound, formulation and skin exposure can also influence skin absorption (Howes et al., 1996; Karadzovska et al., 2012). These include the vehicle, the dose applied, and the duration of exposure. Vehicles in which the compound is dissolved can have an impact on the absorption rate. They can modify the drug diffusity or drug solubility in skin or a combination of both. This results in an alteration of the structure of the skin, facilitating the drug transport across the skin. During the formulation development stage, a range of vehicles need to be evaluated in order to obtain the desired permeation parameters.

Measuring percutaneous absorption *in vitro* can provide an economical and practical alternative to clinical trials for screening large numbers of topical formulations. This can be achieved by using Franz diffusion cells (Franz, 1975) as described in chapter one. Moreover, designing *in vitro* permeation experiments requires a number of factors to be considered in order to simulate the *in vivo* situation and provide useful data (Bronaugh et al., 2005; OECD, 2010; Finnin et al., 2012). These include the source of skin, the choice of vehicle, membrane temperature, the receptor medium, and the amount of formulation applied as outlined in the main introduction.

3.2 Aims

The aims of this study were firstly to evaluate the solubility of RAM and CILA in different solvent systems in order to identify candidate solvents for designing dermal formulations and secondly to assess the transport of these drugs from the formulations across human epidermis and porcine ear skin.

3.3 Materials

RAM and CILA (purity: unknown) were a donation from Ranbaxy laboratories Ltd (Punjab, India). Cilazaprilat was purchased from Toronto Research Chemicals Inc. (Toronto, Canada). Propylene glycol (PG) and isopropyl myristate (IPM), phenylboronic acid and 1,2 butanediol were purchased from Sigma-Aldrich (UK). Polyethylene glycol (PEG) 200 was from Fluka (UK). Propylene glycol monocaprylate or Capryol® 90 (CAP), propylene glycol monolaurate (PGML), propylene glycol laurate (PGL), dipropylene glycol (DPG), diethyleneglycol monoethyl ether or Transcutol® (TCL), and propylene glycol dicaprylate/dicaprate or Labrafac PG® (LAB) were a gift from Gattefosse (Cedex, France). Methanol, water, potassium dihydrogen phosphate (KH_2PO_4), orthophosphoric acid (all HPLC grade) and phosphate buffer saline (PBS, pH 7.4) tablets were purchased from Fisher Scientific Ltd (Leicestershire, UK). Deionized water was prepared using USF ELGA Option 3 water purifier system.

3.4 Methods

3.4.1 HPLC analysis of CILA and cilazaprilat

CILA and its metabolite, cilazaprilat, were detected and quantified by an Agilent 1200 series HPLC System (Agilent Ltd, UK) which consisted of a G1311A quaternary pump, G1316A UV detector, G1329A auto-sampler, G1322A vacuum degasser, and solvent module. The data were acquired and processed using HP Chemstation software & Computer control. All chromatographic experiments were performed in a gradient mode in order to avoid interfering substances detected at the retention time corresponding to cilazaprilat peak. These substances released from the dermal side of the skin during the permeation studies. The chromatographic procedure was carried out as follows: a Synergi polar-RP (250 x 4.6 mm) HPLC column was operated at 40 ºC. The column was purchased from Phenomenex, UK. The injection volume was 15 µl. The mobile phase consisted of methanol (solvent A) and 0.01 M KH_2PO_4 adjusted to pH 2.5 with orthophosphoric acid (solvent B). The column was equilibrated with a mixture of solvent A and solvent B (45:55 v/v). A linear gradient elution was carried out by increasing the percentage of solvent A to reach 80 % over 12 minutes from the moment of injection followed by decreasing the percentage of solvent A to 45 %. This percentage was maintained for 4 minutes to equilibrate the column before the next sample was injected. Analysis was completed within 16 min with a flow rate of 1 ml/min and the eluate was monitored by an UV detector set at a wavelength of 210 nm. The standard solutions of cilazapril and cilazaprilat were prepared at seven different concentrations 0.5, 1, 2, 5, 10, 15 and 30 µg/ml.

3.4.2 GC analysis of PG and TCL

3.4.2.1 Propylene glycol

The analysis of PG was performed using HP-5 (30 m × 0.32 mm × 0.25 µm) Agilent GC column packed with 5 % phenyl-methylpolysiloxane (Agilent Technologies, UK). Nitrogen was used as a carrier gas at a flow rate of 2 ml/min. The column was operated under the following gradient mode: initial temperature was held at 100 ºC for 2 minutes and then increased to 280 ºC at a rate of 30 ºC/min (with a total run time of 8 minutes). The temperature of the injector and detector was 250 ºC and 300 ºC, respectively. The internal standard (IS) was 1,2 butanediol in methanol at a concentration of 0.6 µmol/ml. In order to increase the peak detection and the method sensitivity, the IS and PG were derivatised with phenylboronic acid using the protocol described by Porter and Auansakul (1982). In brief, a 50 µl aliquot of sample or standard was placed in a 0.5 ml centrifuge tube and then 50 µl of the IS previously prepared was added. After mixing, 100 µl of a 40 mM phenylboronic acid in acetone was immediately added to the mixture before injection. 1 µl of the resultant mixture was injected into the GC under the split mode (25:1) and the data were acquired and processed using HP Chemstation® software and computer control. The standards were prepared in water at different concentrations (0.03, 0.05, 0.13, 0.26, 0.52, 1.04 and 2.07 mg/ml. The concentration of PG in each sample was then determined by comparing the peak area ratio (PG/IS) of the sample directly with the standard curve.

3.4.2.2 Transcutol®

The analysis of TCL was performed using HP-ULTRA 1 (25 m × 0.2 mm × 0.33 µm) Agilent GC column packed with 100 % dimethylpolysiloxane (Agilent

Technologies, UK). Nitrogen was used as a carrier gas at a flow rate of 1 ml/min. The column was operated under the following gradient mode: initial temperature was held at 90 ºC for 3 minutes, increased to 200 ºC at a rate of 30 ºC/min and then held at 200ºC for 1 minute (with a total run time of ~7.7 minutes). The temperature of the injector and detector was 300 ºC and 250 ºC, respectively. The standards were prepared in water at different concentrations (0.03, 0.05, 0.12, 0.25, 0.50, 0.99 and 1.98 mg/ml. 2 µl of the resultant mixture was injected into GC under the split mode (75:1) and the data were acquired and processed using HP Chemstation® software and computer control.

3.4.3 HPLC and GC methods validation

The HPLC and GC methods were validated prior to use for parameters such as linearity, specificity, limits of detection and quantification, accuracy, precision, and system suitability according to the British Pharmacopeia (BP, 2013b) and the ICH guidelines Q2 (R1) for validation of analytical procedures (ICH, 2005).

3.4.4 Solubility studies

The solubility studies of RAM and CILA in various single solvents or solvent mixtures were the first stage of topical formulation development. They were conducted to understand the affinity of the drug for each solvent and therefore to determine the concentration of drug in the final formulation. Either the water bath or rotator method was used in order to determine the drug solubility. For the water bath method (Figure 3-2), excess amounts of the drug were individually transferred to capped soda glass specimen tubes (50 x 25 mm) containing 3 ml of each solvent. The suspensions

were stirred using 12 mm magnetic stirring bars at 32 ˚C for 24 and 48 h. At the end of the specified time the suspensions were transferred into pre-warmed centrifuge tubes and directly centrifuged at 32 ˚C using a temperature controlled centrifuge (Eppendorf® 5415, Germany) for 15 min at 12000 rpm. Aliquots from the supernatants were injected into the HPLC after appropriate dilution with the mobile phase. All the experiments were repeated in triplicate.

Figure 3-2 Determining the solubility of drug using the water bath method

In the rotator method (Figure 3-3), an excess amount of the drug was added to 1 ml of the solvent placed in a 1.5 ml centrifuge tube. The tubes were then closed and attached to the rotary plate rotating at a rate of 25 rpm. The rotator was then placed in a temperature controlled oven held at 32 ˚C and the tubes were rotated for 48 h. This period was adequate to obtain equilibrium in the solvents as there was no significant difference (p > 0.05) between the 24 and 48 h solubility of RAM. The resulting suspensions were directly centrifuged at 32 ˚C using a temperature controlled

Eppendorf® centrifuge for 15 min at 12000 rpm. An aliquot of each supernatant was withdrawn and then analyzed by the HPLC after appropriate dilution with the mobile phase. The solubility was determined in triplicate.

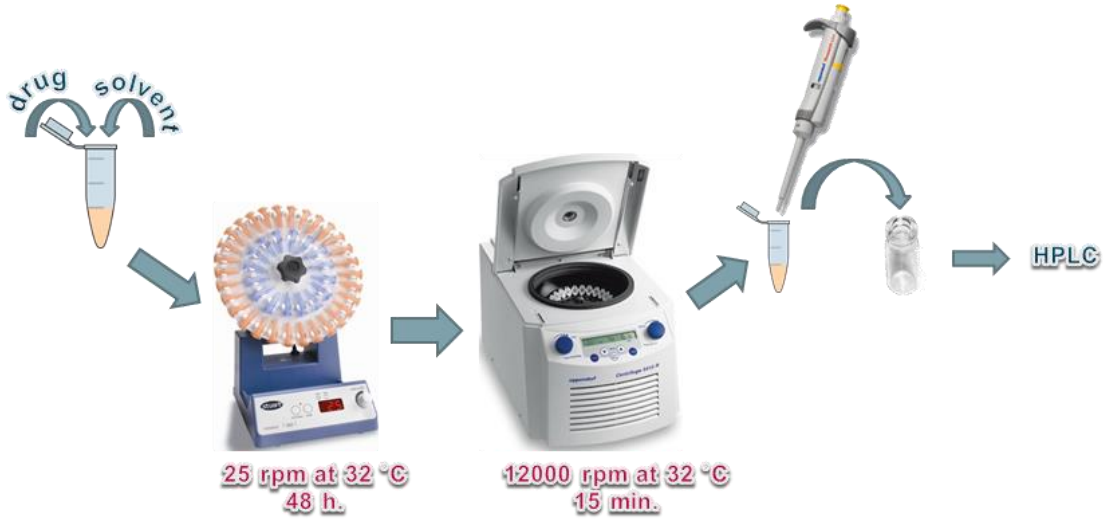

Figure 3-3 Determining the solubility of drug using the rotator method

3.4.5 Solubility parameter

The solubility parameter (δ) has been applied in both the cosmetic and pharmaceutical industries to estimate the co-solubility of two materials. A difference of less than two between the δ of two materials usually indicates mutual solubility (Khalil and Martin, 1967; Vaughan, 1985). The solubility parameters were calculated for RAM and CILA and all vehicles studied using the Molecular Modelling Pro® software (version 6.3.3). The chemical structures of the drugs and vehicles were drawn and then the values of solubility parameter were given by the software. The solubility parameter for a mixture of solvents (δ_{mix}) was calculated (Gonzalez et al., 1994; Herrador and Gonzalez, 1997) using Equation 3.1.

$\delta_{mix} = f_a\delta_a + f_b\delta_b + f_c\delta_c$ …… (3.1)

Where f: the volume fraction of a solvent in the mixed solvents

δ: the solubility parameter of a solvent.

a, b, and c are the solvents.

3.4.6 Miscibility studies

Miscibility studies were conducted with ternary solvent combinations in order to investigate the miscibility of the solvents. The combinations tested were IPM:CAP:PG, IPM:CAP:PEG 200, and IPM:CAP:TCL. A volume fraction of each solvent in each mixture was withdrawn using adjustable Eppendorf® pipettes, transferred to capped soda glass specimen tubes (50 x 12 mm), and then vortexed for 2 minutes. Following vortexing, the mixtures were allowed to settle at room temperature for 24 h. Each mixture was inspected visually for clarity. The mixture was considered miscible when a clear and transparent mixture was visualized. On the other hand, if the mixture formed separate layers or the whole mixture was cloudy, it was considered as immiscible. Methylene blue dye which dissolves more in the aqueous media was added to the mixture. When the dye was added, miscible mixtures had a homogeneous blue colour, but for immiscible mixtures, separate layers with distinct blueness were observed. A ternary phase diagram for each mixture was constructed using the data analysis software, Origin Pro® 8.1 (Origin Lab Corporation, US).

3.4.7 Partition coefficient (n-octanol/water)

The partition coefficient (P) is defined as the ratio of the equilibrium concentrations of a dissolved substance in two immiscible solvents such as water and

n-octanol (OECD, 1995; EPA, 1996). It is usually expressed as its logarithm form (log P) as shown in Equation 3.2.

$$\log P_{o/w} = \log\left[\frac{C_{n-octanol}}{C_{water}}\right] \quad \text{..... (3.2)}$$

Before determining the partition coefficient experimentally (OECD, 1995; EPA, 1996), the two pure solvents were mutually presaturated with each other. This was achieved by shaking the solvents with each other at room temperature for 24 h using a mechanical shaker to achieve a saturation state. The mixture was then let to stand for 24 h to allow the phases to separate. A stock solution of CILA was prepared in n-octanol at a concentration of 2 mg/ml. The actual concentration of this stock solution was determined by HPLC before it was used to determine the partition coefficient. The partition coefficient experiment was carried out in triplicate under three different test conditions. In the first, an equal volume ratio of n-octanol and water was added; in the second, twice the volume of n-octanol was added; and in the third, half the volume of n-octanol was added. The tubes were attached to a rotary plate rotating at 25 rpm for 1 h. The rotator was placed in a temperature controlled room held at 23˚C. In order to separate the two phases, the mixture was left to stand for 24 h at room temperature (23˚C). The concentrations of CILA in the two separated phases were determined. This was done by taking an aliquot from each of the two phases and then analysing them by the HPLC after an appropriated dilution using methanol in order to ensure the miscibility of the octanol with the mobile phase. The total quantity of CILA present in

both phases was calculated and compared with the original quantity introduced. The partition coefficient of RAM was not determined because of its stability issues.

3.4.8 Preparation of the skin membrane

3.4.8.1 Porcine ear skin

Porcine ears were obtained from the slaughter house. After cleaning under cold running water in order to remove all attached residues, the ears were blotted using soft tissues. Any visible hairs on the outer side of the ear were cut carefully using scissors. Care was taken while using the scissors in order to avoid damage to the SC. The whole skin of the outer region of the ear was carefully separated from the underlying cartilage with the aid of a scalpel with small cutting movements in the connective tissues located between the skin and the cartilage. After that both sides of the whole skin were washed under running deionised water and then the skin was placed in a basin containing deionized water. The skin was then removed from the water, floated onto an aluminium foil, and either used immediately or stored at -25 ˚C until required. The preparation stages of porcine ear skin are shown in Figure 3-4

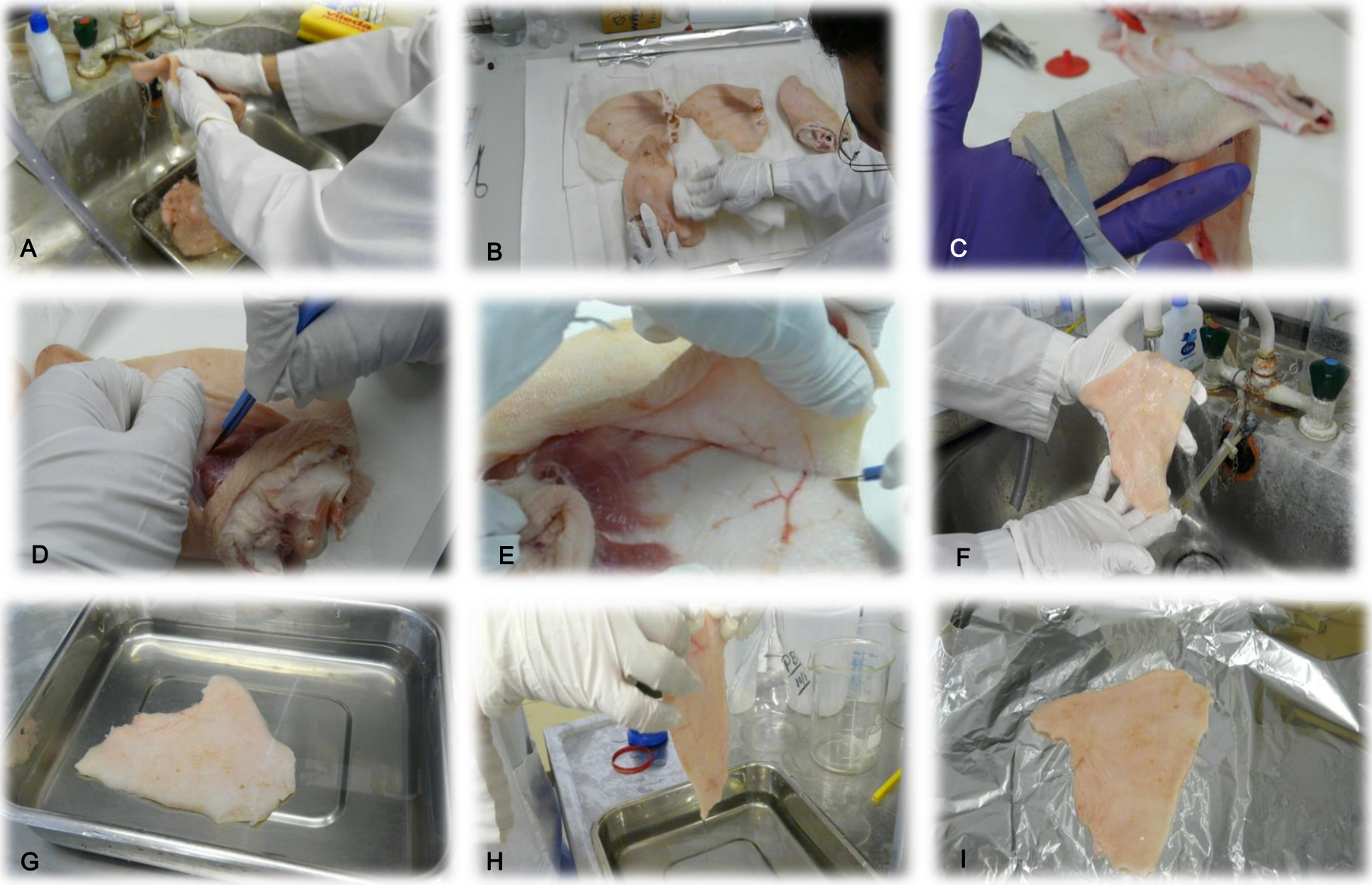

Figure 3-4 The preparation stages of porcine ear skin. A: cleaning; B: drying; C: cutting hair; D and E: separating; F: washing; G: floating in deionized water; H: removing from water; I: spreading the prepared skin on aluminum foil.

3.4.8.2 Human epidermis

Human skin tissue was obtained after cosmetic surgery (research and ethics committee reference “06/HRE04/37”) and stored in a freezer at -20˚C until required. The human epidermis was prepared using the heat separation technique (Kligman and Christophers, 1963). Excised human skin was placed on a cork plate. Part of the subcutaneous layer was trimmed using a scalpel. In a large beaker, the water was heated to about 65°C using a hot plate and then stirred from time to time until its temperature exactly reached 60 ˚C. The skin was tightly held with the aid of a forceps, immersed in the hot water, and stirred for 45 seconds. The skin was then removed from the water and placed on the cork plate again with the dermal side facing down. With the aid of the forceps one of the skin edges was held from the remaining of subcutaneous layer and stretched. The epidermis layer was carefully separated by rubbing and peeling the upper layer using the index finger starting from the sides towards the middle. The skin was kept well stretched at all times. The separated epidermis was carefully uncoiled inside a basin containing deionised water with the SC side up. The epidermis was then removed by placing a filter paper (Whatman grade No.1, UK) underneath it and lifting the filter paper carefully. The separated epidermis was left on another filter paper to dry, covered also with another filter paper, wrapped with aluminium foil, and then stored in the freezer at -20˚C (Swarbrick et al., 1982; Harrison et al., 1984) until required. On the day of the permeation studies the frozen prepared epidermis was removed from the freezer and cut into circles using a stainless steel puncher.

3.4.9 Permeation studies

Permeation studies were carried out using glass Franz-type diffusion cells having a cross-sectional area of approximately 1 cm^2 and a receptor volume of approximately 2.3 ml. Human epidermis or porcine ear skin was cut into circular sections (approximately 2.5 cm in diameter). The skin was then mounted between the two chambers with the SC side facing the donor compartment. Silicone grease was used to avoid leakage between the skin and chambers which in turn were secured with a clamp. Phosphate buffer saline (PBS) solution pH 7.4, containing 0.01 % w/v sodium azide to retard microbial growth (Shaikh et al., 1996), was used as the receptor medium. The receptor fluid was degassed for 25 min. using a Thermolyne Nuova II® magnetic stirrer connected to a vacuum pump. The receptor medium was then transferred to the receptor compartment with a micro magnetic stirring bar (5 mm) in order to keep the receptor solution homogenous in concentration and temperature.

The skin integrity was checked by measuring the electrical resistance (impedance) of each cell (Lawrence, 1997; Fasano et al., 2002; Karande et al., 2006). This was achieved by filling the donor compartment with PBS and then inserting the two stainless steel electrodes of the impedance meter, one in each compartment. The higher the conductivity of ions through the membrane, the lower the impedance value would be recorded and therefore the poorer skin barrier functions. The PBS in the donor compartment was then removed using a plastic Pasteur pipette. The cells were then placed in a water bath held at 34 ˚C and allowed to equilibrate for 1 h, giving a temperature of 32 ºC measured at the SC. To prevent evaporation from the receptor compartment, the side arm of the cell was covered with parafilm. The temperature of the skin surface was confirmed by using a digital thermometer supplied with a 1 m long

cabled insertion probe. Before application of the donor phase, a blank sample of 100 µl was withdrawn from the receptor compartment and immediately replaced with fresh pre-warmed buffer solution. This sample was analysed by the HPLC to ensure the absence of any contamination.

Formulations were applied under infinite or finite dose conditions. In the former, a saturated donor solution (1 ml) of the model drug in the selected solvent systems was added to the donor compartment. Excess solute was present to maintain the saturation level throughout the experiment. In the latter, a small volume of formulation (10 µl/cm^2) was used. The donor compartment was then uncovered or covered with a glass cover slip to prevent evaporation of the solvent. At predetermined time intervals, samples of 100 µl were collected from the receptor medium via the side port of each diffusion cell and immediately replaced with an equal volume of fresh pre-warmed PBS solution. This dilution was taken into account when evaluating the data. The samples were analyzed without dilution using the HPLC. The experiment was repeated five times for each formulation. A minimum of four replicates per formulation was required (OECD, 2004b). Figure 3-5 illustrates a schematic of the permeation study stages.

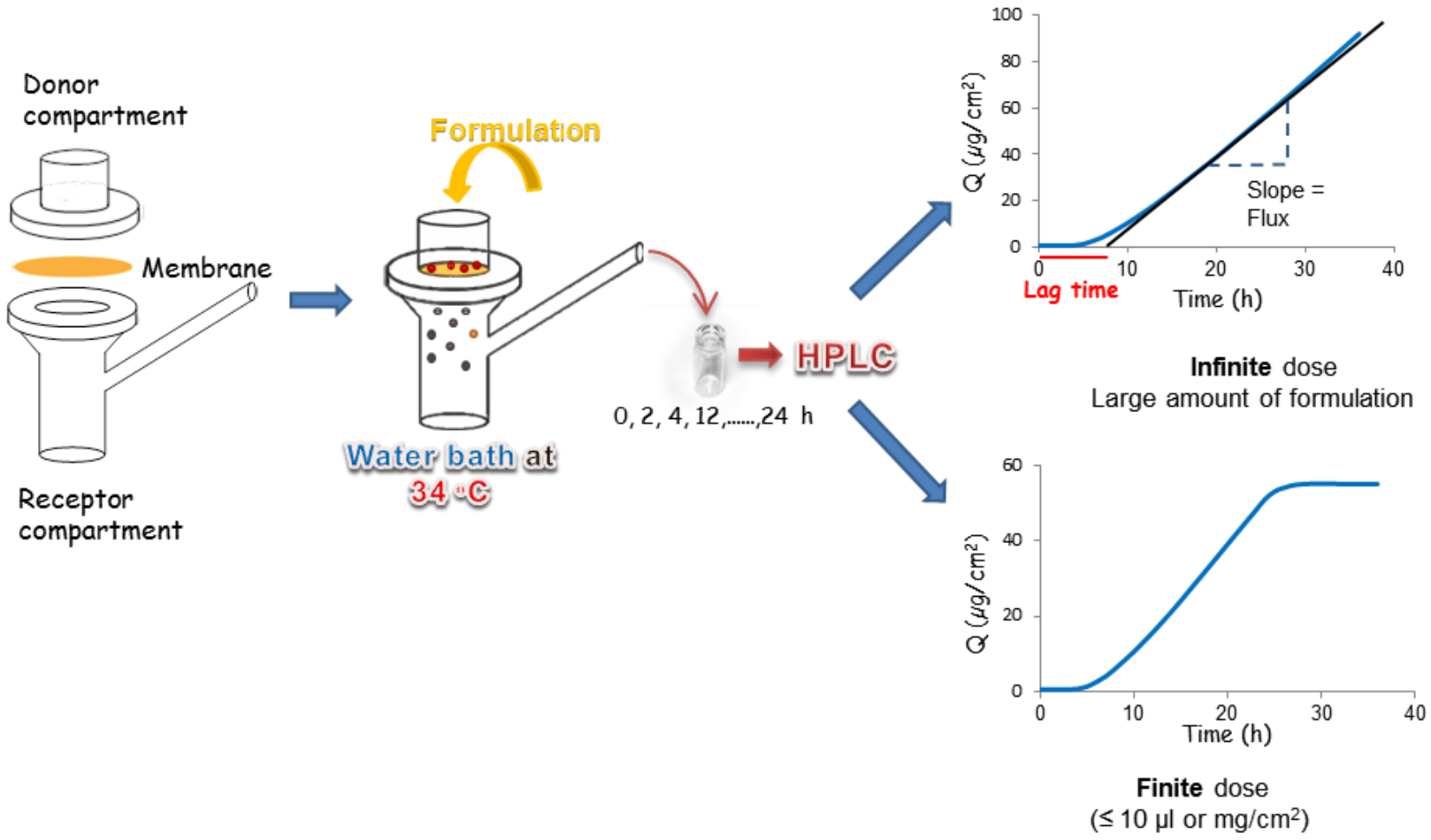

Figure 3-5 Schematic of the permeation study stages.

3.4.9.1 Ramipril

Since RAM was most stable in water, PG, and LA, permeation studies of RAM from these vehicles across human epidermis were conducted under infinite dose conditions.

3.4.9.2 Cilazapril

Permeation studies of CILA from infinite doses (1 ml, suspension) and finite doses (10 µl/cm^2, saturated solutions) were conducted using porcine ear skin. Single, binary, and ternary solvent systems were investigated in order to optimize dermal formulations. The purpose of using binary and ternary solvent combinations was to see if any synergistic enhancement effect can be achieved by these combinations. Finite doses were used since they were much closer to the clinical scenario in terms of the depletion of the drug as well as evaporation and/or depletion of solvents.

3.4.10 Examination of the skin surface with light microscopy

At the end of the permeation experiment of PG and TCL formulations, the skin area in contact with the formulation was carefully cut and then spread on a glass slide. The white precipitate formed on the skin surface was examined by polarized light microscopy (Olympus SZX12, Olympus instruments, Japan). Images were acquired using Insight QE Camera Model 4.2 (Diagnostic Instruments, USA).

3.4.11 Dynamic vapour sorption (DVS)

DVS is a gravimetric technique for studying the sorption properties of materials under controlled conditions of temperature and humidity. A volume of 10 µl of PG and

TCL, which was equal to the formulation dose, was spread on the DVS glass pan. The samples were exposed to controlled temperature and relative humidity, 32 ˚C and 50 % respectively for 48 h. These conditions were equivalent to those of the permeation experiments.

3.4.12 Data analysis

The cumulative amount of drug permeated per unit area (Q_t, μg/cm^2) from a given formulation through the skin at each sampling time was calculated from Equation 3.3 on the basis of the measured receptor fluid concentration and volume.

$$Q_t = V_R \, x \, C_n + [V_s(\sum C_1 + C_2 + \cdots + C_{n-1})]/A \quad \ldots\ldots\ldots\ldots \text{(3.3)}$$

Where C_n is the drug concentration (μg/ml) in the receptor compartment for the corresponding sample time (t); V_R (ml) is the volume of the receptor fluid; V_s (ml) is the volume sampled at each time interval; A (cm^2) is the diffusion area. This amount (Q_t, μg/cm^2) was plotted as a function of time (t, h). The permeation rate, namely flux, (J, μg/cm^2/h) was estimated from the linear portion of permeation profile. For CILA permeation studies, the total amount (cilazapril + cilazaprilat) was used to compare among formulations based on the bioactivity of the metabolite.

Statistical analysis of the differences between the various formulations was performed using one-way analysis of variance (ANOVA) test. The post hoc test used for checking individual differences between the formulations was Tukey test. A 0.05 level of probability (p < 0.05) was considered as the level of significance. The results

were statistically analysed using Microsoft® Office Excel 2010 and GraphPad Prism® (v 6.03) software. All results are presented as mean ± SD.

3.5 Results and discussion

3.5.1 HPLC method validation

3.5.1.1 Linearity

A linear calibration curve was obtained from plotting mean peak areas (y) as a function of the concentration (x) of each working standard solution (Figure 3-6) .The regression equation for CILA and its metabolite, cilazaprilat, was y = 23.66 x - 2.69 and y = 25.98 x – 1.79, respectively, where x is the drug concentration (µg/ml) and y is the peak area. The corresponding correlation coefficient (r^2) was 1. The results showed that within the concentration range (0.5 and 30 µg/ml) there was an excellent correlation between the peak area and concentration of the drugs.

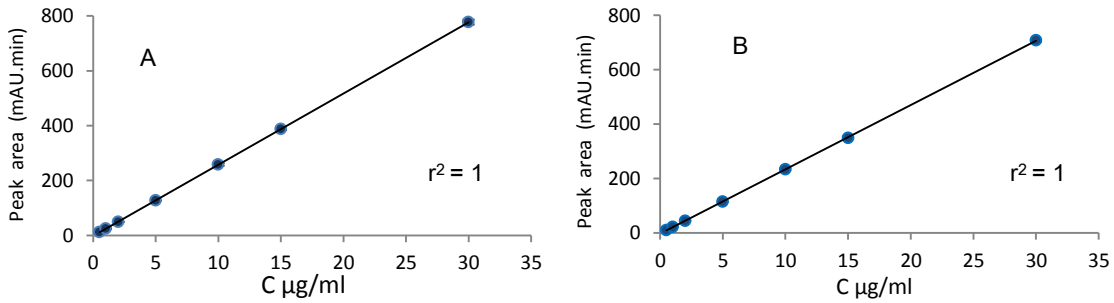

Figure 3-6 Graphical presentation of linearity plots of cilazaprilat (A) and CILA (B) (Mean ± SD, n=3); the SD error bars are too small to be visible.

3.5.1.2 Specificity

From the overlaid HPLC chromatograms of both CILA (20 µg/ml) and cilazaprilat (20 µg/ml) and the mobile phase (Figure 3-7). It was observed that

cilazaprilat and CILA eluted at 8.8 and 12.4 min, respectively. No interfering substances were found at the retention times corresponding to the analyte peaks, indicating the specificity of the method for the analysis of CILA and cilazaprilat.

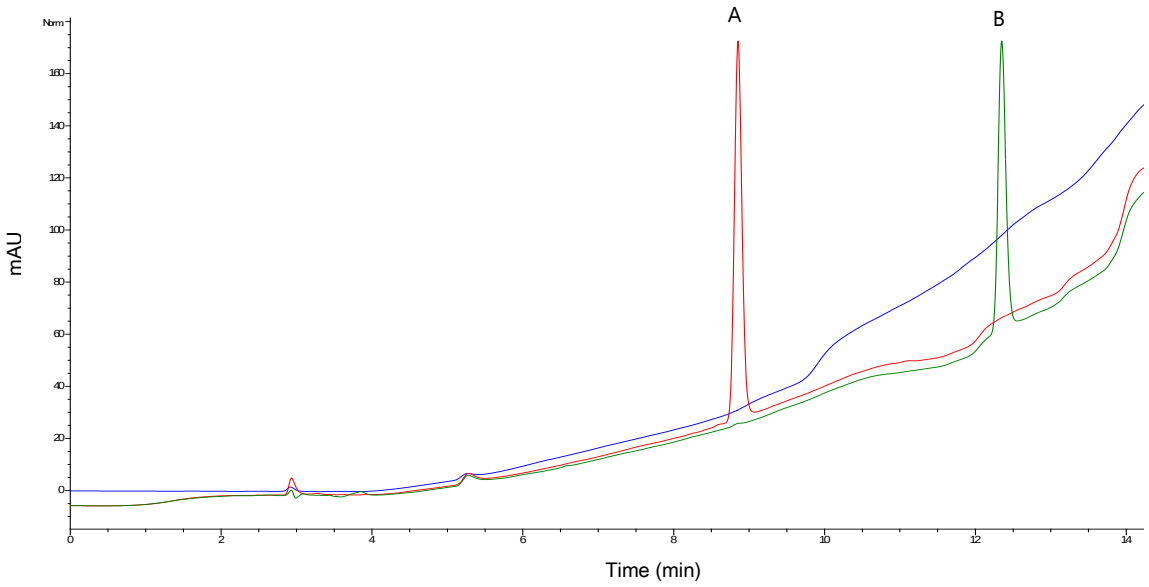

Figure 3-7 Overlaid HPLC chromatograms of cilazaprilat (A) and CILA (B) along with the mobile phase. The blue line represents the chromatogram of the mobile phase.

3.5.1.3 Limits of detection (LOD) and quantification (LOQ)

The LOD and LOQ for CILA and cilazaprilat were 0.25 and 0.5 µg/ml, respectively. These low values were an indication of the sensitivity of the method.

3.5.1.4 Precision

The resulting data for intra- and inter-day precision are provided in Table 3-1. In all cases, the % RSD values were all found to be less than 2 %. The low RSD values demonstrated the repeatability and intermediate precision of the proposed method.

Table 3-1 Results of the precision test. Each value represents the mean ± SD (RSD); n=3

Drug	Conc. (µg/ml)	*Intra-day*			*Inter-day*	
		Day 1	Day 2	Day 3		
Cilazapril	1	1.04 ± 0.01	1.03 ± 0.01	1.03 ± 0.01	1.03 ± 0.01	(0.36)
	15	14.89 ± 0.17	14.86 ± 0.03	14.81 ± 0.17	14.86 ± 0.04	(0.27)
	30	30.06 ± 0.17	30.16 ± 0.21	29.98 ± 0.22	30.06 ± 0.09	(0.30)
Cilazaprilat	1	1.02 ± 0.02	1.00 ± 0.02	1.01 ± 0.02	1.01 ± 0.01	(1.36)
	15	14.99 ± 0.09	14.99 ± 0.04	14.90 ± 0.07	14.96 ± 0.05	(0.35)
	30	30.00 ± 0.29	30.10 ± 0.30	29.95 ± 0.25	30.02 ± 0.08	(0.26)

3.5.1.5 Accuracy

Data listed in Table 3-2 show that the percent accuracy values were within the range from 99 to 104 %. These results were an indication of good accuracy for the method being validated.

Table 3-2 Results obtained from the accuracy test. Each value represents the mean ± SD; n=3

Conc. (µg/ml)	Cilazapril		Cilazaprilat	
	Measured (µg/ml)	Accuracy (%)	Measured (µg/ml)	Accuracy (%)
0.5	0.52 ± 0.01	104.31	0.51 ± 0.01	102.02
15	14.89 ± 0.17	99.25	14.99 ± 0.09	99.90
30	30.05 ± 0.17	100.16	30.00 ± 0.29	100.00

3.5.1.6 System suitability

The results obtained from the system suitability test are shown in Table 3-3. In all cases, % RSD values were less than 2 %, which confirmed the reliability of the method.

Table 3-3 Results obtained from the system suitability test. Each value represents the mean ± SD (RSD); n=6

Parameter	Cilazapril	Cilazaprilat
Retention time (min)	11.76 ± 0.01 (0.06)	7.95 ± 0.01 (0.09)
Peak area (mAU.min)	348.52 ± 2.17 (0.62)	387.23 ± 1.74 (0.45)
Asymmetry	0.89 ± 0.00 (<0.01)	0.95 ± 0.01 (0.55)

3.5.2 GC method validation

3.5.2.1 Linearity

The regression equation for PG and TCL was y = 23.90 x – 0.08 and y = 168.92 x – 1.31 respectively, where x is the vehicle concentration (mg/ml) and y is the peak area. The corresponding correlation coefficient (r^2) was 0.99. The results showed that within this concentration range there was an excellent correlation between the peak area and concentration of vehicle.

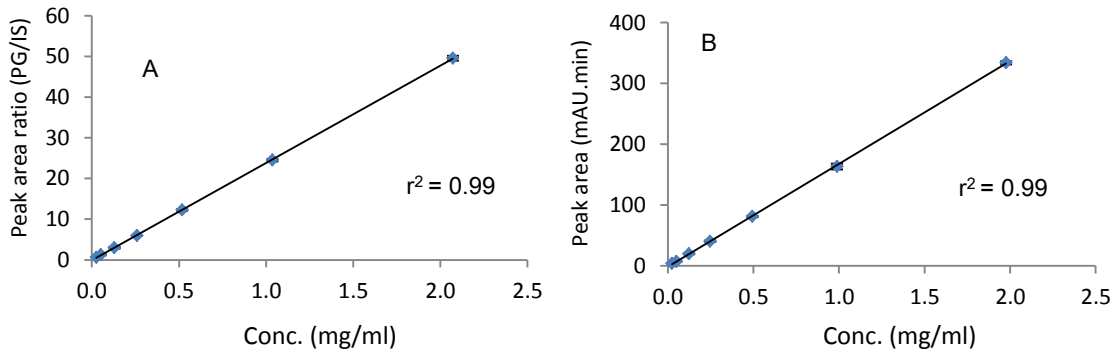

Figure 3-8 Graphical presentation of linearity plots of PG (A) and TCL (B) (Mean ± SD, n=3); the SD error bars are too small to be visible.

3.5.2.2 Specificity

From the GC chromatograms of both PG and TCL at concentrations of 0.13 µg/ml (Figure 3-9), it was observed that PG and TCL eluted at 4.23 and 3.99 min,

respectively. No interfering substances were found at the retention times corresponding to the analyte peaks, indicating the specificity of the methods for the analysis of PG and TCL.

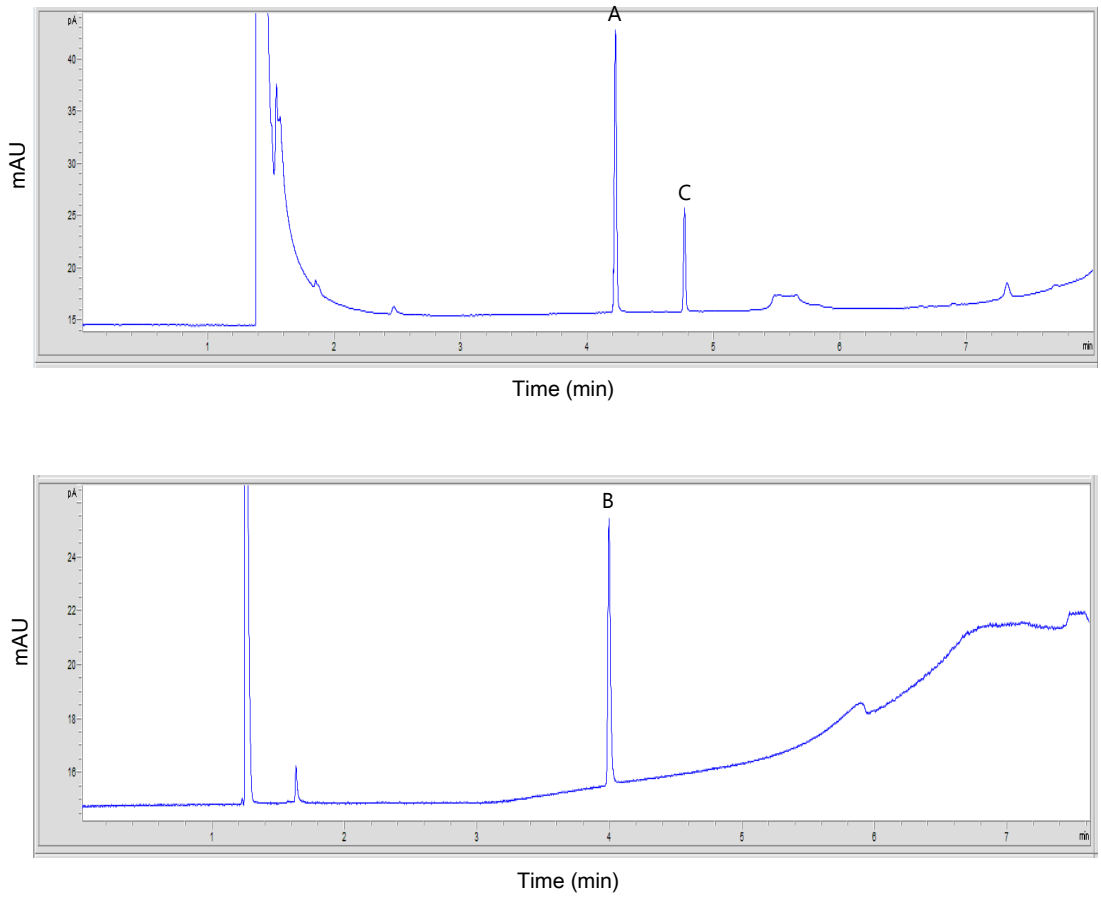

Figure 3-9 GC chromatograms of PG (A) and TCL (B). The peak C is the internal standard.

3.5.2.3 Limits of detection (LOD) and quantification (LOQ)

The LOD and LOQ for both PG and TCL were 0.01 and 0.025 mg/ml, respectively. These low values were an indication of the sensitivity of the method.

3.5.2.4 Precision

The resulting data for intra- and inter-day precision are provided in Table 3-4. The % RSD values were found to be equal or less than 2 %. The low RSD values demonstrated the repeatability and intermediate precision of the proposed method.

Table 3-4 Results of the precision test. Each value represents the mean ± SD (RSD); n=3

Vehicle	Conc. (mg/ml)	*Intra-day*			*Inter-day*
		Day 1	Day 2	Day 3	
PG	0.03	0.03 ± 0.00	0.03 ± 0.00	0.03 ± 0.00	0.03 ± 0.00 (1.62)
	1.04	1.03 ± 0.01	1.07 ± 0.02	1.02 ± 0.02	1.04 ± 0.02 (1.92)
	2.07	2.08 ± 0.02	2.18 ± 0.03	2.08 ± 0.02	2.11 ± 0.06 (2.84)
TCL	0.03	0.03 ± 0.00	0.03 ± 0.00	0.03 ± 0.00	0.03 ± 0.00 (1.91)
	0.99	0.97 ± 0.03	0.96 ± 0.01	0.97 ± 0.02	0.97 ± 0.01 (0.85)
	1.98	1.98 ± 0.02	1.95 ± 0.05	1.98 ± 0.04	1.97 ± 0.02 (0.82)

3.5.2.5 Accuracy

Data listed in Table 3-5 show the percent accuracy values obtained from the accuracy test. These results were an indication of good accuracy for the methods being validated.

Table 3-5 Results obtained from the accuracy test. Each value represents the mean ± SD; n=3

Vehicle	Conc. (mg/ml)	Measured (mg/ml)	Accuracy (%)
PG	0.05	0.053 ± 0.001	102.65
	1.04	1.030 ± 0.011	99.02
	2.07	2.076 ± 0.021	100.29
TCL	0.05	0.051 ± 0.001	102.75
	0.99	0.974 ± 0.028	98.41
	1.98	1.984 ± 0.017	100.18

3.5.2.6 System suitability

The results obtained from the system suitability test using PG and TCL standard solutions at a concentration of 1 mg/ml are shown in Table 3-6. In all cases, % RSD values were equal or less than 2 %, which confirmed the reliability of the methods.

Table 3-6 Results obtained from the system suitability test. Each value represents the mean ± SD; n=5

Parameter	PG/IS	TCL
Retention time (min)	0.89 ± 0.00 (0.00)	3.99 ± 0.00 (0.06)
Peak area (mAU.min)	25.09 ± 0.11 (0.45)	163.60 ± 3.78 (2.31)
Asymmetry	1.03 ± 0.01 (0.85)	0.98 ± 0.02 (2.04)

3.5.3 Solubility studies

3.5.3.1 Ramipril

The solubility of RAM in water and PG was determined using the two methods described in section 3.4.4 and then plotted in Figure 3-10. The drug concentration in each of the saturated supernatants was calculated from the peak area on the basis of the calibration curve equation. It was shown that RAM exhibited low solubility in water in comparison with PG.

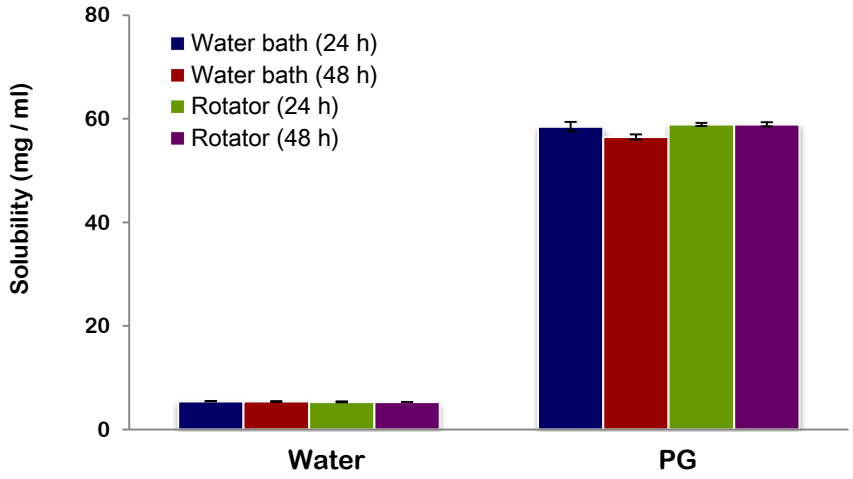

Figure 3-10 Solubility of RAM (mg/ml) in water and PG at 32 °C (mean ± SD; n=3).

Using the water bath method, the 48 h solubility of RAM in water and PG was 5.39 ± 0.04 and 56.49 ± 0.48 mg/ml, respectively. For the rotator method, the 48 h solubility of RAM in the same solvents was 5.32 ± 0.01 and 58.94 ± 0.38 mg/ml. These results illustrated that there was no significant difference ($p > 0.05$) in the drug solubility using either of these two methods or the same method for 24 and 48 h. Since the latter method can be carried out using small amounts of drug, it was selected later to determine the solubility of CILA in a range of different solvents. The solubility values of RAM in PBS pH 7.4 and LA were 6.97 ± 0.18 and 400 ± 5.32 mg/ml, respectively. The purpose of determining RAM solubility in PBS was to ensure that the sink condition is maintained throughout the permeation experiments. The δ_{RAM} calculated using the Molecular Modeling Pro® software was found to be 11.09 $(cal/cm^3)^{1/2}$. This value is much closer to the δ_{PG} [14.07 $(cal/cm^3)^{1/2}$] than the δ_{water} [22.97 $(cal/cm^3)^{1/2}$]. The difference between the δ_{PG} and δ_{RAM} is about a third of that between the δ_{water} and δ_{RAM}. Findings by Sloan et al. (1986) as well as Dias et al. (2007) support the solubility results, where the lower the δ differences, the higher tendency for mutual solubility between two substances (Sloan et al., 1986; Dias et al., 2007).

3.5.3.2 Cilazapril

The solubility of CILA in different single, binary, and ternary solvent systems was measured in triplicate and plotted in Figures 3-11, 3-12, and 3-13. Figure 3-11 highlights the concentration of the saturated solutions of CILA in different single solvents. The solvents are listed in order of increasing CILA solubility.

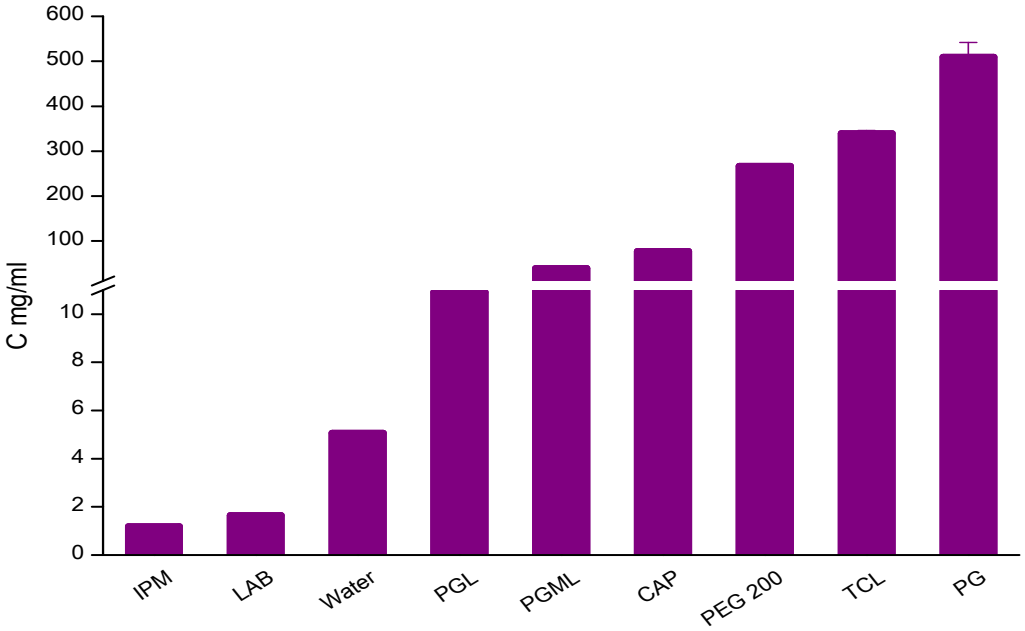

Figure 3-11 Solubility of CILA in a range of single solvent systems at 32 °C (mean ± SD; n=3). The SD values are too small to be visible except for PG.

As shown in Figure 3-11 not all solvents were capable of solubilizing the drug to the same extent. CILA exhibited high solubility in TCL and PG, an intermediate solubility in PGML and CAP, and lowest solubility in IPM and LAB. The solubility of CILA in various pure vehicles increased in the following rank order: IPM (0.95 ± 0.03) < LAB (1.65 ± 0.04) < water (5.07 ± 0.02) < PGL (10.92 ± 0.13) < PGML (39.57 ± 0.50) < CAP (77.18 ± 1.10) < PEG 200 (267.13 ± 2.42) < TCL (339.50 ± 6.32) < PG (509.39 ± 32.2) mg/ml.

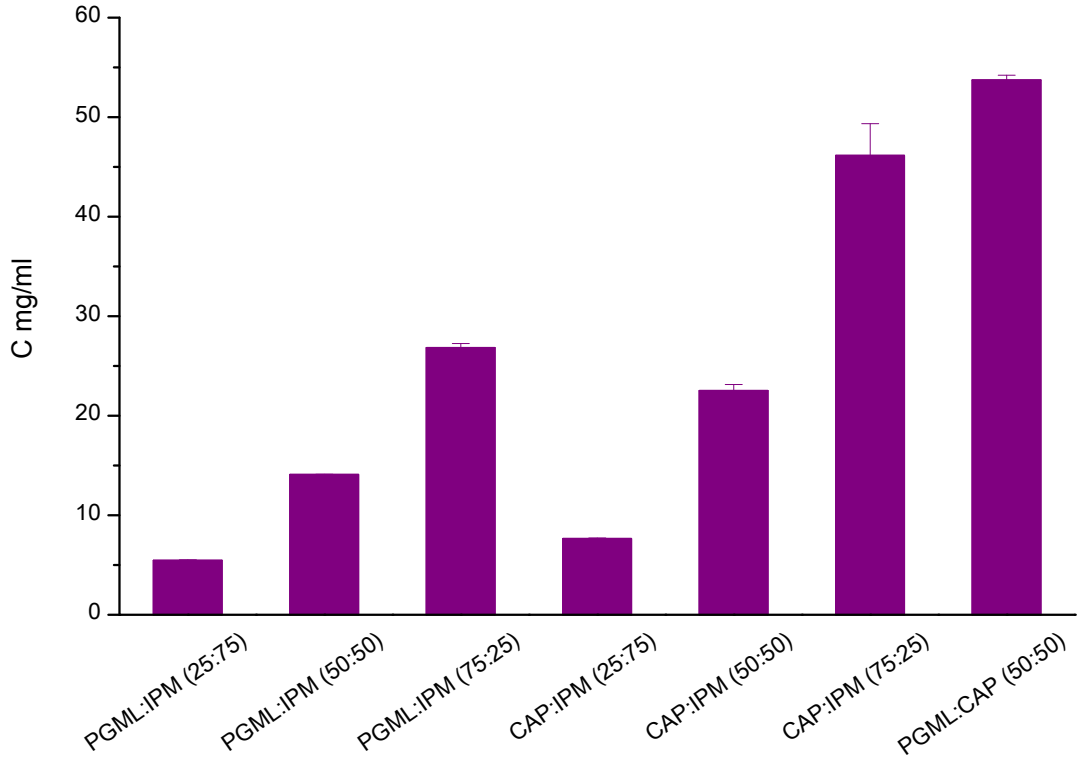

Figure 3-12 Solubility of CILA in a range of binary solvent systems at 32 °C (mean ± SD; n=3).

Expectedly, the solubility of CILA in the binary solvent systems, IPM with either PGML or CAP, decreased as the concentration of IPM increased, which were 26.83 ± 0.43, 14.07 ± 0.06, 5.47 ± 0.05 mg/ml and 46.13 ± 3.22, 22.52 ± 0.61, 7.64 ± 0.08 mg/ml at 25, 50 and 75 % IPM in PGML and CAP, respectively. The addition of TCL, PG, PEG 200 to the binary solvent system (IPM:CAP) resulted in an increase in the solubility of CILA in these ternary solvent systems (Figure 3-13).

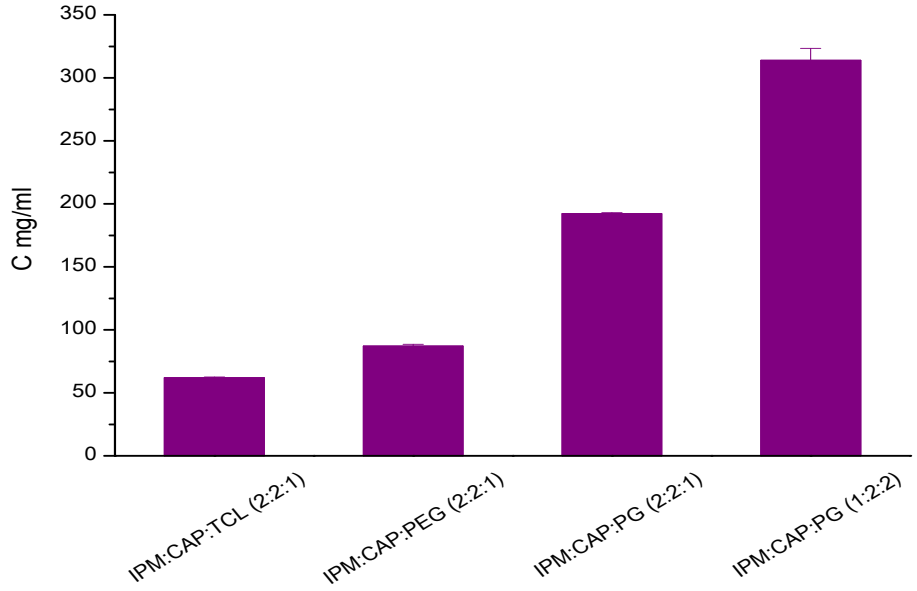

Figure 3-13 Solubility of CILA in a range of ternary solvent systems at 32 °C (mean ± SD; n=3).

3.5.4 The relationship between the solubility of cilazapril and the solubility parameter of different solvent systems

In topical drug delivery, the solubility parameter was used to predict the solubility of the permeant in the vehicle and hence to estimate the co-solubility of two materials (Dias et al., 2007). The solubility parameters (δ) for CILA and for all vehicles were calculated using the Molecular Modelling Pro® software (V6.3.3). The δ_{CILA} was estimated to be 11.55 $(cal/cm^3)^{1/2}$. A relationship was observed between the solubility parameter of the vehicle (δ_V) and the solubility of CILA (Figure 3-14). The closer the δ_V to the δ_{CILA}, the higher the solubility of CILA in this vehicle. This is in accordance with the solubility theory which hypothesizes that a vehicle with a solubility parameter close to that of the drug will be mutually soluble. As shown in Figure 3-14, the lower the δ value of a vehicle, the more lipophilic the vehicle is. IPM, a lipophilic compound, has δ_{IPM} value of 8.21 $(cal/cm^3)^{1/2}$ whereas the δ_{water} is 22.97 $(cal/cm^3)^{1/2}$.

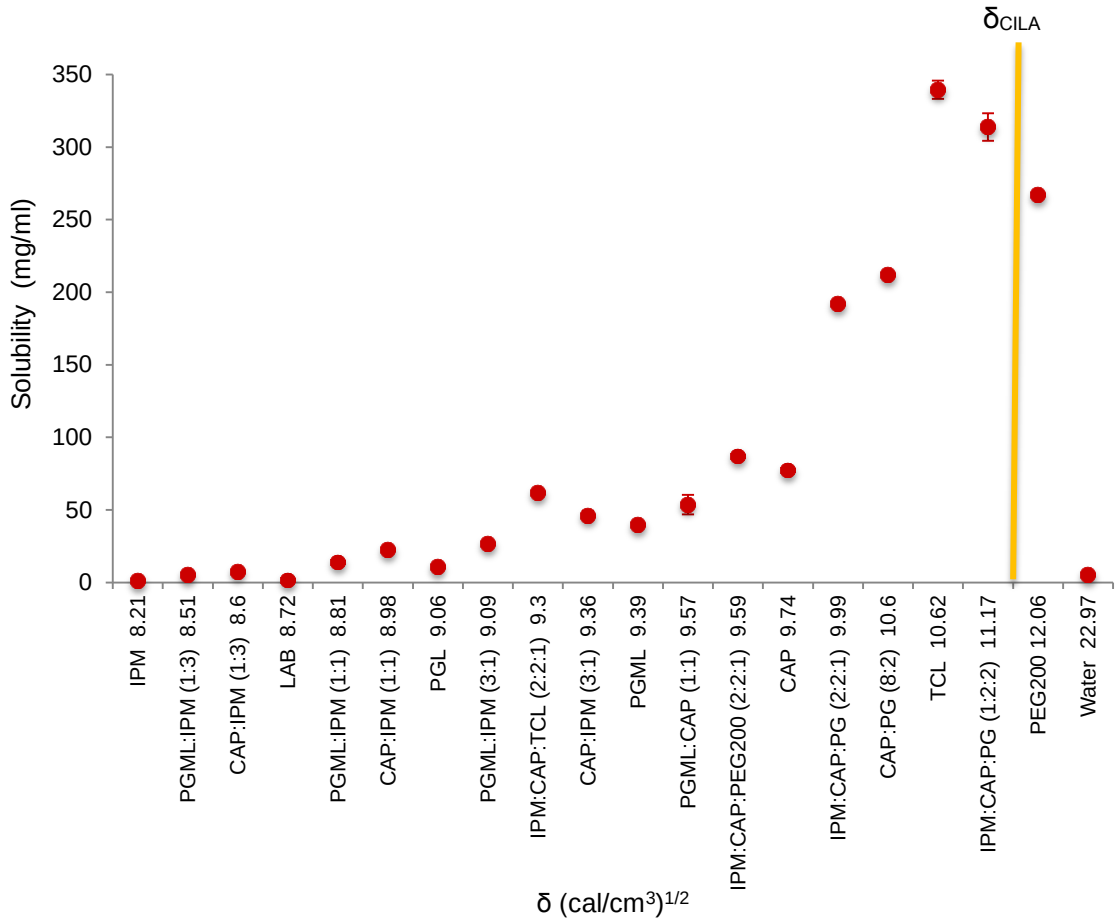

Figure 3-14 The relationship between the solubility of CILA at 32 °C in different solvent systems and the solubility parameter of these systems (mean ± SD; n=3).

The difference between the δ of the solvent system and that of CILA $|\delta_V-\delta_{CILA}|$ was calculated and plotted as a function of CILA solubility in Figure 3-15. As seen from this Figure, the solubility of CILA is inversely proportional to $|\delta_V-\delta_{CILA}|$. The drug solubility in the vehicles with $|\delta_V-\delta_{CILA}|<2$ was much higher than that with $|\delta_V-\delta_{CILA}|>2$. This is in agreement with Khalil and Martin (1967) and Vaughan (1985) who reported that a difference of < 2 usually indicated mutual solubility.

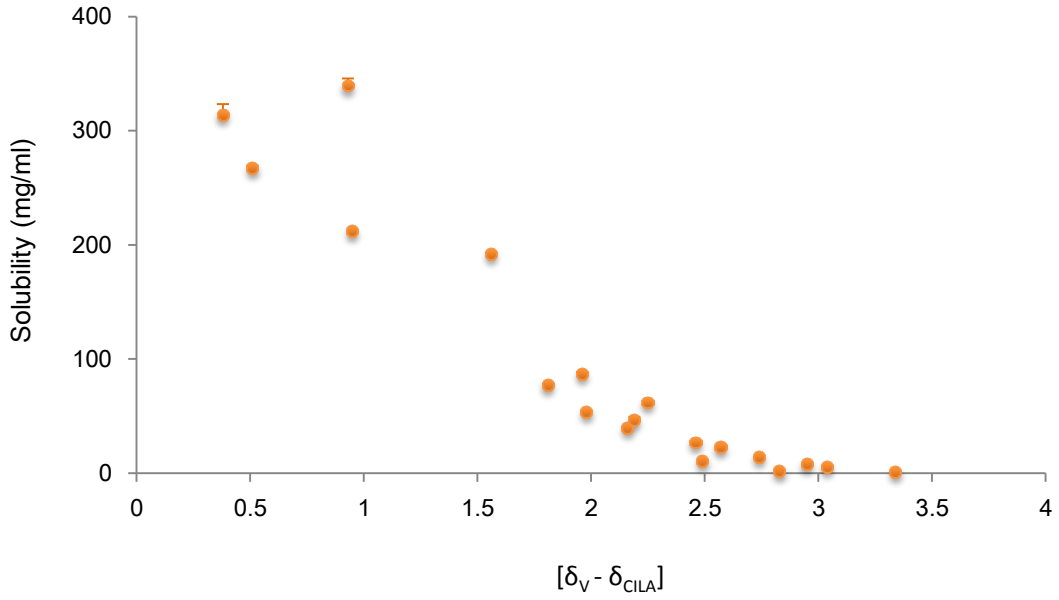

Figure 3-15 The relationship between the solubility of CILA at 32 °C in different solvent systems and the solubility parameter difference between the drug and these systems (mean ± SD; n=3).The SD values are too small to be visible.

3.5.5 Miscibility studies

Miscibility studies were conducted with ternary combinations of five solvents, IPM, CAP, PG, TCL, and PEG 200. IPM, CAP, and TCL were miscible at any combinations, but IPM was not miscible with either PG or PEG 200. CAP was miscible with both PG and PEG 200 over the entire range. The ternary phase diagrams obtained from the miscibility studies data of two ternary solvent systems, IPM:CAP:PG and IPM:CAP:PEG 200 are shown in Figure 3-16. These phase diagrams were useful to design the *in vitro* skin permeation experiment in order to prevent unwanted phase separation, resulting from the solvents mixture or the back diffusion of water into the donor during the permeation study.

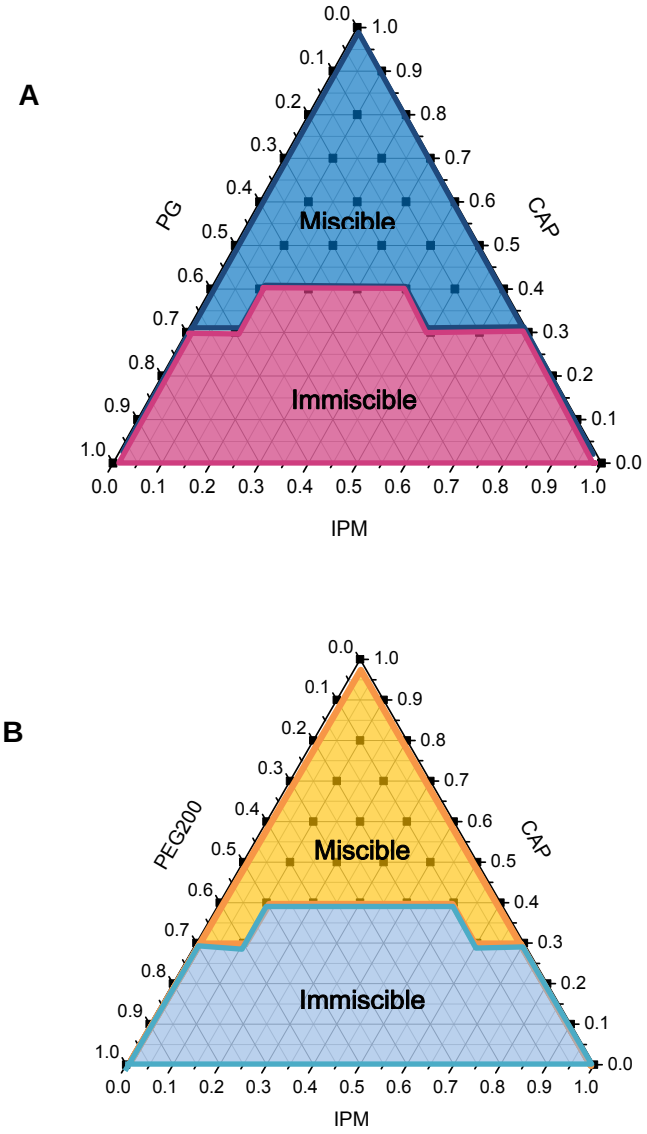

Figure 3-16 Ternary phase diagrams for CAP:IPM:PG (A), CAP:IPM:PEG 200 (B)

The phase diagrams show regions of miscibility and immiscibility. The solvent mixtures of formulation tested were selected from the miscible region. Based on the permeation results obtained with the binary mixtures, the following ternary solvent systems CAP:IPM:PG, CAP:IPM:TCL and CAP:IPM:PEG 200 with the following proportions (40:40:20 v/v) were selected from the ternary phase diagrams to conduct the permeation studies.

3.5.6 Determination of log $P_{o/w}$

The measured concentration of the stock solution of CILA used to determine log P was 2.03 mg/ml. Table 3-7 shows the ratios of the two solvents, the concentrations of CILA in the two separated phases, log P, and the recovery. The determined log P values were all 0.49. The reliability of these values was tested by comparison of the means of the triplicate determinations with the overall mean. The latter value was equal to the means of the triplicate determinations. The recovery results showed that the total quantity of CILA present in both n-octanol and water was close to the original quantity used.

Table 3-7 The partition coefficient results for CILA (mean ± SD; n=3)

The ratio of each phase		Conc (μg/ml)	Log P	Recovery (%)
O:W* (1:1)	O	297.78 ± 1.60	0.49 ± 0.01	98.34
	W	95.57 ± 0.85		
O:W (1:2)	O	479.77 ± 10.57	0.49 ± 0.01	98.40
	W	153.71 ± 0.49		
O:W (2:1)	O	169.05 ± 2.24	0.49 ± 0.02	98.19
	W	54.66 ± 1.08		

*O:W (n-octanol :water)

The experimental log P value (0.49) was close to the log P value (0.73) determined by ChemSpider (www.chemspider.com).

3.5.7 Diffusion studies

3.5.7.1 Ramipril

The effect of three solvents: water, PG, and LA on the permeation of RAM across epidermal human skin was evaluated under infinite dose conditions. The drug concentrations during the diffusion studies were calculated from the peak area on the

basis of the calibration curve equation. The calculated cumulative amount of RAM permeated per unit area versus time was plotted in Figure 3-17

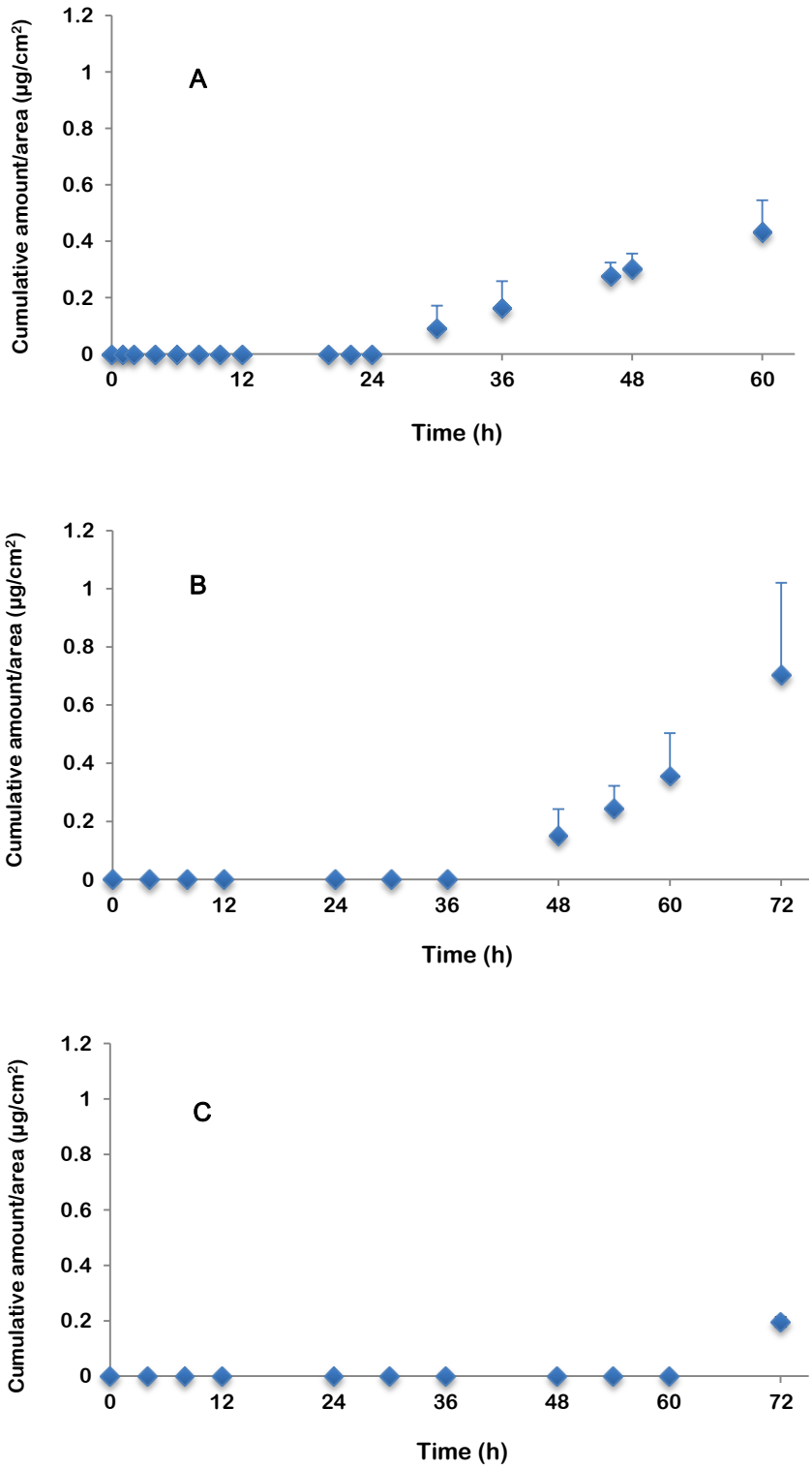

Figure 3-17 Permeation profiles of an infinite dose of RAM in water (A), PG (B), and LA (C) across human epidermis (mean + SD; n=4).

The flux (J, μg/cm²/h) was calculated from the slope of the linear portion of the plot of cumulative amount versus time (Table 3-8). The lag time (t_{lag}, h) was obtained by extrapolating the linear portion of the curve to the time axis. The results showed the low permeability of RAM across human epidermis.

Table 3-8 Fluxes (J) and lag time (t_{lag}) of RAM permeated through human epidermis from infinite doses of RAM in water, PG, and LA (mean ± SD; n=4)

Vehicle	J (x10^{-2} μg/cm²/h)	t_{lag} (h)
Water	1.00 ± 0.54	23.68 ± 0.99
PG	2.26 ± 1.14	42.88 ± 1.24
LA	N/A	N/A

Figure 3-18 shows the cumulative amount per unit area (Q_{72h}, μg/cm²) of the infinite dose of RAM in 72 h where less than 1 μg of RAM per cm² permeated through the skin.

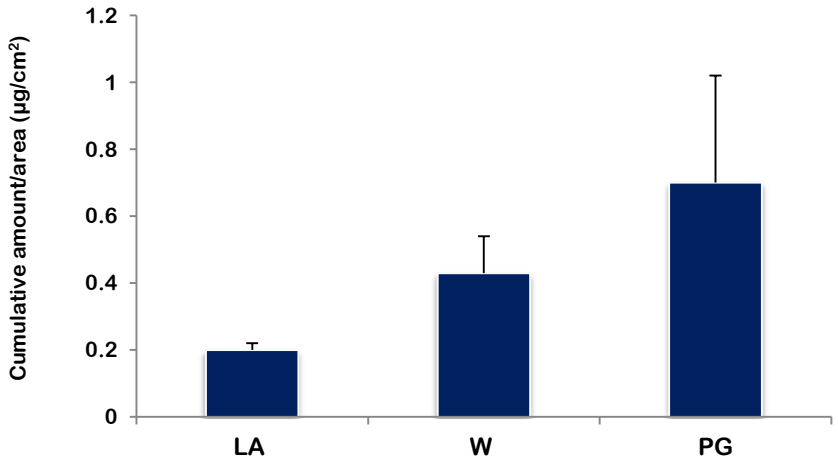

Figure 3-18 The cumulative amount of RAM permeated at 72 h using single solvents under infinite dose conditions through human epidermis (mean + SD; n=4).

The HPLC chromatograms (Figures 3-19 and 3-20) show the presence of ramipril diketopepirazine (RAM-DKP) in the receptor and donor phases. This can be

explained by both the permeation of RAM-DKP, which resulted from RAM degradation in the donor, along with the main compound and the degradation of RAM which permeated in the receptor phase during the time course of experiment.

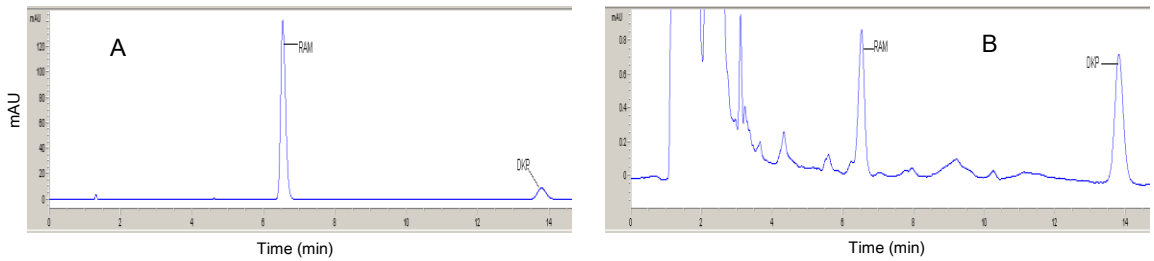

Figure 3-19 HPLC chromatogram of RAM in PG after 72 h from the A: donor; B: receptor compartment. The first peak is RAM and the second one is its degradant.

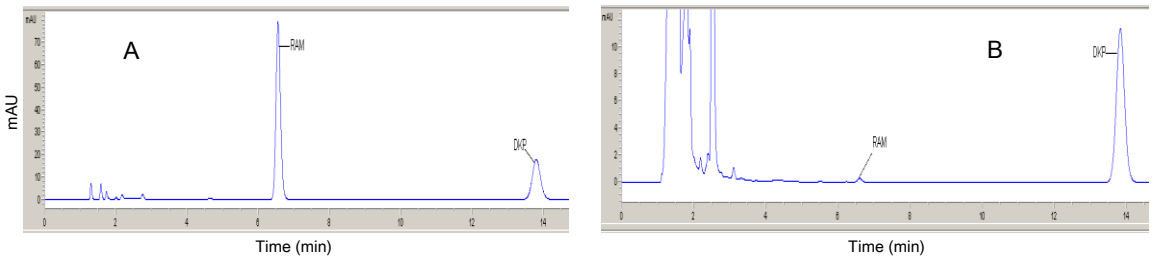

Figure 3-20 HPLC chromatogram of RAM in LA after 72 h from the A: donor; B: receptor compartment. The first peak is RAM and the second one is its degradant.

The molecular weights, calculated log P and calculated solubility parameters of RAM and RAM-DKP are presented in Table 3-9. The log P values of these compounds were determined using the ChemDraw Ultra® 7.0 software and their solubility parameters were calculated using the Molecular Modeling Pro® software. Since the solubility parameter of RAM-DKP is much closer to that of the stratum corneum ~ 10 $(cal/cm^3)^{1/2}$ (Liron and Cohen, 1984), it might be hypothesised that the permeation rate of this compound through the skin would be higher than that of RAM. The high amount of RAM-DKP in the receptor phase might also be attributed to the degradation of RAM to form RAM-DKP in the receptor phase during the permeation experiment. Furthermore, other factors such as the molecular size and shape of molecule might

influence the interaction with the skin and hence the flux as it was reported by Dias et al. (2007)

Table 3-9 Physicochemical properties of RAM and RAM-DKP

Compound	MW	Log P	δ $(cal/cm^3)^{1/2}$
RAM	416.5	3.00	11.09
RAM-DKP	388.5	2.71	10.05

Generally, saturated solutions of a given drug are at equal thermodynamic activities and hence should give the same flux, despite differences in the solubility of the permeant in different vehicles (Higuchi, 1960). Table 3-8 shows that the flux values of RAM from PG and water were not the same and RAM from PG exhibited a higher flux than that from water. Therefore, the flux of RAM from the vehicles used in this study was not thermodynamically controlled. This can be explained by the possibility of interaction between the skin and the vehicle which in turn altered the flux of the permeant.

Water, PG, and LA encompass a range of solubility parameters. The solubility of RAM and the solubility parameters of the vehicles are listed in Table 3-10. The solubility of RAM was the highest in LA with a δ_{LA} of 9.20 $(cal/cm^3)^{1/2}$, which is close to the calculated δ_{RAM} [11.09 $(cal/cm^3)^{1/2}$]. The second peak solubility for RAM was in PG with δ_{PG} = 14.06 $(cal/cm^3)^{1/2}$. RAM had the lowest solubility value in water which has the highest δ_{water} = 22.97 $(cal/cm^3)^{1/2}$. The results are in agreement with those of Dias and co-workers (2007).

Table 3-10 Solubility of RAM in different vehicles at 32 °C and solubility parameter of these vehicles (mean ± SD; n=3)

Vehicle	Solubility (mg/ml)	δ $(cal/cm^3)^{1/2}$
Water	5.39 ± 0.02	22.97
PBS	6.97 ± 0.18	N/A
PG	58.46 ± 0.92	14.06
LA	400.00 ± 5.32	9.20

The calculated δ_{RAM} was close to both the δ_{LA} and δ_{Skin}. The affinity of RAM to leave the formulation and get into the skin was low. Another possible reason why the RAM from LA permeated poorly compared with PG and water probably lies in the inability of LA to interact with and disrupt the skin barrier. The viscosity of the LA formulation might play a role in controlling release of the drug from the formulation to be available for partitioning into the skin. The greatest enhancement was with PG. This could be explained by either an increase in RAM solubility in the skin or a shift of the δ_{Skin} in the direction of that of the drug by PG (Wotton et al., 1985).

3.5.7.2 Cilazapril

3.5.7.2.1 Infinite dose studies

In vitro permeation studies using an infinite dose of CILA were conducted in order to obtain a constant rate of absorption through the skin and therefore evaluate the permeation behaviour of the compound. This allows determining four parameters: flux (J, $\mu g/cm^2/h$), permeability coefficient (k_p, cm/h), cumulative amount (Q_{48h}, $\mu g/cm^2$) permeated over 48 h, and lag time (t_{lag}, h) for all the formulations. The effect of different vehicles/penetration enhancers on CILA transport through porcine ear skin was investigated under infinite dose conditions. CILA was added to each vehicle in an

excess amount of saturated solubility in order to achieve a constant thermodynamic activity. Sink condition was maintained in the receptor phase during the experiment.

3.5.7.2.1.1 Permeation studies using single solvent systems

The permeation profiles of CILA across full thickness porcine ear skin over 54 h following application of 1 ml of saturated solutions of CILA in different neat vehicles are illustrated in Figure 3-21. Various types of vehicles such as LAB, IPM, PG, CAP, PGL, PGML and TCL, were used.

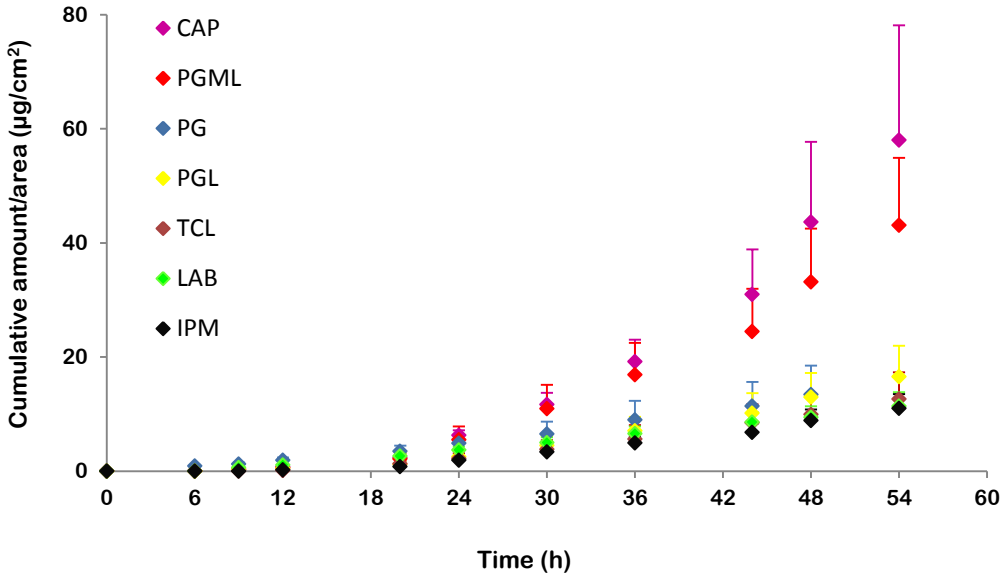

Figure 3-21 Permeation profiles of CILA through porcine ear skin from various single vehicles under infinite dose conditions (mean + SD; n=4).

These profiles are characteristic for the application of an infinite dose, with lag time and flux. They also highlight the variation in absorption due to vehicle used. The permeation parameters calculated from the profiles are presented in Table 3-11. The linear portion of such graphs was used to calculate J. A linear relationship occurs between 36 and 54 h for almost all formulations. The rate of penetration represented by

the k_p was used for comparing the rate of absorption. The ratio of J to the concentration of CILA in each vehicle allowed for the estimation of k_p. The intercept of the linear portion of the cumulative absorption graphs provided t_{lag}. The enhancing effect of each vehicle was assessed on the basis of determining J, k_p, Q_{48h}, and t_{lag}.

Table 3-11 The lag time (t_{lag}), cumulative amount permeated in 48 h (Q_{48h}), permeability coefficient (k_p), and flux $J_{(36-54h)}$ of CILA through porcine ear skin from saturated solutions of different single solvents (mean ± SD; n=4).

Vehicles	Permeation parameters			
	t_{lag} (h)	Q_{48h} (μg/cm²)	k_p (x10⁻⁴ cm/h)	$J_{(36-54h)}$ (μg/cm²/h)
CAP	22.41 ± 1.08	43.69 ± 14.01	0.28 ± 0.10	2.16 ± 0.80
PGML	23.11 ± 1.36	33.19 ± 9.31	0.39 ± 0.09	1.55 ± 0.36
PGL	22.36 ± 3.37	12.96 ± 4.27	0.48 ± 0.16	0.52 ± 0.17
PG	5.58 ± 3.06	13.44 ± 5.08	4.07 ± 2.08	0.39 ± 0.19
TCL	17.08 ± 2.69	9.95 ± 3.70	0.01 ± 0.00	0.39 ± 0.15
IPM	18.47 ± 0.58	8.86 ± 1.98	3.74 ± 0.93	0.34 ± 0.08
LAB	11.17 ± 3.22	9.44 ± 1.95	1.61 ± 0.42	0.26 ± 0.07

The data in Table 3-11 show that the fluxes (J_{36-54h}) of CILA from saturated solutions in LAB, IPM, TCL, PG, and PGL were generally low, ranging from 0.26 ± 0.07 to 0.52 ± 0.17 μg/cm²/h and that the permeability coefficient (k_p) of CILA increased using PG, IPM, and LAB compared with the other vehicles. A relatively short t_{lag} and high k_p was obtained with PG. However, t_{lag} was significantly ($p < 0.05$) prolonged with CAP, PGML, and PGL.

Among the pure vehicles examined, CAP showed the highest permeation rate, which was 2.16 ± 0.80 μg/cm²/h whereas LAB was the lowest (0.26 ± 0.07 μg/cm²/h). Saturated solutions of the same drug are at equal thermodynamic activity. In this case, the flux from all of the vehicles should be equal, despite differences in the solubility of

the drug, provided the vehicle has no effect on the skin barrier (Higuchi, 1960; Twist and Zatz, 1989). It was interesting to note that despite the equal thermodynamic activities, the permeation rates of CILA were different from each vehicle, and the permeation rate of CILA was the greatest in CAP. These results are consistent with those of Leopold et al. (1995) that stated that there was a possibility of reduction in the SC resistance by specific vehicle effects, in addition to any thermodynamically based effects. No significant difference ($p > 0.05$) in $J_{36\text{-}54h}$ and Q_{48h} of CILA among all the single solvent formulations was observed apart from CAP and PGML (Figure 3-21).

3.5.7.2.1.2 Permeation studies using binary solvent systems

The effect of binary vehicle systems on skin permeation was also evaluated. Based on the findings from the permeation studies using single vehicles, the highest Q_{48h} was obtained from CAP and PGML (43.69 ± 14.01 and 33.19 ± 9.31 μg/cm^2, respectively) whereas IPM exerted a high k_p value. Therefore, the influence of combinations of these solvents on CILA permeability across porcine ear skin was interesting to be tested. Three binary vehicle formulations with a ratio of (50:50 v/v) were compared: CAP:IPM, PGML:IPM, CAP:PGML. The highest cumulative amount permeated through the skin was shown for the CAP:IPM combination (Figure 3-22).

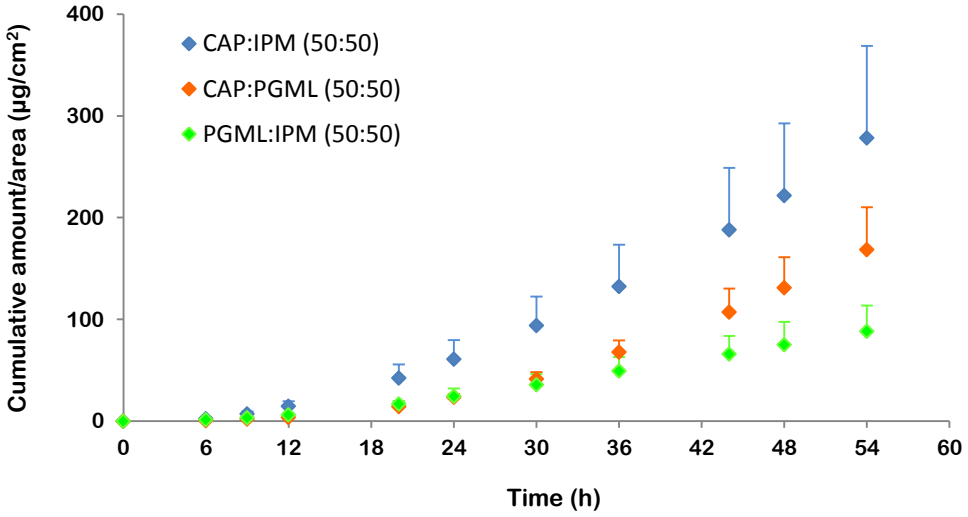

Figure 3-22 Permeation profiles of CILA across porcine ear skin from binary solvent systems under infinite dose conditions (mean + SD; n=4).

It can also be seen from the profiles in Figure 3-22 that no depletion of donor phases occurred during the course of experiments. Furthermore, the binary combination of CAP, IPM and PGML caused a synergistic effect on CILA permeation compared with the neat vehicles. A marked improvement in CILA permeation through the skin was noticed from the binary IPM:CAP (50:50) formulation. A comparison of CILA fluxes ($J_{36\text{-}54h}$) from the binary formulations indicated that the highest permeation rate was observed using CAP:IPM, followed by CAP:PGML and finally PGML:IPM (Table 3-12).

Table 3-12 The lag time (t_{lag}), cumulative amount permeated in 48 h (Q_{48h}), permeability coefficient (k_p), and flux $J_{(36\text{-}54h)}$ of CILA through porcine ear skin from saturated solutions of different binary solvent systems (mean ± SD; n=4).

Vehicles	Permeation parameters			
	t_{lag} (h)	Q_{48h} (µg/cm²)	k_p (x10⁻⁴ cm/h)	$J_{(36\text{-}54h)}$ (µg/cm²/h)
PGML:IPM (50:50)	13.18 ± 1.39	75.15 ± 25.39	1.70 ± 0.48	2.39 ± 0.68
CAP:IPM (50:50)	15.24 ± 0.56	221.71 ± 70.93	3.59 ± 1.21	8.08 ± 2.73
CAP:PGML (50:50)	19.45 ± 1.38	131.26 ± 29.79	1.04 ± 0.32	5.58 ± 1.69

From these findings it was concluded that the major factor that determines the drug permeability across the skin was not the thermodynamic activity but the vehicle effect on the barrier function.

3.5.7.2.2 Finite dose studies

Even though the infinite dose technique was useful for evaluation of the permeation behaviour of a compound, it was not relevant to the clinical scenario where a small amount of a topical formulation is applied to the skin surface. For the finite dose study, both the rate of absorption and total amount of compound absorbed can be different from the infinite dose study. To evaluate the influence of the vehicle when applied at clinically relevant doses, saturated solutions of CILA in different solvent systems were used for the permeation studies under non-occluded and finite dose conditions (10 µl/cm^2). The concentration of CILA in each applied formulation was quantified using HPLC. Based on this and the applied volume, the dose of CILA applied to the porcine ear skin surface was calculated and shown in Figure 3-23.

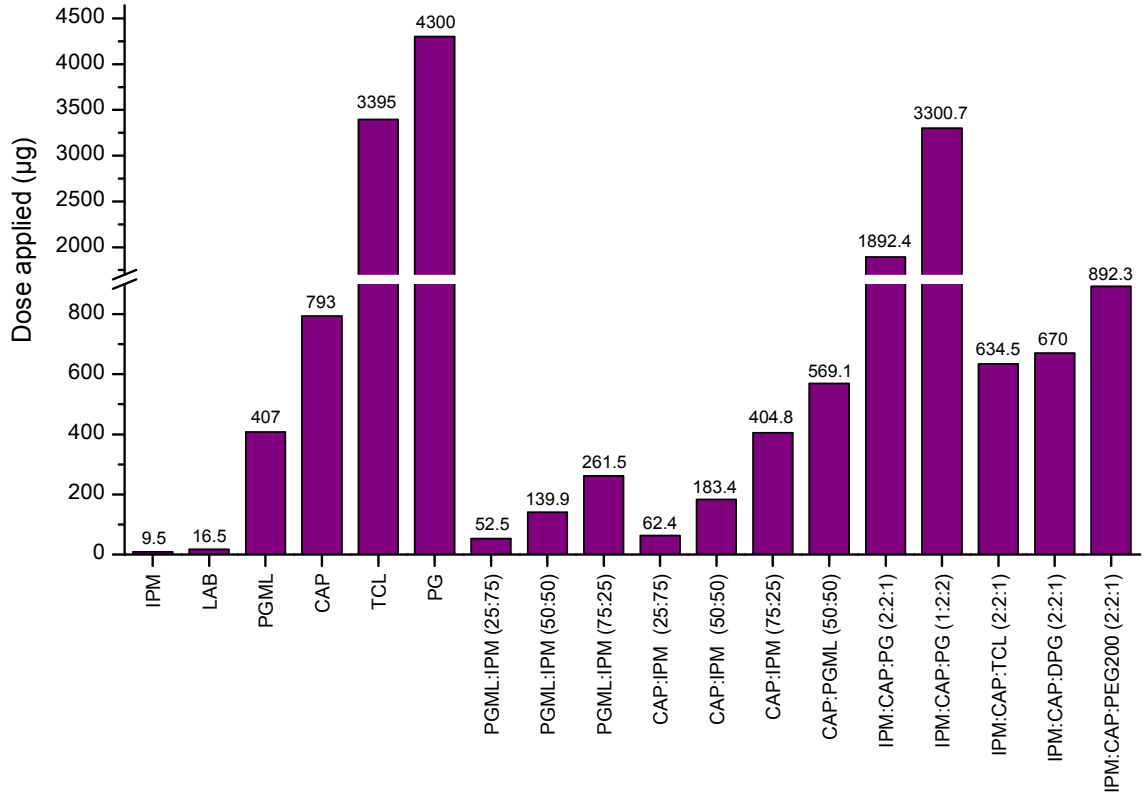

Figure 3-23 The dose applied in µg to 1 cm^2 of the skin surface from different solvent systems under finite dose conditions.

The solvents selected included chemical penetration enhancers which have been investigated (Arellano et al., 1999; Trottet et al., 2004; Mura et al., 2011; Hirata et al., 2013). The enhancement effect was assessed on the basis of determining the total cumulative amount (Q_{48h}, µg/cm^2) of both CILA and cilazaprilat permeated over 48 h for all the formulations.

3.5.7.2.2.1 Permeation studies using single solvent systems

Permeation profiles of CILA from saturated single vehicles under finite conditions are shown in Figure 3-24. These solvents were CAP, PGML, TCL, PG, IPM, and LAB. Each profile represents the cumulative amount of the total CILA permeated (i.e., sum of CILA and cilazaprilat) as a function of time. Measuring the cumulative

amount of both CILA and its metabolite, cilazaprilat, would be more accurate as part of CILA was hydrolysed by skin esterases and in the receptor phase.

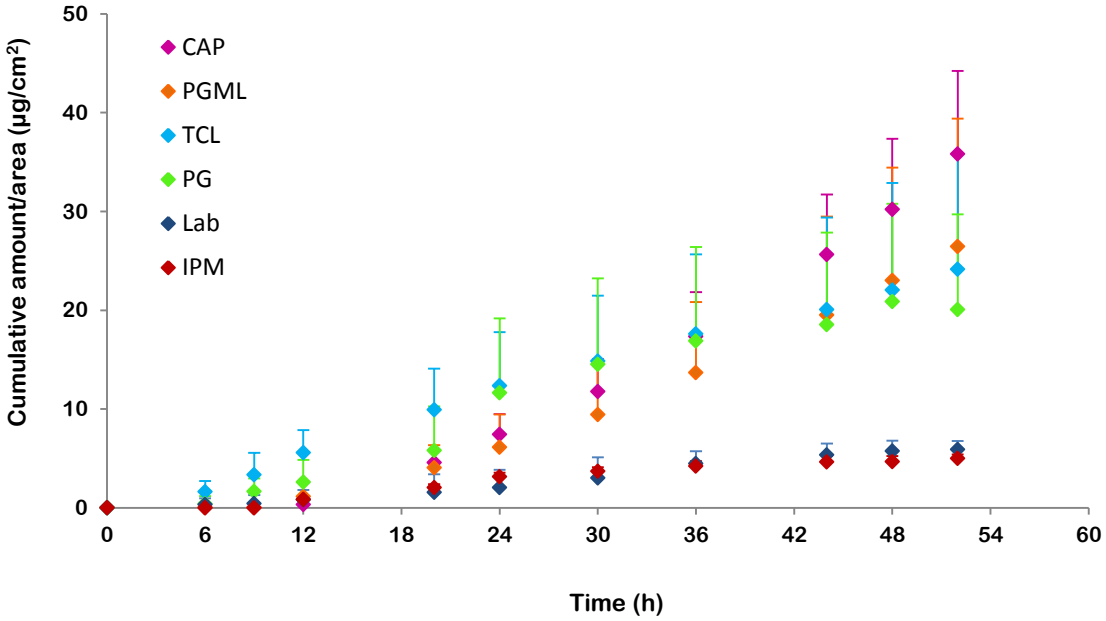

Figure 3-24 Permeation profiles of CILA through porcine ear skin from saturated solutions of single solvents under finite dose conditions (mean + SD; n=4).

Because of the low permeability of CILA compared to the dose applied in some of the formulations, it was difficult to observe donor depletion and to obtain the permeation profile characteristic for finite dose conditions. This was observed when CAP and PGML were used. As seen from the finite dose profiles in Figure 3-24, the shorter estimated lag time resulted from the dose delivered in IPM, PG, and TCL compared with the dose delivered from PGML or CAP vehicles.

It was interesting to note that CILA was applied to the skin surface as an ester form as confirmed by the HPLC analysis of the donor solutions. However, CILA was found in the receptor phase together with variable amounts of its metabolite, cilazaprilat as shown in Figure 3-25. A possible explanation for this phenomenon was that CILA

started to be hydrolysed to cilazaprilat by skin esterases and then both CILA and cilazaprilat diffused into the receptor phase.

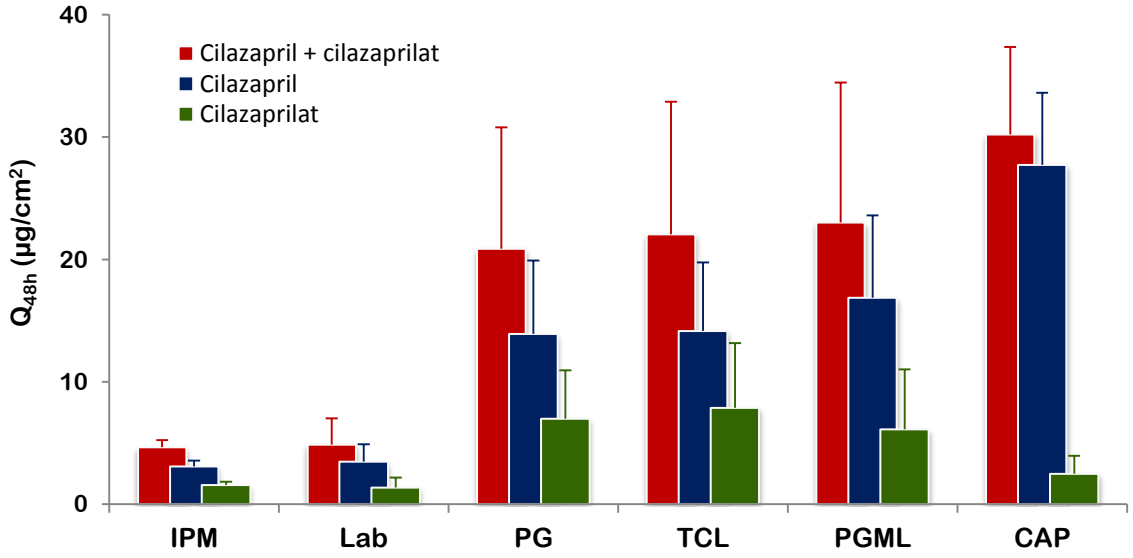

Figure 3-25 The cumulative amount of total CILA (CILA and cilazaprilat), CILA, and cilazaprilat permeated at 48 h through porcine ear skin using single solvents under finite dose conditions (mean + SD; n=4).

The findings are in line with previous studies which indicated the enzymatic conversion of different ester prodrugs to their parent drugs during *in vitro* skin permeation. Ngawhirunpat et al. (2004) compared the skin permeation and metabolism of ethyl nicotinate using porcine and human skin. The authors noted the presence of ethyl nicotinate along with its metabolite, nicotinic acid, in the receptor phase during the permeation experiments. This was attributed to the hydrolysis of the drug by skin esterases with no significant difference ($p > 0.05$) between human and pig skin in terms of their permeability and metabolic capacity. Abla et al. (2006) investigated the percutaneous absorption of valaciclovir across porcine ear skin using iontophoresis. Both valaciclovir and its parent drug, aciclovir, were measured in the receptor fluid and combined to determine the total amount of valaciclovir permeated. From this

observation it was suggested that the former was bio-transformed to the active form during the diffusion process. A further study on evaluating the skin permeation of haloperidol esters across full thickness human and porcine skin was conducted by Morris et al (2009). The findings indicated that these prodrugs underwent enzymatic hydrolysis on their passage across the skin. However, the hydrolysis level was low irrespective of using fresh and frozen skin. All these studies used skin not subject to thermal treatment but stored at -20˚C for up to four months. Under these storage conditions, skin maintained its enzyme capacity (Stinchcomb et al., 1996; Abla et al., 2006; Beydon et al., 2010). On the other hand, Montenegro et al. (2007) evaluated the permeation of ester drugs of quercetin using excised human skin prepared by heat separation. Only quercetin esters were found in the receptor phase. The absence of their parent drugs was explained by the damage of skin enzymes by the heat used during the skin preparation.

Furthermore, some of the cilazaprilat detected in the present study might be also formed by chemical hydrolysis of intact CILA permeated into the receptor phase. This is in agreement with a number of studies that showed the contribution of the chemical hydrolysis in drug metabolism (Bundgaard et al., 1983; Wang et al., 2007). The authors reported that incubation of the ester prodrugs of 5-fluorouracil and morphine in a phosphate buffer exhibited more resistance to the chemical hydrolysis compared with the emzymatic hydrolysis. It was also found that the rate of the chemical hydrolysis was much slower than that of the enzymatic hydrolysis (Stinchcomb et al., 1996; Vaddi et al., 2005). Based on the findings of the present study, it was suggested that the presence of cilazaprilat in the receptor phase was caused by both enzymatic

and chemical ester bond cleavage in CILA structure. This was confirmed by the metabolism studies of CILA in porcine skin as described in chapter four.

It was also possible that CILA hydrolysis was mediated not only by esterases inside the skin but also by esterases released from the dermal side into the receptor phase during the permeation studies. Bundgaard et al. (1983) demonstrated the 20 h leaching of esterases from human skin into the receptor phase compartment of the diffusion cell. They incubated metronidazole benzoate and butyryloxymethyl 5-fluorouracil with the receptor phase collected at different time intervals from a blank diffusion study. They noted that the hydrolysis rate of the esters increased with time. Wang et al. (2007) linked the flattening in the permeated amount of morphine enanthate with the experiment time to the leakage of enzymes into the receptor fluid.

Interestingly, samples taken from the donor compartment and analysed by the HPLC showed the absence of cilazaprilat, indicating that the ester bond cleavage occurred during the diffusion process and in the receptor phase. As shown in Figure 3-25, the quantity of cilazaprilat formed was less than that of CILA. The ratio of CILA to cilazaprilat was different among the formulations. The differences in the ratio may be due to inter-individual variability in the enzyme activity of skin. The interindividual variability in the enzymes level was previously reported (Rolsted et al., 2009). The amount of the metabolite of lidocaine formed after topical application of lidocaine on 9 healthy human volunteers varied from 1.6 to 7.4 ng/mm^2 skin. This was due to the variability in the enzyme level among the subjects. These differences might also result from the effect of vehicle on the enzyme activity, which needs to be explored further in future work.

The 48 h cumulative amount of CILA permeated (Q_{48h}, μg/cm^2) can be ranked according to the following order: CAP > PGML > TCL > PG > LAB > IPM. CAP exhibited significant enhancing effects ($p < 0.05$) on CILA permeation compared with IPM and LAB. In addition, Q_{48h} was statistically higher ($p < 0.05$) in PGML than IPM. The percentage of CILA permeated over 48 h was calculated by dividing the cumulative amount permeated (Q_{48h}, μg/cm^2) by the applied dose (μg/cm^2). As illustrated in Figure 3-26, less than 6 % of the applied dose was absorbed in 48 h from most of the tested vehicles. LAB and IPM were unique in that 33.84 ± 6.41 and 48.22 ± 4.89 % of the applied dose permeated, respectively.

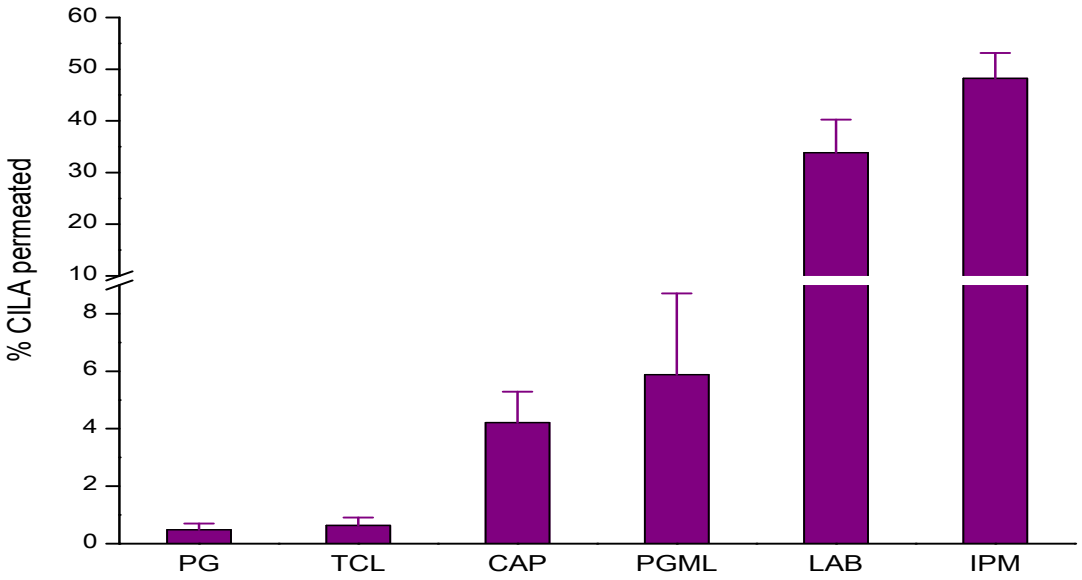

Figure 3-26 The percentage of CILA permeated at 48 h through porcine ear skin from saturated solutions of single solvent systems under finite dose conditions (mean + SD; n=4).

At 48 h, the percentage of CILA permeated can be ranked according to the following order: IPM > LAB > PGML > CAP > TCL > PG. As shown in Figures 3-11 and 3-25, the vehicles, CAP and PGML, in which CILA had high solubility (77.18 ± 1.10 and 39.57 ± 0.05 mg/ml, respectively) showed the highest Q_{48h}. IPM had the lowest

Q_{48h} value of 4.66 ± 0.59 µg/cm^2. IPM was not able to exhibit a very high enhancing effect, due to the extremely low CILA solubility (0.95 ± 0.03 mg/ml) and applied dose (9.5 µg/cm^2). Furthermore, the drug percentage permeated from IPM was high 48.22 ± 4.89 %. This percentage was significantly greater ($p < 0.05$) compared to that observed from PG, TCL, CAP, PGML. It was reported that IPM reduces the barrier function of the skin by interacting with the ordered lipid bilayers of the SC increasing the lipid fluidity and thus increasing the molecule diffusion in skin (Leopold and Lippold, 1995; Brinkmann and Muller-Goymann, 2005). Addition of CAP or PGML, in which the drug possessed a high solubility, to IPM will enable loading a higher amount of the drug for diffusion across porcine skin. These binary combinations were tested in section 3.5.7.2.2.2.

3.5.7.2.2.1.1 Effect of PG and TCL on CILA permeation

After the initial application of CILA in PG and TCL, the vehicles remained visible on the skin surface for a couple of hours. When they disappeared, a solid material deposited on the skin surface. As illustrated in Figure 3-27, CILA flux decreased with time, indicating a reduction of the CILA amount permeated. Even though the CILA dose applied from TCL and PG was very high, 3395 and 4300 µg/cm^2 respectively, the permeation profiles of CILA from these formulations started to flatten.

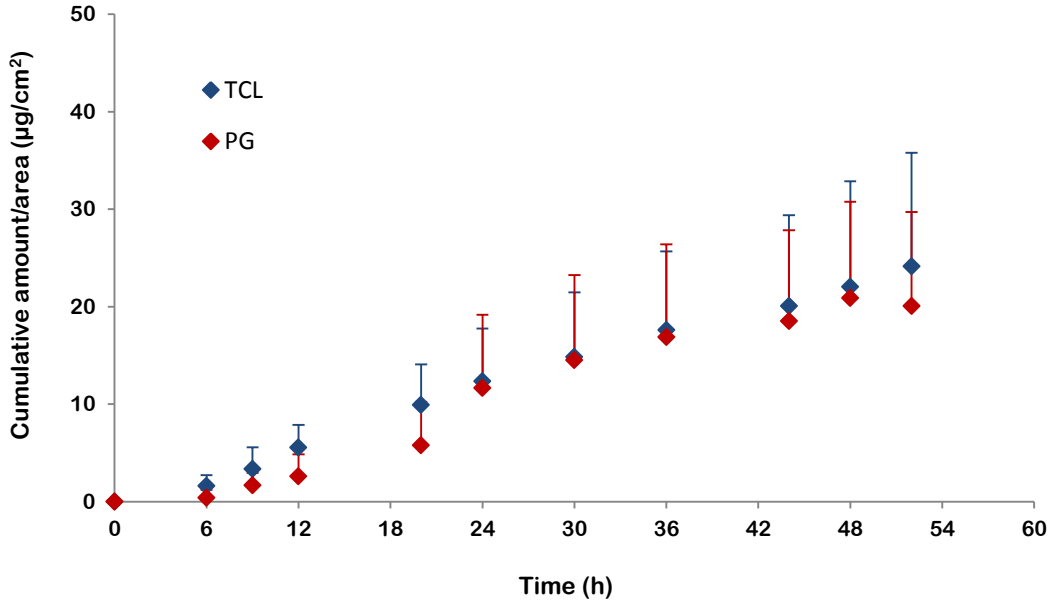

Figure 3-27 Permeation profiles of CILA through porcine ear skin from saturated solutions of PG and TCL under finite dose conditions (mean + SD; n=4).

Furthermore, the white precipitate visually observed on the skin surface was examined by polarized light microscopy which revealed a crystalline material. The crystals exhibited a long needle-shaped morphology as shown in Figure 3-28. Based on these findings, it was unlikely that the lack of CILA permeation was caused by the depletion of the drug itself. Therefore, the only logical explanation of such a pattern is that CILA started to be absorbed slowly from the formulation until PG and TCL disappeared by evaporation and/or rapid percutaneous diffusion across the skin.

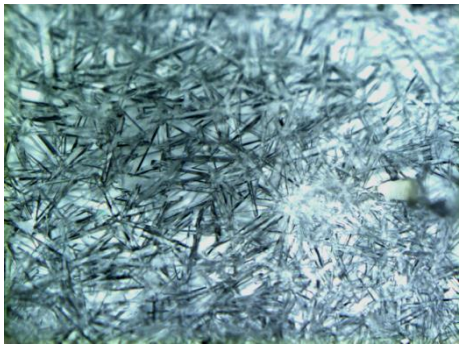

Figure 3-28 Crystal formation and growth on the porcine skin surface from a saturated solution of CILA in PG.

In order to understand further the permeation behaviour of PG and TCL, the permeation of these solvents across the porcine skin into the receptor phase was monitored by GC. As shown in Figure 3-29, the permeation profile of PG indicated that the cumulative amount of PG increased with time to reach a peak at 20 h followed by a gradual decrease.

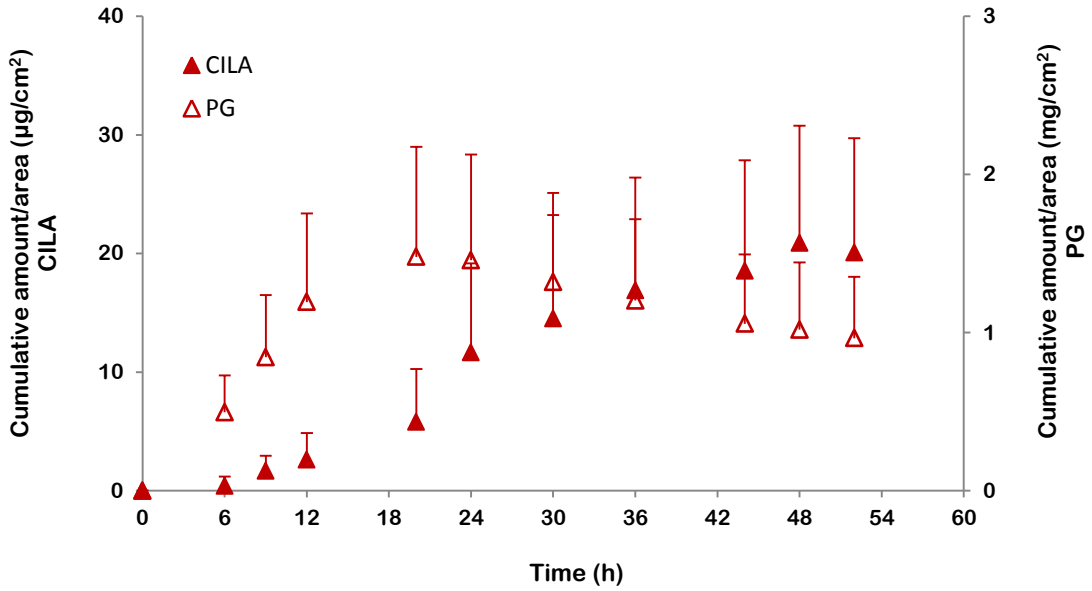

Figure 3-29 Permeation of CILA and PG across porcine skin after the application of a finite dose (10 µl/cm^2) of PG formulation (mean + SD; n=4).

A plausible explanation for this phenomenon is that PG might diffuse back from the receptor through the skin and/or evaporate from the sampling ports of the diffusion cells (see Appendix A). Therefore, further investigations are needed in order to identify the rationale for this phenomenon. These can be achieved by conducting two sets of permeation experiments and comparing the resultant permeation profiles. For the first set, porcine ear skin is mounted on five Franz diffusion cells and a dose of 10 µl PG is spread on each skin surface. Samples are collected at 0, 6, 9, 12, 20, 24, 30, 36, 44,

48, and 52 h. However, in the second set the skin is replaced with aluminium foil (to prevent PG back diffusion) and the receptor fluid is spiked with PG at a concentration similar to that achieved at 20 h. Samples are then collected at 20, 24, 30, 36, 44, 48, and 52 h.The two profiles obtained from the skin and aluminium foil experiments need to be compared in order to verify the existence of PG back diffusion and/or PG evaporation via the sampling port. One of the following three scenarios is possible:

1) If the amount of PG remained constant till the end of the aluminium foil experiment (its profile showed a plateau level), this indicates that the decrease in the permeation profile of PG obtained from the skin experiment resulted from the PG back diffusion only.
2) If the declining parts of the two profiles were overlaid in both experiments, then the PG back diffusion did not exist in the skin experiment and only PG evaporation occurred via the sampling port when porcine skin is used.
3) If the cumulative amount of PG decreased with time in the aluminium foil experiment but to a lesser extent than what we obtained in the skin experiment, it is an indication of both the PG back diffusion across the skin and its evaporation from the receptor phase via the sampling port occurred in the porcine skin experiment.

Furthermore, a comparison of the permeation profile of PG with that of the drug indicated that PG diffused across the skin and appeared in the receptor phase more quickly than CILA. After 6 h of the application of the PG formulation, only 0.4 μg/cm^3 of CILA compared with 500 μg/cm^2 of PG found in the receptor phase. This finding is in agreement with Bowen and Heard (2006) who indicated that the amount of PG

permeated across porcine ear skin was always higher than that of ketoprofen, irrespective of the PG content in the formulation.

PG is a small molecule with a MW of 76 Da whereas CILA has a MW of 435 Da. Since the permeation of a molecule across the skin is governed by passive diffusion, small molecules can traverse skin faster than larger molecules. Therefore, it is most likely for PG to cross the skin faster than the drug. Moreover, the cumulative amount of PG determined in the receptor phase at the end of the experiment was 1 mg/cm^2. This represents 10 % of the applied dose. GC analysis of the skin surface washes and skin extraction showed the absence of PG in the samples, suggesting that the remaining amount of PG was lost by evaporation. Based on the findings, the plateau of the permeation profile observed with CILA formulation in PG was as a result of the depletion of PG, leaving the drug to crystallise on and inside the skin.

The results are in line with Trottet et al (2004) who demonstrated that PG crossed the skin barrier more quickly than the model drug, loperamide, and that the amount of PG permeated through the skin was proportional to the amount of PG present in the formulation (Trottet et al., 2004). They attributed this to the big difference in the MW of these molecules, and therefore the possible interaction with the SC leading to a delay in crossing the skin. The rate and extent at which the topically applied drug, ibuprofen, crossed the SC depended not only on its physicochemical properties but also on the behaviour of vehicles in which the drug was dissolved (Nicoli et al., 2009). The authors evaluated the clearance of ibuprofen, formulated as a saturated solution in 75:25 PG:water, from the SC. They noted that the drug was trapped in the SC as a result of the loss of PG by evaporation or rapid diffusion into the SC. They also found that this

phenomenon was prevented by occlusion that enabled ibuprofen to remain in solution and hence to diffuse out from the SC. In more recent studies, the lack of oxybutynin and fentanyl penetration through human skin from PG/water formulations was reported by Santos and colleagues (2010; 2011). They linked the crystallisation of the drug on or in human skin to PG depletion from the 25 % PG formulation, indicating the importance of maintaining the drug in solution in order to attain transdermal delivery.

Like PG, the 6 h sample from the TCL formulation showed a higher amount of TCL compared with CILA (Figure 3-30). However, the permeation profile of TCL reached a plateau after 36 h. In addition, for each time point, the level of TCL in the receptor phase was higher than that of CILA. The permeation data of TCL and CILA indicated that the former permeated faster than the latter.

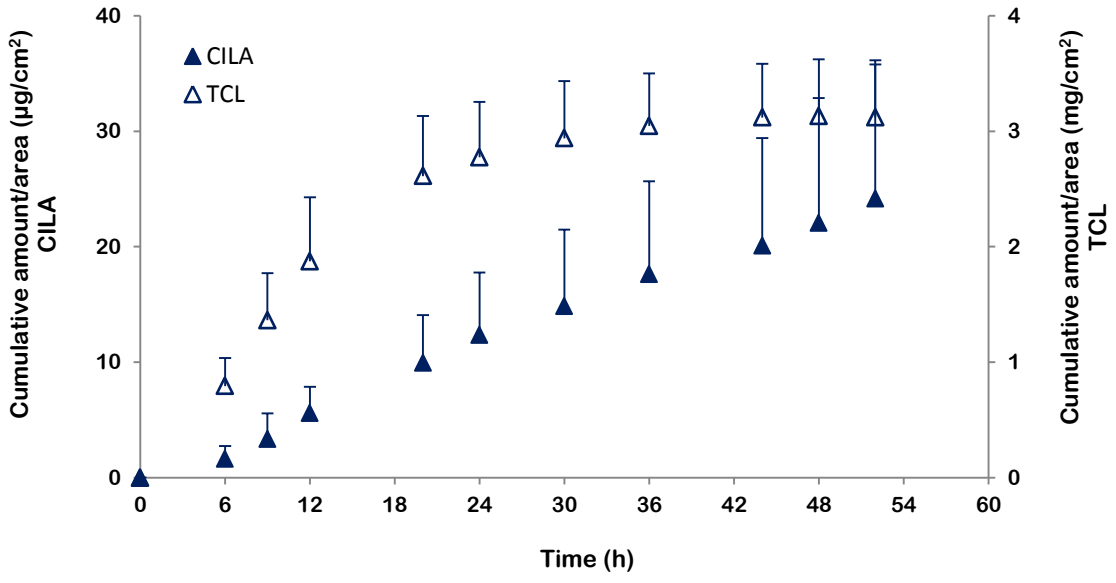

Figure 3-30 Permeation of CILA and TCL across porcine skin after the application of a finite dose (10 µl/cm^2) of TCL formulation (mean + SD; n=4).

TCL is also a small molecule compared with CILA with a MW of 134 Da, which is more than three times smaller than the drug. This implies the possibility of TCL to cross the skin faster than CILA. As can be seen from the permeation profile of CILA in Figure 3-30, the permeated amount of CILA started to decrease very slowly after 30 h. However, the profile did not reach a plateau level as observed with CILA formulation in PG. A possible explanation for this was that although TCL amount decreased with time but the remaining amount was enough to maintain a part of the drug in solution. This in turn was essential for drug to diffuse out of the skin.

Based on the results obtained from the permeation behaviour of PG and TCL and in an attempt to estimate the amount of the solvents lost by evaporation, dynamic vapour sorption (DVS) was used. The change in mass was recorded and plotted as a function of the time as shown in Figure 3-31.

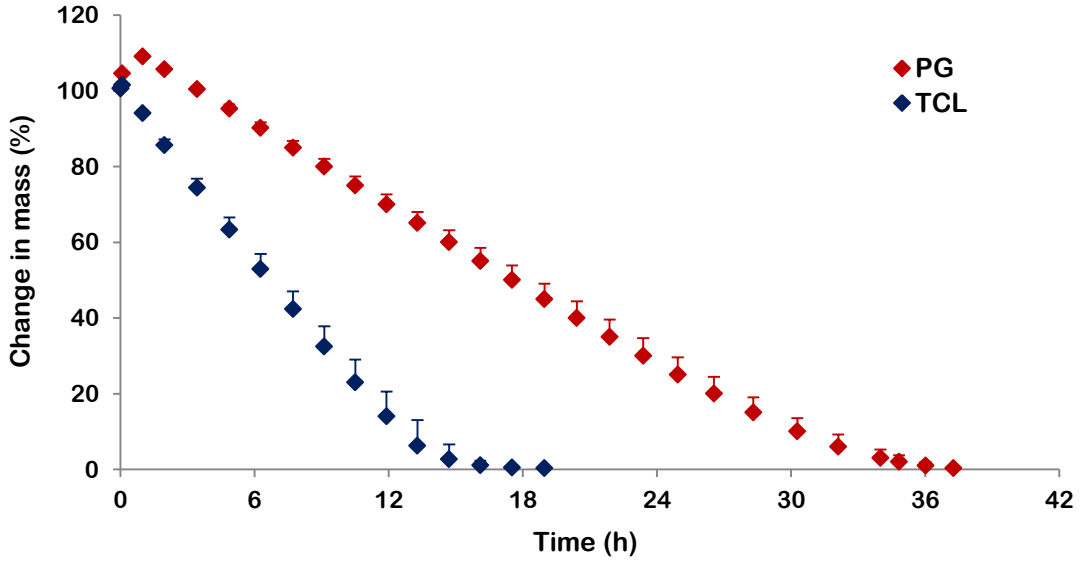

Figure 3-31 The evaporation profiles of PG and TCL at 32 °C and 50 % RH (mean + SD; n=3)

From the PG and TCL evaporation profiles, it is apparent that TCL evaporated more quickly than PG. TCL completely evaporated after ~16 h of application whereas this process took ~36 h for PG. As can be seen from the PG profile in Figure 3-31, a small peak was observed at the beginning of the profile. This implies that PG absorbed an amount of water before starting to evaporate. This was not surprising as PG has hygroscopic properties. Although the experimental conditions of DVS did not completely mimic the *in vitro* permeation conditions where the formulation was applied on the skin surface instead of a glass pan, however, it gave convincing evidence of the contribution of solvent evaporation in the drug crystallisation and therefore the lack of CILA permeation across the skin. Tsai and his colleges (1992) who studied the evaporation of PG from a ternary solvent system observed that the smaller the loading dose (20 µl/cm^2), the higher the degree of evaporation with time. The evaporation of PG led to precipitation of the drug on and within the skin and, thus, poor percutaneous penetration of drug through the skin (Tsai et al., 1992).

3.5.7.2.2.2 Permeation studies using binary solvent systems

Because of the relatively high Q_{48h} and percentage permeated observed with (PGML, CAP) and IPM respectively, further permeation studies (finite doses) were conducted using binary solvent systems. Representative profiles of the permeation of the drug permeated using PGML:IPM and CAP:IPM at different ratios are shown in Figures 3-32 and 3-33.

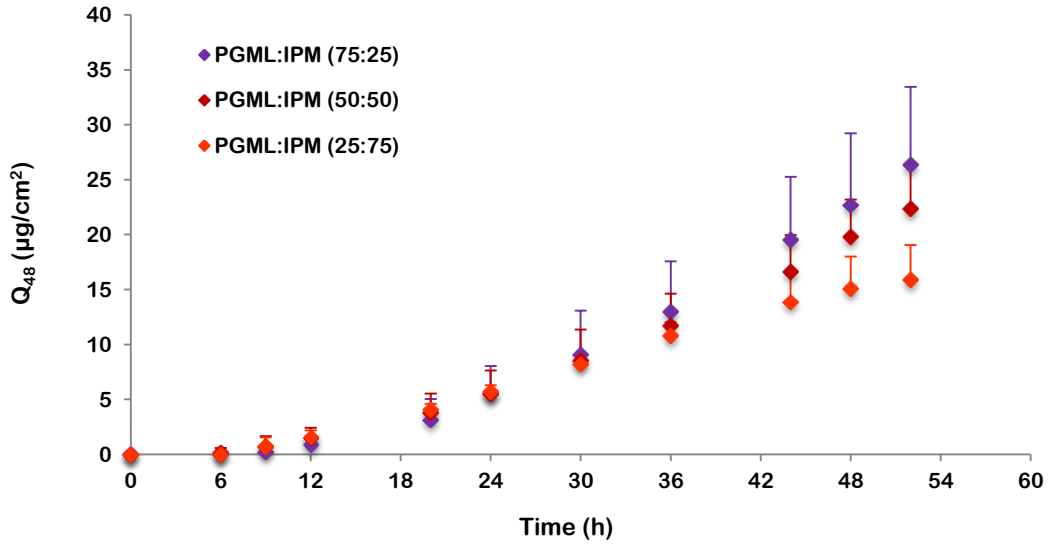

Figure 3-32 Permeation profiles of total CILA under finite dose conditions using PGML:IPM as a binary solvent system at different proportions across porcine ear skin (mean + SD; n=4).

Among the three different proportions of the binary solvent system (PGML:IPM), PGML:IPM (75:25) produced the highest flux. With increasing PGML concentration in the co-solvents, the permeation rate increased. However, Q_{48h} did not significantly change ($p > 0.05$) among all the PGML:IPM formulations. When IPM was combined with CAP, a further enhancement in CILA permeation was observed (Figure 3-33).

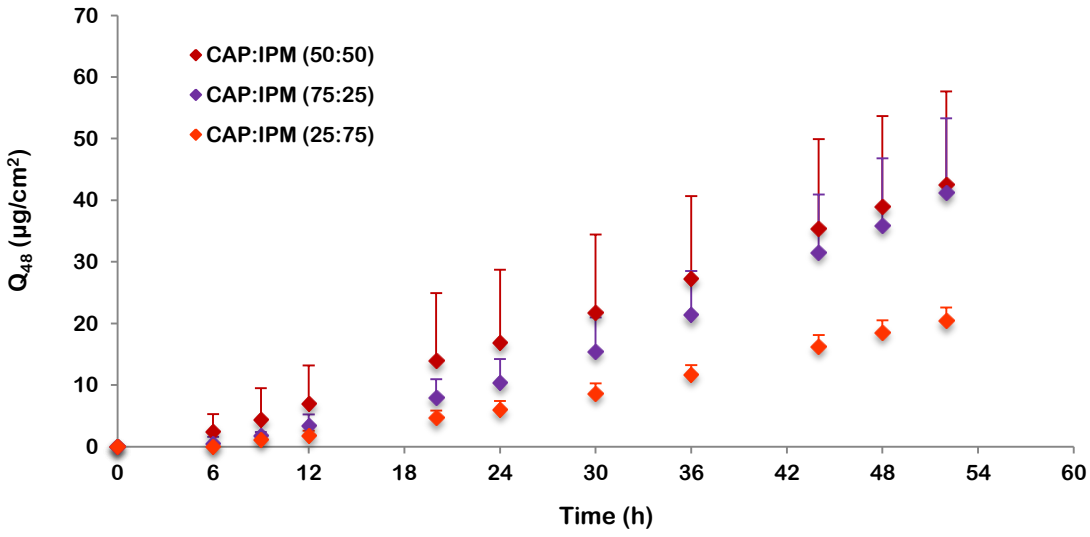

Figure 3-33 Permeation profiles of total CILA under finite dose conditions using CAP:IPM as a binary solvent system at different proportions across porcine ear skin (mean + SD; n=4).

The Q_{48h} of CILA as well as cilazaprilat formed during the permeation were measured, combined and illustrated in Figure 3-34. With regard to cilazaprilat formation, the findings of the permeation studies using binary solvent systems were similar to those using single solvent systems. The presence of cilazaprilat in the receptor phase was attributed to the metabolism process that occurred during the passage of CILA through the skin and inside the receptor medium.

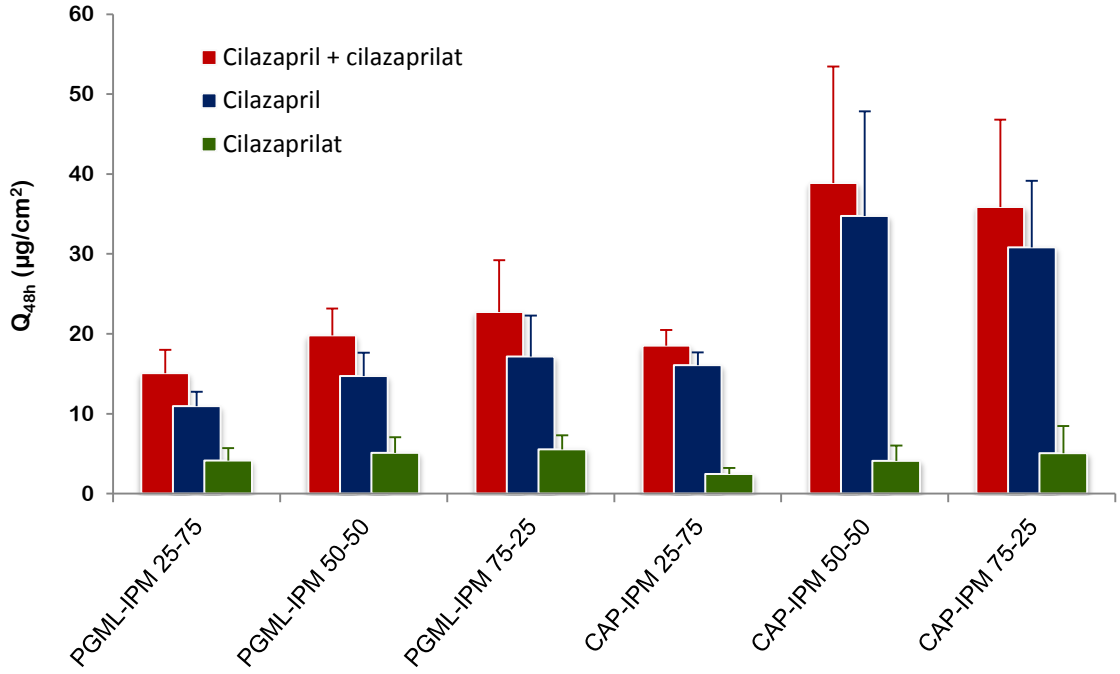

Figure 3-34 The cumulative amount of total CILA (CILA and cilazaprilat), CILA, and cilazaprilat permeated at 48 h using binary solvent systems under finite dose conditions through porcine ear skin (mean + SD; n=4).

As shown in Figure 3-34, the amount of cilazaprilat formed was less than that of CILA. The low level of bioconversion to cilazaprilat may be explained by the low level of enzyme activity in skin. The metabolic activity in skin was reported to be much lower than that in liver (Prusakiewicz et al., 2006; Harville et al., 2007). Morris et al. (2009) demonstrated that the metabolism of haloperidol esters in a porcine skin extract was

limited compared with that in the liver extract, where a complete hydrolysis was observed in the latter. The percentage of CILA permeated from the binary formulations was also calculated and illustrated in Figure 3-35.

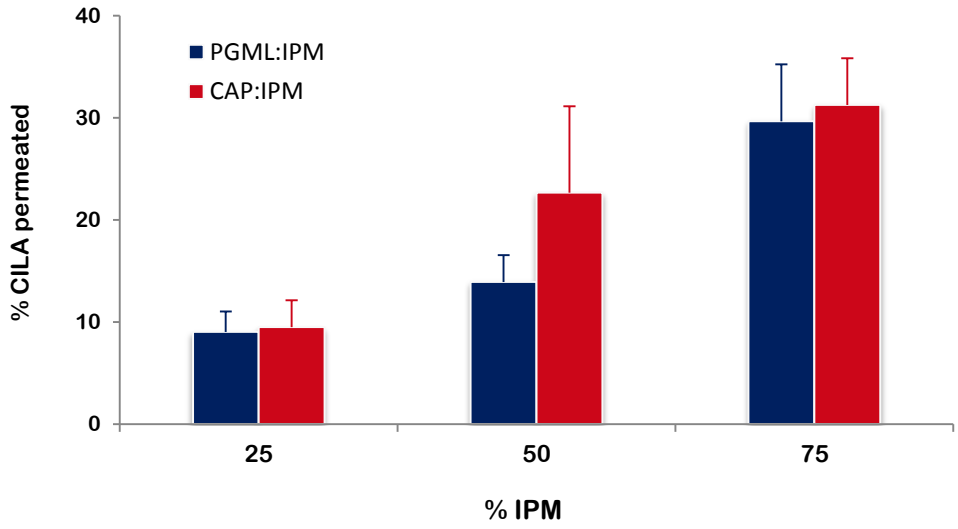

Figure 3-35 The percentage of CILA permeated through porcine ear skin from saturated solutions of the drug in binary solvent systems (mean + SD; n=4).

Interestingly, with increasing IPM concentration in the PGML:IPM and CAP:IPM formulations, the percentage of CILA permeated increased (i.e. the greater the IPM amount available, the higher the CILA percentage permeated). At the same time, an increase in the amount of PGML and CAP in the formulations resulted in an increase in Q_{48h} (Figure 3-34). Therefore, the rank order of Q_{48h} was in reverse to that of percentage permeated across the skin. However, this increase was not significant ($p > 0.05$) among all PGML:IPM formulations with different proportions.

Compared to the neat IPM, the amount of CILA permeated was enhanced between 3 and 8 fold by combining IPM with PGML or CAP with different proportions, 25, 50, and 75 % v/v. This may be attributed to the enhancement of CILA diffusion in

SC by adding IPM to PGML or CAP. The highest Q_{48h} (38.86 μg/cm^2) was obtained from the CAP:IPM (50:50) combination. Statistical comparison of Q_{48h} among the binary formulations showed that Q_{48h} in CAP:IPM (50:50) was significantly higher ($p < 0.05$) than that from PGML:IPM (50:50) and CAP:IPM (25:75). This was due to the increase in the amount of CILA available for permeation. As the highest Q_{48h} was achieved with CAP:IPM (50:50), it was selected for incorporation of a third solvent for further permeation studies.

3.5.7.2.2.3 Permeation studies using ternary solvent systems

Based on the results obtained from the penetration studies from the binary solvent formulations and in an attempt to increase the flux of CILA, more complex formulations using ternary solvent systems were selected. A hydrophilic vehicle, PG, TCL, DPG or PEG 200 was added to the selected binary combination (CAP:IPM). The CILA concentration in the different formulations applied was at saturated solubility level. As illustrated in Figure 3-36, among the various combinations examined, the formulations containing PG exhibited the greatest permeation rate through the porcine ear skin.

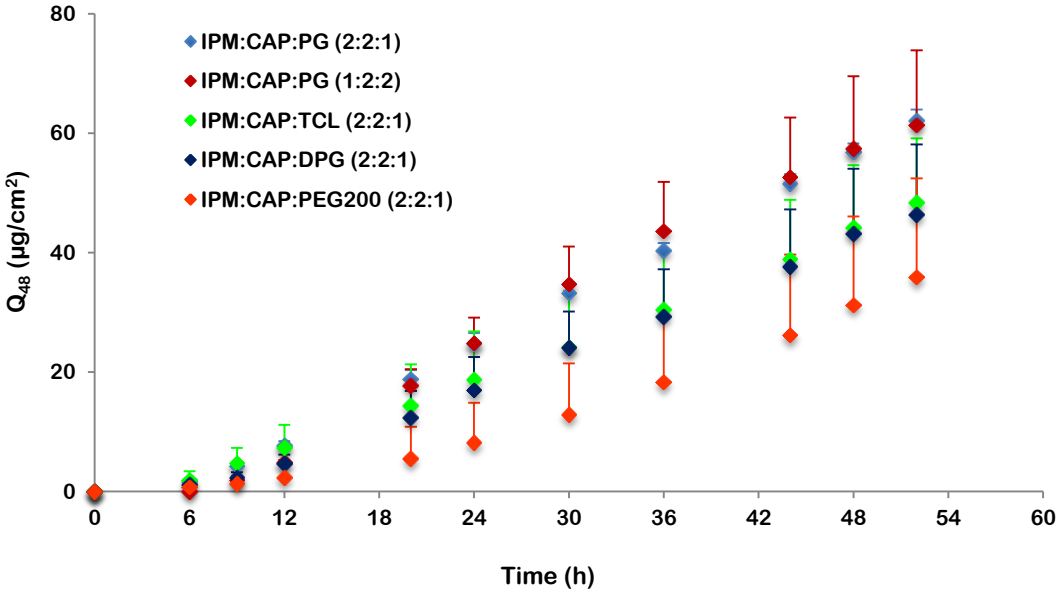

Figure 3-36 Permeation profiles of total CILA under finite dose conditions using different ternary solvent systems across porcine ear skin (mean + SD; n=4).

Furthermore, the shorter estimated lag time resulted from the same formulations. In topical formulations, PG has widely been investigated in terms of its ability to penetrate the human SC successfully and carry drug molecules through the skin (Wotton et al., 1985; Bendas et al., 1995; Trottet et al., 2004; Bowen and Heard, 2006; Karadzovska et al., 2012). X-ray scattering and diffraction and DSC studies showed that PG did not interfere with the SC lipids. However, it was likely that PG incorporated laterally with the head group region of the lipid bilayers (Bouwstra et al., 1991). The data from another study revealed the lateral and perpendicular integration of PG molecules between the polar head groups of the lipid bilayers (Brinkmann and Muller-Goymann, 2005). The conversion of CILA to cilazaprilat was observed in all skin permeation studies. The Q_{48h} of CILA, cilazaprilat, and the total (CILA + cilazaprilat) were also determined and illustrated in Figure 3-37. The Q_{48h} was unaffected by increasing the PG content from 20 to 40 %, where 56.9 ± 1.42 and 57.41 ± 12.13

µg/cm^2 of CILA permeated, respectively. The difference was not statistically significant (p > 0.05). Therefore, increasing the PG amount in formulation did not promote CILA permeation. These findings proposed that the drug on or in the skin may start to crystallize as a result of PG depletion from the formulation.

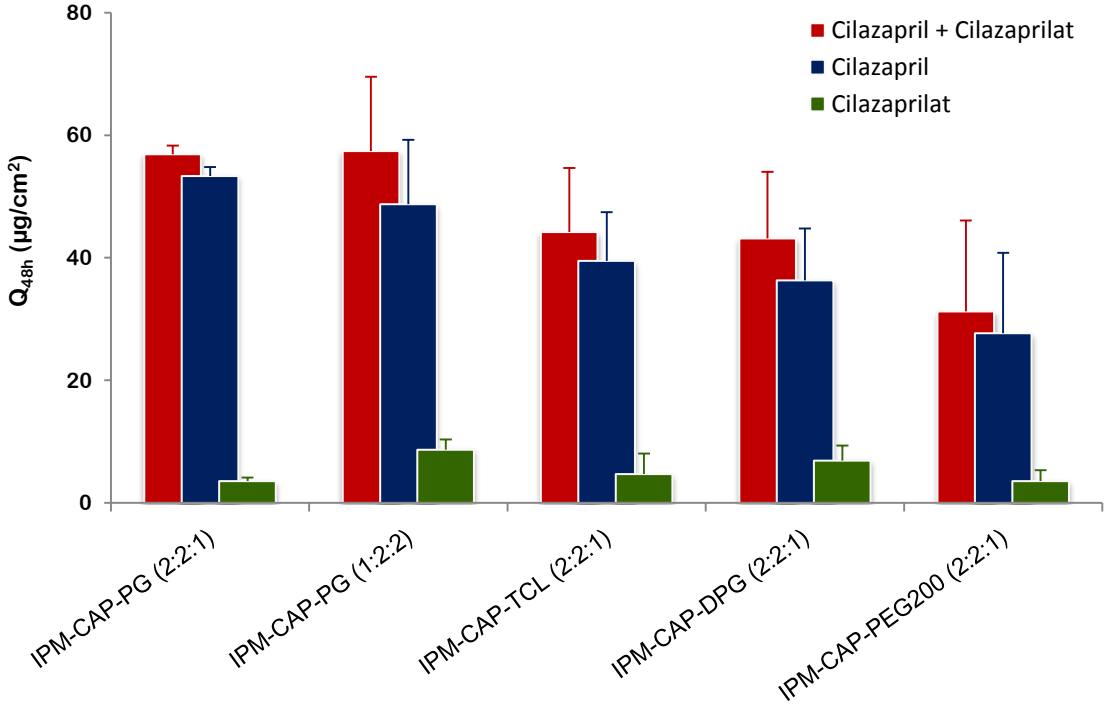

Figure 3-37 The cumulative amount of total CILA (CILA and cilazaprilat), CILA, and cilazaprilat permeated at 48 h using ternary solvent systems under finite dose conditions through porcine ear skin (mean + SD; n=4).

When PG was replaced by an equivalent volume of TCL, DPG, or PEG 200, the Q_{48h} decreased 1.2 -1.8 fold. Combining TCL with IPM and CAP enhanced the percutaneous absorption of CILA compared with the CAP:IPM binary formulations. TCL is a water miscible penetration enhancer. It was reported that TCL can modify skin permeability by increasing the drug solubility in the SC which, in turn, improves the flux (Harrison et al., 1996). The use of TCL in combination with other CPEs increased the

penetration of various drugs through excised human skin (Puglia and Bonina, 2008; Hirata et al., 2013). Hirata and colleagues (2013) reported that incorporation of TCL in carbenoxolone binary and ternary formulations of CPEs resulted in higher fluxes compared with the other formulations in the absence of TCL.

A reduction in Q_{48h} was observed when PG was replaced by DPG. This finding is in line with Fasano et al. (2011) who evaluated the *in vitro* absorption of PG and DPG through human skin. Both PG and DPG penetrated across the skin. However, the permeation rate of PG was 2.5 fold greater than that of DPG. Furthermore, the measured impedance before and after 24 h exposure showed 70 % reduction in the skin integrity when PG was applied whereas DPG had a minor effect on the impedance (Fasano et al., 2011).

Replacement of PG with an alternative glycol, PEG 200, produced the lowest Q_{48h} in comparison with the rest of the formulations (Figure 3-37). The Q_{48h} of CILA from IPM:CAP:PG (40:40:20) formulation was about 2 fold higher than the formulation when PG was substituted for PEG 200. The plausible explanation is the inability of the drug to be released from PEG 200 which might not properly penetrate the skin itself. This needs to be evaluated in future studies. Among the tested ternary formulations, only IPM:CAP:PG and IPM:CAP:PEG 200 with the same ratio (40:40:20) showed a significant difference ($p < 0.05$) in Q_{48h}.

3.5.7.2.2.4 Comparison among the single, binary, and ternary vehicle formulations.

Isopropyl myristate (IPM) is a non-polar enhancer. CAP is a fatty acid ester of propylene glycol used as penetration enhancer. Both of them are water immiscible.

CILA permeation with IPM in which CILA had low solubility (0.95 mg/ml) was low compared to that with CAP in which CILA had 77 fold higher solubility. At the same time the CILA percentage permeated through porcine ear skin using CAP and IPM as single solvent systems was 3.86 ± 0.86 and 48.22 ± 4.89 %, respectively. A combination of vehicles may modify the structure of the skin barrier and thus altering the penetration rate of drugs. The permeation of CILA was enhanced by the CAP:IPM (50:50) formulation when compared with the single vehicle formulations, IPM or CAP (Figure 3-38). Interestingly, this binary formulation showed 8.4 fold greater enhancement effect compared with the IPM vehicle. Combining a hydrophilic vehicle (PG) with lipophilic vehicles (CAP and IPM) resulted in a synergistic enhancement of CILA penetration across porcine skin as illustrated in Figure 3-38. This combination caused a decrease in the lag time with an increase in Q_{48h} by 31 % compared to IPM:CAP (50:50) formulation (Figure 3-39).

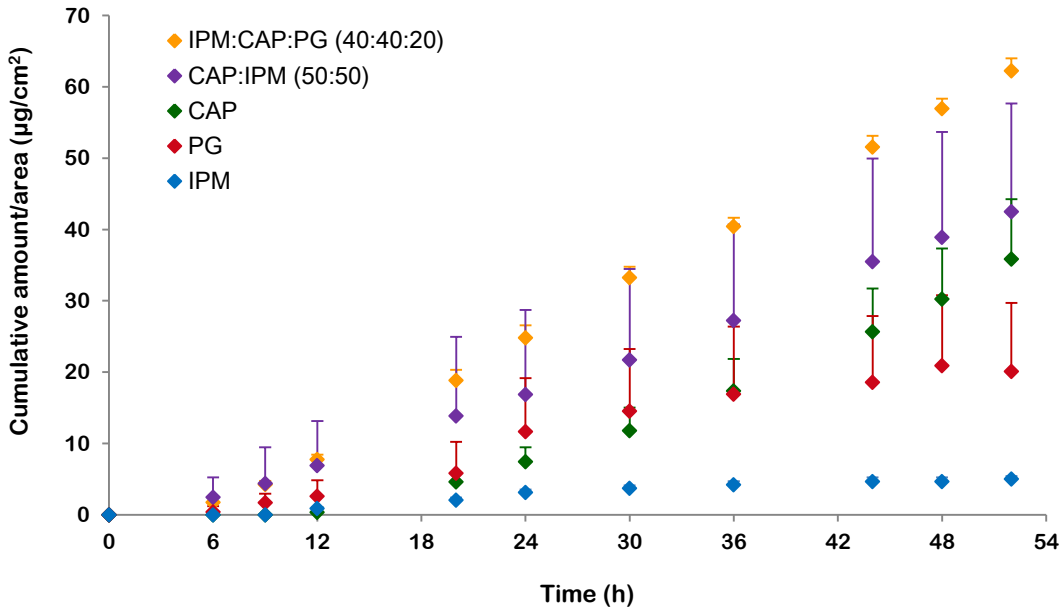

Figure 3-38 Permeation profiles of total CILA under finite dose conditions using single, binary, and ternary solvent systems across porcine ear skin (mean + SD; n=4).

All the formulations in Figure 3-38 were applied to the skin surface as finite doses. Therefore, it was expected that the drug would deplete resulting in a reduction in the permeation rate and an eventual plateau in the permeation profile. This was observed in IPM and PG formulations. However, CILA had high solubility in and at the same time relatively low permeability from CAP, CAP:IPM (50:50), and CAP:IPM:PG (40-40-20). Therefore it was difficult to observe donor depletion and to obtain the permeation profiles characteristic for finite dose application with these formulations. Interestingly, PG had the ability to penetrate the skin successfully and CILA solubility in this vehicle was very high (509 ± 32.23 mg/ml), yet the cumulative permeation profile with PG formulation reached a plateau. This was attributed to the depletion of PG from the skin surface leading to drug crystallisation.

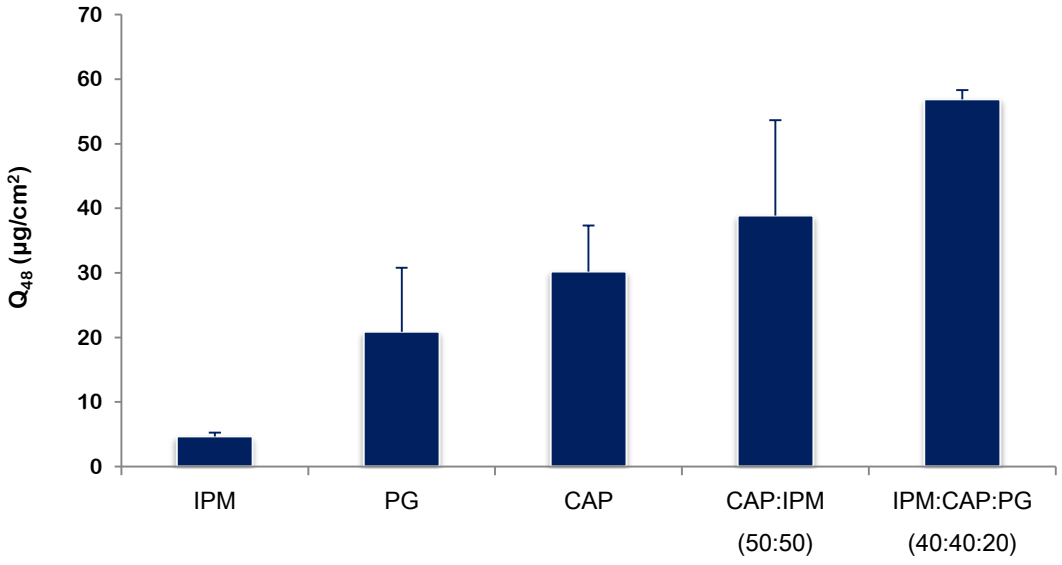

Figure 3-39 The cumulative amount permeated of total CILA in 48 h using different solvent systems under finite dose conditions through porcine ear skin (mean + SD; n=4).

As shown in Figure 3-39, CAP:IPM:PG (40:40:20) in comparison with IPM, PG and CAP improved the Q_{48h} of CILA permeated by 12.2, 2.7 and 1.9 fold, respectively. Compared to the single formulations, IPM and PG, the ternary formulation enhanced the Q_{48h} significantly ($p < 0.05$). These findings demonstrated that the combination of permeation enhancers, lipophilic and hydrophilic ones, was able to improve the permeation rate and decrease the lag time.

3.6 Conclusions

The development of topical formulations containing angiotensin converting enzyme inhibitors was achieved in this chapter. Ramipril and cilazapril were selected as model drugs. A wide range of solvents was investigated individually or in combination in order to optimize dermal formulations. Initially, the affinity of RAM and CILA for different solvent systems was determined at 32 °C. The capability of each system to solubilize the drugs varied from one to another. A relationship was observed between the solubility parameter of the vehicle and the solubility of CILA. The solubility of CILA was high in the solvent systems with solubility parameters close to 11.55 $(cal/cm^3)^{1/2}$, which corresponds to the calculated δ_{CILA}. It was also found that the solubility of CILA was inversely proportional to the difference between the solubility parameter of the solvent (δ_V) and that of the drug (δ_D). CILA solubility in the vehicles with $|\delta_V-\delta_D| < 2$ was much higher than that with $|\delta_V-\delta_D| > 2$.

In vitro permeation studies of RAM and CILA across epidermal human and porcine ear skin, respectively, were conducted. For RAM, the results showed low permeability when applied under infinite dose conditions. Furthermore, RAM-DKP was

detected in both the donor and receptor phase during the time course of experiment as a result of RAM degradation. For CILA, formulations were applied under both infinite and finite dose conditions. Under infinite dose applications, the fluxes of CILA were different among the pure vehicles examined despite the equal thermodynamic activities. This implies that the major factor that determined the drug permeability across the skin was not only the thermodynamic activity but also the specific vehicle effects on the skin barrier. The highest Q_{48h} was obtained from CAP and PGML whereas IPM and PG exerted the highest k_p. Based on the findings obtained from the permeation studies, binary formulations with a ratio of (50:50 v/v) were investigated: CAP:IPM, PGML:IPM, CAP:PGML. Compared with the neat solvents, a remarkable increase in permeation was observed when CILA was formulated in the binary solvent systems.

Further permeation studies under finite dose conditions were conducted. For individual solvents, it was difficult to observe donor depletion and to obtain the permeation profiles characteristic for the finite dose because of the low permeability of CILA compared to the dose applied. However, application of the PG and TCL formulations resulted in precipitation of CILA on the skin and a plateau of the permeation profiles, yet the CILA dose applied from these vehicles was very high. This was as a result of the depletion of the vehicle from the formulation applied by evaporation and rapid diffusion across the skin. The percentage of the applied dose permeated was low at 48 h from the majority of the singles vehicles. IPM was unique in that 48.22 % of the applied dose permeated. Because of the relatively high Q_{48h} and percentage permeated observed with (PGML, CAP) and IPM respectively, further

permeation studies were investigated using binary solvent systems, PGML:IPM and CAP:IPM. Interestingly, the greater the IPM amount was available, the higher the CILA percentage permeated. Compared to the neat IPM, the amount of CILA permeated enhanced 3 - 8 fold by combining IPM with PGML and CAP. In an attempt to increase the flux of CILA, more complex formulations using ternary solvent systems were selected for further permeation studies. Incorporating a hydrophilic vehicle with both IPM and CAP resulted in further improvement in the drug permeation. Among the various combinations examined the formulation IPM:CAP:PG exhibited the greatest permeation rate.

Finally, it was interesting to note that in all tested formulations, HPLC analysis showed the presence of the metabolite, cilazaprilat, together with CILA in the receptor phase, indicating that CILA underwent metabolism during the permeation. Further investigations in order to identify the rationale for this conversion were conducted in Chapter 4, confirming the enzymatic and chemical hydrolysis of CILA.

Chapter 4

The fate of cilazapril in porcine skin homogenate

4 The fate of cilazapril in porcine skin homogenate

4.1 Introduction

Skin is considered as an active metabolizing organ. It is capable of phase I and phase II biotransformation reactions (Wilkinson and Williams, 2007). Phase I, namely functionalization reactions, includes oxidative, reductive and hydrolytic reactions while phase II involves conjugation reactions. Skin possesses the major enzymes found in the liver and therefore plays an important role in the metabolism of exogenous compounds (Kao and Carver, 1990; Korinth et al., 2007; Traynor et al., 2008; Rolsted et al., 2009). Metabolism processes in the skin can make lipophilic compounds more hydrophilic (Mollgaard et al., 1982; Wang et al., 2007; OECD, 2010) and at the same time can influence the biological activity of these compounds.

The epidermis and dermis are considered the major site of metabolism in both porcine and human skin (Montagna, 1955; Meyer and Neurand, 1976; Bickers and Mukhtar, 1990; Wilkinson and Williams, 2007; OECD, 2010; Lau et al., 2012). Montagna (1955) demonstrated the abundance of esterase activity in human epidermis between the stratum granulosum and SC, hair follicles, and sebaceous glands. Meyer and Neurand (1976) confirmed the presence of oxidative and hydrolytic enzymes in porcine skin and the similarities of these enzymes to those in human skin in terms of distribution and activity. Lau et al (2012) findings were in line with Montagna (1955), yet the former used porcine ear skin.

It is strongly recommended that freshly excised skin should be used for the assessment of skin metabolism, and the storage period and temperature depend on

the enzyme being investigated (OECD, 2004b). Generally, metabolism is less significant for *in vitro* experiments compared with the *in vivo* experiments due to the lack of skin viability (Wester et al., 1998), but at the same time leakage of enzymes from the dermal side into the receptor phase during *in vitro* permeation studies can lead to overestimation of the metabolism (Bundgaard et al., 1983).

A number of compounds, including aciclovir, haloperidol and retinoic acid were synthesized in a prodrug form (Abdulmajed et al., 2006; Abla et al., 2006; Morris et al., 2009). A prodrug by definition is a form of a drug that exhibits its pharmacological effect after undergoing chemical and/or enzymatic conversion (Wermuth et al., 1998). Metabolism of these prodrugs and others by esterases in porcine and human skin has been previously studied (Bonina et al., 2001; Ngawhirunpat et al., 2004; Valiveti et al., 2005; Abdulmajed et al., 2006; Jewell et al., 2007b; Morris et al., 2009; Beydon et al., 2010). These studies showed that both parent compounds and their metabolites were found in the receptor fluid of the diffusion cells when viable skin was used. Esterases, a group of enzymes that hydrolyze carboxylic acid esters of alcohols and phenols, are found in all organisms from microorganisms to mammals (Wilkinson and Williams, 2007; Gruning et al., 2009). They are relatively stable enzymes and responsible for hydrolytic biotransformation of endo- and exogenous compounds. Esterases can not only function in viable epidermis and dermis but also in non-viable cells, the stratum corneum (Meyer and Neurand, 1976; Guzek et al., 1989; Jewell et al., 2007c; Lau et al., 2012). Skin esterase was reported to maintain its activity when skin was stored at or below – 20˚C (Hewitt et al., 2000; Beydon et al., 2010). However, this activity can be affected by a number of physiological factors such as species differences

(Ngawhirunpat et al., 2004; Prusakiewicz et al., 2006; Oesch et al., 2007), the anatomical site, and gender (Hikima and Maibach, 2007; Jewell et al., 2007c).

In recent years, porcine skin has been considered as an optimal animal model for studying enzymatic activity. A comparison of the esterase activity in human skin with that in porcine skin was investigated (Ngawhirunpat et al., 2004; Prusakiewicz et al., 2006; Jewell et al., 2007a; Jewell et al., 2007b). The esterase activity of porcine skin was reported to be very similar to that of human. However, rat skin showed greater esterase activity than porcine and human skin (Prusakiewicz et al., 2006; Harville et al., 2007) and hence porcine skin was considered as a surrogate model of biotransformation for human skin. Morris et al. (2009), Prusakiewicz et al. (2006) and Harville et al. (2007) demonstrated that the rate of hydrolysis in skin was much lower than liver. It was also reported that back and ear skin of porcine was the closest to human breast in terms of metabolism of ester compounds (Jewell et al., 2007c).

Cilazapril, one of several ester-based prodrugs has been used in oral formulations for the treatment of hypertension and heart failure (Jackson, 2006). After oral administration, it is hydrolysed by the liver esterases to its diacid active metabolite, cilazaprilat (Moffat et al., 2011). However, the behaviour of this drug in the presence of skin enzymes has not been evaluated to date.

4.2 Aims

The primary aim of this study was to evaluate the effect of freezing on esterase activity in porcine ear skin. The secondary aim was to investigate the role of porcine

skin homogenate in the metabolism of CILA in order to confirm the conversion of CILA to cilazaprilat that occurred during the permeation studies.

4.3 Materials

Cilazapril [CILA] was a gift from Ranbaxy laboratories Ltd (Punjab, India). Cilazaprilat was purchased from Toronto Research Chemicals Inc. (Toronto, Canada). Dimethyl sulfoxide (DMSO), *p*-nitrophenyl butyrate (PNPB), sodium azide, phenylmethanesulfonyl fluoride (PMSF), Bradford reagent, and tryptone soya agar (TSA) were obtained from Sigma-Aldrich, UK. Penicillin-Streptomycin (P/S) liquid (10000 U/ml-10000 µg/ml) was from Invitrogen, UK. Bovine serum albumin (BSA) standard (2 mg/ml), methanol, water, orthophosphoric acid as well as phosphate buffer saline (PBS) tablets were purchased from Fisher Scientific Ltd (Leicestershire, UK). Potassium dihydrogen phosphate (KH_2PO_4) was obtained from BDH, UK. Deionized water was prepared using a USF ELGA Option 3 water purifier system (Scotland, UK).

4.4 Methods

4.4.1 Analysis of cilazapril and its metabolite, cilazaprilat, by HPLC

CILA and its metabolite, cilazaprilat, were detected and quantified by an Agilent 1200 series HPLC System (Agilent Ltd, UK) with the same chromatographic conditions as described in section 3.4.1

4.4.2 Preparation of porcine ear skin homogenate

Fresh porcine ears were obtained from a local slaughterhouse. The ears were cleaned with cold running water in order to remove all attached residues. Skin was

dissected from the cartilage with a scalpel. The technique used for the preparation of the skin homogenate was developed by modifying the method described by Woolfson et al. (1990) and Jewell et al. (2007b). Porcine ear skin from three different donors was used. The skin was sliced into small pieces. These pieces were rapidly frozen and ground with liquid nitrogen to a fine powder using a pestle and mortar. Liquid nitrogen was added from time to time to keep the frozen status. The frozen powdered skin was then transferred into a 7 ml glass homogenizer (Omni Int., USA) with PBS and homogenized. The temperature was kept cool at all times by surrounding the skin suspension with ice and by cooling the homogenizer head with ice before each homogenization. The resultant mixture was centrifuged at 4°C for 20 min at 13000 rpm using a controlled temperature centrifuge (Eppendorf®5415, Germany). Figure 4-1 illustrates the steps for preparing porcine ear homogenate. Aliquots of the supernatant were used immediately for metabolism and esterase activity studies. Some of the supernatant was transferred to a 2 ml centrifuge tube, heated in boiling water for four hours and then autoclaved at 121˚C for 20 min in order to denature enzymes. This was used as a control in metabolism studies.

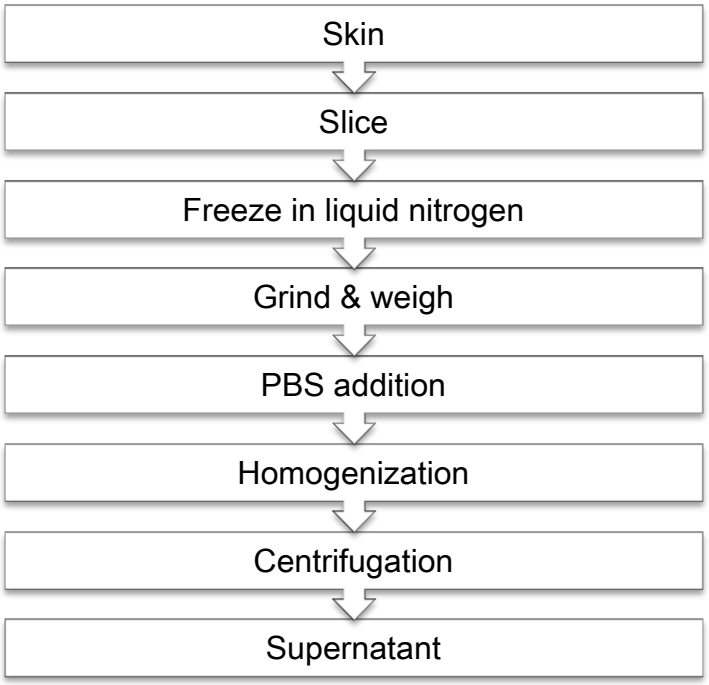

Figure 4-1 Flow chart of preparing porcine ear skin homogenate

4.4.3 Determination of the protein concentration in porcine skin

Total protein concentration in the skin homogenate was determined by the Bradford protein assay (Bradford, 1976) using bovine serum albumin (BSA) as a standard. It is a dye-binding assay in which a colour change of the dye occurs in response to the protein concentrations.

This assay was performed in a 96 well plate in accordance with the Sigma-Aldrich protocol (2011). Bradford reagent was gently mixed in the bottle and brought to room temperature. Protein standards in buffer ranging from 0.125 – 1.7 mg/ml were prepared using the BSA standard. 5 µl of the protein standards as well as homogenate samples with unknown concentrations were added to separate wells in the 96 well plate (Figure 4-2). To the blank well, 5 µl of PBS pH 7.4 was added. Protein solutions were assayed in triplicate. To each well being used, 250 µl of the Bradford reagent was added and

mixed on a shaker for ~30 seconds. The resultant mixtures were incubated at room temperature for 20 minutes. The absorbance was then measured at 595 nm. The net absorbance at 595 nm versus the protein concentration of each standard was plotted. If necessary, homogenate samples were diluted to ensure the concentrations were within the linear range of 0.125 -1.7 mg/ml. The total concentration of protein present in the skin homogenate was calculated based on the calibration curve equation.

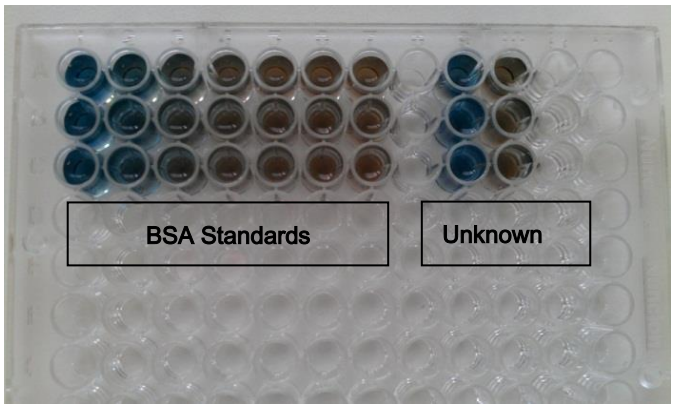

Figure 4-2 The 96 well plate method for protein assay. As the protein concentration in the BSA standards or test sample increases, the blue colour becomes darker.

4.4.4 Esterase activity studies

Total esterase activity in the skin homogenate was assessed using *p*-nitrophenyl butyrate (PNPB) as a substrate (Jewell et al., 2007c; Sigma-Aldrich, 2012). Jewell and co-workers (2007c) investigated the variability in esterase activity from different sites of porcine skin. The substrate was added to the skin homogenate and the colour change resulted from the formation of *p*-nitrophenol, the final product of this enzymatic reaction, was measured spectrophotometrically (Equation 4.1).

p-nitrophenyl butyrate + $H_2O \xrightarrow{Esterase}$ *p*-nitrophenol + butyric acid ……. (4.1)

Briefly, 100 µl of the homogenate was added to a 4 ml cuvette containing 30 µl of PNPB (100 mM in DMSO) and 2.870 ml of PBS (pH 7.4) with a blank control containing 100 µl of PBS, 30 µl of PNPB (100mM in DMSO) and 2.870 ml of PBS (pH 7.4) and the difference in absorbance at λ=420 nm was measured by BioMate® spectrophotometer using the kinetics mode over 5 minutes. Reaction mixtures were mixed by cuvette inversion. Reactions were linear (r^2 = 0.99) for the duration of the assay. Measurements were performed in triplicate and the mean was used for calculation of esterase activities as shown in Equations 4.2 and 4.3 (Sigma-Aldrich, 2012).

$$\text{Units/ml Enzyme} = \frac{(\Delta A_{420\,\text{nm}} / \min \text{test} - \Delta A_{420\,\text{nm}} / \min \text{Blank}) \text{ x } 3 \text{ x df}}{5 \text{ x } 0.1} \ldots\ldots\ldots (4.2)$$

Where

$\Delta A_{420\,nm}$ is the absorbance difference at 420 nm for the test sample or blank used.

3: the total volume of assay (ml).

df: dilution factor.

5: millimolar extinction coefficient of *p*-nitrophenol at pH 7.5.

0.1: the volume of enzyme used (ml).

$$\text{Units/mg skin} = \frac{\text{units/ml enzyme}}{\text{mg skin/ml enzyme}} \quad \ldots\ldots\ldots\ldots\ldots\ldots (4.3)$$

4.4.5 The effect of adding sodium azide, P/S, and PMSF on the esterase activity

To see whether or not the addition of sodium azide, P/S, and PMSF can interfere with or has an effect on the esterase activity, 20 µl of the stock solution of sodium azide (1 % w/v, in water), P/S (10000 U/ml - 10000 µg/ml), and PMSF (0.5 % w/v, in ethanol) was separately added to 1 ml of skin homogenate placed in 2 ml centrifuge tubes. The

samples were vortexed for 15 min at room temperature and then incubated at 32 ˚C for 12 h. The total esterase activity was determined as described in section 4.4.4. 1 ml of the pure skin homogenate and boiled homogenate were used as controls.

4.4.6 *In vitro* metabolism studies

Porcine ear skin from three different donors was separately homogenized in PBS pH 7.4 at 4°C as described in section 4.4.2. The supernatant of the homogenate was then used in the metabolism experiments. The rate of CILA hydrolysis was determined at 32 ˚C in the following media: deionized water, PBS pH 7.4, skin homogenate alone and homogenate with one of the following: sodium azide, P/S, PMSF, and P/S plus PMSF in order to explain the contribution of the agents to CILA hydrolysis. When sodium azide, P/S, PMSF, and P/S plus PMSF were added to the homogenate, the mixtures were vortexed for 15 min at room temperature before CILA was added. At t_0 100 µl of CILA (1 mg/ml in PBS) was added to 900 µl of each medium yielding the initial concentration of 0.1 mg/ml in the incubation mixture. 100 µl aliquot was immediately taken and the mixture was then incubated at 32 °C. Samples were collected at 24, 48, and 72 h. At these time intervals, the incubation was terminated by removing 100 µl of the mixture and adding it to 1 ml of methanol at 4°C in order to precipitate proteins and hence quench the esterase activity immediately. The samples were vortexed for 2 min and then diluted with potassium dihydrogen phosphate 0.01 M. The mixtures were then centrifuged at 13000 rpm for 15 min and the amounts of CILA and its metabolite were determined initially and at predetermined time intervals over the study period using the HPLC. Since the concentration of the drug was high, the sorption to vessel walls was considered minimal.

Blank samples of homogenate, P/S, sodium azide, PMSF were also injected into the HPLC. The boiled homogenate prepared as described in section 4.4.2 was used along with water and PBS as controls in the metabolism studies. These controls were incubated and processed in the same way as the skin homogenates.

4.4.7 Preparation and inoculation of agar plates.

Tryptone soya agar (TSA) is a general purpose culture medium for cultivation and isolation of microorganisms (aerobes and anaerobes). TSA medium was prepared as follow: 40 g of dehydrated media was suspended in one litre of deionized water. After sterilization at 121 ˚C for 15 min, the agar was cooled to ~40 °C prior to pouring petri dishes in order to minimize the amount of condensation. 15 to 20 ml of the medium was poured into a sterile plastic petri dish (100 x 10 mm). Once the agar was solidified, plates were used immediately or refrigerated in closed bags until required. Refrigerated plates were warmed to room temperature prior to use.

A reusable glass spreader was flame sterilized by dipping in 70 % ethanol, shaking off the excess alcohol, and igniting the residue. The spreader was then allowed to cool. An inoculum of 50 µl from each of the incubation mixtures prepared in section 4.4.6 was applied on the agar surface. The spreader was then rotated over the agar surface in order to evenly distribute the inoculum and to allow it to be absorbed into the agar. The plates were then inverted and incubated at 37˚C. Plates were prepared in triplicate

4.4.8 Data analysis

One way analysis of variance (ANOVA) was carried out with a significance level set at 0.05 to examine for differences among three or more groups. Furthermore, the Tukey test, a post hoc statistical test, was performed to analyse the individual differences between the groups. The data treatment and statistics were performed using Microsoft® Office Excel (2010) and GraphPad Prism® (v 6.03) software. All results are presented as the mean ± standard deviation.

4.5 Results and discussion

4.5.1 The protein content of porcine skin

The protein content in skin was determined by the Bradford assay with bovine serum albumin as the standard. The Bradford assay has been widely used to determine the protein content (Chao and Nylander-French, 2004; Hammell et al., 2005; Sander et al., 2009). Figure 4-3 illustrates the amount of protein in fresh and frozen (-25 ˚C, 12 weeks) skin.

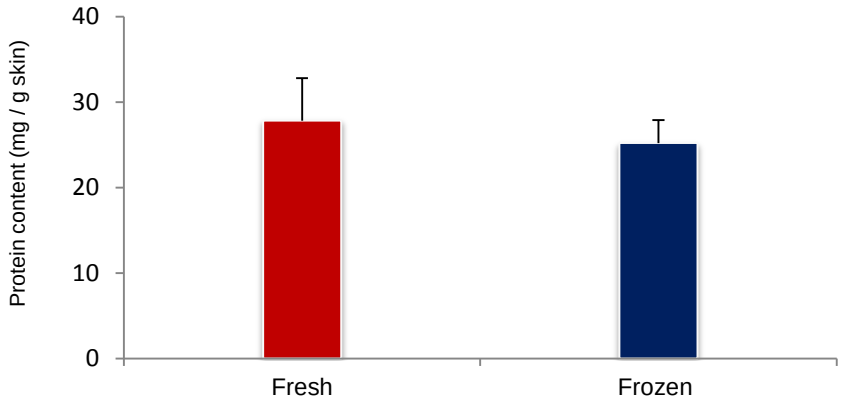

Figure 4-3 Protein content (mg/g skin) in fresh and frozen porcine ear skin at -25 ˚C for 12 weeks (mean + SD; n=3).

The decrease in the protein content after tissue freezing was not statistically significant ($p > 0.05$).

4.5.2 Effect of freezing on skin esterase activity

The presence of esterase in the prepared skin homogenate was previously confirmed by using *p*-nitrophenyl butyrate as a substrate and subsequent spectrophotometry (Woolfson et al., 1990; Jewell et al., 2007c). In the present study, a comparison of the esterase activity in fresh porcine ear skin with that in frozen tissue (-25 ˚C, 12 weeks) is illustrated in Figure 4-4. As expected, there was a tendency for a higher activity in fresh skin (24.8 ± 2.6 units/g skin), yet this activity was not significantly different ($p > 0.05$) when compared with the frozen tissue. Therefore, freezing maintained the metabolic capacity of the skin when fresh skin was stored at -25 ˚C for up to 3 months.

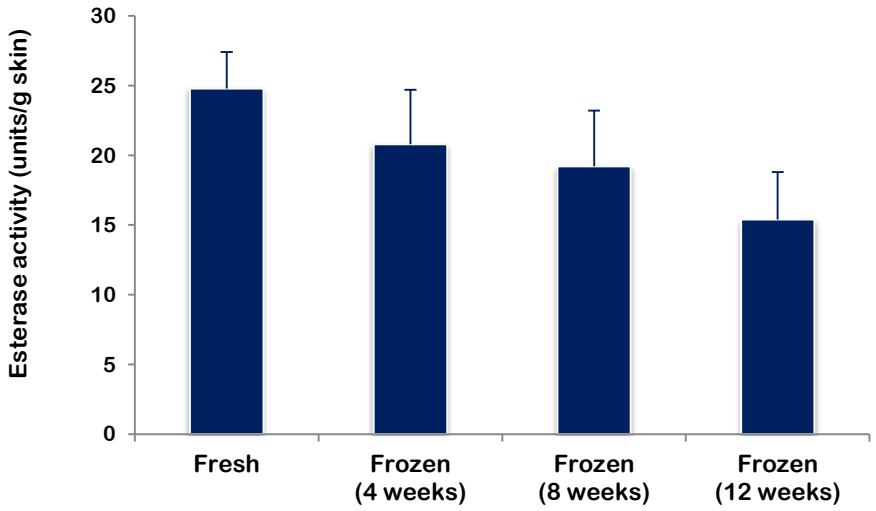

Figure 4-4 Esterase activity (units/g skin) in fresh and frozen porcine ear skin at -25 ˚C (mean + SD; n=3).

Although the statistical analysis did not show a significant difference in the esterase activity, however, a visible drop in the enzyme activity with time existed. Perhaps, with an increase in the number of samples, this trend could be further defined.

These findings are in agreement with those of Hewitt et al. (2000) and Beydon et al. (2010) who demonstrated that skin can maintain its esterase activity if stored at or below -20˚C for up to 6 weeks. Hewitt and colleagues (2000) studied the effect of freezing on the skin absorption and metabolism of two herbicides, fluroxypyr methyl ester and fluroxypyr methylheptyl ester, using full thickness human skin. They demonstrated that the penetration of the tested compounds increased in frozen tissue whereas the metabolic capability was not affected by freezing at -20˚C up to 6 weeks. A comparison of esterase activity in fresh and frozen porcine skin from the same donor was conducted by Beydon et al. (2010). The skin was kept at -20˚C up to 6 weeks before use. The results indicated that both the carboxylesterase activity and percutaneous absorption were not significantly different ($p > 0.05$) between the fresh and frozen tissue. Porcine ear skin stored at -20˚C for a longer period (up to 2 months) was also able to hydrolyze valaciclovir to aciclovir (Abla et al., 2006). The complete hydrolysis of ester prodrugs of buprenorphine across human skin which was kept at -20˚C for up to 4 months has also been reported (Stinchcomb et al., 1996). Conversely, Lau et al (2012) found that esterase activity in porcine ear skin reduced under frozen conditions. The authors compared the esterase activity in fresh skin with that in frozen skin at -20˚C for 1 week. Two methods were used: esterase staining and determination of hydrolysis of acetylsalicylic acid in porcine ear skin by HPLC (Lau et al., 2012).

4.5.3 The effect of adding sodium azide, P/S, and PMSF on the esterase activity

The influence of various substances (sodium azide, P/S, and PMSF) on the esterase activity was also evaluated. Figure 4-5 shows the esterase activity (units/g skin) in both boiled and pure homogenate along with homogenate to which sodium azide, P/S, and PMSF were added separately. The pure homogenate was considered as a control.

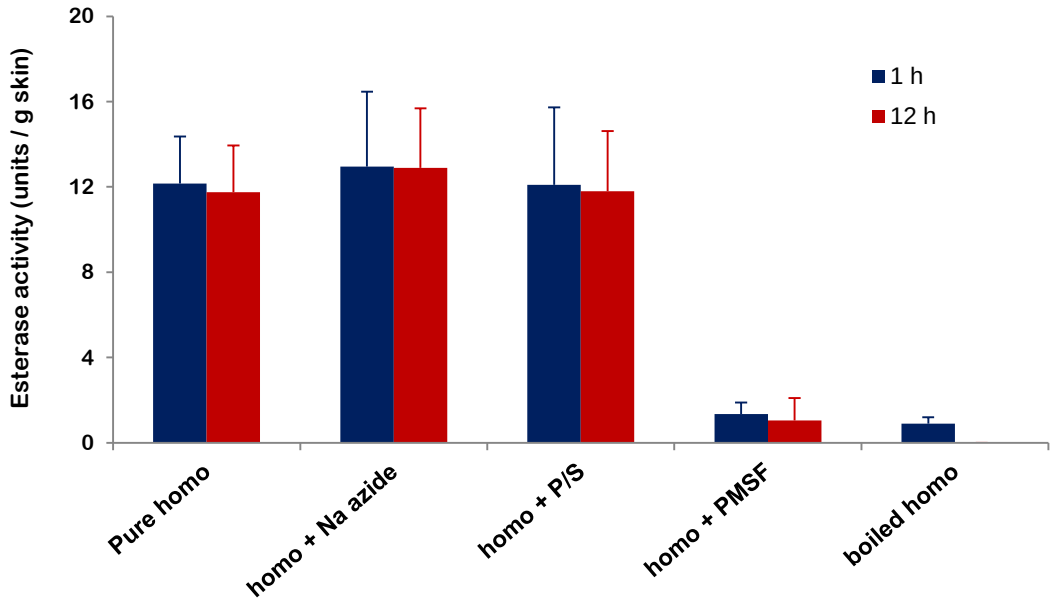

Figure 4-5 Esterase activity (units/g skin) in porcine ear homogenate (homo) containing different additives (mean + SD; n=3).

As illustrated in Figure 4-5, the addition of sodium azide and P/S to the pure homogenate had no significant effect ($p > 0.05$) on the skin esterase activity when compared with the control. No significant differences ($p > 0.05$) were also observed for each sample between 1 and 12 h. Therefore, the presence of these substances in the homogenate should not interfere with the enzyme activity. In an attempt to elucidate the contribution of sodium azide to the hydrolytic activity of esterase, Gaynor assessed the hydrolysis of diclofop methyl in an esterase solution with or without sodium azide

(Gaynor, 1992).The data showed a 7 % reduction in the enzyme capacity to hydrolyse diclofop methyl to diclofop. However, Munjal and Rose (1972) stated that sodium azide did not inhibit the hydrolysis capacity of kidney esterase and the inhibitory effect of this substance on the esterase activity depended on the tissue esterase.

Interestingly, after the skin homogenate was pretreated with PMSF, the amount of esterase activity significantly dropped ($p < 0.05$) and at the same time was similar to the boiled homogenate. Therefore, PMSF exhibited an inhibitory effect on the esterase capacity of the homogenate. The ability of PMSF to inhibit esterases was previously reported (Prusakiewicz et al., 2006; Jewell et al., 2007a). Prusakiewicz and colleagues (2006) characterized esterases in the homogenate of porcine skin using naphthyl acetate as a substrate and PMSF and *bis*-(*p*-nitrophenyl) phosphate (BNPP) as selective esterase inhibitors. PMSF and BNPP showed comparable results in terms of suppression of carboxylesterase responsible for the hydrolysis of naphthyl acetate in skin.

4.5.4 Metabolism studies

A number of experiments were conducted with water, PBS, skin homogenate alone and with sodium azide, P/S, PMSF in an attempt to evaluate the influence of the presence of these agents on CILA metabolism by skin esterases. Sodium azide and P/S were added to the homogenate in order to inhibit the bacterial metabolism of CILA. PMSF was added to inhibit the skin esterases which play a key role in the drug metabolism. The HPLC chromatograms of the blank samples showed no interferences with the peaks of CILA and its metabolite, cilazaprilat. HPLC analysis of the incubation

mixtures in PBS (Figure 4-6) and pure homogenate (Figure 4-7) revealed the main peak of CILA at ~12.4 min. along with another unknown peak at ~8.8 min. The latter gradually increased in area with the incubation time. The retention time of this peak matched with that of the cilazaprilat standard. This confirmed that the metabolism of CILA occurred via the cleavage of the ester bond resulting in cilazaprilat formation.

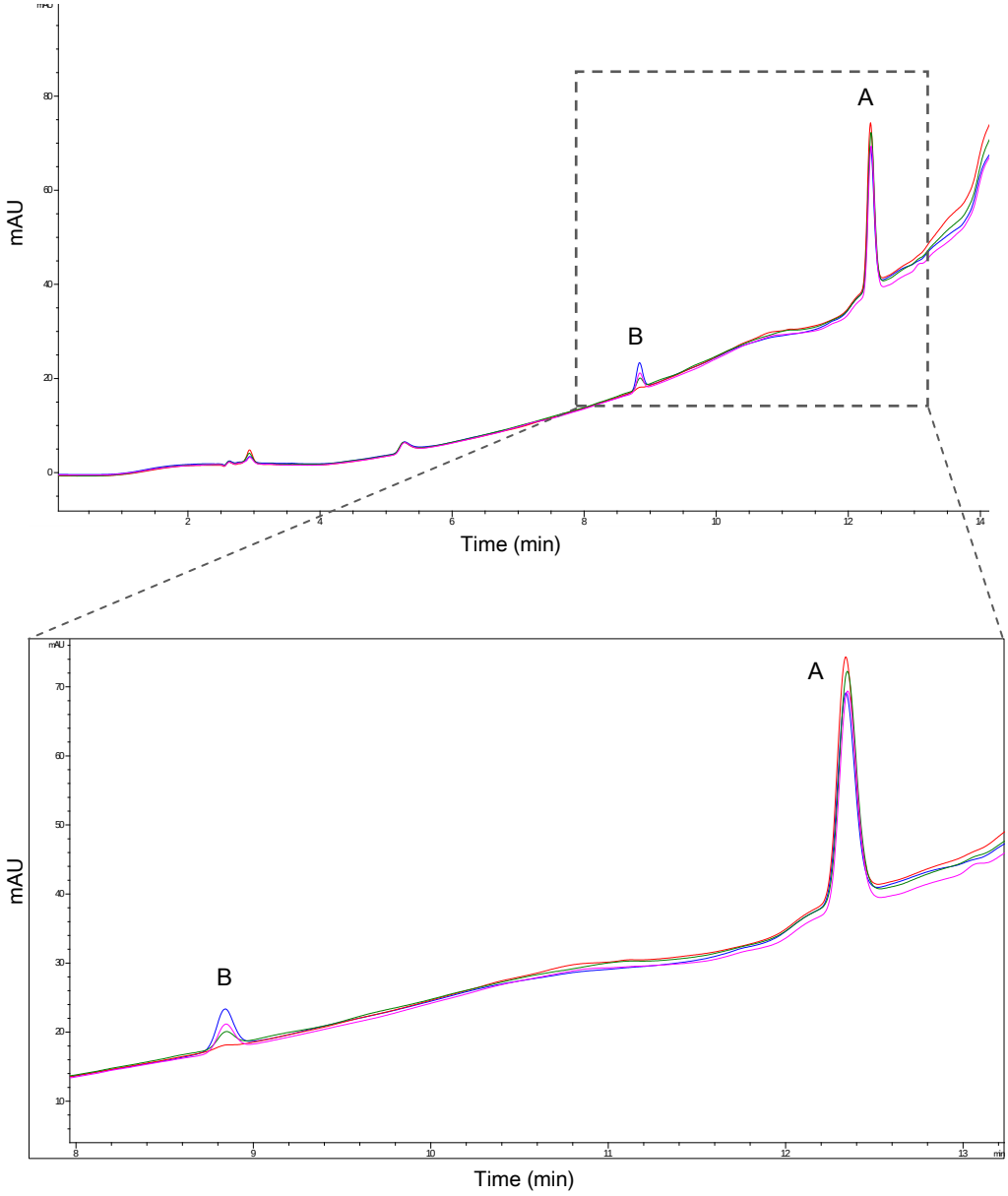

Figure 4-6 Overlaid HPLC chromatograms of CILA (A) and its metabolite, cilazaprilat (B) from PBS pH 7.4 at t_{0h} (red line), t_{24h} (green line), t_{48h} (pink line), amd t_{72h} (blue line)

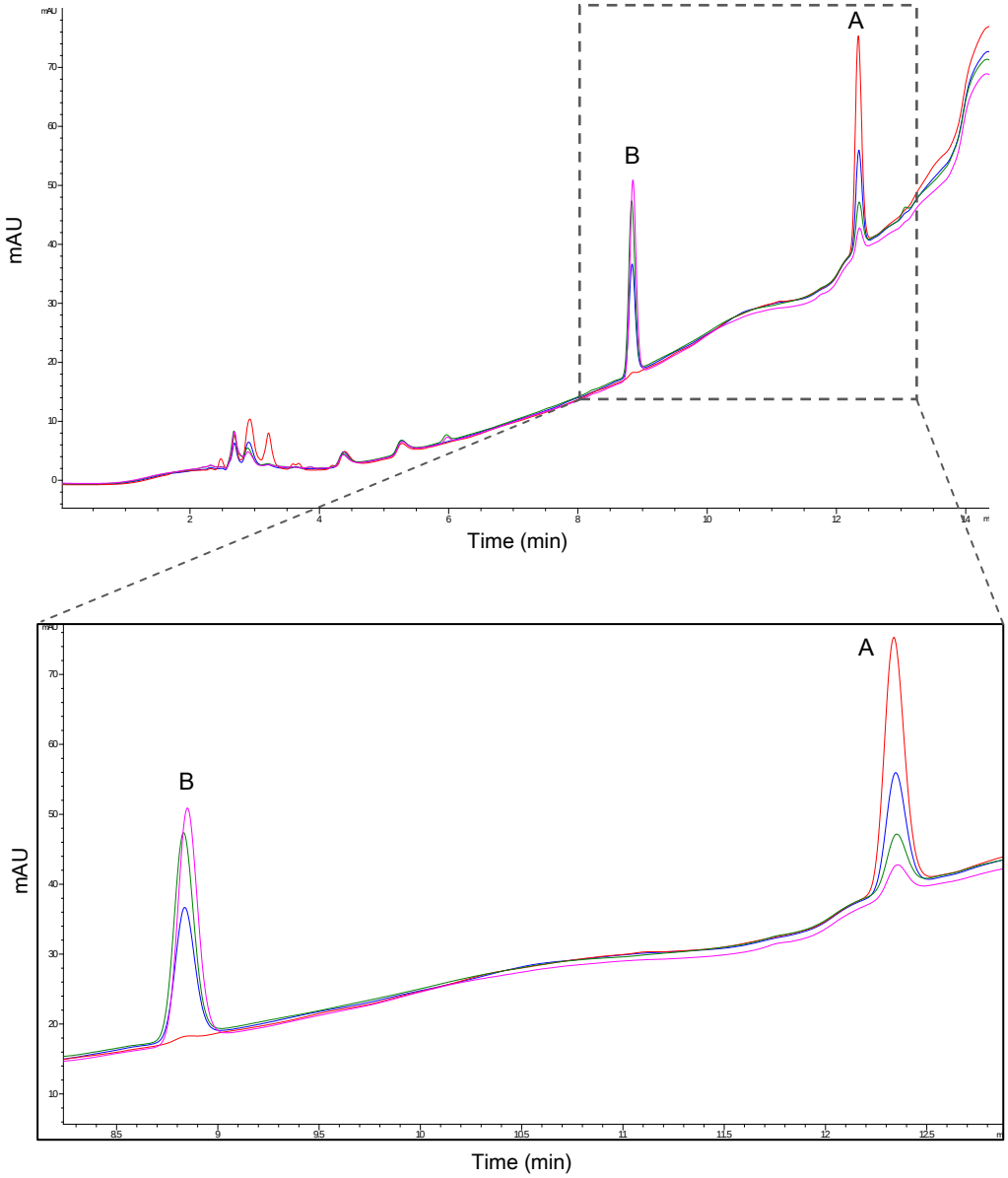

Figure 4-7 Overlaid HPLC chromatograms of CILA (A) and its metabolite, cilazaprilat (B) from porcine skin homogenate at t_{0h} (red line), t_{24h} (blue line), t_{48h} (green line), amd t_{72h} (pink line)

4.5.4.1 Effect of homogenate on CILA metabolism

The parent drug, CILA, was extensively metabolized in the skin homogenate leading to formation of the metabolite, cilazaprilat. After 72 h very small amounts of CILA remained in the pure homogenate (Figure 4-8). This was due to loss of the drug by hydrolysis to cilazaprilat in the presence of esterase activity in the homogenate which was previously assessed in section 4.5.2.

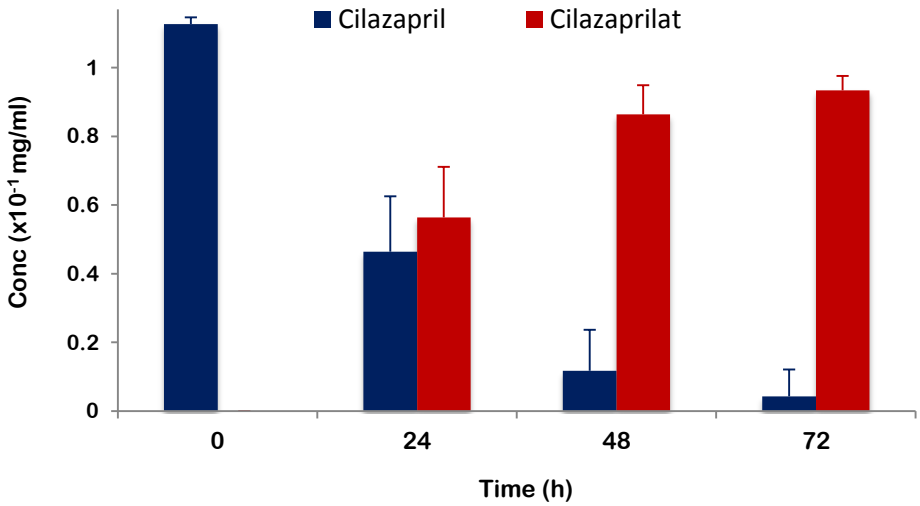

Figure 4-8 Metabolism profile of CILA in porcine ear skin homogenate (mean + SD; n=3).

As shown in Figure 4-8, the amounts of the metabolite formed in the homogenate increased with time throughout the 72 h duration of the experiment. In order to determine whether the drug also underwent chemical hydrolysis, control experiments were carried out in parallel where the skin homogenate was replaced by an equivalent volume of water, PBS, and boiled homogenate separately. The control experiments were important to elucidate the possibility of non-enzymatic transformation involvement in the metabolite formation.

As illustrated in Figure 4-9, a slow increase in the concentration of the metabolite, cilazaprilat, with time was observed in all control samples. The quantities of cilazaprilat formed after 72 h were small if compared with those found in the pure homogenate (Figure 4-8). This is believed to be the result of non-enzymatic metabolism because of the absence of enzymes in the tested samples, confirming that chemical hydrolysis of CILA was also occurring by the cleavage of the ester bond.

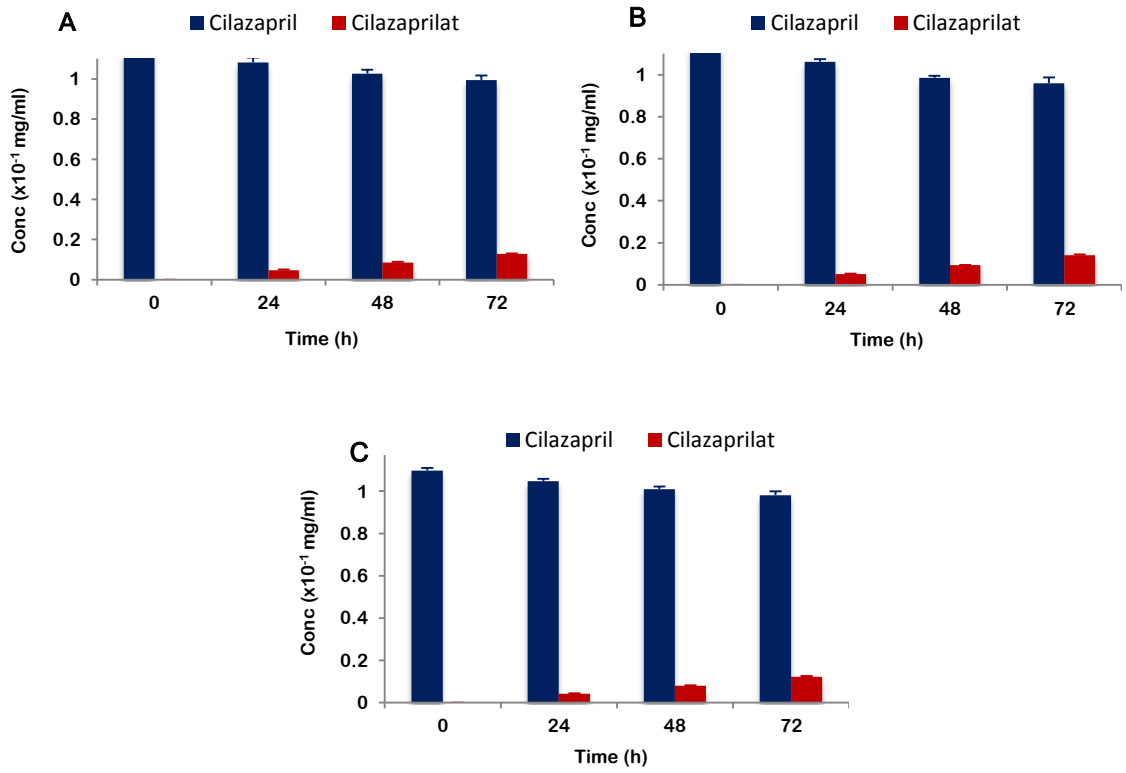

Figure 4-9 Metabolism profiles of CILA in water (A); PBS (B); boiled homogenate (C) (mean + SD; n=3).

The results obtained from the buffer experiment are in agreement with previous research (Bundgaard et al., 1983; Hammell et al., 2005; Wang et al., 2007). The researchers found that the incubation of ester prodrugs of 5-fluorouracil, naltrexone and morphine in pH 6 - 7.4 phosphate buffer exhibited resistance to the chemical

hydrolysis. In the present study, CILA was hydrolysed faster in pure homogenate (41 ± 14 % in 24 h) than in the boiled one (96 ± 1 % in 24 h). These findings along with those obtained from the esterase assay (section 4.5.3) demonstrated that the hydrolysis of CILA was mainly enzymatic. Compared to the control samples (Figure 4-9), CILA concentration significantly decreased ($p < 0.05$) in the homogenate samples (Figure 4-8). These data are consistent with previous research conducted by Guzek et al. (1989). The authors noted a rapid disappearance of a diester derivative of salicylic acid in contact with human skin homogenate. Moreover, the comparison between the amount of the metabolite formed in the homogenate medium and that in PBS confirmed the predominant contribution of enzymatic metabolism over the chemical metabolism. In a recent study, the metabolism of acetylsalicylic acid in the presence of porcine ear skin was studied (Lau et al., 2012). The findings showed a significant decrease ($p < 0.05$) in the compound level when incubated with fresh skin compared with the heated skin and buffer. The thermal treatment of porcine skin at 60 ˚C for 1 min resulted in loss of its esterase activity as confirmed by using an esterase staining kit and by investigating acetylsalicylic acid hydrolysis (Lau et al., 2012). In another study, human epidermis prepared by heat separation (60 ˚C for 2 min) was used to evaluate the permeation of quercetin esters (Montenegro et al., 2007). The authors reported the absence of the parent drug, quercetin, in the receptor phase and attributed this to the thermal denaturation of skin enzymes. The formation of the metabolite, cilazaprilat in both the skin homogenate and PBS confirmed that cilazaprilat was detected in the receptor phase during the permeation experiments was due to enzymatic and chemical hydrolysis.

4.5.4.2 Effect of sodium azide and P/S on CILA metabolism

The microbial role in the hydrolysis of CILA was investigated in skin homogenate in the presence of two different antimicrobials, sodium azide and P/S. This was carried out to determine if bacterial metabolism contributed to cilazaprilat formation along with enzymatic metabolism. On incubation, a marked decrease in CILA in line with increasing cilazaprilat formation was noticed (Figure 4-10).

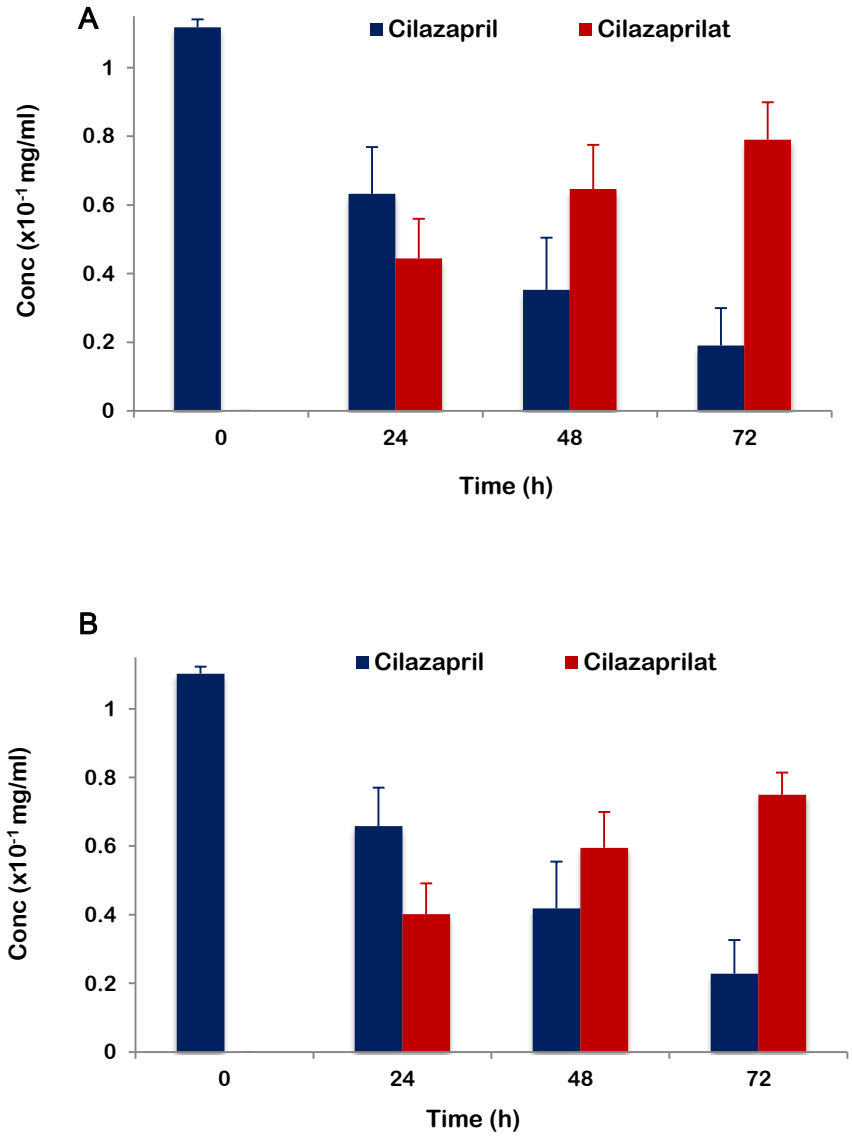

Figure 4-10 Metabolism profiles of CILA in porcine ear skin homogenate with sodium azide (A); homogenate with P/S (B) (mean + SD; n=3)

HPLC results showed small differences in the hydrolysis process with these two substances. These were not statistically different ($p > 0.05$). The amount of cilazaprilat formed at 72 h from the homogenate in the presence of sodium azide and P/S (0.79 ± 0.11 and 0.75 ± 0.06) $x10^{-1}$ mg/ml respectively, was less than that from homogenate alone (0.93 ± 0.04) $x10^{-1}$ mg/ml. CILA hydrolysis with sodium azide and P/S was slower than that obtained from homogenate alone, but at the same time it was much faster than the control. Therefore, the addition of antibacterial to homogenate resulted in the inhibition of bacteria and therefore a reduction of metabolism.

Many aerobic bacteria have been reported to be present on healthy human skin surface and able to produce esterases and lipases (Holt, 1971). Smith and Evans (1972) found that staphylococci were the most abundant bacteria in porcine skin. They can flourish at some depth in the porcine skin such as sebaceous glands and hair follicles similar to human (Montes and Wilborn, 1970). The organisms exhibit esterase activity and may originate from faecal contamination (Holt, 1971). The findings of the previous studies support what it was found in the present study where bacteria might participate in the production of the metabolite via bacterial metabolism.

The efficacy of the antibacterial on the inhibition of bacterial growth was verified by inoculating and incubating samples from the metabolism studies (section 4.5.4) on TSA plates at 37˚C. These conditions were ideal for bacterial growth and multiplication. The supplementation of homogenate with P/S as a preservative resulted in the absence of bacteria when the sample was incubated for 24 h (Figure 4-11-A), thereby preventing interference with bacterial metabolism. On the other hand, sodium azide was not able to completely inhibit the bacterial growth (Figure 4-11-B). The possibility

of microbial contamination may arise as sodium azide did not have as broad a bacteriostatic and bactericidal spectrum as P/S had. However, sodium azide was able to inhibit the esterase producing bacteria as no significant difference ($p > 0.05$) in the CILA amount remained between the homogenate treated with sodium azide and P/S was noticed. Further microbiological tests are needed in order to specify the microorganisms which remained in the homogenate treated with sodium azide.

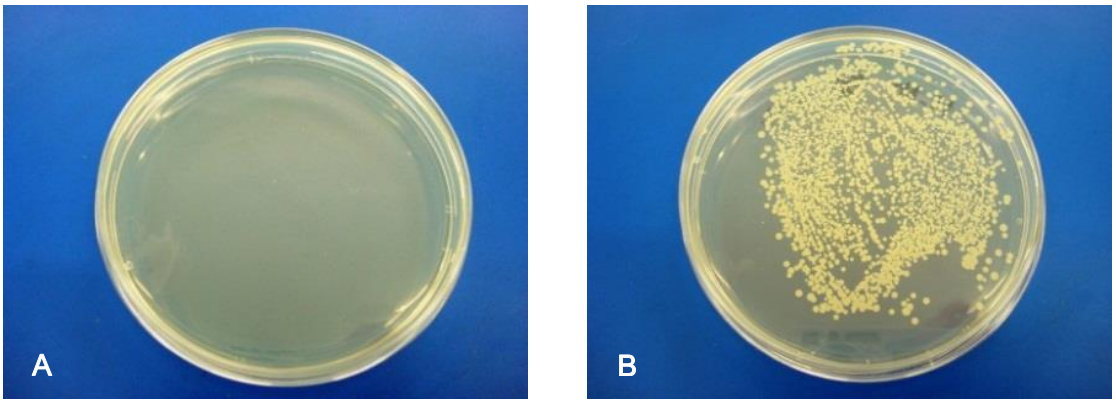

Figure 4-11 TSA spread plates of the porcine skin homogenate treated with P/S (A) and sodium azide (B) incubated at 37°C (n=3).

As can be seen from Figure 4-12-A, the incubation of the boiled homogenate samples proved to be sterile during the time course of the experiment.

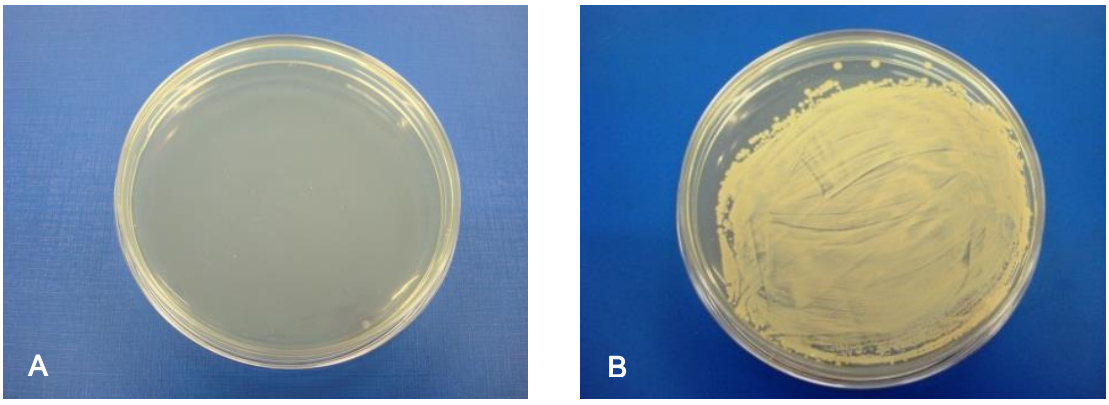

Figure 4-12 TSA spread plates of the boiled (A) and unboiled (B) porcine skin homogenate incubated at 37°C (n=3).

The colonies from plates incubated with homogenate and sodium azide (Figure 4-11-B) were much less than those incubated with pure homogenate (Figure 4-12-B), whereas no colonies were observed on the plates from homogenate with P/S. Based on the incubation results and since the addition of both sodium azide and P/S decreased the rate of CILA hydrolysis when compared with the pure homogenate, it seems that skin microorganisms played a role in the hydrolysis process. Microorganisms reside on the skin surface and are capable of metabolizing topically applied drugs. Skin microorganisms were reported to be responsible for the bioconversion of nandrolone decanoate during skin absorption studies (Foreman and Clanachan, 1975). However, the metabolic contribution of skin microorganisms was negligible (May and Declement, 1982).

4.5.4.3 Effect of PMSF on CILA metabolism

To assess the impact of PMSF on skin esterases, CILA was incubated with homogenate containing PMSF at 32 ˚C. A comparison of the findings from homogenate-PMSF (Figure 4-13) with those from the boiled homogenate (Figure 4-9) showed that the same amounts of CILA were metabolised. Thus, PMSF strongly inhibited the esterase activity in the homogenate over 72 h.

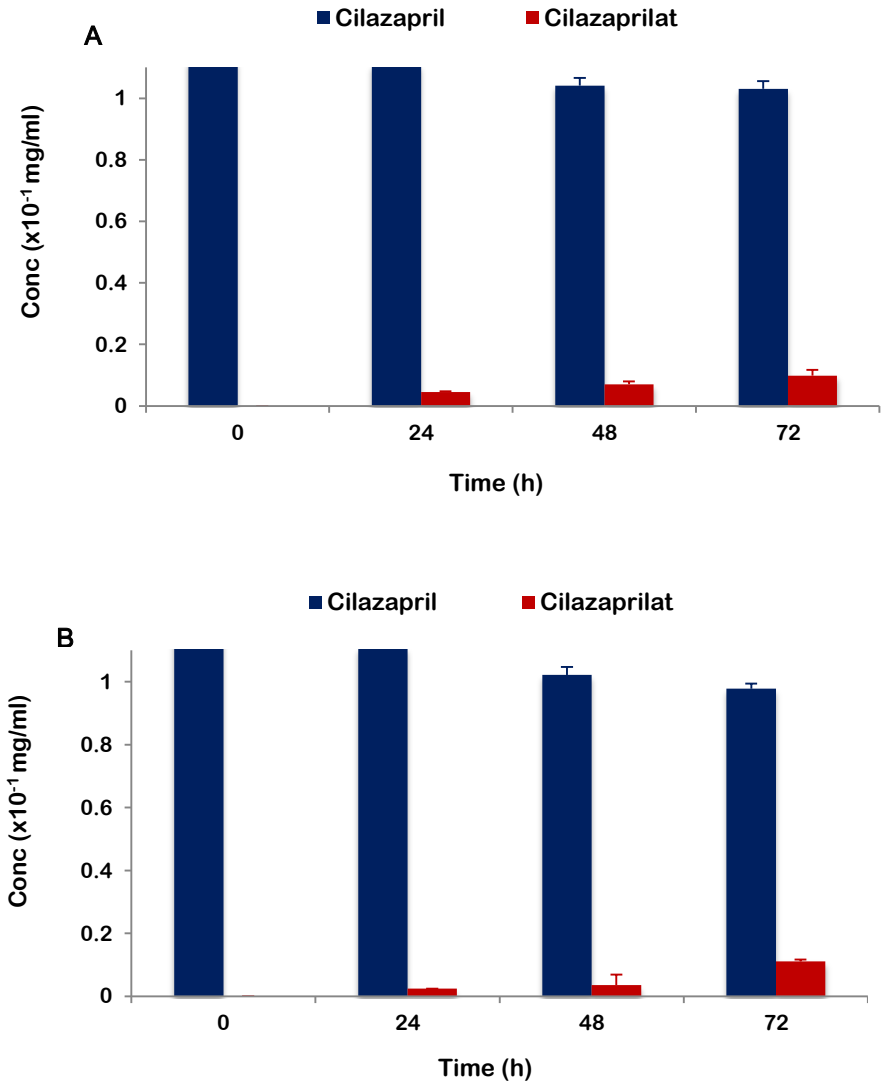

Figure 4-13 Metabolism profiles of CILA in porcine ear skin homogenate with PMSF (A); homogenate with PMSF plus P/S (B) (mean + SD; n=3).

In the presence of PMSF, the esterase activity was reduced and therefore a significant decrease ($p < 0.05$) in the formation of cilazaprilat was observed compared with the homogenate samples in Figure 4-8. For each time point, the amount of CILA which remained unhydrolysed was not significantly different ($p > 0.05$) between PMSF samples and the controls.

PMSF has been used in metabolism studies as a carboxylesterase inhibitor and known to inhibit esterases (Prusakiewicz et al., 2006; Harville et al., 2007; Jewell et al., 2007a). The findings of Prusakiewicz et al. (2006) indicated that carboxylesterases were responsible for the majority of hydrolysis activity in porcine skin. The present results are in agreement with previous studies (Guzek et al., 1989; Prusakiewicz et al., 2006; Zheng et al., 2012) where it was noted that PMSF was able to protect the tested drugs from the enzymatic conversion. Guzek et al. (1989) examined the enzymatic cleavage of salicylate diester using skin homogenate, where rapid hydrolysis of the drug was observed. However, the addition of PMSF resulted in an inhibitory effect. Further studies investigated the effect of PMSF on the hydrolysis of naphtyle acetate (Prusakiewicz et al., 2006) and parabens (Harville et al., 2007). It was found that PMSF completely blocked esterase activity in skin homogenate resulting in suppression of the hydrolysis of these ester compounds.

4.5.4.4 Effect of temperature on CILA metabolism

The effect of temperature on the rate of CILA hydrolysis was also examined. As expected, an increase in the temperature from 32 to 37 ˚C led to an increase in the rate of CILA metabolism by esterases (Figure 4-14). However, this increase was not statistically significant ($p > 0.05$).

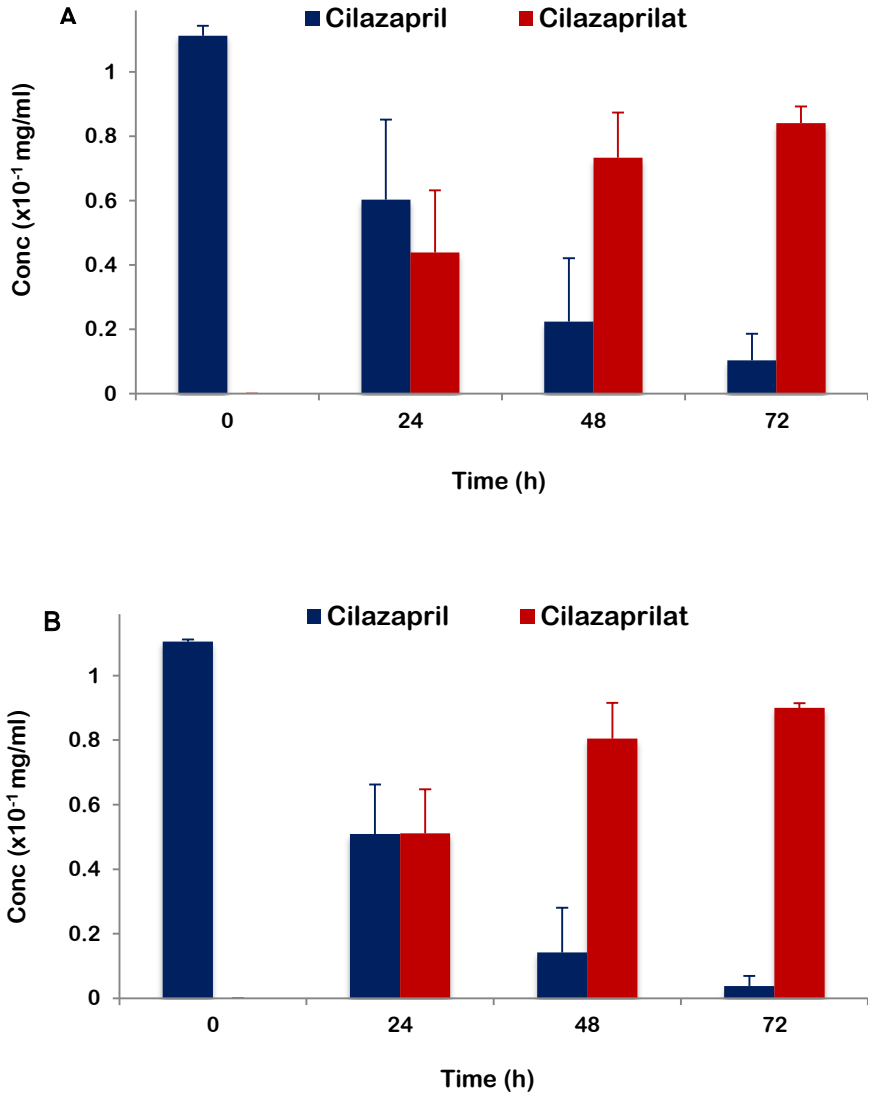

Figure 4-14 The effect of two different temperatures 32 °C (A) and 37 °C (B) on the hydrolysis of CILA (mean + SD; n=3).

4.5.5 Kinetics of cilazapril hydrolysis

The logarithm of the percentage of drug remaining was plotted as a function of time (Figure 4-15) to calculate pseudo-first order rate constants and half-lives of CILA in the different media. The rate constants (k) for the chemical and enzymatic hydrolysis were calculated from the slopes of the linear curves using linear regression analysis.

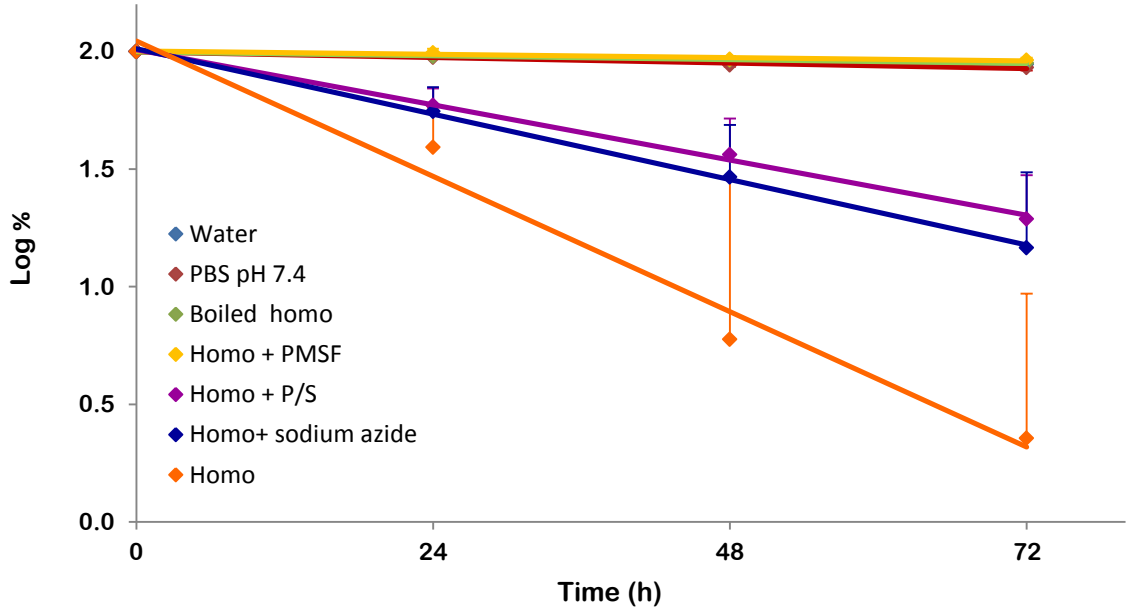

Figure 4-15 Pseudo first order plots for the hydrolysis of CILA in different media at 32 °C (mean + SD; n=3).

As shown in Figure 4-15, the curves of the controls (water, PBS, and boiled homogenate) are overlapped. CILA showed a good stability in controls compared with the homogenate. The rate constants and their corresponding half-lives of CILA hydrolysis in the different incubation media are summarized in Table 4-1.

Table 4-1 Pseudo first order constant rates, (k), and half-lives ($t_{1/2}$) of the hydrolysis of CILA to cilazaprilat in different incubation media (mean ± SD; n=3).

The incubation media	k (x10^{-2} h^{-1})	$t_{1/2}$ (h)
Water	0.18 ± 0.01	394.05 ± 31.02
PBS pH 7.4	0.22 ± 0.04	316.87 ± 53.12
Boiled homo	0.16 ± 0.04	415.37 ± 130.3
Homo	5.52 ± 2.17	14.45 ± 7.25
Homo + sodium azide	2.67 ± 1.05	28.48 ± 9.86
Homo + P/S	2.26 ± 0.60	32.19 ± 8.39
Homo + PMSF	0.13 ± 0.04	561.22 ± 169.29
Homo + P/S + PMSF	0.21 ± 0.08	355.78 ± 136.29

As shown in Table 4-1 the rate of cilazaprilat formation in the controls ranged from (0.16 to 0.22) x10^{-2} h^{-1} with no significant difference ($p > 0.05$) in the constant rates was observed. k values were quite low in controls and their corresponding half-lives were long ($t_{1/2}$ > 300 h). The hydrolysis rate of CILA in the homogenate was approximately 27 fold faster compared with the chemical hydrolysis rates. The hydrolysis rate was lower when CILA was incubated in the homogenate in the presence of antimicrobial agents compared with pure homogenate. However, the differences were not statistically significant ($p > 0.05$). The addition of the esterase inhibitor, PMSF, resulted in low k values which were comparable with those for controls and long half-lives for CILA. The findings suggested that enzymatic metabolism was mainly responsible for the conversion of CILA to cilazaprilat.

4.6 Conclusions

The susceptibility of cilazapril to cutaneous metabolism by using porcine ear skin homogenate was reported for the first time. The esterase activity in the homogenate was measured. The findings demonstrated that frozen porcine ear skin maintained the metabolic capacity of skin when it was stored at -25 ˚C for up to 12 weeks. The *in vitro* fate of CILA showed that CILA was extensively metabolized in the skin homogenate by esterases leading to the metabolite formation, cilazaprilat and only small amounts of CILA remained in the homogenate. This enzymatic conversion was inhibited by the addition of an esterase inhibitor, PMSF and the results were comparable with those of controls. CILA was also subject to non-enzymatic (chemical) metabolism in the presence of deionized water and phosphate buffer. This chemical hydrolysis was significantly slower ($p < 0.05$) than enzymatic hydrolysis, confirming that CILA was less

susceptible to chemical hydrolysis. Furthermore, the supplementation of homogenate with P/S as a preservative resulted in the absence of bacteria and a decrease in the hydrolysis process. However, this decrease was not statistically different ($p > 0.05$) from pure homogenate, indicating that the hydrolysis of CILA was mainly enzymatic. Microbial hydrolysis of CILA was less important than enzymatic hydrolysis. CILA hydrolysis follows pseudo first order kinetics. The calculated constant rates and their corresponding half-lives indicated that CILA was quickly hydrolysed in the enzyme containing media. Evaluation of the drug metabolism in skin homogenate can be regarded as a useful approach for screening of metabolite formation. Such studies provide important information about the susceptibility of the drug to enzymes and the possibility of formation of inactive forms. Ultimately the information reported here will ensure the development of optimal CILA formulation for topical therapy.

Chapter 5

Conclusions and Future work

5 Conclusions and Future work

The involvement of ACEIs in the improvement and recovery of scars has been reported. However, to date, there are no topical products containing ACEIs on the market. Therefore, the proposed work has evaluated the stability of ACEIs (MOX, RAM and CILA) in a range of dermal vehicles. Based on these data, different dermal formulations of RAM and CILA using different solvent systems were developed. In addition, these formulations were screened to ensure that the drugs were released from the formulations and delivered across porcine ear skin.

The stability of active ingredients in pharmaceutical products is of vital importance in the safety, efficacy, and quality of the products. Loss of potency and formation of toxic degradation products are the potential adverse effects of drug instability. Therefore, the assessment of MOX, RAM and CILA stability in a range of lipophilic and hydrophilic topical vehicles at 32 ˚C was investigated in Chapter 2. These included IPM, PGML, CAP, LAB, DMI, PG, EtOH, TCL, PEG 200, and water. The rationale for this temperature was that the topical formulations of the present study were prepared and assessed in terms of their percutaneous absorption at skin temperature. All the test solutions of MOX and RAM were initially clear and colourless under natural light. Some of the MOX solutions exhibited colour change or precipitation during the study. However, the appearance of RAM solutions did not change throughout the study except for DMI. Stability-indicating HPLC analysis showed that both MOX and RAM were not stable in the majority of vehicles under the experimental conditions. The findings illustrated that the type of vehicle in which the drug was dissolved played an important role in the degradation process. For MOX, rapid degradation was observed in

PEG 200 and DMI compared with water, PG, TCL, EtOH, PGL, PGML, and CAP. The percentage of MOX remaining in these vehicles after 5 days ranged from 25.61 ± 2.07 to 90.33 ± 2.16 %. RAM also underwent rapid degradation in IPM, PGL, PGML, DMI, EtOH and CAP. Like MOX, the percentage of unaltered RAM concentration after 5 days varied from 25.67 ± 1.72 to 98.69 ± 1.71 %. Furthermore, HPLC chromatograms showed a separated unknown peak from the main peak of the model drugs. A comparison of the retention times of the main compounds with that of their degradation products indicated that the latter was more hydrophobic than the former. As recommended by FDA, the identification of the degradation products of MOX and RAM was achieved using MS. The MS analysis confirmed that the molecular weight of the unknown compound matched that of the diketopiperazine form of MOX and RAM. The diketopiperazine formed as a result of an intramolecular cyclization process in the main drug molecule. On the other hand, CILA, which belongs to the same category of ACEIs, exhibited a good stability in all the selected vehicles except for DMI. Less than 2 % loss of CILA occurred after 5 days in the test samples. Based on the obtained stability results of MOX, RAM, and CILA and the comparison of the chemical structure of CILA with that of MOX and RAM, it was concluded that the structural element had the greatest influence on the stability properties of ACEIs. CILA seemed to be a promising candidate in terms of its stability and physicochemical properties for design topical formulations and investigating the possibility of delivering this compound across porcine skin.

Besides the importance of the drug stability during formulation development process, its solubility and delivery into the skin are not less important. In Chapter 3, the

solubility studies of RAM and CILA in various single solvents at 32 °C were the first stage of topical formulation development. Not all vehicles were capable of solubilizing the drug to the same extent. RAM had high solubility in PG and LA in comparison with water. The solubility of CILA in various pure vehicles increased in the following rank order: IPM < LAB < water < PGL < PGML < CAP < PEG 200 < TCL < PG < EtOH. Furthermore, the solubility of CILA in binary and ternary solvent systems was also determined. IPM was combined with either CAP or PGML at different ratios 25, 50, and 75 %, resulting in a decrease in CILA solubility as the concentration of IPM increased. The addition of TCL, PG, PEG 200 to the binary mixture (IPM:CAP) resulted in an increase in the solubility of CILA in the ternary solvent systems.

The solubility parameter (δ) was also calculated for the drugs (δ_D) and all vehicles (δ_V) studied and used to estimate the solubility of permeant in the vehicle. A good relationship was observed between the δ_V and solubility of CILA. This was in accordance with the solubility theory which hypothesizes that a vehicle with a solubility parameter close to that of the drug will be mutually soluble. The solubility of CILA was high in the solvent systems with solubility parameters close to 11.55 $(cal/cm^3)^{1/2}$, which corresponds to the calculated δ_D. It was also found that the solubility of CILA was inversely proportional to $|\delta_V-\delta_D|$. CILA solubility in the vehicles with $|\delta_V-\delta_D| < 2$ was much higher than that with $|\delta_V-\delta_D| > 2$.

After the affinity of the drug for each vehicle was determined, the effect of water, PG, and LA on the percutaneous penetration of RAM across human epidermis was evaluated under infinite dose conditions. The results demonstrated the low permeability

of RAM. A possible explanation was that both the permeation of RAM-DKP, resulted from RAM degradation in the donor, along with the main compound and the degradation of RAM permeated in the receptor phase during the time course of experiment.

Percutaneous absorption of CILA across porcine ear skin was also investigated. Formulations were applied under both infinite and finite dose conditions. Single, binary, and ternary solvent systems were tested in order to achieve synergistic enhancement effects for drug permeation and thus optimizing dermal formulations.

For the neat vehicles under an infinite dose study, despite the equal thermodynamic activities, the permeation rates of CILA were different among the pure vehicles examined. CAP showed the highest permeation rate, which was 2.16 ± 0.80 μg/cm^2/h whereas LAB was the lowest (0.26 ± 0.07 μg/cm^2/h). This was attributed to reduction in the SC resistance by specific vehicle effects. Furthermore, the highest Q_{48h} was obtained from CAP and PGML (43.69 ± 14.01 and 33.19 ± 9.31 μg/cm^2, respectively) whereas IPM exerted the highest k_p. Based on the findings from the permeation studies using single vehicles in terms of Q_{48h} and k_p, different binary formulations with a ratio of (50:50 v/v) were compared: CAP:IPM, PGML:IPM, CAP:PGML. The former resulted in the highest CILA skin permeation rate with $J_{36\text{-}52h}$ value of 8.08 ± 2.73 μg/cm^2/h. In comparison with the neat vehicles, a remarkable increase in permeation was observed when CILA was formulated in binary solvent systems. From the obtained results, it was concluded that the major factor that determined the drug permeability across the skin was not only the thermodynamic activity but also the vehicle effect on the barrier function of the skin.

Even though the infinite dose application was useful for evaluation of the permeation behaviour of a compound, however, it was not relevant to the clinical use in terms of the depletion of the drug and solvents. Therefore, further permeation studies under finite dose conditions were conducted. CILA permeation profiles in CAP and PGML were characteristic for infinite dose application. This was explained by the low permeability of CILA compared with the applied dose. Interestingly, a plateau of the permeation profiles with time was observed with TCL and PG formulations, yet the CILA doses applied from these vehicles were very high, 3395 and 4300 μg/cm^2, respectively. This was attributed not to the depletion of the drug itself but to that of the vehicle from the formulation applied, resulting in precipitation of CILA at the skin surface as a deposited film. The crystallised drug had limited ability to permeate through the skin. Furthermore, GC analysis of PG and TCL indicated that these vehicles crossed the skin faster than CILA itself. This was ascribed to the small molecular weights of these molecules which govern their passive diffusion. Depletion of the solvents by evaporation also took part in the drug crystallisation. DVS results showed that TCL and PG completely evaporated after ~16 and ~36 h of application under 32 ˚C and 50 % RH. Therefore, rapid diffusion and evaporation of PG and TCL from the formulation applied limited their penetration enhancement effect.

For individual vehicles, the Q_{48h} of CILA permeated can be ranked according to the following order: CAP > PGML > TCL > PG > LAB > IPM. IPM was not able to exhibit a very high enhancing effect, due to the extremely low CILA solubility (i.e. low applied dose). However, IPM was unique in that 48.22 ± 4.89 % of the applied dose permeated over 48 h. This was significantly greater (p < 0.05) compared to that

observed from PG, TCL, PGML, and CAP. It has been reported that IPM reduces the barrier function of the skin by interacting with the ordered bilayer SC lipid. Because of the relatively high Q_{48h} and % CILA permeated observed with (PGML, CAP) and IPM respectively, further permeation studies were conducted using binary solvent systems, PGML:IPM and CAP:IPM. Interestingly, with increasing IPM concentration in the binary formulations, the percentage permeated of CILA increased. Compared to the neat IPM, the amount of CILA permeated was enhanced between 3 and 8 fold by combining IPM with PGML and CAP. The highest Q_{48h} was achieved with CAP:IPM (50:50) and thus more complex ternary formulations were selected for further permeation studies. Incorporating PG, TCL, or DPG, a hydrophilic vehicle, into the CAP:IPM formulation promoted the drug permeation across porcine skin. The maximum Q_{48h} was obtained with the formulation containing PG. It was suggested that PG can modify skin permeability by partitioning into the SC and increasing drug solubility in the skin. However, the combination of PG and IPM was reported to affect the SC lipid structure in different mechanism from the individual vehicles. IPM enables PG to laterally integrate between the lipid head groups with the absence of its perpendicular integration between the head groups, which was observed with PG alone.

It was interesting to note that CILA was applied to the skin as an ester form, irrespective of the formulation. However, HPLC analysis showed the presence of the metabolite, cilazaprilat, together with CILA in the receptor phase. A plausible explanation for this phenomenon was the biotransformation of CILA by skin esterases. The formation of cilazaprilat may also be caused by the chemical hydrolysis of CILA permeated into the receptor phase and/or the leaching of esterases into the receptor

phase during the permeation studies. These assumptions were confirmed in Chapter 4. It was shown that CILA/cilazaprilat ratio was different among the formulations. This was due to the variability in the enzymes level and/or the effect of vehicle on the skin enzyme activity, which needs to be explored further in future work.

Besides being considered as a portal of entry for compounds, skin is a metabolizing organ and possesses the major enzymes found in the liver. CILA, an ester-based prodrug, was reported to be hydrolysed by the liver to cilazaprilat with no data about its behaviour in the skin. Therefore, Chapter 4 was built on the results of Chapter 3 and focused on the susceptibility of CILA to porcine skin homogenate. Initially, the presence of esterase in the prepared skin homogenate was confirmed by using *p*-nitrophenyl butyrate as a substrate. The effect of freezing on the skin esterase activity was then investigated. The data demonstrated that porcine skin can maintain its esterase activity if it was stored at or below -25 ˚C for up to 12 weeks.

The drug metabolism studies showed that CILA was extensively metabolised in the presence of pure porcine skin homogenate leading to formation of the metabolite, cilazaprilat. Further metabolism studies were conducted to verify the contribution of the chemical and microbial metabolism in CILA hydrolysis. To achieve this goal, sodium azide, P/S, PMSF, and P/S plus PMSF were added to the homogenate to which CILA was then added. Controls were simultaneously run where the skin homogenate was replaced by an equivalent volume of water, PBS, and boiled homogenate separately. At all time points, the quantities of cilazaprilat formed in the controls were statistically smaller ($p < 0.05$) if compared with those found in the pure homogenate. The microbial role in the hydrolysis of CILA was investigated in skin homogenate in the presence of

two different antimicrobials, sodium azide and P/S. The amount of cilazaprilat formed from the homogenate in the presence of sodium azide and P/S was less than that from homogenate alone with no significant difference ($p > 0.05$). The addition of the esterase inhibitor, PMSF, strongly suppressed the metabolism and the results were comparable with those of the controls. A change in the temperature from 32 to 37 ˚C had no significant effect ($p > 0.05$) on CILA hydrolysis. The results of agar plating indicated that sodium azide was not able to completely inhibit the bacterial growth in the homogenate. This was attributed to the fact that sodium azide did not have a broad bacteriostatic and bactericidal spectrum as P/S had. Further microbiological tests are needed in order to specify the microorganisms which are resistant to sodium azide. The calculated constant rates and their corresponding half-lives indicated that CILA was quickly hydrolysed in the enzyme containing media, demonstrating that the prodrug was mainly hydrolysed by the skin esterases.

In general, the design of stable topical formulations containing CILA has been reported for the first time. Furthermore, the permeation data demonstrated the feasibility of dermal delivery of CILA across porcine skin which has been used as a surrogate for human skin. Future work will focus on conducting clinical trials on patients with new surgical wounds or with a scar history in order to test the efficacy of the optimized formulations on prevention of scar development or improvement of scar appearance.

References

Abdou A. G., Maraee A. H., Al-Bara A. M. and Diab W. M. (2011) Immunohistochemical expression of TGF-beta 1 in keloids and hypertrophic scars. American Journal of Dermatopathology, **33**: 84-91.

Abdulmajed K., McGuigan C. and Heard C. M. (2006) Topical delivery of retinyl ascorbate co-drug. *In vitro* degradation studies. Skin Pharmacology and Physiology, **19**: 248-258.

Abiko M., Rodgers K. E., Campeau J. D., Nakamura R. M. and Dizerega G. S. (1996) Alterations of angiotensin II receptor levels in full thickness excisional wounds in rat skin. Wound Repair Regeneration, **4**: 363-367.

Abla N., Naik A., Guy R. H. and Kalia Y. N. (2006) Topical iontophoresis of valaciclovir hydrochloride improves cutaneous aciclovir delivery. Pharmaceutical Research, **23**: 1842-1849.

Abramov Y., Hirsch E., Ilievski V., Goldberg R. P., Botros S. M. and Sand P. K. (2013) Transforming growth factor beta 1 gene expression during vaginal vs cutaneous surgical wound healing in the rabbit. International Urogynecology Journal, **24**: 671-675.

Al-Omari M. M., Abdelah M. K., Badwan A. A. and Jaber A. M. Y. (2001) Effect of the drug-matrix on the stability of enalapril maleate in tablet formulations. Journal of Pharmaceutical and Biomedical Analysis, **25**: 893-902.

Albery W. J. and Hadgraft J. (1979) Percutaneous absorption: *in vivo* experiments. Journal of Pharmacy and Pharmacology, **31**: 140-147.

Allen L. V., Popovich N. G. and Ansel H. C. (2011a) Dosage form design: pharmaceutical and formulation considerations. In: Ansel's Pharmaceutical Dosage Forms and Drug Delivery Systems. Philadelphia, Lippincott Williams & Wilkins. Chapter 4, pp. 90-142

Allen L. V., Popovich N. G. and Ansel H. C. (2011b) New drug development and approval process. In: Ansel's Pharmaceutical Dosage Forms and Drug Delivery Systems. Philadelphia, Lippincott Williams & Wilkins. Chapter 2, pp. 27-65

Allen L. V., Stiles M. L., Prince S. J., Mclaury H. J. and Sylvestri M. F. (1995) Stability of ramipril in water, apple juice, and applesauce. American Journal of Health-System Pharmacy, **52**: 2433-2436.

Amaral P. H., Fernandes R., Eberlin M. N. and Hoeehr N. F. (2011) Direct monitoring of drug degradation by easy ambient sonic-spray ionization mass spectrometry: the case of enalapril. Journal of Mass Spectrometry, **46**: 1269-1273.

Apikian M. and Goodman G. (2004) Intralesional 5-fluorouracil in the treatment of keloid scars. Australasian Journal of Dermatology, **45**: 140-143.

Ardekani G. S., Aghaie S., Nemati M. H., Handjani F. and Kasraee B. (2009) Treatment of a postburn keloid scar with topical captopril: report of the first case. Plastic and Reconstructive Surgery, **123**: 112E-113E.

Ardekani G. S., Ebrahimi S., Amini M., Aslani F. S., Handjani F., Omrani G. R., Ardekani L. S., Alhashem i. S. H. H. and Kasraee B. (2008) Topical captopril as a novel agent against hypertrophic scar formation in New Zealand white rabbit skin. Wounds, **20**: 101-106.

Arellano A., Santoyo S., Martin C. and Ygartua P. (1999) Influence of propylene glycol and isopropyl myristate on the *in vitro* percutaneous penetration of diclofenac sodium from carbopol gels. European Journal of Pharmaceutical Sciences, **7**: 129-135.

Augusti K. T. (1996) Therapeutic values of onion (Allium cepa L.) and garlic (Allium sativum L.). Indian Journal of Experimental Biology, **34**: 634-640.

Barry B. W. (1988) Action of skin penetration enhancers: The lipid protein partitioning theory. International Journal of Cosmetic Science, **10**: 281-293.

Bartek M. J., LaBudde J. A. and Maibach H. I. (1972) Skin permeability *in vivo*: comparison in rat, rabbit, pig and man. The Journal of Investigative Dermatology, **58**: 114-123.

Bataller R., Sancho-Bru P., Gines P., Lora J. M., Al-Garawi A., Sole M., Colmenero J., Nicolas J. M., Jimenez W., Weich N., Gutierrez-Ramos J. C., Arroyo V. and Rodes J. (2003) Activated human hepatic stellate cells express the renin-angiotensin system and synthesize angiotensin II. Gastroenterology, **125**: 117-125.

Beanes S. R., Dang C., Soo C. and Ting K. (2003) Skin repair and scar formation: The central role of TGF-beta. Expert Reviews in Molecular Medicine, **5**: 1-22.

Bendas B., Schmalfuss U. and Neubert R. (1995) Influence of propylene glycol as cosolvent on mechanisms of drug transport from hydrogels. International Journal of Pharmaceutics, **116**: 19-30.

Berman B. (2002) Imiquimod: a new immune response modifier for the treatment of external genital warts and other diseases in dermatology. International Journal of Dermatology, **41**: 7-11.

Berman B. and Kaufman J. (2002) Pilot study of the effect of postoperative imiquimod 5% cream on the recurrence rate of excised keloids. Journal of the American Academy of Dermatology, **47**: S209-S211.

Bettinger D. A., Yager D. R., Diegelmann R. F. and Cohen I. K. (1996) The effect of TGF-beta on keloid fibroblast proliferation and collagen synthesis. Plastic and Reconstructive Surgery, **98**: 827-833.

Beydon D., Payan J. P. and Grandclaude M. C. (2010) Comparison of percutaneous absorption and metabolism of di-n-butylphthalate in various species. Toxicology in Vitro, **24**: 71-78.

Bharate S., Bharate S. and Bajaj A. (2010) Interactions and incompatibilities of pharmaceutical excipients with active pharmaceutical ingredients: a comprehensive review. Journal of Excipients and Food Chemicals, **1**: 3-26.

Bhatia K. S. and Singh J. (1996) Pig ear skin as a model for predicting percutaneous absorption in man. Journal of Pharmaceutical Sciences, **2**: 275-276.

Bickers D. R. and Mukhtar H. (1990) Skin as a portal for entry for systemic effect: Xenobiotic metabolism. In: C. L. Galli, C. N. Hensby and M. Marinovich (eds.) Skin Pharmacology and Toxicology: Recent Advances. New York, Plenum Press. Chapter 5, pp. 85–97.

BNF (2012) Drug affectings the renin-angiotensin system. In: British National Formulary. pp. 115-122

Bodde H. E., Vandenbrink I., Koerten H. K. and Dehaan F. H. N. (1991) Visualization of *in vitro* percutaneous penetration of mercuric chloride: transport through intercellular space versus cellular uptake through desmosomes. Journal of Controlled Release, **15**: 227-236.

Bonina F. P., Puglia C., Barbuzzi T., de Caprariis P., Palagiano F., Rimoli M. G. and Saija A. (2001) *In vitro* and *in vivo* evaluation of polyoxyethylene esters as dermal prodrugs of ketoprofen, naproxen and diclofenac. European Journal of Pharmaceutical Sciences, **14**: 123-134.

Bos J. D. and Meinardi M. M. (2000) The 500 Dalton rule for the skin penetration of chemical compounds and drugs. Experimental Dermatology, **9**: 165-169.

Boulton D. W., Woods D. J., Fawcett J. P. and Tucker I. G. (1994) The stability of an enalapril maleate oral solution prepared from tablets. Australian Journal of Hospital Pharmacy, **24**: 151-156

Bouwstra J. A., Devries M. A., Gooris G. S., Bras W., Brussee J. and Ponec M. (1991) Thermodynamic and structural aspects of the skin barrier. Journal of Controlled Release, **15**: 209-220.

Bouwstra J. A. and Ponec M. (2006) The skin barrier in healthy and diseased state. Biochimica et Biophysica Acta, **1758**: 2080-2095.

Bowen J. L. and Heard C. M. (2006) Film drying and complexation effects in the simultaneous skin permeation of ketoprofen and propylene glycol from simple gel formulations. International Journal of Pharmaceutics, **307**: 251-257.

BP (2013a) Ramipril monograph. In: The British Pharmacopoeia. Vol. 2, pp. 1921-24

BP (2013b) Validation of analytical procedures. In: The British Pharmacopoeia. Vol. 5, Supplementary, Chapter III F pp. A664-666.

Bradford M. M. (1976) Rapid and sensitive method for quantitation of microgram quantities of protein utilizing principle of protein-dye binding. Analytical Biochemistry, **72**: 248-254.

Brinkmann I. and Muller-Goymann C. C. (2005) An attempt to clarify the influence of glycerol, propylene glycol, isopropyl myristate and a combination of propylene glycol and isopropyl myristate on human stratum corneum. Die Pharmazie, **60**: 215-220.

Bronaugh R. L., Kraeling M. E. K. and Yourick J. J. (2005) Determination of percutaneous absorption by *in vitro* techniques. In: R. Bronauch and H. Maibach (eds.) Percutaneous Absorption: Drugs–Cosmetics–Mechanisms–Methodology. New York, Taylor and Francis Group. Chapter 18, pp. 265-270.

Bulstrode N. W., Mudera V., McGrouther D. A., Grobbelaar A. O. and Cambrey A. D. (2005) 5-fluorouracil selectively inhibits collagen synthesis. Plastic and Reconstructive Surgery, **116**: 209-221.

Bundgaard H., Hoelgaard A. and Mollgaard B. (1983) Leaching of hydrolytic enzymes from human skin in cutaneous permeation studies as determined with metronidazole and 5-fluorouracil prodrugs. International Journal of Pharmaceutics, **15**: 285-292.

Cacao F. M., Tanaka V. and de Lourenzo Messina M. C. (2009) Failure of imiquimod 5% cream to prevent recurrence of surgically excised trunk keloids. Dermatologic Surgery, **35**: 629-633.

Campbell D. J. (1987) Circulating and tissue angiotensin systems. Journal of Clinical Investigation, **79**: 1-6.

Chan K. Y., Lau C. L., Adeeb S. M., Somasundaram S. and Nasir-Zahari M. (2005) A randomized, placebo-controlled, double-blind, prospective clinical trial of silicone gel in prevention of hypertrophic scar development in median sternotomy wound. Plastic and Reconstructive Surgery, **116**: 1013-1020.

Chanprapaph K., Tanrattanakorn S., Wattanakrai P., Wongkitisophon P. and Vachiramon V. (2012) Effectiveness of onion extract gel on surgical scars in asians. Dermatology Research and Practice: DOI: 10.1155/2012/212945.

Chao Y. C. E. and Nylander-French L. A. (2004) Determination of keratin protein in a tape-stripped skin sample from jet fuel exposed skin. Annals of Occupational Hygiene, **48**: 65-73.

Chau D., Mancoll J. S., Lee S., Zhao J. G., Phillips L. G., Gittes G. K. and Longaker M. T. (1998) Tamoxifen downregulates TGF-beta production in keloid fibroblasts. Annals of Plastic Surgery, **40**: 490-493.

Chernoff W. G., Cramer H. and Su-Huang S. (2007) The efficacy of topical silicone gel elastomers in the treatment of hypertrophic scars, keloid scars, and post-laser exfoliation erythema. Aesthetic Plastic Surgery, **31**: 495-500.

Chilcott R. P. (2008) Cutaneous anatomy and function. In: R. P. Chilcott and S. A. Price (eds.) Principles and Practice of Skin Toxicology. UK, Wiley. Chapter 1, pp. 3-16.

Cho Y. A. and Gwak H. S. (2004) Transdermal delivery of ketorolac tromethamine: Effects of vehicles and penetration enhancers. Drug Development and Industrial Pharmacy, **30**: 557-564.

Chung V. Q., Kelley L., Marra D. and Jiang S. B. (2006) Onion extract gel versus petrolatum emollient on new surgical scars: a prospective double-blinded study. Dermatologic Surgery, **32**: 193-197.

Clark R. A. F. (1996) Wound repair: overview and general considerations. In: R. A. F. Clark (eds.) The Molecular and Cellular Biology of Wound Repair. New York., Plenum Press. Chapter 1, pp. 3-50.

Cruz N. I. and Korchin L. (1994) Inhibition of human keloid fibroblast growth by isotretinoin and triamcinolone acetonide *in vitro*. Annals of Plastic Surgery, **33**: 401-405.

Darougheh A., Asilian A. and Shariati F. (2009) Intralesional triamcinolone alone or in combination with 5-fluorouracil for the treatment of keloid and hypertrophic scars. Clinical and Experimental Dermatology, **34**: 219-223.

De Diego M., Godoy G., Mennickent S., Olivares M. and Godoy R. (2010) Stress degradation studies of ramipril by a validated stability-indicating liquid chromatographic method. Journal of the Chilean Chemical Society, **55**: 450-453.

De Oliveira G. V., Nunes T. A., Magna L. A., Cintra M. L., Kitten G. T., Zarpellon S. and do Amaral C. M. R. (2001) Silicone versus nonsilicone gel dressings: a controlled trial. Dermatologic Surgery, **27**: 721-726.

Dias M., Hadgraft J. and Lane M. E. (2007) Influence of membrane-solvent-solute interactions on solute permeation in model membranes. International Journal of Pharmaceutics, **336**: 108-114.

Dick I. P. and Scott R. C. (1992) Pig ear skin as an *in vitro* model for human skin permeability. Journal of Pharmacy and Pharmacology, **44**: 640-645.

Dunkin C. S. J., Pleat J. M., Gillespie P. H., Tyler M. P. H., Roberts A. H. N. and McGrouther D. A. (2007) Scarring occurs at a critical depth of skin injury: precise measurement in a graduated dermal scratch in human volunteers. Plastic and Reconstructive Surgery, **119**: 1722-1732.

Engelbrecht T. N., Deme B., Dobner B. and Neubert R. H. H. (2012) Study of the influence of the penetration enhancer isopropyl myristate on the nanostructure of stratum corneum lipid model membranes using neutron diffraction and deuterium labelling. Skin Pharmacology and Physiology, **25**: 200-207.

Enoch S. and Leaper D. J. (2008) Basic science of wound healing. Surgery, **26**: 31-37.

EPA (1996) Partition coefficient (n-octanol/water): shake flask method (OPPTS 830.7550). EPA Product Properties Test Guidelines: 1-7.

Espana A., Solano T. and Quintanilla E. (2001) Bleomycin in the treatment of keloids and hypertrophic scars by multiple needle punctures. Dermatologic Surgery, **27**: 23-27.

Fasano W. J., Manning L. A. and Green J. W. (2002) Rapid integrity assessment of rat and human epidermal membranes for *in vitro* dermal regulatory testing: correlation of electrical resistance with tritiated water permeability. Toxicology in Vitro, **16**: 731-740.

Fasano W. J., ten Berge W. F., Banton M. I., Heneweer M. and Moore N. P. (2011) Dermal penetration of propylene glycols: measured absorption across human abdominal skin *in vitro* and comparison with a QSAR model. Toxicology in Vitro, **25**: 1664-1670.

Fauzee A. F. B. and Walker R. B. (2013) Forced degradation studies of clobetasol 17-propionate in methanol, propylene glycol, as bulk drug and cream formulations by RP-HPLC. Journal of Separation Science, **36**: 849-856.

FDA (2006) Guidance for industry: Impurities in new drug products (Q3B). Food and Drug Administration. [online]. Available from: http://www.fda.gov/downloads/Drugs/GuidanceComplianceRegulatoryInformation/Guidances/ucm073389.pdf [Accessed 8 April 2013]

FDA (2008) Guidance for industry: Drug stability guidelines. Food and Drug Administration. [online]. Available from: http://www.fda.gov/downloads/AnimalVeterinary/GuidanceComplianceEnforcement/GuidanceforIndustry/ucm051556.pdf [Accessed 8 April 2013]

Finnin B., Walters K. A. and Franz T. J. (2012) *In vitro* skin permeation methodology. In: H. A. Benson and A. C. Watkinson (eds.) Transdermal and Topical Drug Delivery: Principle and Practice. USA, Wiley. Chapter 5, pp. 85-108.

Fitzpatrick R. E. (1999) Treatment of inflamed hypertrophic scars using intralesional 5-FU. Dermatologic Surgery, **25**: 224-232.

Foreman M. I. and Clanachan I. (1975) Percutaneous penetration of nandrolone decanoate. British Journal of Dermatology, **93**: 47-52.

Franz T. J. (1975) Percutaneous absorption. On the relevance of *in vitro* data. Journal of Investigative Dermatology, **64**: 190-195.

Gallant-Behm C. L. and Mustoe T. A. (2010) Occlusion regulates epidermal cytokine production and inhibits scar formation. Wound Repair and Regeneration, **18**: 235-244.

Gattefosse (2010a) Lauroglycol 90 - Technical Data Sheet. [online]. Available from: http://www.gattefosse.com/media/document/tds_lauroglycol_90.PDF [Accessed 8 April 2013]

Gattefosse (2010b) Lauroglycol FCC - Technical Data Sheet. [online]. Available from: http://www.gattefosse.com/media/document/tds_lauroglycol_fcc.PDF [Accessed 8 April 2013]

Gawkrodger D. J. (2003) Basic principles. In: D. J. Gawkrodger (eds.) Dermatology: An Illustrated Colour Text. New York, Churchill Livingstone. Chapter 1, pp. 1-24.

Gaynor J. D. (1992) Microbial hydrolysis of diclofop-methyl in soil. Soil Biology and Biochemistry, **24**: 29-32.

Gonzalez A. G., Herrador M. A. and Asuero A. G. (1994) Solubility of theophylline in aqueous n,n-dimethylformamide mixtures. International Journal of Pharmaceutics, **108**: 149-154.

Gragnani A., Warde M., Furtado F. and Ferreira L. M. (2010) Topical tamoxifen therapy in hypertrophic scars or keloids in burns. Archives of Dermatological Research, **302**: 1-4.

Graham-Brown R. and Burns T. (2007) Structure and function of the skin, hair and nails. In: Dermatology. UK, Blackwell. Chapter 1, pp. 1-9

Gruning B., Hills G., Veit T., Weitemeyer C., Favre-Bulle O., Lefevre F., Nguyen H. K. and Ravot G. (2009) Thermostable esterases from thermophilic bacteria, United States Patent: 7595181.

Gu L. and Strickley R. G. (1987) Diketopiperazine formation, hydrolysis, and epimerization of the new dipeptide angiotensin converting enzyme inhibitor Rs-10085. Pharmaceutical Research, **4**: 392-397.

Gu L. and Strickley R. G. (1990) A profound solvent effect on the diketopiperazine formation of the new dipeptide angiotensin converting enzyme inhibitor, Moexipril. International Journal of Pharmaceutics, **60**: 99-107.

Gu L., Strickley R. G., Chi L. H. and Chowhan Z. T. (1990) Drug-excipient incompatibility studies of the dipeptide angiotensin-converting enzyme-inhibitor, moexipril hydrochloride - dry powder vs wet granulation. Pharmaceutical Research, **7**: 379-383.

Guzek D. B., Kennedy A. H., McNeill S. C., Wakshull E. and Potts R. O. (1989) Transdermal drug transport and metabolism. I. Comparison of *in vitro* and *in vivo* results. Pharmaceutical Research, **6**: 33-39.

Gwak H. S., Kim S. U. and Chun I. K. (2002) Effect of vehicles and enhancers on the in vitro permeation of melatonin through hairless mouse skin. Archives of Pharmacal Research, **25**: 392-396.

Hadgraft J. (2001) Skin, the final frontier. International Journal of Pharmaceutics, **224**: 1-18.

Hadgraft J. (2004) Skin deep. European Journal of Pharmaceutics and Biopharmaceutics, **58**: 291-299.

Hadgraft J. and Lane M. E. (2011) Skin: the ultimate interface. Physical Chemistry Chemical Physics, **13**: 5215-5222.

Hammell D. C., Stolarczyk E. I., Klausner M., Hamad M. O., Crooks P. A. and Stinchcomb A. L. (2005) Bioconversion of naltrexone and its 3-O-alkyl-ester prodrugs in a human skin equivalent. Journal of Pharmaceutical Sciences, **94**: 828-836.

Hanysova L., Vaclavkova M., Dohnal J. and Klimes J. (2005) Stability of ramipril in the solvents of different pH. Journal of Pharmaceutical and Biomedical Analysis, **37**: 1179-1183.

Harrison J. E., Watkinson A. C., Green D. M., Hadgraft J. and Brain K. (1996) The relative effect of Azone and Transcutol on permeant diffusivity and solubility in human stratum corneum. Pharmaceutical Research, **13**: 542-546.

Harrison S. M., Barry B. W. and Dugard P. H. (1984) Effects of freezing on human skin permeability. Journal of Pharmacy and Pharmacology, **36**: 261-262.

Harville H. M., Voorman R. and Prusakiewicz J. J. (2007) Comparison of paraben stability in human and rat skin. Drug Metabolism Letters, **1**: 17-21.

Hatamipour E., Mehrabi S., Hatamipour M. and Ghafarian Shirazi H. R. (2011) Effects of combined intralesional 5-Fluorouracil and topical silicone in prevention of keloids: a double blind randomized clinical trial study. Acta Medica Iranica, **49**: 127-130.

Hendriks T., Martens M., Huyben C. and Wobbes T. (1993) Inhibition of basal and TGF-beta induced fibroblast collagen synthesis by antineoplastic agents: implications for wound healing. British Journal of Cancer, **67**: 545-550.

Herkenne C., Naik A., Kalia Y. N., Hadgraft J. and Guy R. H. (2006) Pig ear skin *ex vivo* as a model for *in vivo* dermatopharmacokinetic studies in man. Pharmaceutical Research, **23**: 1850-1856.

Herrador M. A. and Gonzalez A. G. (1997) Solubility prediction of caffeine in aqueous N,N-dimethylformamide mixtures using the Extended Hildebrand Solubility Approach. International Journal of Pharmaceutics, **156**: 239-244.

Hewitt P. G., Perkins J. and Hotchkiss S. A. M. (2000) Metabolism of fluroxypyr, fluroxypyr methyl ester, and the herbicide fluroxypyr methylheptyl ester. I. During percutaneous absorption through fresh rat and human skin *in vitro*. Drug Metabolism and Disposition, **28**: 748-754.

Higuchi T. (1960) Physical chemical analysis of percutaneous absorption process from creams and ointments. Journal of the Society of Cosmetic Chemists, **11**: 85-97.

Hikima T. and Maibach H. I. (2007) Gender differences of enzymatic activity and distribution of 17 beta-hydroxysteroid dehydrogenase in human skin *in vitro*. Skin Pharmacology and Physiology, **20**: 168-174.

Hirata K., Helal F., Hadgraft J. and Lane M. E. (2013) Formulation of carbenoxolone for delivery to the skin. International Journal of Pharmaceutics, **448**: 360-365.

Holt R. J. (1971) Esterase and lipase activity of aerobic skin bacteria. British Journal of Dermatology, **85**: 18-23.

Hosnuter M., Payasli C., Isikdemir A. and Tekerekoglu B. (2007) The effects of onion extract on hypertrophic and keloid scars. Journal of Wound Care, **16**: 251-254.

Houben E., De Paepe K. and Rogiers V. (2007) A keratinocyte's course of life. Skin Pharmacology and Physiology, **20**: 122-132.

Howes D., Guy R., Hadgraft J., Heylings J., Hoeck U., Kemper F., Maibach H., Marty J.-P., Merk H., Parra J., Rekkas D., Rondelli I., Schaefer H., Täuber U. and Verbiese N. (1996) Methods for assessing percutaneous absorption. The report and recommendations of ECVAM workshop 13, **24**: 81-106.

Iannello S., Milazzo P., Bordonaro F. and Belfiore F. (2006) Low dose enalapril in the treatment of surgical cutaneous hypertrophic scar and keloid: two case reports and literature review. Medscape General Medicine, **8**: 60-68.

ICH (2003) Guidance for industry: Stability testing of new drug substances and products Q1A (R2). The International Conference on Harmonisation. [online]. Available from: http://www.fda.gov/downloads/regulatoryinformation/guidances/ucm128204.pdf [Accessed 8 April 2013]

ICH (2005) Validation of analytical procedures: Text and methodology Q2 (R1). The International Conference on Harmonisation [online]. Available from: http://www.ich.org/products/guidelines/quality/quality-single/article/validation-of-analytical-procedures-text-and-methodology.html [Accessed 8 April 2013]

Irion G. L. (2010a) Anatomy and physiology of skin. In: Comprehensive Wound Management. USA, Slack Inc. Chapter 1, pp. 3-10

Irion G. L. (2010b) Normal wound healing. In: Comprehensive Wound Management. USA, Slack Inc. Chapter 2, pp. 13-18

Jackson B. A. and Shelton A. J. (1999) Pilot study evaluating topical onion extract as treatment for postsurgical scars. Dermatologic Surgery, **25**: 267-269.

Jackson E. K. (2006) Renin and angiotensin. In: L. Brunton, J. Lazo and K. L. Parker (eds.) Goodman & Gilman's The Pharmacological Basis of Therapeutics, McGraw-Hill. Chapter 30, pp. 789-821.

Jacobi U., Kaiser M., Toll R., Mangelsdorf S., Audring H., Otberg N., Sterry W. and Lademann J. (2007) Porcine ear skin: an *in vitro* model for human skin. Skin Research and Technology, **13**: 19-24.

Jain R., Wu Z., Bork O. and Tucker I. G. (2012) Pre-formulation and chemical stability studies of penethamate, a benzylpenicillin ester prodrug, in aqueous vehicles. Drug Development and Industrial Pharmacy, **38**: 55-63.

Janssens M., van Smeden J., Gooris G. S., Bras W., Portale G., Caspers P. J., Vreeken R. J., Hankemeier T., Kezic S., Wolterbeek R., Lavrijsen A. P. and Bouwstra J. A. (2012) Increase in short-chain ceramides correlates with an altered lipid organization and decreased barrier function in atopic eczema patients. Journal of Lipid Research, **53**: 2755-2766.

Jewell C., Ackermann C., Payne N. A., Fate G., Voorman R. and Williams F. M. (2007a) Specificity of procaine and ester hydrolysis by human, minipig, and rat skin and liver. Drug Metabolism and Disposition, **35**: 2015-2022.

Jewell C., Prusakiewicz J. J., Ackermann C., Payne N. A., Fate G., Voorman R. and Williams F. M. (2007b) Hydrolysis of a series of parabens by skin microsomes and cytosol from human and minipigs and in whole skin in short-term culture. Toxicology and Applied Pharmacology, **225**: 221-228.

Jewell C., Prusakiewicz J. J., Ackermann C., Payne N. A., Fate G. and Williams F. M. (2007c) The distribution of esterases in the skin of the minipig. Toxicology Letters, **173**: 118-123.

Johnson A. W. (2009) Function and the skin barrier. In: Z. D. Draelos (eds.) Cosmeceuticals. USA, Saunders. Chapter 2, pp. 7-14.

Kao J. and Carver M. P. (1990) Cutaneous metabolism of xenobiotics. Drug Metabolism Reviews, **22**: 363-410.

Karadzovska D., Brooks J. D. and Riviere J. E. (2012) Experimental factors affecting *in vitro* absorption of six model compounds across porcine skin. Toxicology in Vitro, **26**: 1191-1198.

Karande P., Jain A. and Mitragotri S. (2006) Relationships between skin's electrical impedance and permeability in the presence of chemical enhancers. Journal of Controlled Release, **110**: 307-313.

Karlsson C., Lindell K., Ottosson M., Sjostrom L., Carlsson B. and Carlsson L. M. S. (1998) Human adipose tissue expresses angiotensinogen and enzymes required for its conversion to angiotensin II. Journal of Clinical Endocrinology and Metabolism, **83**: 3925-3929.

Kawaguchi Y., Takagi K., Hara M., Fukasawa C., Sugiura T., Nishimagi E., Harigai M. and Kamatani N. (2004) Angiotensin II in the lesional skin of systemic sclerosis patients contributes to tissue fibrosis via angiotensin II type 1 receptors. Arthritis and Rheumatism, **50**: 216-226.

Ketchum L. D., Smith J., Robinson D. W. and Masters F. W. (1966) Treatment of hypertrophic scar keloid and scar contracture by triamcinolone acetonide. Plastic and Reconstructive Surgery, **38**: 209-218.

Khalil S. A. and Martin A. N. (1967) Drug transport through model membranes and its correlation with solubility parameter. Journal of Pharmaceutical Sciences, **56**: 1225-1233.

Kikwai L., Kanikkannan N., Babu R. J. and Singh M. (2002) Effect of vehicles on the transdermal delivery of melatonin across porcine skin *in vitro*. Journal of Controlled Release, **83**: 307-311.

Kim D. Y., Han Y. S., Kim S. R., Chun B. K. and Park J. H. (2012) Effects of a topical angiotensin converting enzyme inhibitor and a selective COX-2 inhibitor on the prevention of hypertrophic scarring in the skin of a

rabbit ear. Wounds: Compendium of Clinical Research and Practice, **24**: 356-364.

Kligman A. M. and Christophers E. (1963) Preparation of isolated sheets of human stratum corneum. Archives of Dermatology, **88**: 702-705.

Kong R. and Bhargava R. (2011) Characterization of porcine skin as a model for human skin studies using infrared spectroscopic imaging. Analyst, **136**: 2359-2366.

Kontochristopoulos G., Stefanaki C., Panagiotopoulos A., Stefanaki K., Argyrakos T., Petridis A. and Katsambas A. (2005) Intralesional 5-fluorouracil in the treatment of keloids: an open clinical and histopathologic study. Journal of the American Academy of Dermatology, **52**: 474-479.

Korinth G., Jakasa I., Wellner T., Kezic S., Kruse J. and Schaller K. H. (2007) Percutaneous absorption and metabolism of 2-butoxyethanol in human volunteers: a microdialysis study. Toxicology Letters, **170**: 97-103.

Krieger L. M., Pan F., Doong H. and Lee R. C. (1993) Thermal response of the epidermis to surface gels. Surgical Forum, **44**: 738-740.

Kuhn M. A., Moffit M. R., Smith P. D., Lyle W. G., Ko F., Meltzer D. D. and Robson M. C. (2001) Silicone sheeting decreases fibroblast activity and downregulates TGF-β in hypertrophic scar model. International Journal of Surgical Investigation, **2**: 467-474.

Kurosaka M., Suzuki T., Hosono K., Kamata Y., Fukamizu A., Kitasato H., Fujita Y. and Majima M. (2009) Reduced angiogenesis and delay in wound healing in angiotensin II type 1a receptor-deficient mice. Biomedicine and Pharmacotherapy, **63**: 627-634.

Kusuma S., Vuthoori R. K., Piliang M. and Zins J. E. (2010) Skin anatomy and physiology. In: M. Z. Siemionow and M. EisenmannKlein (eds.) Plastic and Reconstructive Surgery, Springer. Chapter 13, pp. 161-171.

Lampe M. A., Burlingame A. L., Whitney J., Williams M. L., Brown B. E., Roitman E. and Elias P. M. (1983) Human stratum corneum lipids: characterization and regional variations. Journal of Lipid Research, **24**: 120-130.

Lane M. E. (2013) Skin penetration enhancers. International Journal of Pharmaceutics, **447**: 12-21.

Lane M. E., Santos P., Watkinson A. C. and Hadgraft J. (2012) Passive skin permeation enhancement. In: H. A. Benson and A. Watkinson (eds.) Transdermal and Topical Drug Delivery: Principles and Practice. NJ, Wiley. Chapter 2, pp. 23-42.

Lau W. M., Ng K. W., Sakenyte K. and Heard C. M. (2012) Distribution of esterase activity in porcine ear skin, and the effects of freezing and heat separation. International Journal of Pharmaceutics, **433**: 10-15.

Lawrence J. N. (1997) Electrical resistance and tritiated water permeability as indicators of barrier integrity of *in vitro* human skin. Toxicology in Vitro, **11**: 241-249.

Lee K. E., Choi Y. J., Oh B. R., Chun I. K. and Gwak H. S. (2013) Formulation and in vitro/in vivo evaluation of levodopa transdermal delivery systems. International Journal of Pharmaceutics, **456**: 432-436.

Lee T. Y., Chin G. S., Kim W. J. H., Chau D., Gittes G. K. and Longaker M. T. (1999) Expression of transforming growth factor beta 1, 2, and 3 proteins in keloids. Annals of Plastic Surgery, **43**: 179-184.

Leopold C. S. and Lippold B. C. (1995) An attempt to clarify the mechanism of the penetration enhancing effects of lipophilic vehicles with differential scanning calorimetry (DSC). Journal of Pharmacy and Pharmacology, **47**: 276-281.

Lindpaintner K., Jin M., Wilhelm M. J., Suzuki F., Linz W., Schoelkens B. A. and Ganten D. (1988) Intracardiac generation of angiotensin and its physiologic role. Circulation, **77**: 18-23.

Lippold B. C. (1992) How to optimize drug penetration through the skin. Pharmaceutica Acta Helvetiae **67**: 294-300.

Lippold B. C. and Schneemann H. (1984) The influence of vehicles on the local bioavailability of betamethasone-17-benzoate from solution type and suspension type ointments. International Journal of Pharmaceutics, **22**: 31-43.

Liron Z. and Cohen S. (1984) Percutaneous absorption of alkanoic acids: application of regular solution theory. Journal of Pharmaceutical Sciences, **73**: 538-542.

Lynch S. E., Colvin R. B. and Antoniades H. N. (1989) Growth factors in wound healing: single and synergistic effects on partial thickness porcine skin wounds. Journal of Clinical Investigation, **84**: 640-646.

Ma C. M., Cai J. L., Niu F. Y., Zong X. L., Chen Y. and Liu L. B. (2012) Skin needle roller importing triamcinolone acetonide into scar to treat hypertrophic scars. Chinese Journal of Plastic Surgery, **28**: 185-189.

Magnusson B. M., Anissimov Y. G., Cross S. E. and Roberts M. S. (2004) Molecular size as the main determinant of solute maximum flux across the skin. Journal of Investigative Dermatology, **122**: 993-999.

Malhotra A. K., Gupta S., Khaitan B. K. and Sharma V. K. (2007) Imiquimod 5% cream for the prevention of recurrence after excision of presternal keloids. Dermatology, **215**: 63-65.

May S. R. and Declement F. A. (1982) Development of a radiometric metabolic viability testing method for human and porcine skin. Cryobiology, **19**: 362-371.

McGrath J. A. and Uitto J. (2010) Anatomy and organization of human skin. In: T. Burns, S. Breathnach, N. Cox and C. Griffiths (eds.) Rook's Textbook of Dermatology. UK, Wiley-Blackwell. Chapter 3, pp. 1-53.

Menon G. K., Cleary G. W. and Lane M. E. (2012) The structure and function of the stratum corneum. International Journal of Pharmaceutics, **435**: 3-9.

Meyer W. and Neurand K. (1976) The distribution of enzymes in the skin of the domestic pig. Laboratory Animals, **10**: 237-247.

Michaels A. S., Chandrasekaran S. K. and Shaw J. E. (1975) Drug permeation through human skin: theory and *in vitro* experimental measurement. AIChE Journal, **21**: 985-996.

Modhave D. T., Handa T., Shah R. P. and Singh S. (2011) Successful characterization of degradation products of drugs using LC-MS tools: application to piroxicam and meloxicam. Analytical Methods, **3**: 2864-2872.

Moffat A. C., Osselton M. D., Widdop B. and Watts J. (2011) Cilazapril. In: A. C. Moffat, M. D. Osselton, B. Widdop and J. Watts (eds.) Clarke's Analysis of Drugs and Poisons. London, UK, Pharmaceutical Press.

Moghimipour E., Salimi A. and Zadeh B. S. M. (2013) Effect of the Various Solvents on the In Vitro Permeability of Vitamin B-12 through Excised Rat Skin. Tropical Journal of Pharmaceutical Research, **12**: 671-677.

Mollgaard B., Hoelgaard A. and Bundgaard H. (1982) Prodrugs as drug delivery systems. Improved dermal delivery of 5-fluorouracil through human skin via N-acyloxymethyl prodrug derivatives. International Journal of Pharmaceutics, **12**: 153-162.

Montagna W. (1955) Histology and cytochemistry of human skin: the distribution of non-specific esterases. Journal of Biophysical and Biochemical Cytology, **1**: 13-16.

Monteiro-Riviere N. A., Bristol D. G., Manning T. O., Rogers R. A. and Riviere J. E. (1990) Interspecies and interregional analysis of the comparative histologic thickness and laser doppler blood-flow measurements at 5 cutaneous sites in 9 species. Journal of Investigative Dermatology, **95**: 582-586.

Montenegro L., Carbone C., Maniscalco C., Lambusta D., Nicolosi G., Ventura C. A. and Puglisi G. (2007) *In vitro* evaluation of quercetin-3-O-acyl esters as topical prodrugs. International Journal of Pharmaceutics, **336**: 257-262.

Montes L. F. and Wilborn W. H. (1970) Anatomical location of normal skin flora. Archives of Dermatology, **101**: 145-159.

Montesano R. and Orci L. (1988) Transforming growth factor-beta stimulates collagen-matrix contraction by fibroblasts: implications for wound healing. Proceedings of the National Academy of Sciences of the United States of America, **85**: 4894-4897.

Morihara K., Takai S., Takenaka H., Sakaguchi M., Okamoto Y., Morihara T., Miyazaki M. and Kishimoto S. (2006) Cutaneous tissue angiotensin converting enzyme may participate in pathologic scar formation in human skin. Journal of the American Academy of Dermatology, **54**: 251-257.

Morris A. P., Brain K. R. and Heard C. M. (2009) Skin permeation and *ex vivo* skin metabolism of O-acyl haloperidol ester prodrugs. International Journal of Pharmaceutics, **367**: 44-50.

Mousavi S. R., Raaiszadeh M., Aminseresht M. and Behjoo S. (2010) Evaluating tamoxifen effect in the prevention of hypertrophic scars following surgical incisions. Dermatologic Surgery, **36**: 665-669.

Muneuchi G., Suzuki S., Onodera M., Ito O., Hata Y. and Igawa H. H. (2006) Long-term outcome of intralesional injection of triamcinolone acetonide for the treatment of keloid scars in Asian patients. Scandinavian Journal of Plastic and Reconstructive Surgery and Hand Surgery, **40**: 111-116.

Munjal D. and Rose N. R. (1972) Purification and immunochemical characterization of a human specific urine and tissue esterase EC-3.1.1.1. Biochimica et Biophysica Acta, **285**: 352-363.

Mura S., Manconi M., Valenti D., Sinico C., Vila A. O. and Fadda A. M. (2011) Transcutol containing vesicles for topical delivery of minoxidil. Journal of Drug Targeting, **19**: 189-196.

Naeini F. F., Najafian J. and Ahmadpour K. (2006) Bleomycin tattooing as a promising therapeutic modality in large keloids and hypertrophic scars. Dermatologic Surgery, **32**: 1023–1030.

Nanda S. and Reddy B. S. N. (2004) Intralesional 5-fluorouracil as a treatment modality of keloids. Dermatologic Surgery, **30**: 54-57.

Nemanic M. K. and Elias P. M. (1980) In situ precipitation: a novel cyotchemical technique for visualization of permeability pathways in mammalian stratum corneum. Journal of Histochemistry and Cytochemistry, **28**: 573-578.

Ngawhirunpat T., Opanasopit P. and Prakongpan S. (2004) Comparison of skin transport and metabolism of ethyl nicotinate in various species. European Journal of Pharmaceutics and Biopharmaceutics, **58**: 645-651.

Nicoli S., Bunge A. L., Delgado-Charro M. B. and Guy R. H. (2009) Dermatopharmacokinetics: factors influencing drug clearance from the stratum corneum. Pharmaceutical Research, **26**: 865-871.

Norlen L., Nicander I., Rozell B. L., Ollmar S. and Forslind B. (1999) Inter- and intra-individual differences in human stratum corneum lipid content related to physical parameters of skin barrier function *in vivo*. Journal of Investigative Dermatology, **112**: 72-77.

OECD (1995) Partition coefficient (n-octanol/water): shake flask method. OECD Guideline for the Testing of Chemicals, **107**: 1-4.

OECD (2004a) Guidance document for the conduct of skin absorption studies. [online]. Available from: http://search.oecd.org/officialdocuments/displaydocumentpdf/?doclanguage=en&cote=env/jm/mono(2004)2 [Accessed 8 April 2013]

OECD (2004b) OECD Guideline 428 for the Testing of Chemicals: Skin absorption: *in vitro* methods. [online]. Available from: http://www.oecd-ilibrary.org/environment/test-no-428-skin-absorption-in-vitro-method_9789264071087-en [Accessed 8 April 2013]

OECD (2010) OECD guidance notes on dermal absorption. [online]. Available from: http://www.oecd.org/env/ehs/testing/46257610.pdf [Accessed 8 April 2013]

Oesch F., Fabian E., Oesch-Bartlomowicz B., Werner C. and Landsiedel R. (2007) Drug-metabolizing enzymes in the skin of man, rat, and pig. Drug Metabolism Reviews, **39**: 659-698.

Otto A., du Plessis J. and Wiechers J. W. (2009) Formulation effects of topical emulsions on transdermal and dermal delivery. International Journal of Cosmetic Science, **31**: 1-19.

Otto A., Wiechers J. W., Kelly C. L., Hadgraft J. and du Plessis J. (2008) Effect of penetration modifiers on the dermal and transdermal delivery of drugs and cosmetic active ingredients. Skin Pharmacology and Physiology, **21**: 326-334.

Pan C., Jiang Y., Wen H. and Motto M. (2012) Identification of a drug degradation product found in a stressed dosage form using LC/MS, LC/TOF MS and on-line H/D exchange MS. Journal of Pharmaceutical and Biomedical Analysis, **57**: 99-103.

Parmar N., Amin S., Singla N. and Kohli K. (2012) The solution, solid state stability and kinetic investigation in degradation studies of

lercanidipine: study of excipients compatibility of lercanidipine. Pharmaceutical Development and Technology, **17**: 730-740.

Paul M., Bader M., Steckelings U. M., Voigtlander T. and Ganten D. (1993) The renin angiotensin system in the brain: localization and functional significance. Drug Research, **43**: 207-213.

Perkins K., Davey R. B. and Wallis K. A. (1983) Silicone gel: a new treatment for burn scars and contractures. Burns, **9**: 201-204.

Phan T. T., Lim I. J., Chan S. Y., Tan E. K., Lee S. T. and Longaker M. T. (2003) Quercetin inhibits fibronectin production by keloid derived fibroblasts: implication for the treatment of excessive scars. Journal of Dermatological Science, **33**: 192-194.

Porter W. H. and Auansakul A. (1982) Gas chromatographic determination of ethylene-glycol in serum. Clinical Chemistry, **28**: 75-78.

Potts R. O. and Guy R. H. (1992) Predicting skin permeability. Pharmaceutical Research, **9**: 663-669.

Prausnitz M. R., Mitragotri S. and Langer R. (2004) Current status and future potential of transdermal drug delivery. Nature Reviews Drug Discovery, **3**: 115-124.

Prusakiewicz J. J., Ackermann C. and Voorman R. (2006) Comparison of skin esterase activities from different species. Pharmaceutical Research, **23**: 1517-1524.

Puglia C. and Bonina F. (2008) Effect of polyunsaturated fatty acids and some conventional penetration enhancers on transdermal delivery of atenolol. Drug Delivery, **15**: 107-112.

Rao P. S., Ray U. K., Hiriyanna S. G., Rao S. V., Sharma H. K., Handa V. K. and Mukkanti K. (2011) Identification of oxidative degradation impurities of Olanzapine drug substance as well as drug product. Journal of Pharmaceutical and Biomedical Analysis, **56**: 413-418.

Ren S., Park M. J., Sah H. and Lee B. J. (2008) Effect of pharmaceutical excipients on aqueous stability of rabeprazole sodium. International Journal of Pharmaceutics, **350**: 197-204.

Reynolds D. W., Facchine K. L., Mullaney J. F., Alsante K. M., Hatajik T. D. and Motto M. G. (2002) Available guidance and best practices for conducting forced degradation studies. Pharmaceutical Technology, **26**: 48-56.

Rodgers K., Abiko M., Girgis W., Amand K., Campeau J. and Dizerega G. (1997) Acceleration of dermal tissue repair by angiotensin II. Wound Repair Regeneration, **5**: 175-183.

Rolsted K., Benfeldt E., Kissmeyer A. M., Rist G. M. and Hansen S. H. (2009) Cutaneous *in vivo* metabolism of topical lidocaine formulation in human skin. Skin Pharmacology and Physiology, **22**: 124-127.

Roskar R., Simoncic Z., Gartner A. and Kmetec V. (2009) Stability of new potential ACE inhibitor in the aqueous solutions of different pH. Journal of Pharmaceutical and Biomedical Analysis, **49**: 295-303.

Rowe R. C., Sheskey P. J. and Quinn M. E. (2009) Handbook of Pharmaceutical Excipients, 6th ed. Pharmaceutical Press: London.

Sandby-Moller J., Poulsen T. and Wulf H. C. (2003) Epidermal thickness at different body sites: relationship to age, gender, pigmentation, blood content, skin type and smoking habits. Acta Dermato-Venereologica, **83**: 410-413.

Sander I., Fleischer C., Meurer U., Bruening T. and Raulf-Heimsoth M. (2009) Allergen content of grass pollen preparations for skin prick testing and sublingual immunotherapy. Allergy, **64**: 1486-1492.

Santos P., Watkinson A. C., Hadgraft J. and Lane M. E. (2010) Oxybutynin permeation in skin: the influence of drug and solvent activity. International Journal of Pharmaceutics, **384**: 67-72.

Santos P., Watkinson A. C., Hadgraft J. and Lane M. E. (2011) Formulation issues associated with transdermal fentanyl delivery. International Journal of Pharmaceutics, **416**: 155-159.

Saray Y. and Gulec A. T. (2005) Treatment of keloids and hypertrophic scars with dermojet injections of bleomycin: a preliminary study. International Journal of Dermatology, **44**: 777-784.

Sato K., Sugibayashi K. and Morimoto Y. (1991) Species differences in percutaneous absorption of nicorandil. Journal of Pharmaceutical Sciences, **80**: 104-107.

Saulis A. S., Mogford J. H. and Mustoe T. A. (2002) Effect of Mederma on hypertrophic scarring in the rabbit ear model. Plastic and Reconstructive Surgery, **110**: 177-183.

Sawada Y. and Sone K. (1992) Hydration and occlusion treatment for hypertrophic scars and keloids. British Journal of Plastic Surgery, **45**: 599-603.

Schlatter J. and Saulnier J. L. (1997) The stability of enalapril maleate solution prepared from tablet in sterile water. Australian Journal of Hospital Pharmacy, **27**: 395-397.

Schmid P., Cox D., Bilbe G., McMaster G., Morrison C., Stahelin H., Luscher N. and Seiler W. (1993) TGF-βs and TGF-β type-II receptor in human epidermis: differential expression in acute and chronic skin wounds. Journal of Pathology, **171**: 191-197.

Shaikh N. A., Ademola J. I. and Maibach H. I. (1996) Effects of freezing and azide treatment of *in vitro* human skin on the flux and metabolism of 8-methoxypsoralen. Skin Pharmacology, **9**: 274-280.

Shetgiri N. P., Bhure S., Rakhe A., Patil S., Anwari A. and Mukherjee R. (2008) Synthesis and structural elucidation of impurities in ramipril tablets. Current Trends in Mass Spectrometry.

Shumer S. M. and O'Keefe E. J. (1983) Bleomycin in the treatment of recalcitrant warts. Journal of the American Academy of Dermatology, **9**: 91-96.

Sigma-Aldrich (2011) Technical bulletin - Bradford Reagent. [online]. Available from: http://www.sigmaaldrich.com/catalog/product/sigma/b6916?lang=en&region=GB [Accessed 8 April 2013]

Sigma-Aldrich (2012) Enzymatic assay of esterase (EC 3.1.1.1).

Signorini M. and Clementoni M. T. (2007) Clinical evaluation of a new self drying silicone gel in the treatment of scars: a preliminary report. Aesthetic Plastic Surgery, **31**: 183-187.

Singh B. N., Singh R. B. and Singh J. (2005) Effects of ionization and penetration enhancers on the transdermal delivery of 5-fluorouracil through excised human stratum corneum. International Journal of Pharmaceutics, **298**: 98-107.

Singh S., Zhao K. and Singh J. (2002) *In vitro* permeability and binding of hydrocarbons in pig ear and human abdominal skin. Drug and Chemical Toxicology, **25**: 83-92.

Sinha V. R. and Kaur M. P. (2000) Permeation enhancers for transdermal drug delivery. Drug Development and Industrial Pharmacy, **26**: 1131-1140.

Sloan K. B., Koch S. A. M., Siver K. G. and Flowers F. P. (1986) Use of solubility parameters of drug and vehicle to predict flux through skin. Journal of Investigative Dermatology, **87**: 244-252.

Smith R. F. and Evans B. L. (1972) Bacteria of porcine skin, xenografts, and treatment with neomycin sulfate. Applied Microbiology, **23**: 293-297.

Stanisz B. (2004) The influence of relative humidity and temperature on stability of moexipril hydrochloride in solid phase. Acta Poloniae Pharmaceutica, **61**: 91-96.

Stanisz B., Regulska K., Kania J. and Garbacki P. (2013) Effect of pharmaceutical excipients on the stability of angiotensin-converting enzyme inhibitors in their solid dosage formulations. Drug Development and Industrial Pharmacy, **39**: 51-61.

Steckelings U. M., Henz B. M., Wiehstutz S., Unger T. and Artuc M. (2005) Differential expression of angiotensin receptors in human cutaneous wound healing. British Journal of Dermatology, **153**: 887-893.

Steckelings U. M., Wollschlager T., Peters J., Henz B. M., Hermes B. and Artuc M. (2004) Human skin: Source of and target organ for angiotensin II. Experimental Dermatology, **13**: 148-154.

Steiling W., Kreutz J. and Hofer H. (2001) Percutaneous penetration/dermal absorption of hair dyes *in vitro*. Toxicology in Vitro, **15**: 565-570.

Stinchcomb A. L., Paliwal A., Dua R., Imoto H., Woodard R. W. and Flynn G. L. (1996) Permeation of buprenorphine and its 3-alkyl-ester prodrugs through human skin. Pharmaceutical Research, **13**: 1519-1523.

Stojadinovic O., Lee B., Vouthounis C., Vukelic S., Pastar I., Blumenberg M., Brem H. and Tomic-Canic M. (2007) Novel genomic effects of glucocorticoids in epidermal keratinocytes: Inhibition of apoptosis, interferon-gamma pathway, and wound healing along with promotion of terminal differentiation. Journal of Biological Chemistry, **282**: 4021-4034.

Suetake T., Sasai S., Zhen Y. X., Ohi T. and Tagami H. (1996) Functional analyses of the stratum corneum in scars: sequential studies after injury and comparison among keloids, hypertrophic scars, and atrophic scars. Archives of Dermatology, **132**: 1453-1458.

Suetake T., Sasai S., Zhen Y. X. and Tagami H. (2000) Effects of silicone gel sheet on the stratum corneum hydration. British Journal of Plastic Surgery, **53**: 503-507.

Swarbrick J., Lee G. and Brom J. (1982) Drug permeation through human skin: effect of storage conditions of skin. Journal of Investigative Dermatology, **78**: 63-66.

Takahashi K., Komai M., Kinoshita N., Nakamura E., Hou X.-L., Takatani-Nakase T. and Kawase M. (2011) Application of hydrotropy to transdermal formulations: hydrotropic solubilization of polyol fatty acid monoesters in water and enhancement effect on skin permeation of 5-FU. Journal of Pharmacy and Pharmacology, **63**: 1008-1014.

Takahashi K., Sakano H., Yoshida M., Numata N. and Mizuno N. (2001) Characterization of the influence of polyol fatty acid esters on the permeation of diclofenac through rat skin. Journal of Controlled Release, **73**: 351-358.

Takeda H., Katagata Y., Hozumi Y. and Kondo S. (2004) Effects of angiotensin II receptor signaling during skin wound healing. American Journal of Pathology, **165**: 1653-1662.

Tandara A. A., Kloeters O., Mogford J. E. and Mustoe T. A. (2007) Hydrated keratinocytes reduce collagen synthesis by fibroblasts via paracrine mechanisms. Wound Repair and Regeneration, **15**: 497-504.

Tang H. T., Cheng D. S., Jia Y. T., Ben D. F., Ma B., Lv K. Y., Wei D., Sheng Z. Y. and Xia Z. F. (2009) Angiotensin II induces type I collagen gene expression in human dermal fibroblasts through an AP-1/TGF-beta1 dependent pathway. Biochemical and Biophysical Research Communications, **385**: 418-423.

Terunuma A., Aiba S. and Tagami H. (2001) Cytokine mRNA profiles in cultured human skin component cells exposed to various chemicals: a simulation model of epicutaneous stimuli induced by skin barrier perturbation in comparison with that due to exposure to haptens or irritant. Journal of Dermatological Science, **26**: 85-93.

Thappa D. M. (2009) Physiology, biochemistry, and immunology of the skin. In: Textbook of Dermatology, Venereology and Leprology. India, Elsevier. Chapter 2, pp. 16-22

Tobin D. J. (2011) The anatomy and physiology of the skin. In: M. J. Hertenstein and S. J. Weiss (eds.) The Handbook of Touch: Neuroscience, Behavioral, and Health Perspectives. NY, Springer. Chapter 1, pp. 3-32.

Traynor M. J., Wilkinson S. C. and Williams F. M. (2008) Metabolism of butoxyethanol in excised human skin *in vitro*. Toxicology Letters, **177**: 151-155.

Trottet L., Merly C., Mirza M., Hadgraft J. and Davis A. F. (2004) Effect of finite doses of propylene glycol on enhancement of *in vitro* percutaneous permeation of loperamide hydrochloride. International Journal of Pharmaceutics, **274**: 213-219.

Tsai J. C., Cappel M. J., Flynn G. L., Weiner N. D., Kreuter J. and Ferry J. J. (1992) Drug and vehicle deposition from topical applications: use of *in vitro* mass balance technique with minoxidil solutions. Journal of Pharmaceutical Sciences, **81**: 736-743.

Twist J. N. and Zatz J. L. (1986) Influence of solvents on paraben permeation through idealized skin model membranes. Journal of the Society of Cosmetic Chemists, **37**: 429-444.

Twist J. N. and Zatz J. L. (1989) The effect of solvents on solute penetration through fuzzy rat skin *in vitro*. Journal of the Society of Cosmetic Chemists, **40**: 231-242.

Vaddi H. K., Hamad M. O., Chen J. H., Banks S. L., Crooks P. A. and Stinchcomb A. L. (2005) Human skin permeation of branched-chain 3-O-alkyl ester and carbonate prodrugs of naltrexone. Pharmaceutical Research, **22**: 758-765.

Valiveti S., Paudel K. S., Hammell D. C., Hamad M. O., Chen J. H., Crooks P. A. and Stinchcomb A. L. (2005) *In vitro / in vivo* correlation of transdermal naltrexone prodrugs in hairless guinea pigs. Pharmaceutical Research, **22**: 981-989.

Vaughan C. D. (1985) Using solubility parameters in cosmetics formulations. Journal of the Society of Cosmetic Chemists, **36**: 319–333.

Viswanathan M. and Saavedra J. M. (1992) Expression of angiotensin II AT2 receptors in the rat skin during experimental wound healing. Peptides, **13**: 783-786.

Wagner J., Danser A. H. J., Derkx F. H. M., deJong P., Paul M., Mullins J. J., Schalekamp M. and Ganten D. (1996) Demonstration of renin mRNA, angiotensinogen mRNA, and angiotensin converting enzyme mRNA expression in the human eye: evidence for an intraocular renin-angiotensin system. British Journal of Ophthalmology, **80**: 159-163.

Walters K. A. and Roberts M. S. (2002) The structure and function of skin. In: K. A. Walters (eds.) Dermatological and Transdermal Formulations. New York, Marcel Dekker. Chapter 1, pp. 1-30.

Wang J., Dodd C., Shankowsky H. A., Scott P. G. and Tredget E. E. (2008) Deep dermal fibroblasts contribute to hypertrophic scarring. Laboratory Investigation, **88**: 1278-1290.

Wang J. J., Sung K. C., Huang J. F., Yeh C. H. and Fang J. Y. (2007) Ester prodrugs of morphine improve transdermal drug delivery: a mechanistic study. Journal of Pharmacy and Pharmacology, **59**: 917-925.

Watkinson A. C., Joubin H., Green D. M., Brain K. R. and Hadgraft J. (1995) The Influence of vehicle on permeation from saturated solutions. International Journal of Pharmaceutics, **121**: 27-36.

Watkinson R. M., Guy R. H., Hadgraft J. and Lane M. E. (2009) Optimisation of cosolvent concentration for topical drug delivery. II. Influence of propylene glycol on ibuprofen permeation. Skin Pharmacology and Physiology, **22**: 225-230.

Watson D. G. (2012) High pressure liquid chromatography. In: Pharmaceutical Analysis. Churchill Livingstone. Chapter 12, pp. 301-357

Weerheim A. and Ponec M. (2001) Determination of stratum corneum lipid profile by tape stripping in combination with high-performance thin-layer chromatography. Archives of Dermatological Research, **293**: 191-199.

Wendling J., Marchand A., Mauviel A. and Verrecchia F. (2003) 5-fluorouracil blocks transforming growth factor-beta-induced alpha(2)

type I collagen gene (COL1A2) expression in human fibroblasts via c-Jun NH2-terminal kinase/activator protein-1 activation. Molecular Pharmacology, **64**: 707-713.

Wermuth G., Ganellin C. R., Lindberg P. and Mitscher L. A. (1998) Glossary of terms used in medicinal chemistry (IUPAC Recommendations 1998). Pure and Applied Chemistry, **70**: 1129-1143.

Wertz P. W., Swartzendruber D. C., Madison K. C. and Downing D. T. (1987) Composition and morphology of epidermal cyst lipids. Journal of Investigative Dermatology, **89**: 419-425.

Wester R. C., Christoffel J., Hartway T., Poblete N., Maibach H. I. and Forsell J. (1998) Human cadaver skin viability for *in vitro* percutaneous absorption: storage and detrimental effects of heat-separation and freezing. Pharmaceutical Research, **15**: 82-84.

Wester R. C. and Maibach H. (1985) Structure-activity correlations in percutaneous absorption. In: R. Bronauch and H. Maibach (eds.) Percutaneous Absorption: Mechanisms-Methodology-Drug Delivery. New York, Marcel Dekker. Chapter 8, pp. 107-123.

Wilkinson S. C. (2008) Biochemistry of the skin. In: R. P. Chilcott and S. A. Price (eds.) Principles and Practice of Skin Toxicology. UK, Wiley. Chapter 2, pp. 17-49.

Wilkinson S. C. and Williams F. M. (2007) Cutaneous metabolism. In: M. S. Roberts and K. A. Walters (eds.) Dermal Absorption and Toxicity Assessment, Informa Healthcare USA, Inc., New York. Chapter 6, pp. 89-115.

Wolff H. H. (2009) Introduction to the skin and dermatology. In: W. H. C. Burgdorf, G. Plewig, H. H. Wolff and M. Landthaler (eds.) Braun-Falco´s Dermatology. UK, Springer. Chapter 1, pp. 1-16.

Woolfson A. D., Mccafferty D. F. and Mcgowan K. E. (1990) The metabolism of amethocaine by porcine and human skin extracts: influence on percutaneous anesthesia. International Journal of Pharmaceutics, **62**: 9-14.

Wotton P. K., Mollgaard B., Hadgraft J. and Hoelgaard A. (1985) Vehicle effect on topical drug delivery: effect of azone on the cutaneous permeation of metronidazole and propylen glycol. International Journal of Pharmaceutics, **24**: 19-26.

Wu H. J., Liu H. W., Cheng B., Gu Y. F., Xie B., Xiao L. L., Shao J. L. and Lu J. Q. (2011) The change of angiotensin II production and its receptor expression during wound healing: possible role of angiotensin II in wound healing. Chinese Journal of Plastic Surgery, **27**: 124-128.

Wu W. S., Wang F. S., Yang K. D., Huang C. C. and Kuo Y. R. (2006) Dexamethasone induction of keloid regression through effective

suppression of VEGF expression and keloid fibroblast proliferation. Journal of Investigative Dermatology, **126**: 1264-1271.

Yahata Y., Shirakata Y., Tokumaru S., Yang L. J., Dai X. J., Tohyama M., Tsuda T., Sayama K., Iwai M., Horiuchi M. and Hashimoto K. (2006) A novel function of angiotensin II in skin wound healing. Induction of fibroblast and keratinocyte migration by angiotensin II via heparin-binding epidermal growth factor (EGF)-like growth factor-mediated EGF receptor transactivation. Journal of Biological Chemistry, **281**: 13209-13216.

Zheng N., Fung E. N., Buzescu A., Arnold M. E. and Zeng J. (2012) Esterase inhibitors as ester-containing drug stabilizers and their hydrolytic products: potential contributors to the matrix effects on bioanalysis by liquid chromatography/tandem mass spectrometry. Rapid Communications in Mass Spectrometry, **26**: 1291-1304.

Appendix A

The effect of the evaporation and back diffusion of propylene glycol on its permeation profile

The possible processes in the permeation of propylene glycol (PG) across porcine skin (Figure A-1) are:

A. The diffusion of PG across the skin from the donor toward the receptor.

B. The back diffusion of PG from the receptor to the donor.

C. The evaporation of PG via the sampling port of the diffusion cell.

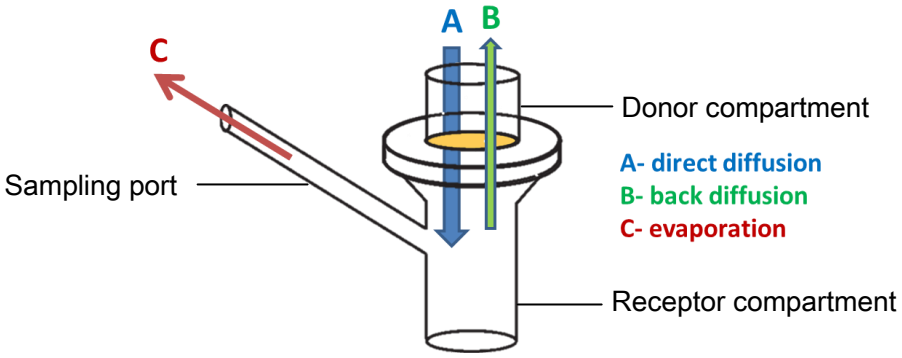

Figure A-1 Franz diffusion cell

In order to derive the equation for the permeation profile of PG, a number of equations were used:

Any collection time (0, 6, 9, 12, 20, 24, 30, 36, 44, 48 or 52 h) was denoted by (i); where i=1 represents the collection time at 6 h; i=2 represents the collection time at 9 h...etc.

The mass of PG that reached the receptor by the direct diffusion (*dd*) through the porcine skin (Figure A-1-A) from the beginning of the experiment until a specific

collection time (n) was denoted by M_{dd_n}. However, the mass of PG that reached the receptor by the direct diffusion between two consecutive collection times (i and i-1) was denoted by m_{dd_i}, therefore

$$M_{dd_n} = \sum_{i=1}^{n} m_{dd_i} \qquad (1)$$

The mass of PG that back diffused (*bd*) through the porcine skin (Figure A-1-B) from the beginning of the experiment until a specific collection time (n) was denoted by M_{bd_n}. However, the mass of PG that escaped from the receptor by back diffusion between two consecutive collection times (i and i-1) was denoted by m_{bd_i}, therefore:

$$M_{bd_n} = \sum_{i=1}^{n} m_{bd_i} \qquad (2)$$

The mass of PG that escaped from the receptor by evaporation (*ev*) via the sampling port (Figure A-1-C) from the beginning of the experiment until a specific collection time (n) was denoted by M_{ev_n}. However, the mass of PG that escaped from the receptor by evaporation between two consecutive collection times (i and i-1) was m_{ev_i}, therefore:

$$M_{ev_n} = \sum_{i=1}^{n} m_{ev_i} \qquad (3)$$

The mass of PG that was sampled via the sampling port (M_{S_n}) between the beginning of the experiment and before a specific collection time (n):

$$M_{S_n} = \sum_{i=1}^{n-1} m_{S_i} = \sum_{i=1}^{n-1} C_i \,.\, V_{S_i} \qquad (4)$$

Where C_i is the concentration of PG in the sample collected at each collection time

V_{S_i} is the volume of sample (constant)

Since the sample collected from the receptor medium (V_{S_i}) was immediately replaced with an equal volume of a fresh pre-warmed buffer solution (V_{buf_i}), the mass of PG in each of the buffer solution samples (m_{buf_n}) was equal to zero. Therefore, the mass of PG that reached the receptor from the buffer (M_{buf_n}) before a specific collection time (n) was equal to zero:

$$M_{buf_n} = \sum_{i=1}^{n-1} m_{buf_i} = 0 \qquad (5)$$

The mass of PG that accumulated in the receptor phase at the collection time, n (M_{r_n})

$$M_{r_n} = C_{r_n}.V_r \qquad (6)$$

Where C_{r_n} is the concentration of PG in the receptor phase

V_r is the volume of the receptor phase

The amount of PG in the receptor until a specific collection time (n) is the difference between the PG amount which entered the receptor (M_{in}) and that left the receptor (M_{out}), i.e., $M_{r_n} = (\sum M_{in} - \sum M_{out})_n$. The mass of PG which reached the receptor phase from buffer replacement and direct diffusion was $\sum M_{in} = M_{buf_n} + M_{dd_n}$and that which left the receptor by sampling, evaporation, and back diffusion was $\sum M_{out} = M_{S_n} + M_{ev_n} + M_{bd_n}$. Therefore:

$$M_{r_n} = (\sum M_{in} - \sum M_{out})_n = M_{buf_n} + M_{dd_n} - (M_{S_n} + M_{ev_n} + M_{bd_n}) \qquad (7)$$

$$M_{buf_n} = 0 \quad \rightarrow \quad M_{r_n} + M_{S_n} = M_{dd_n} - \left(M_{ev_n} + M_{bd_n}\right) \qquad (8)$$

Using Equations 1, 2, 3, 4 and 6, Equation 8 can be rewritten as follows

$$C_{r_n}.V_r + \sum_{i=1}^{n-1} C_i\,.V_{S_i} = \sum_{i=1}^{n} m_{dd_i} - \left[\sum_{i=1}^{n} m_{ev_i} + \sum_{i=1}^{n} m_{bd_i}\right] \qquad (9)$$

From Equations 8 and 9,

$$M_{r_n} + M_{S_n} = C_{r_n}.V_r + \sum_{i=1}^{n-1} C_i\,.V_{S_i} = Q_{t_n} \qquad (10)$$

The cumulative amount at a specific collection time (Q_{t_n}) is the sum of PG mass in the receptor phase (M_{r_n}) at this time and the PG masses in all the samples collected before this time (M_{S_n}).

From Equations 9 and 10,

$$Q_{t_n} = \sum_{i=1}^{n} m_{dd_i} - \left[\sum_{i=1}^{n} m_{ev_i} + \sum_{i=1}^{n} m_{bd_i}\right] \qquad (11)$$

Furthermore, the cumulative amount of PG in the receptor at the collection time (n-1) would be:

$$Q_{t_{n-1}} = \sum_{i=1}^{n-1} m_{dd_i} - \left[\sum_{i=1}^{n-1} m_{ev_i} + \sum_{i=1}^{n-1} m_{bd_i}\right] \qquad (12)$$

Subtracting Eq.12 from Eq.11results in:

$$Q_{t_n} - Q_{t_{n-1}} = \left[\sum_{i=1}^{n} m_{dd_i} - \sum_{i=1}^{n-1} m_{dd_i}\right] - \left[\sum_{i=1}^{n} m_{ev_i} - \sum_{i=1}^{n-1} m_{ev_i}\right] - \left[\sum_{i=1}^{n} m_{bd_i} - \sum_{i=1}^{n-1} m_{bd_i}\right]$$

$$Q_{t_n} - Q_{t_{n-1}} = m_{dd_n} - m_{ev_n} - m_{bd_n}$$

$$Q_{t_n} - Q_{t_{n-1}} = m_{dd_n} - \left(m_{ev_n} + m_{bd_n} \right) \qquad (13)$$

Where $m_{dd_n} \geq 0$, $m_{bd_n} \geq 0$, and $m_{ev_n} \geq 0$

Discussion:

One of the following three possible cases can be observed:

1) If the back diffusion and evaporation are absent $(m_{bd_n} = m_{ev_n} = 0)$, Equation 13 can be rewritten as follows: $Q_{t_n} - Q_{t_{n-1}} = m_{dd_n} \geq 0$. Therefore, the permeation profile (Q_t *vs.* time) will either increase with time or have a plateau level.

2) If the direct diffusion is absent $(m_{dd_n} = 0)$, while the back diffusion and/or evaporation are/is present, Equation 13 can be rewritten as follows $Q_{t_n} - Q_{t_{n-1}} = -\left(m_{ev_n} + m_{bd_n} \right) \leq 0$. Therefore, the permeation profile will have a negative slope (a decrease with time).

3) If the direct diffusion, back diffusion and evaporation are all present, the right side of Equation 13 can be positive, negative or zero. Therefore, all shapes of the permeation profile can be observed. Further experiments with aluminum foil replacing the skin should be conducted. In these experiments the effect of the direct and back diffusion is excluded $(m_{dd_n} = m_{bd_n} = 0)$ and Equation 13 can be rewritten in the following form $Q_{t_n} - Q_{t_{n-1}} = -m_{ev_n} \leq 0$. Either of two possible permeation profiles can be obtained: a plateau curve as an indication of the absence of the evaporation or a decrease in the permeation profile with

time indicating to the presence of PG evaporation from the receptor via the sampling port.

Example:

If we assume that the volume of Franz cell's receptor was 1 ml and the volume of the sample collected at each collection time was 0.1 ml. If the PG amount in the receptor phase at 20 h was 4 µg and its amount from previous collections was 1 µg, therefore, the cumulative amount of PG would be 4 + 1 = 5 µg.

Since the sample volume withdrawn at 20 h was 0.1 ml, the PG amount in this sample was 0.4 µg and the remaining amount of PG in the receptor phase would be (4 - 0.4 = 3.6) µg after the 20 h collection time.

If the PG diffusion between 20 and 24 h (the next collection) stopped and 1 µg of PG evaporated from the receptor phase during this period, the remaining amount of PG in the receptor would be (3.6 – 1 = 2.6) µg. This would result in a cumulative amount of PG equal to 4 µg at 24 h [2.6 µg + 1 µg (the old collections before 20 h) + 0.4 µg (the PG amount present in 0.1 ml sample from the previous collection at 20 h]. Since 4 < 5, a decrease in the permeation profile will be noticed. This phenomenon was observed in my PG permeation profile.